NUMERICAL SIMULATION OF BRINE MIGRATION IN THE VICINITY OF A POTASH MINE

A Thesis Submitted to the College of Graduate Studies and Research

in Partial Fulfilment of the Requirements for the

Degree of Master of Science in the Department of Geological Sciences

at the University of Saskatchewan, Saskatoon.

By

Michelle Uwiera

January 9, 1998

© Copyright Michelle Uwiera, 1998. All Rights Reserved.

DISTRIBUTION NOTICE

In presenting this thesis in partial fulfilment of the requirements for a Postgraduate degree from the University of Saskatchewan, the author has agreed that the liberties of this University may make it freely available for inspection. Further more, the author has agreed that permission for copying this thesis in any manner, in whole or in part, for scholarly purposes may be granted by the professors who supervised the thesis work recorded herein or, in their absence, by the Head of the Department of the Dean of the College in which the thesis work was done. It is understood the due recognition will be given to the author of this thesis and to the University of Saskatchewan in any use of the materials in this thesis. Copying of publication or any other use of this thesis or parts thereof for financial gain without the author's written permission is prohibited.

Requests for permission to copy or to make other use of material in this thesis in whole or part should be addressed to:

Department Head
Department of Geological Sciences
University of Saskatchewan
114 Science Place
Saskatoon, Saskatchewan
S7N 5E2

ABSTRACT

The development and results of a 3-D site-specific groundwater flow and transport study of the Potash Corporation of Saskatchewan Incorporated Cory Division Potash Mine (PCS Cory Mine) and surrounding area are presented. The mine is located approximately 10 km southwest of Saskatoon, Saskatchewan, Canada. The objectives of the study are to simulate, analyze and predict the extent of brine migration, originating from the PCS Cory Mine Waste Management Area (WMA), in the groundwater flow system.

The hydrogeology of interest to the study is Late Cretaceous to Quaternary in age. A 3-D finite element mesh representing the hydrogeology of the study area is constructed. The FEMWATER code is used to simulate steady-state and transient groundwater flow and solute transport processes. Calibration of the model using observed hydraulic heads is reported.

Fifty years of brine plume migration at the PCS Cory Mine WMA, beginning in 1969, are simulated. Detailed analysis of the position and concentration of the brine plume in the surficial stratified deposits, the Floral Aquifer, the Judith River Aquifer and in vertical cross-sections are conducted for the years 1979, 1986, 1995 and 2019. Analysis of the base case model indicates that after 50 years of simulated brine transport, the contaminant plume migrated past the freshwater bypass ditch in the surficial stratified deposits and infiltrates the Floral Aquifer reaching concentrations in excess of 100 g/L.

Sensitivity studies indicate that the engineered containment devices are ineffective at inhibiting brine plume migration. These studies also show that brine mounding in the tailings pile is a critical control on plume migration to the Floral Aquifer and in vertical section. Varying the coefficient of tortuosity has little effect on brine migration.

ACKNOWLEDGMENTS

I would like to thank a number of people and institutions that had an important part in the completion of this thesis study. Firstly, I sincerely thank my supervisor, Dr. Malcolm J. Reeves for his support and guidance he provided throughout my thesis study. His input, discussion and knowledge of this area of research have not only enlightened me, but also provided me with a solid foundation for my future career.

Secondly, I would like to thank, NSERC, Dr. Graeme Strathdee of the Potash Corporation of Saskatchewan and the College of Graduate Studies and Research for project funding throughout my postgraduate education.

Finally, I would like to thank my family for their continued support throughout this thesis study.

TABLE OF CONTENTS

LIST OF TABLES

LIST OF FIGURES

LIST OF ABBREVIATIONS

1-D	One Dimensional
2-D	Two Dimensional
3-D	Three Dimensional
Δt	Time Step
DFR	Driving Force Ratio
FEM	Finite Element Method
GMS	Groundwater Modelling System
KCl	Sylvite
MAE	Mean Absolute Error
ME	Mean Error
MWR	Method of Weighted Residuals
NaCl	Halite
PCS	Potash Corporation of Saskatchewan
ppt	Parts Per Thousand
RMS	Root Mean Square
SRC	Saskatchewan Research Council
SWC	Saskatchewan Water Corporation
TDS	Total Dissolved Solids
TIN	Triangulated Irregular Network
UTM	Universal Tranverse Mercator
WF	Weighting Factor
WMA	Waste Management Area

CHAPTER 1

INTRODUCTION

Potash mining in Saskatchewan began in 1962. The potash ore is extracted from the upper 70 m of the Prairie Evaporite Formation located between depths of 1000 and 2500 m (Tallin *et al.*, 1990).

The ore consists of halite (NaCl), sylvlite (KCl), sometimes carnallite ($KMgCl_3 \cdot 6H_2O$), minor sulphates and approximately 1 to 5% insoluble minerals. For every tonne of KCl refined, 2 tonnes of NaCl and 1 to 2 m^3 of brine are produced. At operating capacity the Saskatchewan potash industry produces 28×10^6 tonnes of salt tailings and 11×10^6 m^3 of brine each year. Over 250×10^6 tonnes of tailings and lesser amounts of brine are stored on the ground surface in waste management areas (WMAs) adjacent to the mine site. Mining is expected to continue for the next 100 years and thus presents a potentially large scale waste management problem (Tallin *et al.*, 1990). Brine, due to its high concentration relative to native groundwater, can adversely affect the local environment if it migrates out of the WMA (Meneley, 1989).

Environmental regulations for Saskatchewan potash mines are established by the provincial government. However, when mining began, environmental assessment investigations were not conducted and thus environmental factors were not considered when determining the mine locations. Experience indicates that the locations of the WMA, with respect to surface hydrology and subsurface hydrogeology, are the most important factors controlling the long term success of environmental management (Meneley, 1989).

The Potash Corporation of Saskatchewan Incorporated (PCS) is currently developing decommissioning plans for PCS Cory Mine and its other Saskatchewan potash mines. The objective of the decommissioning strategy is to reduce the potential for a serious environmental waste management problem. Some of the requirements for a viable decommissioning plan include the ability to remove all

tailings stored on the ground surface, to control the rate of brine released into the subsurface from the containment facility and to obtain a reasonable level of care and maintenance of the WMA (Meneley, 1989). One aspect of a mine decommissioning plan is to predict long term brine migration, from the WMA, into the regional and local groundwater flow systems.

1.1 Project Objectives

The primary objective of this thesis was to assess and predict long term brine migration from the PCS Cory Mine WMA into the groundwater flow system. To meet this objective a three dimensional (3-D), variable density, groundwater flow and solute transport numerical model was utilized.

More specifically, the objectives of the groundwater flow and solute transport modelling investigation for PCS Cory Mine and surrounding area were to:

1. Develop a 3-D conceptual representation of the hydrostratigraphy at PCS Cory Mine and surrounding area from existing geological databases;
2. Construct a 3-D hydrogeological conceptual model that represents the groundwater flow system and active contaminant transport processes;
3. Calibrate a numerical model using available hydrogeological data, results from regional groundwater flow studies and observations of the brine plume position at the mine;
4. Simulate transient brine migration from the WMA;
5. Analyze the effectiveness of existing engineered brine migration control measures; and
6. Determine the limitations of the numerical simulation by conducting sensitivity analysis.

The United States, Department of Defense Groundwater Modeling System (GMS) was developed by Engineering Computer Graphics Laboratory of Brigham

Young University, Utah and United States Army Engineer Waterways Experiment Station, Vicksburg, Mississippi. GMS is a comprehensive graphical interface used for the constructing 3-D hydrogeological models and groundwater flow and contaminant transport simulations (ECGL, 1996). The groundwater flow and solute transport codes, MODFLOW, MT3D, MODPATH, FEMWATER, SEEP2D and RT3D are supported by the GMS interfaces. All the tools required for site characterization, model conceptualization, mesh and grid generation, geostatistical data interpolation and post-processing are provided in the GMS graphical interface (ECGL, 1996).

The groundwater flow and solute transport code, FEMWATER, was used to simulate groundwater flow and brine transport at PCS Cory Mine. FEMWATER is a 3-D finite element, saturated-unsaturated, variable density, groundwater flow and transport code developed by coupling the 3DFEMWATER (flow) and 3DLEWASTE (transport) codes (ECGL, 1996 and Lin *et al.*, 1996). During the 1990s FEMWATER was modified slightly so that it could be supported by GMS.

1.2 Study Area Location

The region selected for the near-field groundwater contaminant migration study was located in south, central Saskatchewan, Canada, between Saskatoon and Vanscoy. The study area covers approximately 400 km^2 of Saskatchewan prairie (Map 1, Appendix F). The boundary of the groundwater flow and brine transport study was selected based on topography, surficial hydrology, hydrogeology, well data and results from regional numerical simulations of groundwater flow. The approximate UTM (Universe Tranverse Mercator) coordinates defining the roughly shaped hexagonal perimeter of the contaminant migration study area were 375800E/5782800N, 372300E/5783100N, 358400E/5781400N, 361700E/576400N, 373200E/5762900N, 373200E/5762900N, and 381700E/5765000N.

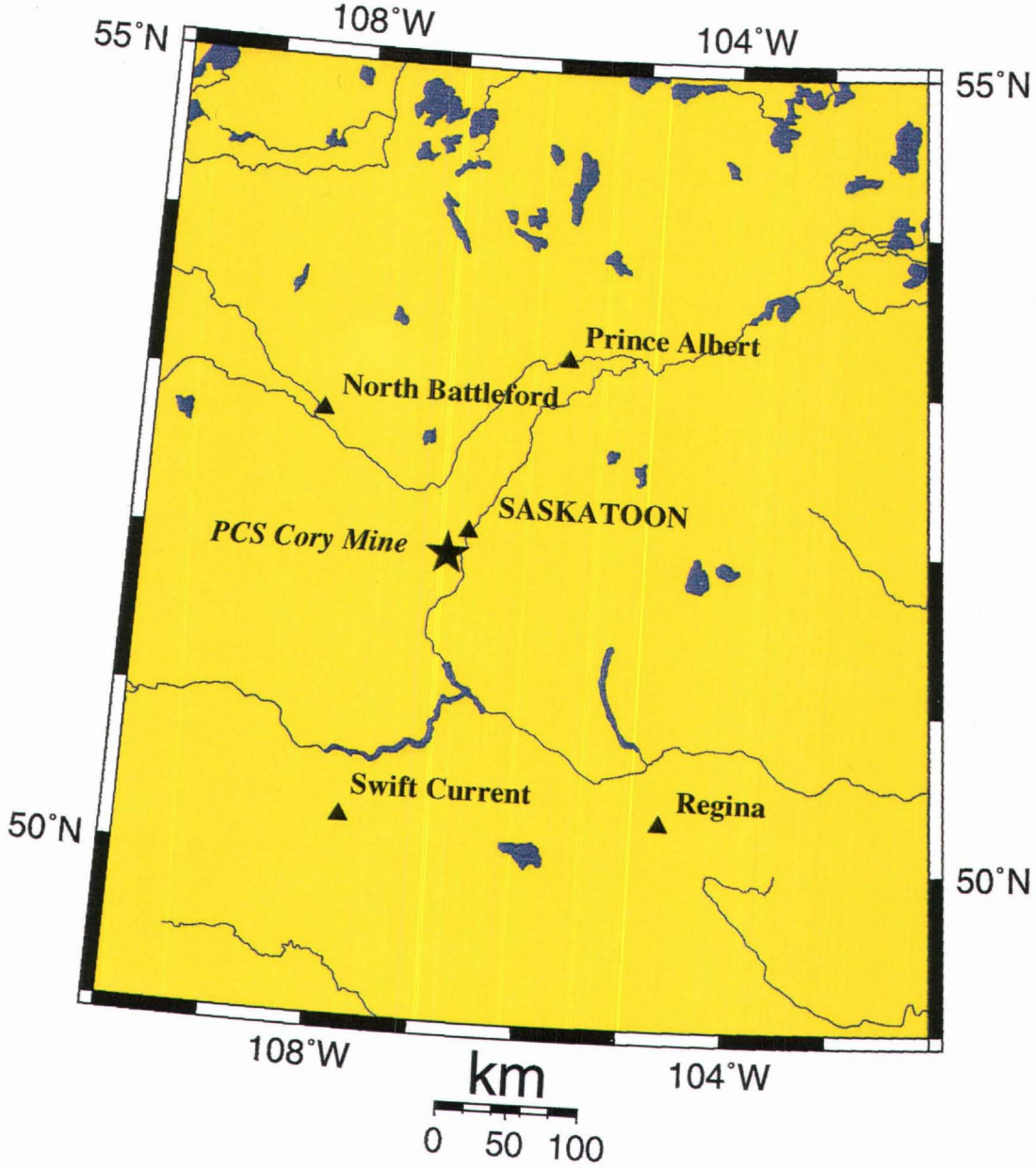

Figure 1.1 - Location of PCS Cory Mine

1.2.1 PCS Cory Mine Location

The PCS Cory Mine is located approximately 10 km west of Saskatoon along Highway 7 (Map 1, Appendix F). The approximate perimeter of the mine site is defined by the UTM coordinates 370600E/5769900N, 370600E/5774300N, 373350E/5774300N and 373350E/5769900N. The mine property includes all or parts of Range 6, Township 36, Section 7,18, and 19, and Range 7, Township 36, Sections 11-14, 23 and 24 (Maathuis *et al.*, 1994), west of the third meridian. Figure 1.1 illustrates the location of PCS Cory Mine in Saskatchewan, Canada. A photograph of the western side of the mine site viewed from Highway 7 is shown in Figure 1.2.

Figure 1.2 - Photograph of PCS Cory Mine Viewed From Highway 7

1.2.1.1 Containment Structures at PCS Cory Mine

Since mining began at PCS Cory in 1962 and the initial construction of the WMA in 1968, the WMA developed considerably, as knowledge and understanding of the site hydrogeology improved. Numerous containment structures were installed to protect the environment from stored solid wastes and surficial brine contamination. Illustrated in Figure 1.3 is the layout of the WMA showing the location of tailings pile, brine pond and other site features important to the numerical modelling study.

At PCS Cory Mine the brine pond, slimes settling area and mine tailings are contained by external dykes that are approximately 6 km long and at an elevation of 497.1 m. The internal dykes used to separate the brine pond from the tailings pile and slimes settling area are approximately 2 km in length.

The flood containment pond is also confined by dykes that are at an elevation of 497.1 m. The elevation of the dykes in the slimes storage pond is 498.0 m in order to prevent overflowing of slimes into brine pond. The slimes storage pond dykes are 1.2 km long.

A slurry trench was installed to impede brine plume migration from the WMA. The slurry trench was installed in 1979 around the north, west and south sides of the WMA (Figure 1.2). The slurry trench is 5.3 km long, 1 m wide, 5 to 8 m deep and is keyed into the Floral Formation till. A mixture of fine sand and till hydrated with brine was used to construct the slurry trench.

The freshwater bypass ditch was also installed in 1979 along the southwestern edge of the WMA in order to intercept brine that may have migrated through or from the slurry trench. The elevation of the bottom of the drainage ditch varies from 494.26 m in the north to 491.81 m in the south. In 1986 two-small, buried drains, known as the east drain and west drain, were installed south of the tailings pond. In 1995 the west drain was extended to intercept the bypass ditch. Brine intersecting the drains and ditch is pumped into the slimes storage pond.

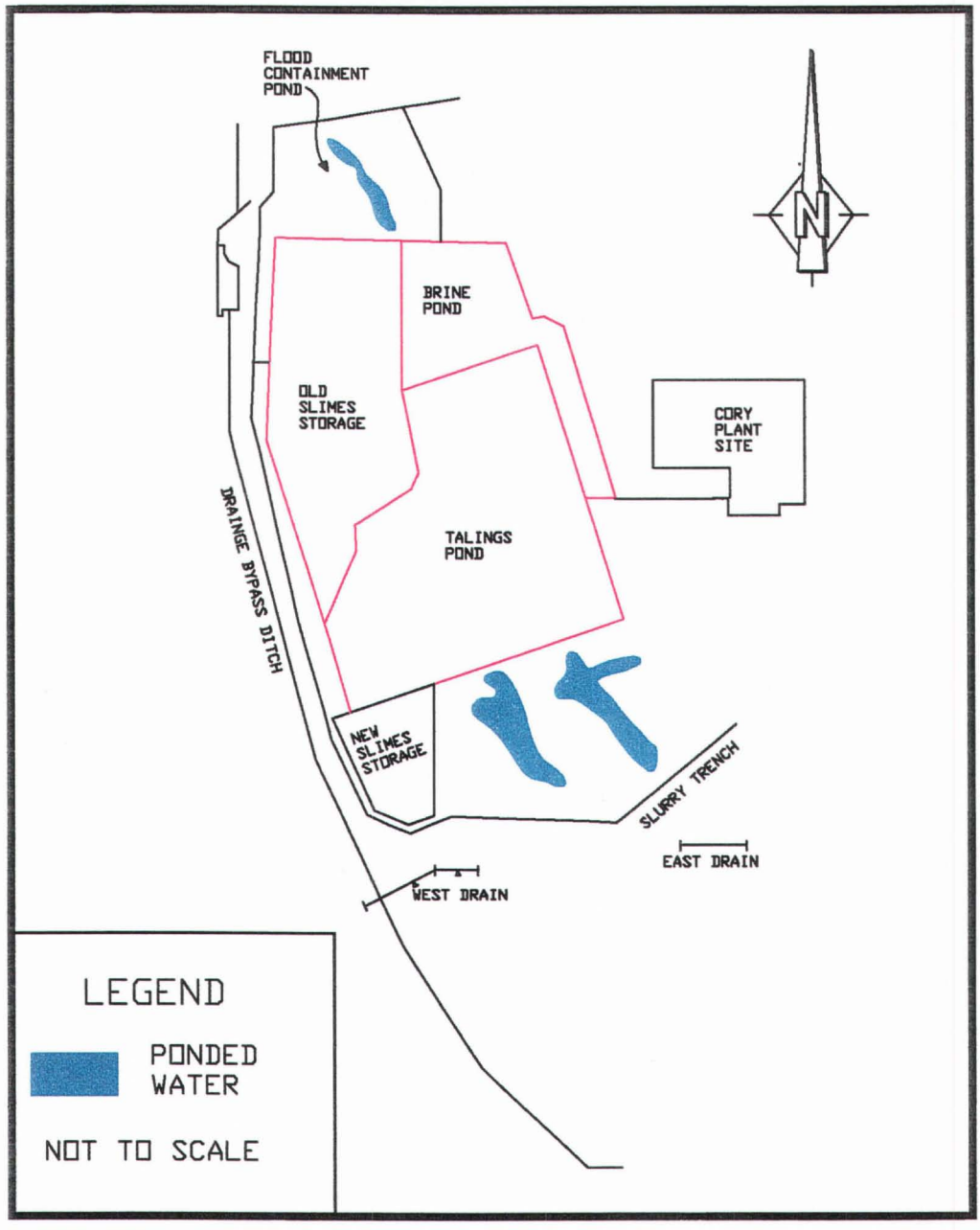

Figure 1.3 - Plan view of PCS Cory Mine Showing the Location of the Tailings Facility, the Containment Structures and the Plant Site

1.3 Site Topography and Drainage

Over the past two million years, Saskatchewan's landscape altered significantly especially during the Pleistocene glaciation. The Wisconsinan deglaciation occurring 10,000 to 17,000 years ago was the last glacial event affecting Saskatchewan (Christansen, 1979). During these glacial events large ice sheets, originating from present day northern Canada, flowed over and eroded the Precambrian Shield. Eroded material was transported and deposited on the Interior Plains forming a succession of till, glaciolacustrine, glaciofluvial and ice-contact stratified deposits (Lennox *et al.*, 1988 and Stephenson *et al.*, 1988). The repeated advance and retreat of the glacial ice front modified the stress regime, particularly in the consolidated tills, thereby causing them to fracture in preferential directions (Penner, 1986 and Stauffer and Gendzwill, 1987).

The terrain in the study area is gently undulating. The total topographic variation is approximately 50 m (Figure 1.4 and Map 1, Appendix F). Topographic lows ranging from 475 to 480 m are found near the South Saskatchewan River and Moon Lake, located at the southeastern corner of the study area. Along the southwestern margin of the study area and also northwest of PCS Cory Mine are the highest elevations, ranging from 520 and 530 m.

There are numerous factors influencing the hydrological conditions within the study area. The climate at the study area and over most of central and southern Saskatchewan is semi-arid. The majority of groundwater infiltration and recharge originates from water filled depressions in upland areas and discharges in local and regional topographic lows. Throughout most of the study area where numerous seasonal and permanent sloughs are present, the water table is located near the ground surface. Most surficial water flow in the study area is directed towards the South Saskatchewan River Valley. Surficial drainage immediately southwest of the study area discharges towards Rice Lake, which is subject to evaporation and is situated in an enclosed low with no outflowing streams.

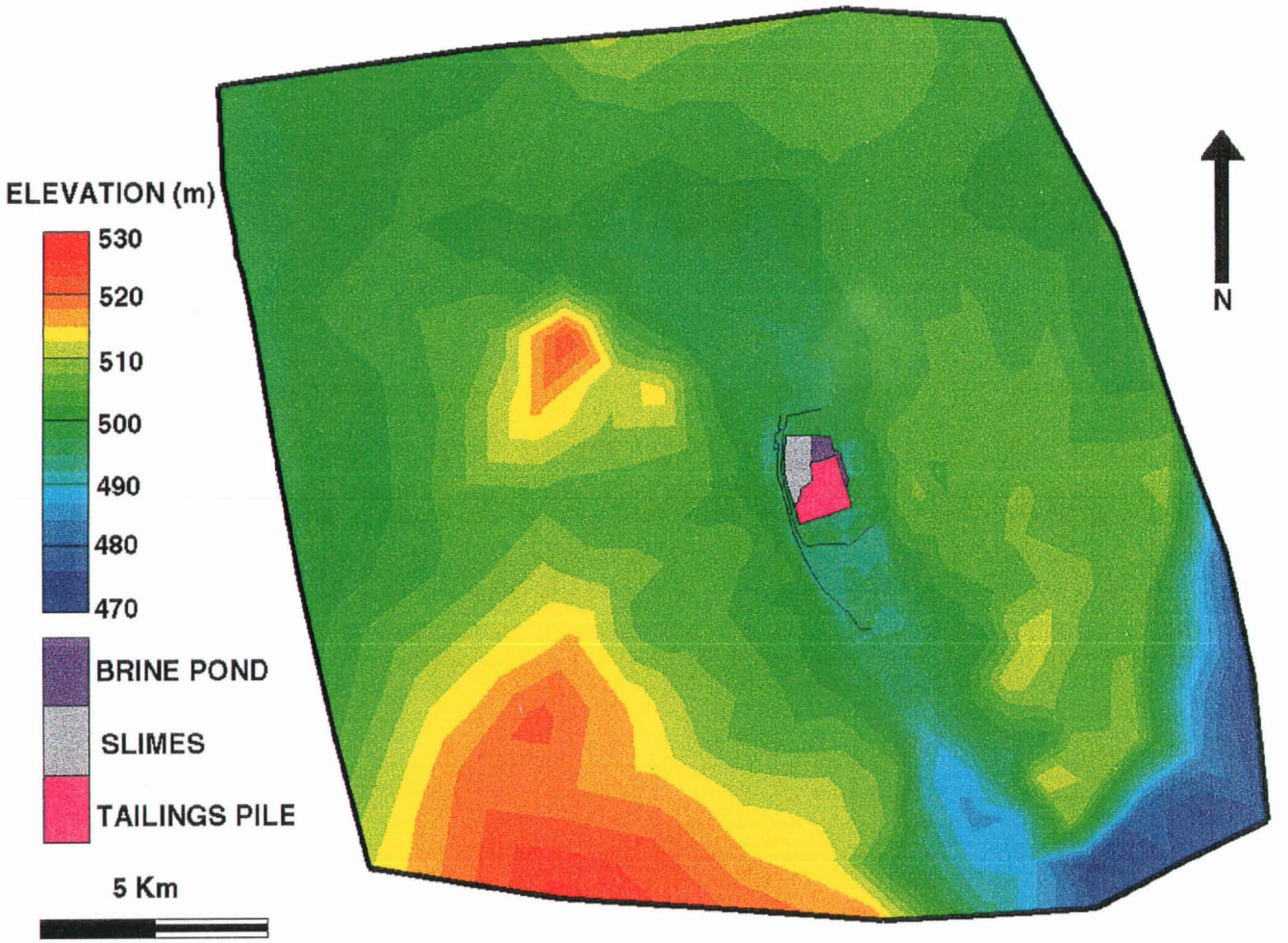

Figure 1.4 - Topography of the Study Area

PCS Cory Mine is situated on surficial sands, silts and clays that overlay low permeability aquitards, permeable channel aquifers and Cretaceous bedrock sediments. The mine site is located on a glacial lake plain and in particular, within a broad, shallow, meltwater channel depression defined by the 500 m contour on Figure 1.5. This depression originates northwest of the mine and extends southeast towards Moon Lake and the South Saskatchewan River (Maathuis *et al.*, 1994). Along the eastern boundary of the study area is another parallel meltwater channel. Both meltwater channels were formed during the final stage of Wisconsinan deglaction (Christansen and Sauer, 1994).

Approximately 5 km west of PCS Cory Mine, the topography rises approximately 25 m and forms a surface water catchment boundary. Surficial drainage east of the divide flows towards the South Saskatchewan River. Drainage west of the divide flows into the Rice Lake depression.

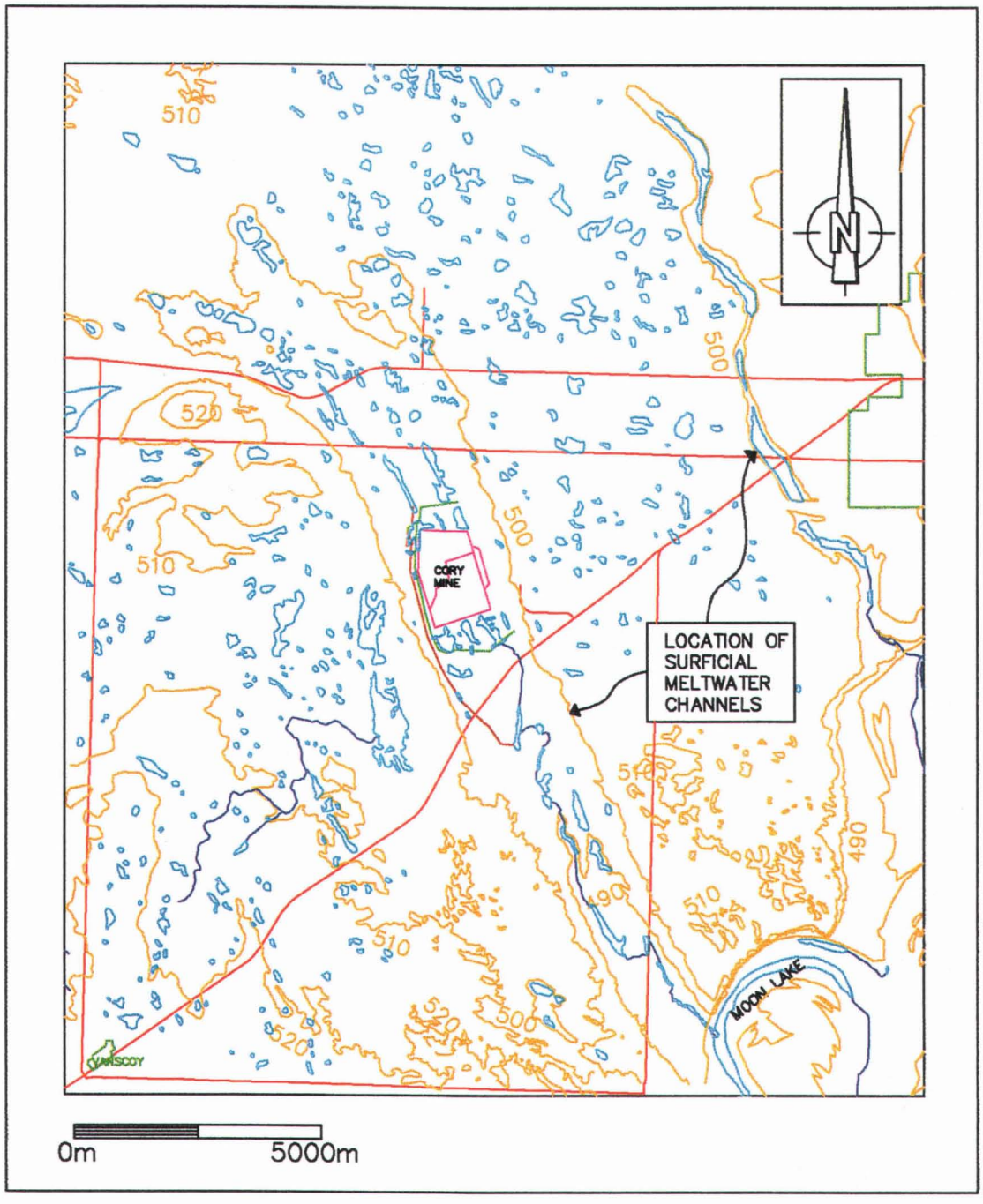

Figure 1.5 - Location of Surficial Meltwater Channels

CHAPTER 2

GEOLOGY AND HYDROGEOLOGY

Extensive geological research in Saskatchewan began in the mid 1940s. During these investigations the Saskatchewan prairie soil was classified, mapped and analyzed in detail. From these investigations the foundations of an in depth knowledge of Saskatchewan's geological history was synthesized.

The regional geological setting at PCS Cory Mine and surrounding area is described by Christiansen (1967, 1970 and 1979), Meneley (1970), Maathuis *et al.* (1994) and Maathuis and van der Kamp (1994). The geological setting of the study area is qualitatively determined from testhole logs and cross-sections. Stratigraphy at PCS Cory Mine and surrounding region was subdivided into Bedrock stratigraphy and Quaternary glacial stratigraphy. Figure 2.1 outlines the stratigraphic framework of PCS Cory Mine and the surrounding area.

2.1 Bedrock Stratigraphy

The bedrock stratigraphic units important to the study of brine migration at PCS Cory Mine, were, in order of increasing age:

1. Bearpaw Formation;
2. Judith River Formation; and
3. Lea Park Formation.

The bedrock formations were deposited from 84 to 66 MA ago during the Late Cretaceous Period. The Lea Park, Judith River and Bearpaw formations were differentiated in stratigraphic drillhole logs by lithological and geotechnical properties, relative stratigraphic position and electrical signatures.

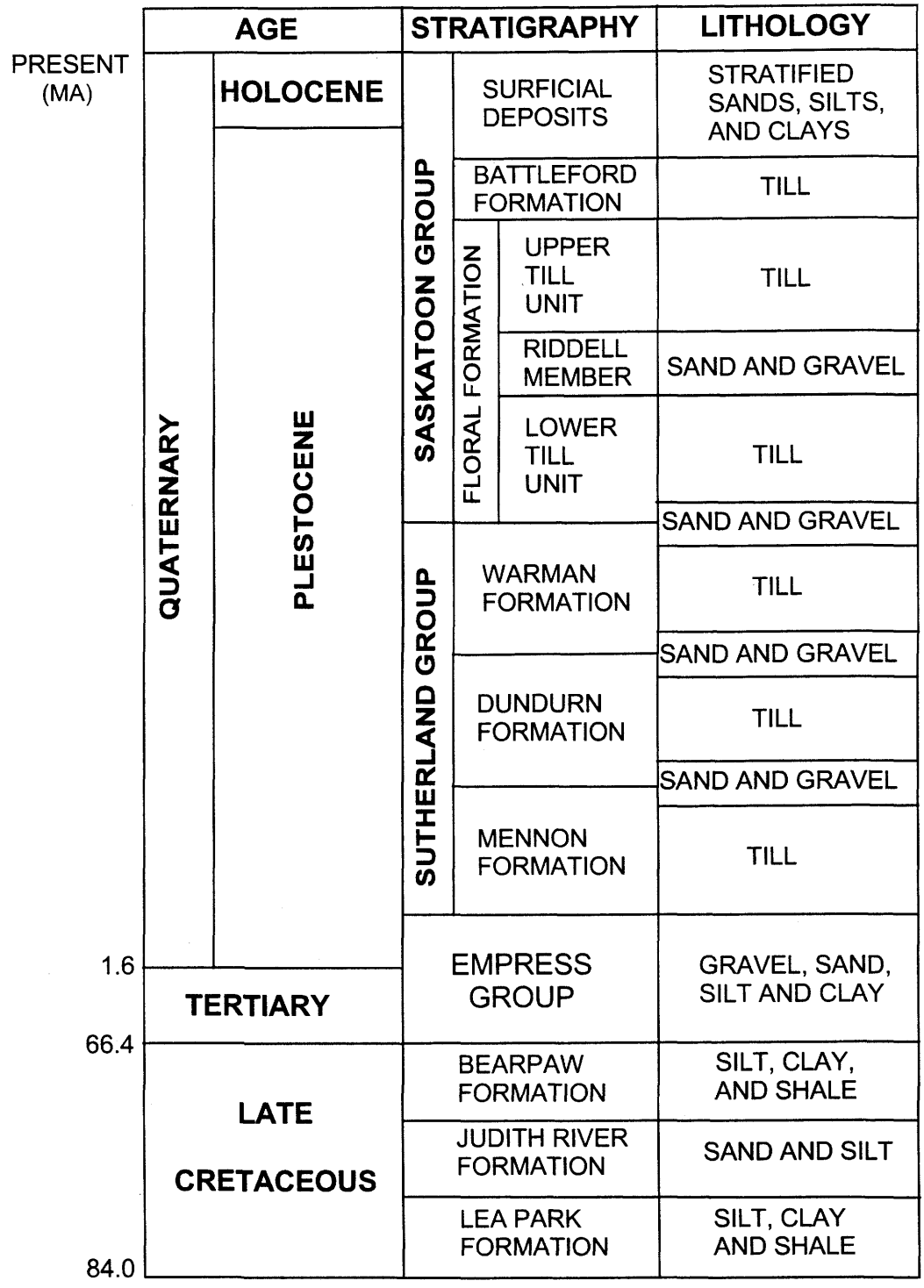

Figure 2.1 - Stratigraphic Framework of the Study Area
(after Maathuis *et al.*, 1994)

The elevation of the bedrock surface at PCS Cory Mine and surrounding area ranges from approximately 365 to 485 m ASL (Maathuis *et al.*, 1994) corresponding to a typical thickness of 60 to 100 m of glacial deposits. Collapse structures, resulting from the dissolution of salt from the Elk Point Group and Prairie Evaporite Formation (Christiansen, 1967 and 1970) and glacial and fluvial erosion (Maathuis *et al.*, 1994) affects the bedrock topographic profile. Geological investigations indicate that collapse structures are absent beneath the mine site, however, this conclusion may involve some uncertainty due to the limited number of deep stratigraphic drill holes (Maathuis *et al.*, 1994).

2.1.1 Lea Park Formation

The Lea Park Formation is the lowermost stratigraphic unit considered in this study. This formation consists of mainly non-calcareous, overconsolidated, marine, silts and clays. The lowermost portion of the Lea Park Formation is calcareous (Christiansen, 1970 and Maathuis *et al.*, 1994). Drill hole data indicates that in the study area the Lea Park Formation is more than 250 m thick (Maathuis *et al.*, 1994).

2.1.2 Judith River Formation

Conformably overlying the Lea Park Formation is the Judith River Formation which consists of marine and non-marine deltatic silts and clays and also fine-grained sands and silts. The Judith River Formation is also interbedded with carbonaceous and concretionary material (Christiansen, 1970 and Maathuis *et al.*, 1994).

The Judith River Formation is present throughout most of the study area. The maximum thickness of the Judith River below the WMA is 16 m and throughout the remainder of the study area no more than 40 m. The Judith River Formation is laterally continuous below the WMA (Maathuis *et al.*, 1994) but is not continuous throughout the study area.

2.1.3 Bearpaw Formation

The Bearpaw Formation is the youngest bedrock stratigraphic unit found in the study area. This formation is composed of non-calcareous, marine silts and clays that are preserved in collapse structures or as erosional remnants (Christiansen, 1970 and Maathuis *et al.*, 1994).

At the PCS Cory Mine WMA and most of the surrounding area the Bearpaw Formation has a maximum thickness of approximately 10 m. However near the southeast corner study area thickness of the Bearpaw Formation increases to almost 85 m. Large variations in formation thickness are attributed to its preservation in collapse features.

2.2 Quaternary Stratigraphy

The Quaternary sediments, also known as "drift", are located between the bedrock and the ground surface (Christiansen, 1970 and Maathuis *et al.*, 1994). In descending order, the Quaternary drift at PCS Cory Mine and surrounding area is divided into three sections; the Saskatoon Group, the Sutherland Group and the Empress Group. Some of the Empress Group sediments may be Tertiary in age but are described here for convenience. The Sutherland and Saskatoon Groups can be further divided into formations and subunits. It is not always possible to differentiate between the formations of the Sutherland Group from test hole logs or to locate the exact position of the stratigraphic contact between the Sutherland and Saskatoon Group.

2.2.1 Empress Group

The Empress Group sediments are Tertiary to Late Quaternary in age and are composed of stratified gravel, sand, silt and clay located between the Cretaceous bedrock and the Sutherland Group (Christiansen, 1970 and Whitaker

and Christiansen, 1972). These stratified sediments are fluvial, lacustrine and colluvial in origin (Whitaker and Christiansen, 1972). The contact between the bedrock surface and Empress Group is a preglacial erosional unconformity that is identified by a quartzite or cherty gravel with minor amounts of petrified wood, carbonates and igneous pebbles (Christiansen, 1970 and Christiansen, 1992).

Empress Group sediments are not encountered below PCS Cory Mine, however they are found in the western portion of the study area. The stratigraphic thickness of the Empress Group is highly variable ranging from 0 to 75 m.

2.2.2 Sutherland Group

The Sutherland Group sediments, which are predominately composed of till, are located between the base of the lower most till unit and the Saskatoon Group (Christiansen, 1992). Stratified deposits consisting of sand, gravel, silt and clay are found sporadically throughout the Sutherland Group (Christiansen, 1992). The contact between the Sutherland and Empress Group is easily located as the lithology changes from stratified gravels, sands, silts and clays to a till.

The Sutherland and Saskatoon Group tills are differentiated by carbonate content, texture, Atterberg Limits, electrical log signatures and preconsolidation pressures. In general, the carbonate content and electrical resistivity of the Sutherland Group till is less than the tills of the Saskatoon Group. The Mennon, Dundurn and Warman Formations are subdivisions of the Sutherland Group (Christiansen, 1992).

The thickness of the Sutherland Group is highly variable throughout the study area reaching a maximum greater than 50 m. The predominant lithology is a hard, dense, grey unoxidized till. Soil analysis of samples taken from the WMA indicate that the Sutherland Group is mostly comprised of the Dundurn Formation, a relatively high carbonate till and a sandy silt lithology similar to the Floral Formation till. Assigning formation names to the Sutherland Group sediments is possible only at a few test holes where carbonate analysis was conducted (Maathuis *et al.*, 1994).

Below the WMA, a stratified sand unit is found within in the Sutherland Group sediments. This sand unit is thought to be part of a regional complex channel fill system, even though it has only been encountered in a small number of test holes drilled at the mine site (Maathuis *et al.*, 1994). The sand unit is believed to be present under the tailings facility and northwest of the plant site. It is absent under the north perimeter dyke (Maathuis *et al.*, 1994). The maximum thickness of the stratified sand is approximately 16 m.

2.2.3 Saskatoon Group

The Saskatoon Group sediments are located between the Sutherland Group and the ground surface (Christiansen, 1970 and Christiansen, 1992). The Saskatoon Group is divided into the surficial stratified deposits, the Battleford Formation and the Floral Formation.

2.2.3.1 Floral Formation

The Floral Formation is the lowermost stratigraphic unit in the Saskatoon Group and is situated between the Sutherland Group and Battleford Formation. The Floral Formation can consist of a basal stratified sand and two informally subdivided tills that are separated by a discontinuous stratified sand unit. Compositional differences between the two till units are insufficient to warrant a formal stratigraphic name (Christiansen, 1992).

The stratified sand unit separating the two till units is the Riddell Member. This unit contains stratified and cross bedded sands that are heavily stained with iron and manganese oxides. Fossilized bone, shells and wood are abundant in the Riddell Member (Skwarawoolf, 1980). The measured maximum thickness of the Riddell sand is approximately 16 m in the study area.

The two Floral Formation tills have similar lithological characteristics. They are both hard, have a high carbonate content and a silty-sandy grey appearance.

The upper till is weathered and macroscopically fractured showing evidence of iron and manganese oxidation. The lower till is unoxidized (Christiansen, 1970 and Maathuis *et al.*, 1994). The combined thickness of these till units is highly variable in the study area, reaching a maximum thickness of approximately 20 m.

Preconsolidation pressures were measured for the Floral Formation till. The range of preconsolidation pressure measurements are between 1500 and 2200 kPa indicating that the thickness of the overlying glacial ice the till was between 170 to 240 m (Sauer and Christiansen, 1991).

The basal stratified sand unit in the Floral Formation is part of a regional complex channel fill system trending northwest-southeast in the study area. This sand channel is carved into the Sutherland Group till. It is thought that sand deposition began during the late stages of Sutherland Group till deposition (Maathuis *et al.*, 1994). The maximum measured thickness of the channel sand is over 26 m.

2.2.3.2 Battleford Formation

The Battleford Formation is composed of drift located between the Floral Formation and surficial stratified deposits (Christiansen, 1992). The Battleford Formation, in the study area, consists of an unstained, soft, friable till. The contact between the Battleford and Floral Formation is unconformable and often denoted by a stratified boulder pavement. In the study area, the stratigraphic contact is gradational consisting of deformed soil fractures and disseminated oxidized stains similar to that of the Floral Formation (Christiansen, 1992).

In addition to the macroscopic separation of the Battleford and Floral Formations, the tills are differentiated on the basis of their preconsolidation pressures. The preconsolidation pressures measured in the Battleford Formation till vary from 350 to 750 kPa, significantly lower than the pressures measured in the Floral Formation till (Sauer and Christiansen, 1991).

The maximum measured thickness of the Battleford Formation at the PCS Cory Mine WMA is about 5 m and in study area approximately 14 m. At the WMA, the Battleford Formation till is only found near the southern end of the slurry trench, however, it is found sporadically throughout the study area.

2.2.3.3 Surficial Stratified Deposits

The surficial stratified deposits accumulated during the Holocene. These deposits include the preglacial and postglacial sediments located between the Battleford Formation and ground surface. The Battleford - Surficial Stratified Deposits contact is conformable and gradational where glaciolacustrine deposits are inculcated with Battleford Formation till (Christiansen, 1992). The surficial stratified deposits are found as a complex arrangement of sands, silts and clays within the study area . The thickness is variable ranging from less than 2 m to more than 12 m, in the study area (Maathuis *et al.*, 1994).

2.3 Soil Properties

Knowledge of the stratigraphic framework at the study area is a prerequisite for the successful design of a groundwater flow and solute transport model. In addition to understanding the stratigraphic framework of the study area, the geotechnical soil properties must also be known.

2.3.1 Dry Density

One of the important geotechnical properties is dry density. Table 2.1 indicates density ranges for different lithologies.

Table 2.1 - Dry Density Ranges for Various Lithologies

Lithology	Dry Density (kg/m^3)
Gravel	1450 - 2100[1],[2]
Sand	1350 - 1900[1]
Silt	1450 - 1950[1],[2]
Clay	1400 - 2100[1]
Till	
Oxidized	1900 - 2200[1],[3]
Unoxidized	2150 - 2300[1],[3]

(1) Bell (1993)
(2) Eyles (1983)
(3) Holtz and Kovacs (1981)

2.3.2 Hydraulic Properties

For modelling purposes it is necessary to develop a hydrostratigraphic model and assign hydraulic parameters, such as hydraulic conductivity, porosity, compressibility and specific storage, to the different lithologic units. The stratigraphic section must be subdivided into aquifer and aquitard units. Knowing the hydraulic properties of the sediments and how they vary with position within the study area is crucial for analyzing groundwater flow and brine transport.

Hydraulic properties were estimated from the literature. Table 2.2 lists the hydraulic conductivity ranges and Table 2.3 summarizes the ranges of compressibility, porosity and specific storage for the various lithologies encountered in the study area.

2.3.2.1 High Hydraulic Conductivity Units

The high hydraulic conductivity units in the study area represented the aquifer units. These aquifer units consisted of bedrock sands and silts and also Quaternary gravels, sands and some silts.

The Judith River Formation, which consists of partially consolidated, fine-grained silts and sands, has an estimated hydraulic conductivity ranging from $6x10^{-6}$ to $1.2x10^{-5}$ m/s at PCS Cory Mine (Maathuis *et al.*, 1994).

The hydraulic conductivity of the Empress Group sands, silts and clays in the study area were not measured. Freeze and Cherry (1979) indicate that the range of hydraulic conductivity for a silty sand is between $1x10^{-7}$ to $3x10^{-3}$ m/s.

The Sutherland intertill sands are classified as fine to medium grained and the hydraulic conductivity is thought to fall within the range of $6x10^{-5}$ to $1.2x10^{-4}$ m/s (Maathuis *et al.*, 1994).

The channel fill sands and Riddell Member sands of the Floral Formation are medium to course grained. The hydraulic conductivity of the channel sands varies from $3.5x10^{-5}$ to $4x10^{-4}$ m/s (Maathuis *et al.*, 1994). The hydraulic conductivity of the Riddell Member sands was not measured, however they are thought to fall within the same range as the channel fill sands.

The surficial stratified deposits in the study area are extremely heterogenous. The hydraulic conductivity of the sand is greater than $1x10^{-7}$ m/s (Maathuis *et al.*, 1994) and likely falls within the range of a silty sand ($1x10^{-7}$ to $3x10^{-3}$ m/s) to a clean sand ($8x10^{-3}$ to $1x10^{-2}$ m/s) reported by Freeze and Cherry (1979).

2.3.2.2 Low Hydraulic Conductivity Units

The low hydraulic conductivity units found throughout the study area form aquitards that impede groundwater flow and brine transport. The low hydraulic conductivity units were associated with clay, till, shale and some silt. The hydraulic conductivities of these units were very low however significantly increased if fracturing existed. The documented hydraulic conductivity ranges for low hydraulic conductivity till units in Saskatchewan were summarized by Maathuis and van der Kamp (1994):

1. Tills that are oxidized, fractured and shallow (less than10 m below the ground surface) have a hydraulic conductivity between $1x10^{-8}$ to $1x10^{-7}$ m/s. Such tills are found in the Floral Formation.
2. Tills that are unoxidized, fractured and situated at depths less than 30 m generally have a hydraulic conductivity value ranging from $1x10^{-9}$ to $1x10^{-8}$ m/s. Such tills are found in the Floral Formation.
3. Unoxidized and unfractured tills located at least 10 m below the ground surface with a thickness more than 30 m have hydraulic conductivities falling within the range of $1x10^{-11}$ to $1x10^{-10}$ m/s. This category includes tills of the Sutherland Group and the thick unfractured tills of the Floral Formation.

Unoxidized surficial silts and clays have hydraulic conductivities as low as $4x10^{-10}$ m/s. Oxidized silts may have a hydraulic conductivity greater than 10^{-7} m/s. Intact bedrock silts and clays have a hydraulic conductivity less than 10^{-10} m/s. If the bedrock is fractured or was subjected to glacial shearing the hydraulic conductivity can be several orders of magnitude higher (Maathuis and van der Kamp, 1994).

Table 2.2 - Ranges of Hydraulic Conductivity for the Geological Units in the Study Area

Stratigraphic Unit	**Hydraulic Conductivity (m / s)**
Surficial Stratified Deposits	
Sand	$1x10^{-5}$ - $1x10^{-2}$ (5)
Silt	$1x10^{-7}$ - $1x10^{-3}$ (1,5)
Clay	$1x10^{-9}$ - $3x10^{-9}$ (1)
Floral Formation Till	
Oxidized	$1x10^{-8}$ - $1x10^{-7}$ (2)
Unoxidized	$1x10^{-9}$ - $1x10^{-8}$ (2)
Riddell Member Sand	$3.5x10^{-5}$ - $4x10^{-4}$ (1)
Floral Formation Sand	$3.5x10^{-5}$ - $4x10^{-4}$ (1)
Sutherland Group Till	$1x10^{-11}$ - $1x10^{-10}$ (3)
Sutherland Group Sand	$6x10^{-5}$ - $1.2x10^{-4}$ (1)
Empress Group Sand	$1x10^{-7}$ - $3x10^{-3}$ (5)
Empress Group Silt	$1x10^{-7}$ - $3x10^{-3}$ (5)
Bearpaw Formation	$< 1x10^{-9}$ (1)
Judith River Formation	$6x10^{-6}$ - $1.2x10^{-5}$ (1)
Lea Park Formation	$<10^{-10}$ (2)

(1) Maathuis *et al.* (1994)
(2) Maathuis and van der Kamp (1994)
(3) Keller *et al.* (1989) and Keller *et al.* (1988)
(4) Therrien and Sudicky (1996)
(5) Estimation based on Freeze and Cherry (1979)

2.3.2.3 Storage Properties

The porosity of the hydrostratigraphic units in the study area was not measured. Freeze and Cherry (1979) documented typical ranges of porosity for different lithologies. These ranges were assigned to the high and low hydraulic conductivity units encountered in the numerical study.

The porosity range documented by Freeze and Cherry (1979) for Cenozoic and Mesozoic sandstones similar to that of the Judith River Formation is between 20 and 30%. The porosity of sands and silts in the Sutherland and Saskatoon Groups is probably between 25 and 50%.

The porosity of the low hydraulic conductivity units were determined from water content analysis by previous workers. The equivalent porosity of surficial silts and clays generally range from 40 to 50%. Both Floral Formation and Sutherland Group till samples were analyzed and found that porosity generally varied from 20 to 30% and 30 to 35% respectively (Maathuis and van der Kamp, 1994). The porosity documented by Freeze and Cherry (1979) for consolidated bedrock silts and clays, such as the Bearpaw and Lea Park Formation, is less than 10%.

Figure 2.2a and 2.2b illustrate the relationship between hydraulic conductivity and moisture content with suction pressure (negative pressure head). Most surficial stratified deposits in the study area are unsaturated.

Soils in the unsaturated zone have a hydraulic conductivity and moisture content lower than the same soil located below the water table. In the unsaturated zone the moisture content is less than the soil porosity (Ranjitkar, 1989). In general, hydraulic conductivity and moisture content of soils in the unsaturated zone is dependent on suction pressure. Below the water table, hydraulic conductivity and moisture content are independent of pressure head.

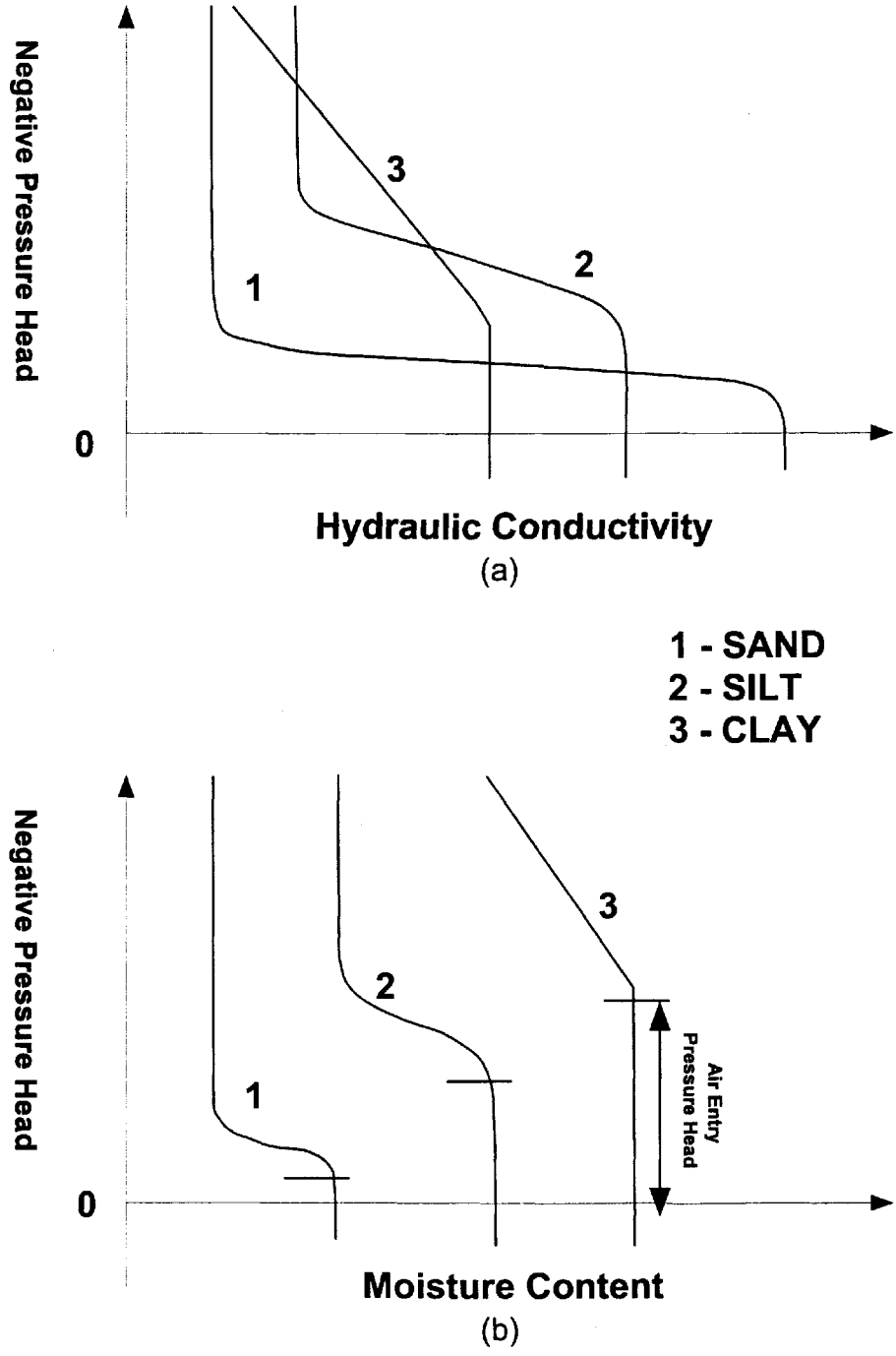

Figure 2.2 - Characteristic Curves for a (1) Sand, (2) Silt and (3) Clay Relating
(a) Hydraulic Conductivity with Suction Pressure and
(b) Moisture Content with Suction Pressure

2.3.2.4 Unsaturated Soil Properties

Table 2.3 lists the possible ranges for compressibility, porosity and specific storage of soils encountered in the study area.

Table 2.3 - Ranges of Soil Compressibility (after Dominico and Schwartz, 1990), Porosity and Specific Storage for Soils in the Study Area.

Stratigraphic Unit	Soil Compressibility (m^2 / N)	Porosity (%)	Specific Storage (m^{-1})
Surficial Stratified Drift			
Sand	$5.2x10^{-8}$ - $1.0x10^{-7}$	25 - 50 (3)	$6.9x10^{-4}$ - $1.9x10^{-3}$
Silt	$5.2x10^{-8}$ - $1.0x10^{-7}$	35 - 50 (3)	$7.4x10^{-4}$ - $1.9x10^{-3}$
Clay	$6.9x10^{-8}$ - $1.3x10^{-7}$	40 - 50 (1,2)	$9.5x10^{-4}$ - $2.7x10^{-3}$
Floral Formation Till	$1.3x10^{-9}$ - $6.9x10^{-8}$	20 - 30 (1)	$2.8x10^{-5}$ - $1.3x10^{-3}$
Riddell Member Sand	$1.3x10^{-8}$ - $2.0x10^{-8}$	25 - 50 (3)	$1.7x10^{-4}$ - $3.8x10^{-4}$
Floral Formation Sand	$1.3x10^{-8}$ - $2.0x10^{-8}$	25 - 50 (3)	$1.7x10^{-4}$ - $3.8x10^{-4}$
Sutherland Group Till	$2.6x10^{-9}$ - $1.3x10^{-7}$	30 - 35 (2)	$5.9x10^{-5}$ - $2.7x10^{-3}$
Sutherland Group Sand	$1.3x10^{-8}$ - $2.0x10^{-8}$	25 - 50 (3)	$1.7x10^{-4}$ - $3.8x10^{-4}$
Empress Group Sand	$1.3x10^{-8}$ - $2.0x10^{-8}$	25 - 50 (3)	$1.7x10^{-4}$ - $3.8x10^{-4}$
Empress Group Silt	$2.0x10^{-9}$ - $1.3x10^{-8}$	35 - 50 (3)	$3.8x10^{-5}$ - $1.9x10^{-4}$
Bearpaw Formation	$2.6x10^{-5}$ - $1.3x10^{-7}$	0 -10 (3)	$5.9x10^{-5}$ - $2.7x10^{-3}$
Judith River Formation	$1.3x10^{-8}$ - $2.0x10^{-8}$	5 - 30 (3)	$1.7x10^{-4}$ - $3.8x10^{-4}$
Lea Park Formation	$2.6x10^{-9}$ - $1.3x10^{-7}$	0 - 10 (3)	$5.9x10^{-5}$ - $2.7x10^{-3}$

* Compressibility of Water at 25°C is $4.8x10^{-10}$ m^2 / N

(1) Maathuis and van der Kamp (1994)
(2) Therrien and Sudicky (1996)
(3) Estimation based on Freeze and Cherry (1979)

Specific storage is the volume of water released from a confined unit volume of porous medium per unit decline in hydraulic head per unit thickness.

Specific storage is related to the compressibility of the porous medium and that of water, together with the porosity:

$$S_s = (a + nb)\gamma_w \tag{2.1}$$

where:

S_s	=	specific storage
a	=	soil compressibility
b	=	water compressibility
n	=	porosity
γ_w	=	specific weight of water

Van Genuchten (1980) developed an empirical equation relating the relative hydraulic conductivity and moisture content as a function of suction pressure. This analytical expression developed from the theory of Mualem (1976) involves three independent parameters determined empirically by fitting the soil-water retention model to experimental data (van Genuchten, 1980).

Equations 2.2, 2.3 and 2.4 (Fetter, 1992, Lin *et al.*, 1996, Mualem, 1976 and van Genuchten, 1980) indicate the empirical expressions used by van Genuchten to define the relationship between hydraulic conductivity, moisture content and suction pressure. The storage characteristics of the porous media were determined from the derivative of the soil-water characteristic profiles.

$$K_r = S_e^{0.5}\left[1 - \left(1 - S_e^{1/\gamma}\right)^{\gamma}\right]^2 \tag{2.2}$$

$$S_e = \left[1 + (\alpha\psi)^{\beta}\right]^{-\gamma} \gamma < 0 \tag{2.3}$$

$$\gamma = 1 - \frac{1}{\beta} \tag{2.4}$$

where:

K_r	=	relative hydraulic conductivity ranging from 0.0 to 1.0
S_e	=	degree of saturation ranging from 0.0 to 1.0
β,γ	=	soil-specific exponents
α	=	soil-specific coefficient

Equation 2.3 applies to soils in the unsaturated zone. The degree of saturation, S_e, equals one when the pressure head is equaled to or greater than 0 m. Equation 2.5 demonstrates the relationship between moisture content and effective moisture content.

$$\theta_w = \theta_r + S_e(n - \theta_r) \tag{2.5}$$

where:

θ_w	=	soil moisture content
θ_r	=	residual moisture content

2.4 Study Area Hydrostratigraphy

The hydrogeological units present in the study area were subdivided into Bedrock and Quaternary aquifers and aquitards. Figure 2.3 outlines the hydrogeological units present at PCS Cory Mine and surrounding area.

In the study area the sands of the Judith River Formation, Empress Group, Sutherland Group, Saskatoon Group and surficial stratified deposits comprised a series of aquifers. With the exception of the Surficial Aquifer, these aquifers were confined by aquitards. The aquitards included the shales of the Lea Park and Bearpaw Formation, the tills of the Sutherland and Saskatoon Group and the clays

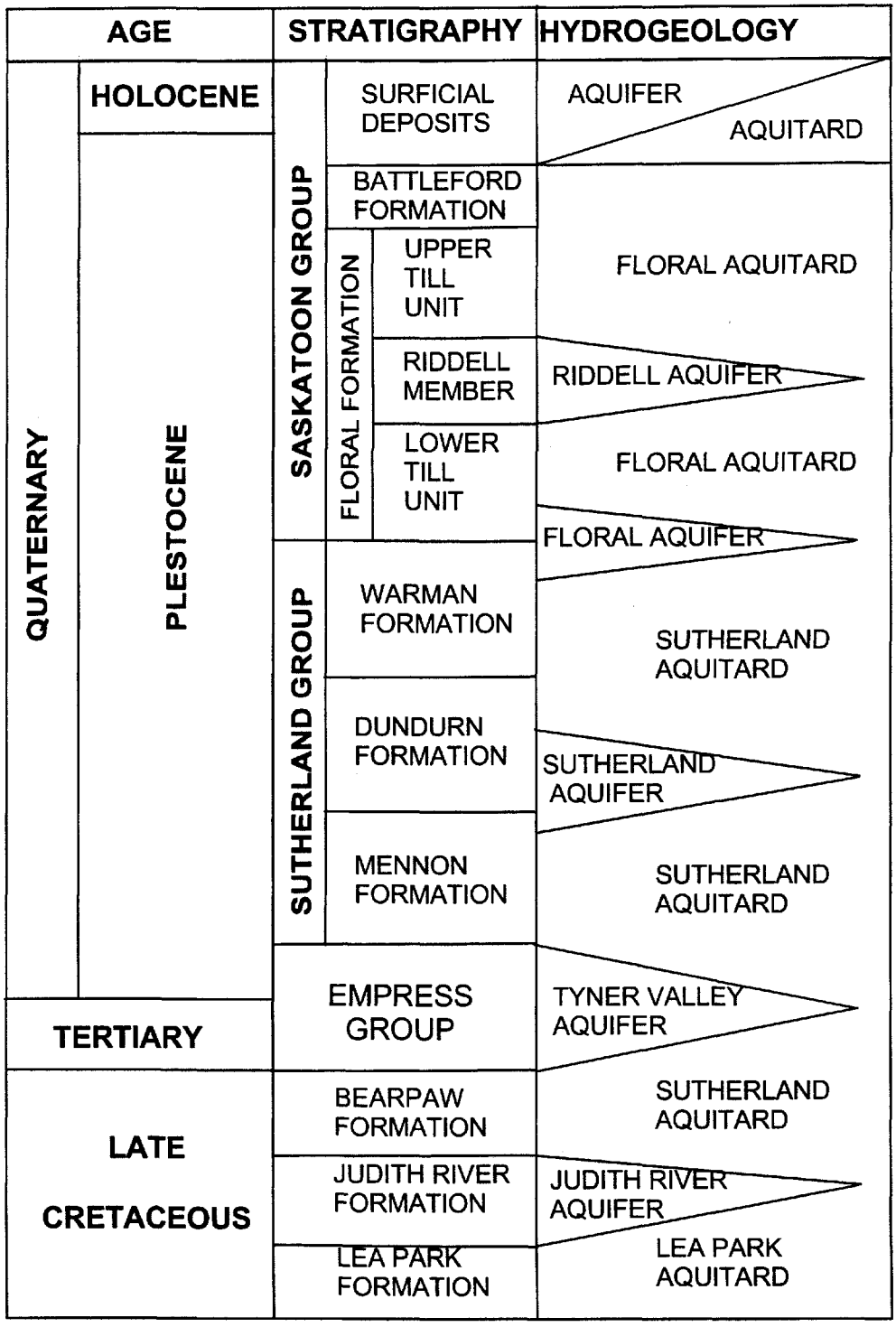

Figure 2.3 - Hydrostratigraphic Framework of the Study Area

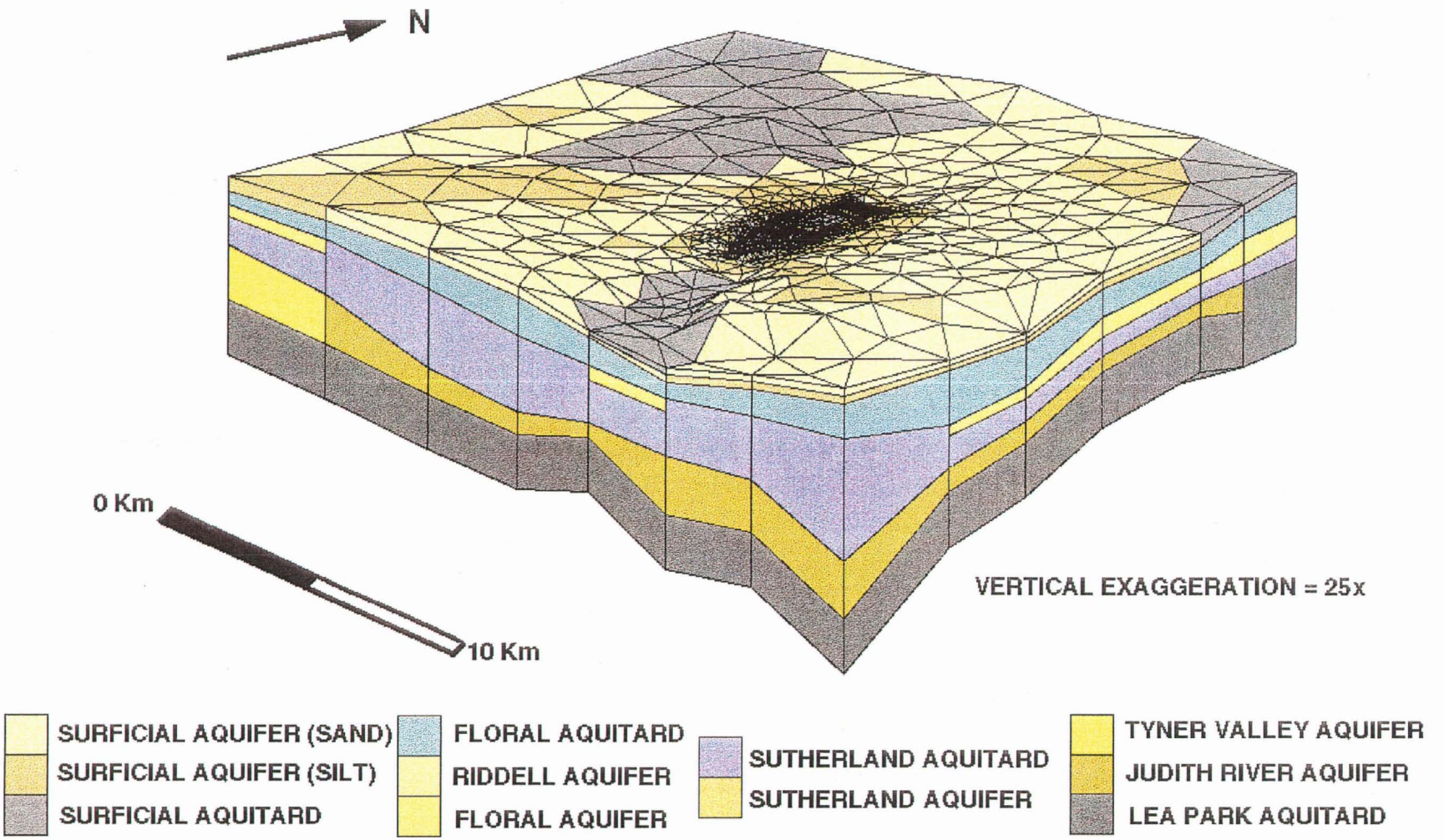

Figure 2.4 - 3-D Hydrostratigraphic Conceptual Model for the Study Area

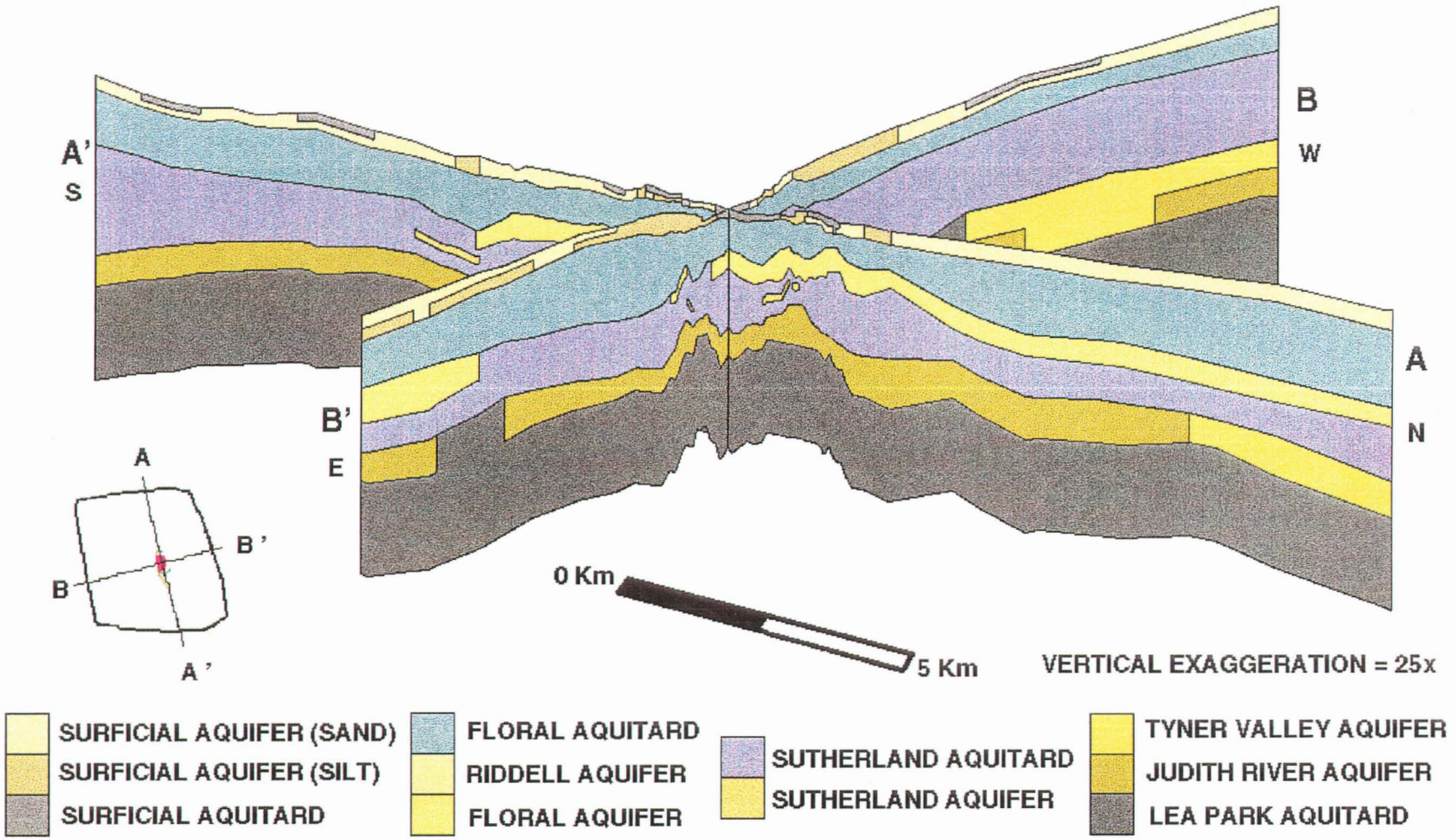

Figure 2.5 - Hydrostratigraphic Cross-Sectional Views of the Study Area

of the surficial stratified deposits. Figure 2.4 shows the 3-D hydrostratigraphic conceptual model constructed for the study area. Figure 2.5 shows cross-sections taken from the hydrostratigraphic conceptual model.

Sources for the geological information referred to in the development of the 3-D hydrostratigraphic conceptual model include:

1. Saskatchewan Research Council (SRC) drillhole logs;
2. Geological publications by Christiansen (1967, 1970,1992), Christiansen and Sauer (1994) and Sauer and Christiansen (1991);
3. Hydrogeological reports by Meneley (Meneley, 1970 and Meneley, 1989);
4. Preliminary hydrogeological investigations conducted by Maathuis *et al.*, (1994); and
5. AGRA (1996) geological database for drillholes west of Saskatoon.

2.4.1 Lea Park Aquitard

The silts and clays of the Lea Park Formation form the Lea Park Aquitard in the hydrogeological model. The base of the Lea Park Aquitard was considered to be an impermeable boundary for the numerical study because of its low hydraulic conductivity, depth below the WMA, thickness and continuity.

2.4.2 Judith River Aquifer

The Judith River Aquifer was the lowermost aquifer of interest in the study area and is composed of partially consolidated sands and silts. The Judith River Formation is bounded by the underlying Lea Park Aquitard and the overlying Bearpaw Formation and Sutherland Group tills. Well yields are low in the Judith River Aquifer because of the abundance of fine grained sand and silt (Maathuis *et al.*, 1994).

The Judith River Aquifer is found throughout the study area except where it is interrupted by collapse structures and glacial erosion. To the northwest of PCS Cory Mine the Judith River Aquifer is eroded and infilled by Empress Group sands (Maathuis *et al.*, 1994). The Judith River Aquifer is laterally continuous below the mine site.

2.4.3 Tyner Valley Aquifer

The Tyner Valley Aquifer is part of an extensive and productive aquifer system in the Saskatoon area. This aquifer is part of one of the largest buried valley aquifer systems in southern Saskatchewan. The Tyner Valley Aquifer consists of alluvial and glaciofluvial silts, sands and gravels of the Empress and Sutherland Groups (Meneley, 1970). Alluvial sediments were deposited in valleys present in the Upper Cretaceous bedrock sediments and also those formed during the Pleistocene glaciation. In the later stages of glaciation these valleys were covered by till thereby forming a buried valley aquifer (Lennox *et al.*, 1988).

The Tyner Valley Aquifer is present near the western margin of the study area. It is not found below the mine site. The aquifer is bounded by the overlying Sutherland Aquitard and underlying Lea Park Aquitard and Judith River Aquifer.

In the study area, the Tyner Valley Aquifer is predominantly continuous and composed mostly of coarse stratified sediments. Near Grandora, Saskatchewan (364600E, 5777400N), the continuity of the aquifer is interrupted by a collapse structure. Here the Tyner Valley Aquifer is filled with lithology similar to the Sutherland till. This results in a reduction in permeability causing an abrupt increase in the hydraulic gradient near Grandora. Gravity faulting resulting from salt dissolutions is thought to be the cause of the lithology change and permeability reduction (Maathuis *et al.*, 1994 and Meneley, 1970).

The Tyner Valley Aquifer System is an interconnected group of aquifers that includes the Battleford Valley Aquifer, the Tyner Valley Aquifer and the Judith River Aquifer. The Judith River and Tyner Valley Aquifers are grouped into one aquifer

system because the Judith River sands are contiguous with the Tyner Valley Aquifer, causing the aquifers to function as a single, continuous, hydrological unit (Meneley, 1970).

The Tyner Valley Aquifer System is confined by the Sutherland Group, Floral Formation and the Lea Park Aquitard. Figure 2.6 shows the position of the Judith River Aquifer and the Tyner Valley Aquifer within the aquifer system.

2.4.4 Sutherland Aquitard

The Sutherland Aquitard is composed of the Sutherland Group tills and the silts and clays of the Bearpaw Formation. Throughout most of the study area the Sutherland Aquitard separates the basal sands of the Floral Formation from the sands of the Sutherland Group. It also separates the Floral and Sutherland sands from the Tyner Valley and Judith River Aquifers. The Bearpaw Formation and Sutherland Group were combined to form the Sutherland Aquitard because of their similar hydraulic properties.

2.4.5 Sutherland Aquifer

Within the Sutherland Aquitard is a small, discontinuous intertill aquifer composed of Sutherland Group sands. Little is known about lateral extent of this intertill aquifer at the study area because of limited geological and hydrogeological information. It is hypothesized that the width of the channel aquifer below the tailings pile and also northeast of the plant is over 900 m, however, there is no direct evidence to confirm these dimensions (Maathuis *et al.*, 1994).

Figure 2.6 - Areal Extent and Direction of Groundwater Flow in the Tyner Valley Aquifer System

At most 8 m of Sutherland Aquitard separates the Sutherland and Judith River Aquifers. The Sutherland Aquifer is separated from the basal sands of the Floral Formation by approximately 3 to 10 m of Sutherland Aquitard.

2.4.6 Floral Aquifers

Glaciofluvial sands and gravels of the Floral Formation were divided into two confined aquifer units; the Floral Aquifer and the Riddell Aquifer. The Floral Aquifer is a channel aquifer confined by the underlying Sutherland Aquitard and overlying the Floral Formation till. The Riddell Aquifer is a discontinuous aquifer of limited extent and is confined above and below by the Floral Formation till.

2.4.6.1 Floral Aquifer

The Floral Aquifer was the most important hydrogeological unit in the groundwater flow and brine transport study. It was the most likely conduit for advective brine flow. The location of the Floral Aquifer was determined from drillhole information and inferred from topographic characteristics of the study area.

The topography of the study area includes a broad, channel like, shallow depression outlined by the 500 m contour (Figure 1.4 and Map 1, Appendix F). This depression originates northwest of PCS Cory Mine and extends southeast towards Moon Lake. The surficial channel formed a conduit for meltwaters during glacial retreat (Christiansen and Sauer, 1994). Maathuis *et al.* (1994) hypothesized that buried channel aquifers are likely a reflection of this meltwater channel. During glacial retreat, subglacial meltwater from the ice followed pre-existing channel depressions on the ground surface. Over time these subglacial channels eroded the overlying ice and became exposed (Maathuis *et al.*, 1994). The repetition of this cycle during multiple glacial events formed stacked channels as drainage re-occupied the previously formed valleys.

The Floral Aquifer consists of a series of channels with limited areal extent, possibly originating from the Dalmeny Aquifer located north of the study area. The channel aquifer below the mine site was the most important channel in the numerical study. A second buried channel is found along the eastern border of the study area below the topographic channel like meltwater depression (Figure 1.4 and Map 1, Appendix F). A third possible channel is also found in the northwest corner of the study site. Figure 2.7 shows the location and extent of the Floral Aquifer channels.

2.4.6.2 Riddell Aquifer

The Riddell Aquifer is a small, discontinuous aquifer composed of cross-bedded sand lens (Skwarawoolf, 1980) in the Floral Formation. The extent of the Riddell Aquifer is not exactly known because of limited geological data.

2.4.7 Floral Aquitard

The Floral Aquitard is a continuous aquitard unit found throughout the study area. The Floral Aquitard is composed of the Floral and Battleford Formation tills.

The Floral Aquitard separates the Floral and Riddell Aquifers from each other and also from the surficial stratified drift deposits. This aquitard is a low hydraulic conductivity unit impeding vertical brine migration from the WMA to the Floral Aquifer. Fracturing in the aquitard, however, provides a possible accelerated pathway for brine from the WMA to reach the Floral Aquifer.

2.4.8 Surficial Aquifers and Aquitards

The surficial stratified deposits form the Surficial Aquifer and Surficial Aquitard in the hydrogeological model. The sands and silts form the Surficial Aquifers while the clays form the Surficial Aquitard. The arrangement of the

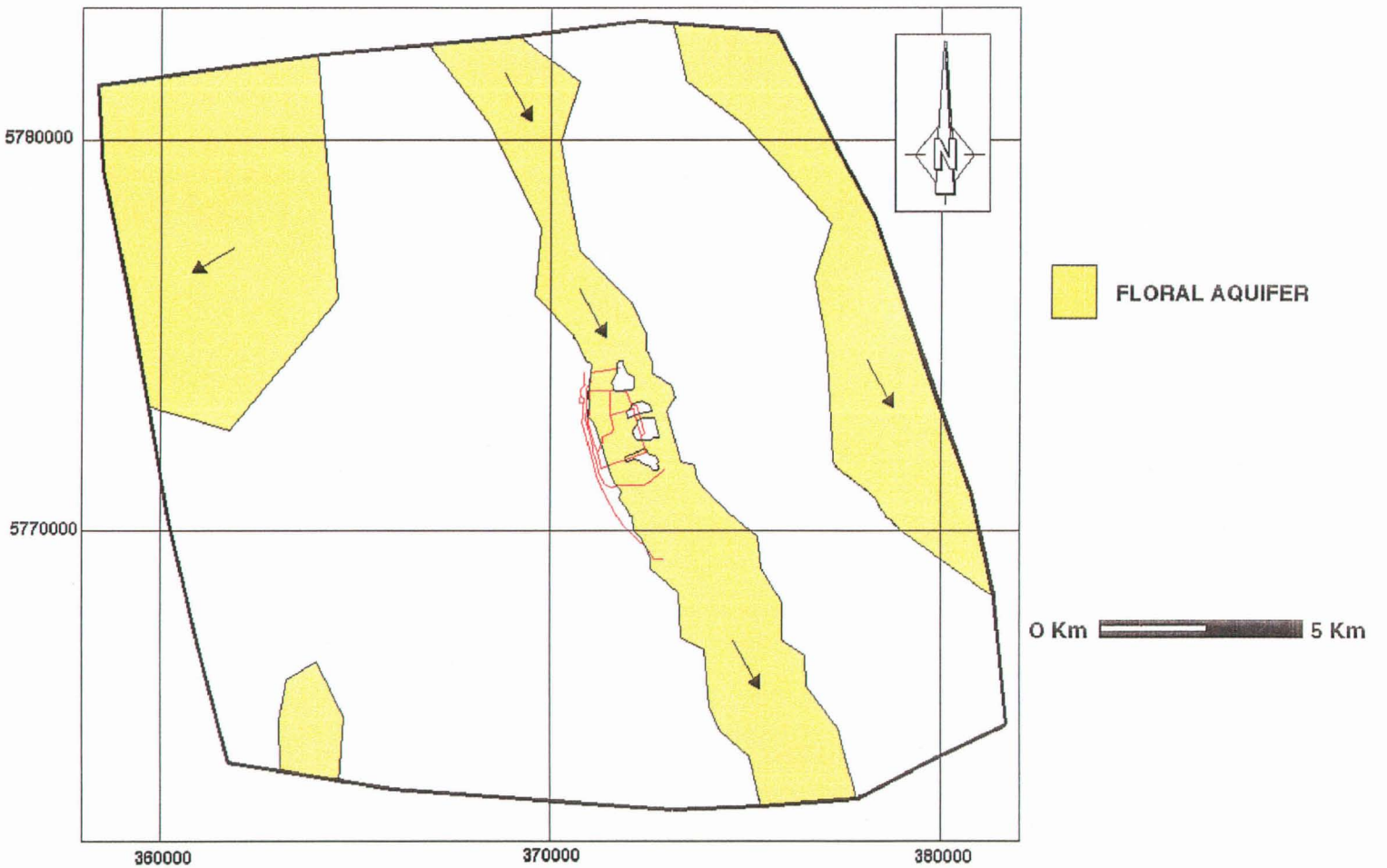

Figure 2.7 - Areal Extent and Direction of Groundwater Flow in the Floral Aquifer

aquifers and aquitards in the study area is very complex as these units are discontinuous.

2.5 Groundwater Flow and Recharge

Knowing the characteristics of the groundwater flow system in the study area is very important when constructing a 3-D hydrogeological model for the numerical simulation. Information about the flow system is acquired through water level measurements and environmental measurements of annual precipitation and evaporation rates.

Regional groundwater flow in the prairies was first subjected to extensive study during the 1960s. At high elevations water infiltrates the ground surface and recharges the flow system. At topographic lows, groundwater discharges from the local, intermediate and regional systems via seepages and springs (Tóth, 1962 and Tóth, 1963).

The amount of recharge depends on many factors. In the Interior Plains the amount of evaporation far exceeds precipitation (Fortin *et al.*, 1989). Christiansen (1970) quotes that the mean precipitation west of Saskatoon is approximately 350 mm/yr while the rate of evaporation is approximately 1000 mm/yr. Average recharge rates are likely to be very low (5-10 mm/yr). Studies of a depression focused recharge suggest that local rates may be as high as 30 mm/yr but most authors agree that 5 to 10 mm/yr is consistent with large scale water balance calculations (Fortin *et al.*, 1989).

2.5.1 Flow in the Tyner Valley Aquifer System

Groundwater enters the Tyner Valley Aquifer System in the study area via vertical flow from overlying glacial deposits and also from regional flow outside the study area. The Tyner Valley Aquifer functions as a drain funneling groundwater into the channel aquifer from the laterally continuous Judith River Aquifer. Meneley

(1970) estimates that nearly 90% of the flow in the Tyner Valley Aquifer originates from the Judith River Aquifer. Once groundwater flow enters the Tyner Valley Aquifer it is diverted north towards the Battleford Valley arm where it then flows westward ultimately discharging into the North Saskatchewan River (Karvonen, 1997 and Meneley, 1970). The direction of groundwater flow in the Tyner Valley Aquifer System is shown in Figure 2.6.

The hydraulic gradient in the Tyner Valley Aquifer increases significantly near Grandora due to a permeability blockage resulting from collapse structures. This blockage causes the hydraulic head north of Grandora to be controlled by the elevation of the North Saskatchewan River. South of the permeability blockage the hydraulic head is much higher and artesian conditions result from the impeded groundwater flow (Meneley, 1970). Water levels measured in monitoring wells completed in the Tyner Valley Aquifer are higher south of the permeability blockage than they are north of the blockage.

Monitoring wells completed in the Judith River Aquifer have been flowing since their installation at the mine site. Monitoring wells 77-702 and 86-103 have high fluid levels suggesting that the Judith River Aquifer is poorly connected at these sites (Maathuis *et al.*, 1994). Artesian conditions in the Judith River Aquifer near PCS Cory Mine indicate that an upward, vertical hydraulic gradient exists in this area.

2.5.2 Flow in the Sutherland Aquifer

Monitoring wells 86-101 and 93-102 are completed in the intertill channel aquifer while 86-104 and MW 86-106 are completed in the intertill sand lens. Maathuis *et al.* (1994) indicated that water level data obtained from these wells cannot be used for indicating the direction groundwater flow within the Sutherland Aquifer as the aquifer is poorly defined. It is thought, however, that flow in the Sutherland Aquifer is southward.

2.5.3 Flow in the Floral Aquifers

Little is known about the flow regime in the Floral and Riddell Aquifers, however, it is hypothesized that the Floral Aquifer acts as buried drain collecting groundwater from neighboring tills and directing it towards the South Saskatchewan River. Figure 2.7 illustrates the inferred direction of groundwater flow in the Floral Aquifer.

Monitoring wells 18, 77-802, 77-804, 77-805, 86-107 and 93-103 were completed in the Floral Aquifer. Analysis of well data indicates that groundwater flow in the vicinity of PCS Cory Mine is southwards and the corresponding hydraulic gradient is approximately 0.5 to 0.7 m/km (Maathuis *et al.*, 1994). Water levels recorded from 18 and 86-107 are higher than the level measured in the neighboring well 77-802, thus suggesting that a localized narrow channel may exist within the larger Floral Aquifer. This narrow channel, as interpreted by Maathuis *et al.* (1994) acts as a drain for the neighboring sands. Monitoring wells were not completed in the Riddell Aquifer.

2.5.4 Flow in the Surficial Aquifers

Water infiltrating the Surficial Aquifer moves either laterally or downward. Lateral groundwater flow discharges in depressions, seasonal ponds, sloughs, streams or at road side drainage ditches. Downward groundwater flow recharges underlying aquifers.

2.5.5 Flow in the Vicinity of the Tailings Pile

When WMAs are sited above a saturated aquitard or aquifer, the change in the total stress changes the pore pressure distribution within the groundwater system. Variations in pore pressures in these conditions are most noticeable in thick, low permeability, highly compressible formations; that is, the aquitards.

The increase in total stress resulting from the weight of the WMA increases the hydraulic head within the aquitards. If the aquitard is thick the excess head developed within the aquitard can be large and remain for many years after loading stops. This excess head may act as a hydrodynamic barrier impeding the downward flow of contaminants from the WMA. In this situation an upward flow gradient from the middle of the aquitard to the base of the tailings pile and a downward flow gradient towards the underlying aquifer may exist (Maathuis and van der Kamp, 1994 and van der Kamp and Maathuis, 1985).

If loading stops, the excess head dissipates and the hydraulic barrier disappears. However, the overlying weight may have caused the aquitard to consolidate thereby reducing both the vertical hydraulic conductivity and the rate of flow and transport through the aquitard (Maathuis and van der Kamp, 1994 and van der Kamp and Maathuis, 1985).

This situation is more complex if a highly concentrated, dense fluid, such as brine, is involved. The high fluid density creates a density-driven buoyancy force causing brine to move downwards. The density-driven buoyancy force is of a similar magnitude to the upward advective gradient and may prevent the development of a hydrodynamic barrier.

CHAPTER 3

MECHANICS OF FLUID TRANSPORT

The physical and chemical properties of brine have a significant affect on brine migration. Since the density of brine is greater than native groundwater, buoyancy forces influence the position of the brine plume in the groundwater flow system. Predicting the location of the brine plume with time is important for analyzing the environmental impact and also for developing mine decommissioning plans.

3.1 Brine Properties

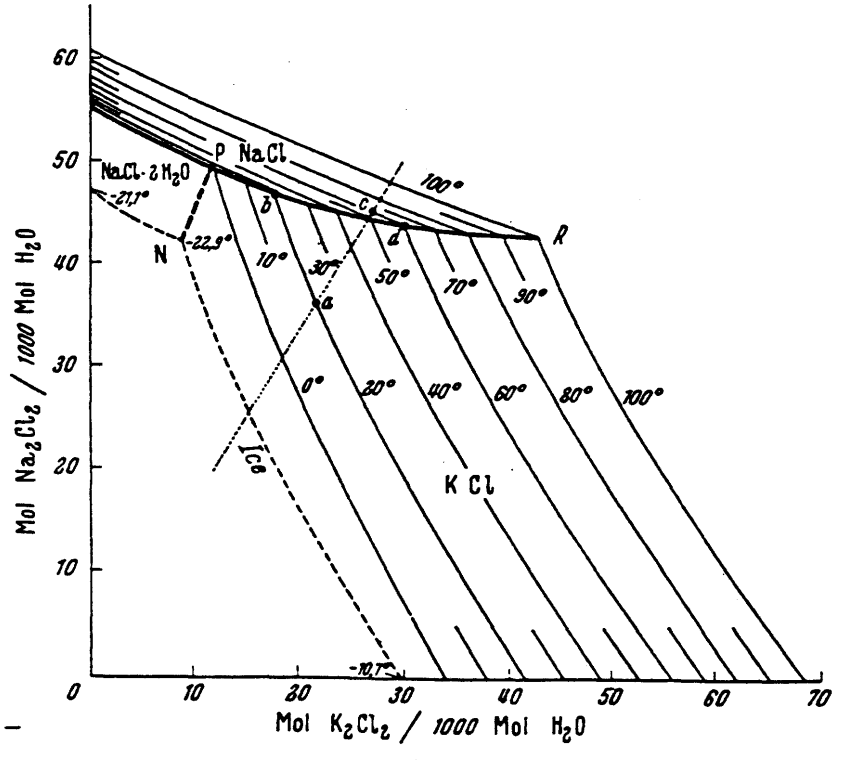

Figure 3.1 - The system NaCl-KCl-H_2O for temperatures ranging from -22.9 to 100°C (Braitsch, 1971)

A temperature solubility diagram for a NaCl-KCl-H_20 system is shown in Figure 3.1. Line R represents a solution that is mutually saturated with NaCl and KCl at 100°C. The figure indicates the strong temperature dependence of solubility. Brine, composed of NaCl and KCl and stored in the PCS Cory Mine WMA, is saturated and has a density and TDS (Total Dissolved Solids) concentration of approximately 1,280 kg/m^3 and 300,000 mg/L respectively at 0°C. This is equivalent to a 5.3 M solution (Braitsch, 1971, Ho *et al.*, 1989 and Kestin *et al.*, 1981). The approximate density and TDS concentration of native groundwater are 1,000 kg/m^3 and 1,000 mg/L respectively.

The relationship between the density and concentration of brine is empirically represented by the polynomial indicated in equation 3.1. Equation 3.2 gives a similar empirical relationship between the absolute or dynamic viscosity and brine concentration (Lin *et al.*, 1996).

$$\frac{\rho}{\rho_o} = a_1 + a_2 C + a_3 C^2 + a_4 C^3 \qquad (3.1)$$

$$\frac{\mu}{\mu_o} = a_5 + a_6 C + a_7 C^2 + a_8 C^3 \qquad (3.2)$$

where:

C	=	chemical concentration of the fluid in ppt (parts per thousand)
$a_1, a_2, \ldots a_8$	=	parameters required to define concentration dependance of water density and viscosity
ρ	=	fluid density at a given chemical concentration
ρ_o	=	referenced fluid density at zero chemical concentration
μ	=	dynamic viscosity of fluid at given chemical concentration
μ_o	=	referenced dynamic viscosity at zero chemical concentration

The coefficients a_1 to a_8 are slightly pressure dependent and strongly temperature dependent. A constant pressure and temperature of 5 MPa and 0°C respectively were used for interpolating values for the coefficients from data documented by Kestin *et al.* (1981) and Rowe and Chou (1970). The mean annual temperature in Saskatoon is close to 0°C and natural groundwater temperatures in the shallow subsurface are no more than 8°C. Groundwater temperatures are normally subject to small fluctuations and the values used in the model are considered valid for the anticipated range of pressure and temperature. Table 3.1 lists the parameters used for qualifying the relationship of brine density and dynamic viscosity with concentration.

Table 3.1 - Parameters Used to Determine the Dependance of Chemical Concentration on the Density and Dynamic Viscosity of Brine and Freshwater

Coefficients	Value
a_1	1.0006
a_2	6.9787×10^{-4}
a_3	-4.2801×10^{-7}
a_4	1.4352×10^{-10}
a_5	1.0002
a_6	0.0013
a_7	3.3092×10^{-6}
a_8	1.8854×10^{-9}

3.1.1 Clay-Brine Interaction

Research on the effects of brine on clay soils indicate that when a highly concentrated solution of NaCl is introduced into a soil, it can either increase or decrease in the hydraulic conductivity of that soil. The change in hydraulic conductivity is most dependent on the magnitude of the confining stress.

When brine invades the pore spaces between clay particles, the microstructure changes from a dispersed to a flocculated condition (Yang and Barbour, 1992). The Na^+ cations in brine interact with negatively charged clay particles, thereby changing the soil properties. The physiochemical interactions between the Na^+ cation and the negatively charged clay surface may cause the clay to osmotically consolidate and develop fractures (Barbour and Fredlund, 1989, Barbour and Yang, 1993 and Ho *et al.*, 1989). Osmotic consolidation results from the shrinkage of the diffuse double layer. This may account for approximately 1.5 to 2.4 % volume reduction in till (Barbour, 1990).

Osmotic consolidation within tills is reduced when a confining stress is applied. When clay is subjected to a large confining stress, such as that created by the weight of a tailings pond or tailings pile, the strain generated by osmotic consolidation is restricted. This can prevent an increase in the effective void ratio between the clay aggregates (Barbour and Yang, 1993 and Yang and Barbour, 1992). Because the magnitude and direction of changes in hydraulic conductivity beneath the WMA cannot be reliably predicted, it was assumed that any such changes were small and could be neglected. This could be the subject of a sensitivity analysis in a numerical model at a future date.

3.2 Brine Migration Pathways

Figure 3.2 illustrates the main pathways for brine migration outside the PCS Cory Mine WMA. The elevation of brine ponded in the WMA is higher than the elevation of the regional water table generating a radial, outward hydraulic gradient. Density and concentration differences between brine and freshwater create strong buoyancy forces, together with the hydraulic gradient, results in an unbalanced flow and transport system. To attain equilibrium conditions, brine has a tendency to move radial and downwards out of the WMA into the flow system where it will then continue to migrate until equilibrium is reached.

Brine can move downwards through the surficial stratified deposits and into

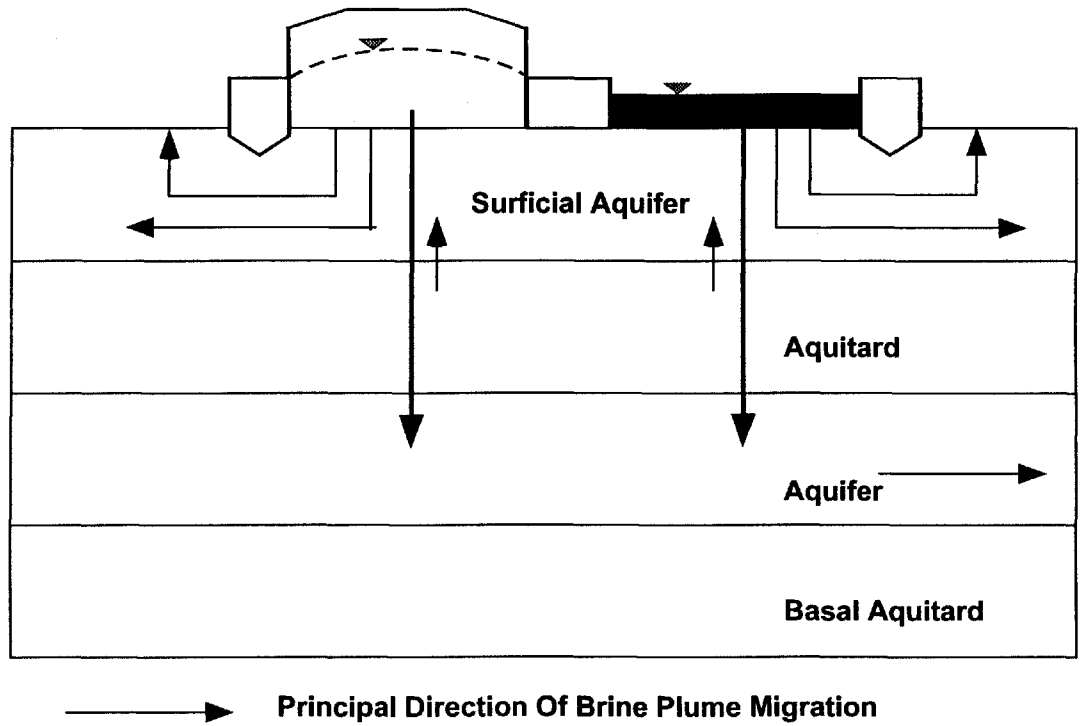

Figure 3.2 - Schematic Illustration of the Principal Brine Migration Pathways at the PCS Cory Mine WMA (after Maathuis and van der Kamp, 1994)

the Floral Aquitard. The mobility of brine in the Floral Aquitard may be greater in the vertical direction than the horizontal because of its high density compared to native groundwater and also due to preferential flow along vertical fractures within the aquitard. The load generated by the weight of the WMA may form a hydraulic barrier within the aquitard generating an upward flow gradient and possibly impeding the downward transport of brine (Maathuis and van der Kamp, 1994).

The numerical model does not allow for consolidation of the aquitards to be included in the analysis. Calculation of the relative magnitudes of the buoyancy forces and the advective gradients driving flow suggests that both may be similar in magnitude.

3.3 Hydraulic Head in Groundwater of Variable Density

Davies (1987), Oberlander (1989) and Bachu (1995) discussed the difficulties and pitfalls when relating groundwater hydraulic head and flow directions in porous media containing variable density fluids. The problem was originally investigated by Lusczynski (1961).

The hydraulic head for a constant density fluid is described by equation 3.3. Lusczynski (1961) introduced the concept of freshwater head and environmental head in an attempt to predict the flow directions in chemically inhomogeneous and density-driven fluids. Freshwater head (equation 3.4) in the flow system is defined by Lusczynski (1961) as the equivalent height of the water column if the "environmental" water is replaced by freshwater.

$$h = z + \frac{p}{\rho g} \tag{3.3}$$

$$h_o = z + \frac{p}{\rho_o g} \tag{3.4}$$

where:

h	=	hydraulic head
h_o	=	freshwater head
z	=	elevation
p	=	fluid pressure
ρ	=	environmental water density
ρ_o	=	freshwater density

The environmental head (equation 3.5) is the freshwater head reduced by an amount corresponding to the difference in density between the column of water to a specified depth and an equivalent freshwater column (Lusczynski, 1961).

$$h_e = h_o + \frac{\Delta z(\rho_e - \rho_o)}{\rho_o} \tag{3.5}$$

where:

h_e	=	environmental head
ρ_e	=	the average density of the in the column
Δz	=	depth of the fluid column

The average density of the fluid is given by:

$$\rho_e = \left(\frac{1}{\Delta z}\right)\int \rho dz \tag{3.6}$$

The driving force per unit mass in fluid flow was first described by Hubbert (1940) and further described by Davies (1987), Oberland (1989) and Bachu (1995). Hubbert (1940) indicated that the impelling force per unit mass (equation 3.7) of fluid is related to the freshwater head gradient and buoyancy resulting from variations in fluid density. Figure 3.3 shows the vector components of the driving forces affecting fluid flow.

Equation 3.7 indicates that freshwater heads specify the horizontal vector component of the impelling force. The vertical vector component of the impelling force, however, cannot accurately be determined from freshwater head

measurements (Bachu, 1995). Changes in fluid density, temperature, pressure, and salinity are important parameters to consider when analyzing the vertical component of the impelling force (Bachu,1995 and Oberland, 1989).

$$F = -\left(\frac{\rho_o}{\rho}\right)\left[\nabla h_o + \left(\frac{\Delta\rho}{\rho_o}\right)\Delta z\right]$$

The driving force ratio (DFR) is used to evaluate the relative magnitude of freshwater hydraulic head and buoyancy forces in groundwater flow. When the DFR is greater than 0.5, density-driven groundwater flow in a variable density environment is significant. Neglecting these density related gravity effects may result in erroneous interpretations of flow systems (Davies, 1987). When the DFR is greater than 1.0, a free convection regime exists and fluid motion is governed by density differences within the flow field. When the DFR is less than 1.0, a forced convection system exists indicating that fluid flow is driven by external forces such as advection (Bear, 1972). Equation 3.8 describes the DFR expression:

$$DFR = \frac{\left(\frac{\Delta\rho}{\rho_o}\right)\nabla z}{\nabla h_o} \qquad (3.8)$$

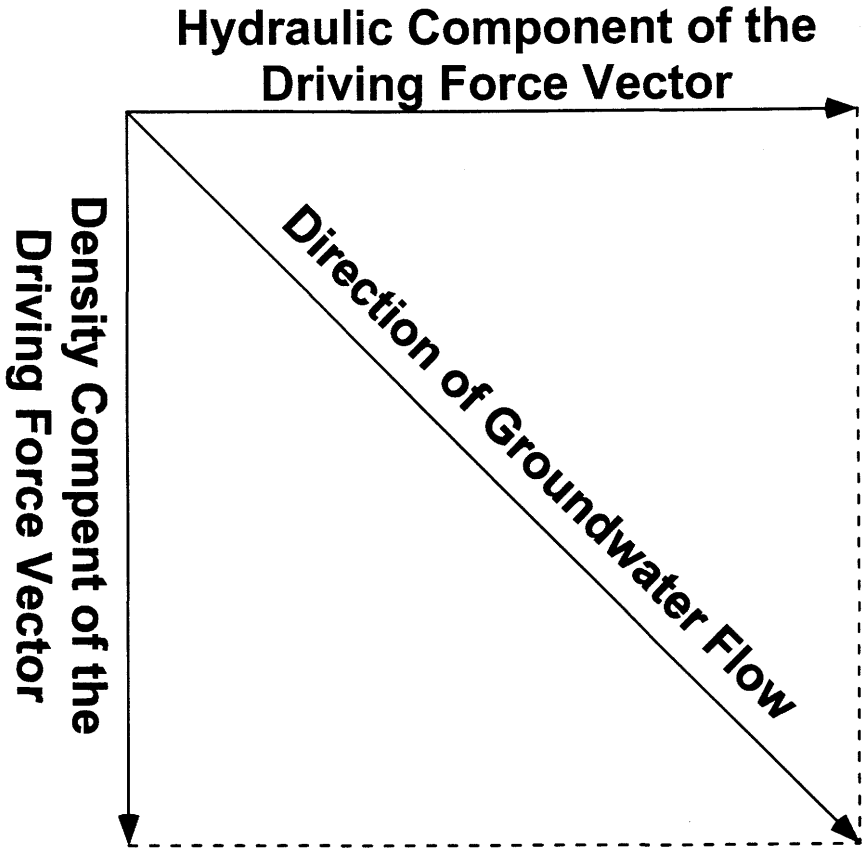

Figure 3.3 - Vector Components of the Driving Force

3.4 Groundwater Flow and Mass Transport Principles

Two transport processes influencing brine migration in the groundwater flow system are mechanical dispersion and molecular diffusion. The attenuation of brine concentrations resulting from the physiochemical reaction between brine and the porous media are assumed to be negligible for the purposes of this numerical investigation. The interaction between dissolved salts and clay, however, can effect the formation permeability through osmotic consolidation (van der Kamp, 1989) but it has been argued earlier that such effects are difficult to quantify.

3.4.1 Advection and Mechanical Dispersion

Advection is the movement of solute with the flowing groundwater. The amount of dissolved material that is transported depends on the fluid concentration and the groundwater flow velocity (Fetter, 1992 and Freeze and Cherry, 1979).

The advective movement of a solute is not affected by variable density or chemical reactions within the subsurface. The equation for one dimensional (1-D) advective mass flux (3.9a) and advective transport (3.9b) are shown below.

$$F = vnC \tag{3.9a}$$

$$\frac{\partial C}{\partial t} = -v\frac{\partial C}{\partial x} \tag{3.9b}$$

where:

F	=	1-D mass flux
n	=	effective porosity of the porous medium
v	=	average linear velocity
C	=	concentration of the solute
$\partial C / \partial t$	=	concentration gradient with time
$\partial C / \partial x$	=	concentration gradient with position

When groundwater flows through a porous medium it does not move at a constant velocity. It moves at rates different to the average linear velocity on a microscopic scale.

1. Flow is faster near the center of voids compared to the edges where fluid-solid interactions occur;
2. Some solute particles will travel along longer flow paths; and
3. Flow velocities change as the pore diameters change.

Mechanical dispersion is the mixing and spreading associated with groundwater flow through porous media resulting in the "smearing" of the sharp advective front. Longitudinal dispersion occurs in the direction of groundwater flow while transverse dispersion occurs perpendicular to flow (Fetter, 1992).

3.4.2 Molecular Diffusion

Molecular diffusion gradually spreads the solute through the random movement of particles. Diffusion causes the contaminant to migrate from areas of high chemical concentration to low chemical concentration even in the absence of flowing groundwater (Rowe, 1996). Fick's first law (equation 3.10) represents the diffusive movement of a solute in 1-D;

$$F = -nD_e\left(\frac{\partial C}{\partial x}\right) \tag{3.10}$$

where:

D_e = effective diffusion coefficient

The effective diffusion coefficient is dependent on the valence, ionic radius, temperature, the solute species, lithology and pore size and distribution (Rowe, 1996). The self diffusion coefficient for most ionic solute species varies from $1x10^{-9}$ to $2x10^{-9}$ m^2/s (Fetter, 1992). The effective diffusion coefficient for chloride ranges from $1x10^{-10}$ to $5x10^{-10}$ m^2/s (Maathuis and van der Kamp, 1995). The effective diffusion coefficient can be reduced into two components;

$$D_e = \omega D_o \tag{3.11}$$

where;

ω = coefficient of tortuosity

D_o = self diffusion coefficient

3.4.3 Hydrodynamic Dispersion

Hydrodynamic dispersion describes mass transport including the effects of molecular diffusion and mechanical dispersion. Dispersion coefficients are usually described by the empirical equations:

$$D_L = \alpha_L v_i + D_e \tag{3.12a}$$

$$D_T = \alpha_T v_i + D_e \tag{3.12b}$$

where:

D_L	=	hydrodynamic dispersion coefficient in the direction of flow (longitudinal)
D_T	=	hydrodynamic dispersion coefficient in the direction perpendicular to flow (transverse)
α_L	=	longitudinal dynamic dispersivity
α_T	=	transverse dynamic dispersivity
v_i	=	velocity in the longitudinal direction

Dynamic dispersivity is a property that is dependent on the characteristics of the porous media. The longitudinal dispersivity of a geological material is often at least one order of magnitude greater than the transverse dispersivity (Fetter, 1992 and Maathuis and van der Kamp, 1994). Neuman (1990) commented on the scale dependence of dispersivity and developed an empirical relationship between the apparent longitudinal dynamic dispersivity and the length of the flow path, provided that the flow path is less than 3,500 m. The longitudinal dynamic dispersivity can be estimated by using the following empirical formula:

$$\alpha_L = (0.0175)\ L^{1.46} \tag{3.13}$$

where;

L	=	Length of the flow path

3.4.4 Breakthrough Curve

When solute particles are traveling along different flow paths and at different velocities the sharp concentration front expected for "piston-flow" is smeared because of dispersion. The classical experiment illustrating dispersion involved a tracer being continuously injected at the up gradient end of a sand column through which water was flowing under steady-state conditions. The concentration of the injected tracer at the inflow is Co and the concentration of the tracer at the outlet of the sand column is measured as the relative concentration expression, C/Co. The graph (Figure 3.4) shows the relative concentration of the tracer with time for the outlet. This characteristic sigmoidal curve is known as a breakthrough curve. If the tracer moved through the column without being dispersed (piston-flow), the breakthrough curve would be a step function (Wang and Anderson, 1995).

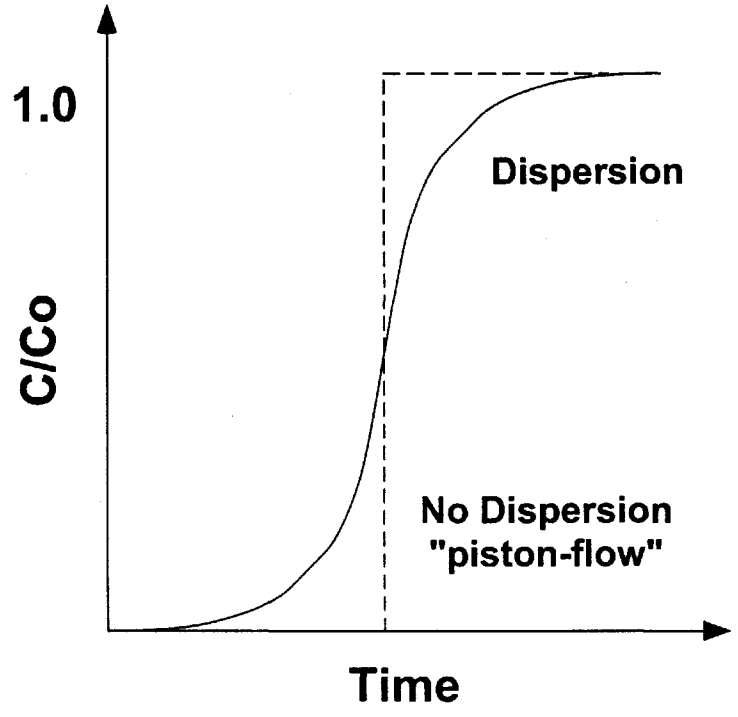

Figure 3.4 - Typical Breakthrough Curve

CHAPTER 4

MODEL DEVELOPMENT

Once the hydrogeological conceptual model is developed, the native groundwater water and brine properties are known and the processes affecting brine migration are understood, a computer model that mathematically simulates groundwater flow and transport can be constructed. Spatial and temporal discretization of the problem domain must be carefully designed to ensure that the model represents the natural system. Design is necessary to avoid, as much as possible, artifacts created by the numerical calculations. The most serious of these artifacts in solute transport modelling is an artificial "mixing" caused by the calculation process (numerical dispersion).

4.1 Spatial Discretization

Developing a numerical model requires that the problem domain be represented by a finite number of nodal points and elements. Elements are formed from the areas or volumes enclosed by lines connecting the nodal points. Nodes are the points where groundwater head and solute concentration are calculated or specified. Hydraulic properties are assigned to the elements in the problem domain. Boundary conditions are applied either at nodal points or over the surface of elements. The spatial discretization process is an attempt to faithfully represent the hydrogeological units and to provide the most detail in areas of practical interest, such as the WMA.

4.1.1 Finite Element Mesh Design

Mesh design is very important for the successful use of any numerical method including the finite element method (FEM). Computational accuracy and the level of computational effort are directly related to the mesh design. Well

designed, finite element meshes provide more accurate solutions with less computational effort. Poorly designed meshes can result in wasted computational effort and loss of accuracy. Refining the finite element mesh increases accuracy but computational effort is also increased. Coarse meshes require less computational effort but both accuracy and spatial resolution of physical boundaries are lost.

4.1.1.1 Two Dimensional Finite Element Mesh

The 2-D mesh used in the numerical investigation of PCS Cory Mine consisted of 2356 nodes and 4685 triangular elements. The nodes located along the boundary of the mesh coincided with the body-centered grid nodes of the finite difference grid constructed by Karvonen (1997) for investigating regional groundwater flow west of Saskatoon. Matching the x,y coordinates of the 2-D mesh nodes with those of the regional flow model grid nodes allowed the hydraulic heads determined at these locations in the regional model to be used as boundary conditions for the local PCS Cory Mine model.

The 2-D finite element mesh was coarse along the perimeter of the study area and was refined towards the PCS Cory Mine WMA. The mesh was designed to provide both accuracy and detailed spatial resolution in the vicinity of the WMA.

Numerical dispersion is an artifact of the mesh and time-stepping used for numerical results. The smallest distance that the contaminant will travel in one model time step is the distance between adjacent mesh nodes. If either the time step or the mesh spacing are too large then artificial mixing occurs. Fine time discretization and small mesh elements are required to avoid "numerical mixing" that exceeds the rate of the physical diffusive process. Problems with numerical dispersion occur where imposed concentration gradients are high, hydrostratigraphy is complex or the stresses imposed on the flow system due to the installation of various containment devices are highly variable in time.

The aspect ratio of mesh elements (the ratio of maximum to minimum

element dimensions) need to be relatively small so that errors in the estimation of gradients between elements are controlled. The aspect ratio was designed to be no greater than 5:1 (Anderson and Woessner, 1992 and Istok, 1989). The transition from a coarse mesh to fine mesh was gradual. Elements were chosen so that they did not cross or straddle hydrostratigraphic boundaries (Lin *et al.*, 1996).

4.1.1.2 Three Dimensional Finite Element Mesh

The method of constructing a 3-D finite element mesh in GMS involves the use of both a 2-D mesh and TINs (Triangular Irregular Networks). TINs are a series of connected x,y,z points that map the surface of a hydrostratigraphic contact. The 2-D mesh is projected through the TIN surfaces representing the top and bottom contact of a hydrostratigraphic unit (Figure 4.1). In projecting the 2-D mesh the number of element layers used to model the hydrogeological unit is specified thus creating a vertical column of 3-D elements (Figure 4.2). Refinement of the vertical mesh is made in locations where the hydraulic head or concentration gradients are high and in the unsaturated zone (Lin *et al.*, 1996). Care is taken when constructing the 3-D finite element mesh to ensure that the depth of the constructed elements is not too large or too small relative to its horizontal length. This is particularly significant if vertical flow components are an important part of the model.

The advantage of creating a 3-D element mesh in this fashion is that the procedure is relatively fast for simple hydrostratigraphic systems. However, when the hydrostratigraphy is relatively complex, the technique used to construct the 3-D mesh must be modified. In some parts of the mesh, changes of material properties of elements within layers are required. Figure 4.3 shows lens and pinchouts are represented in a 3-D mesh.

The TIN surfaces created for representing the hydrostratigraphy of the study area were, in ascending order; the Lea Park Aquitard, Tyner Valley Aquifer System, Sutherland Aquitard, Floral Aquifer, Floral Aquitard and the topographic surface. TIN surfaces were not constructed for the complex and discontinuous

hydrogeological units, such as sand units of the Sutherland Aquifer, Riddell Aquifer, Surficial Aquifer and Surficial Aquifer. Constructing TIN surfaces for these units would result in a 3-D mesh having vertical elements of zero thickness. It is necessary to avoid constructing meshes containing hydrostratigraphic units of zero thickness. The elements in the 3-D mesh corresponding to the Judith River Aquifer, Tyner Valley Aquifer, Sutherland Aquifer, Riddell Aquifer, Surficial Aquifer and Surficial Aquitard were assigned the appropriate hydraulic properties. The final 3-D mesh contained 18 layers and a total of 44673 nodes and 84058 elements. Table 4.1 lists the number of layers constructed within each aerially extensive hydrogeological unit.

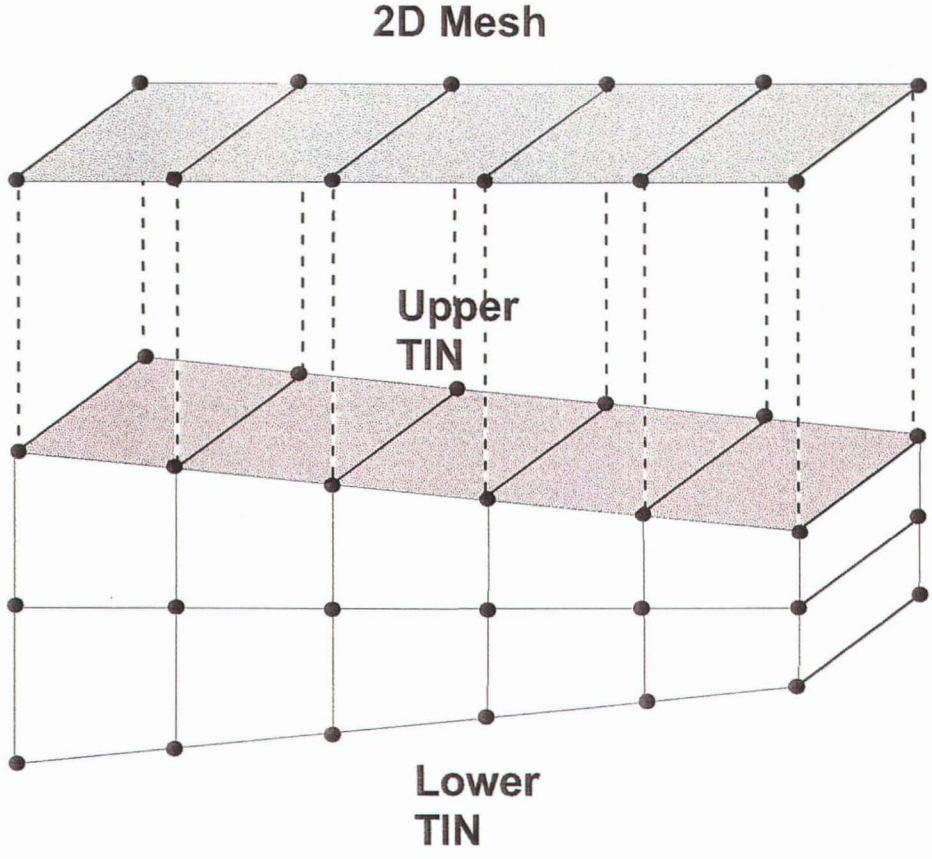

Figure 4.1 - Projection Technique used for Constructing a 3-D Mesh

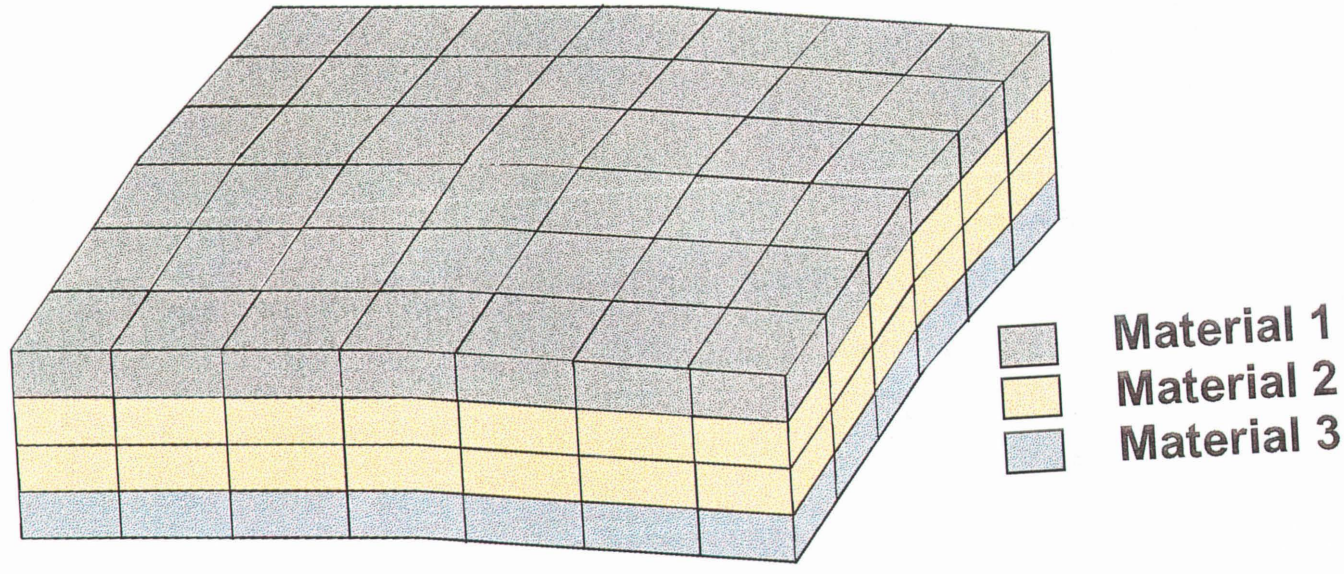

Figure 4.2 - 3-D Mesh Showing Multiple Hydrostratigraphic Units Represented by Vertical Columns of 3-D Elements

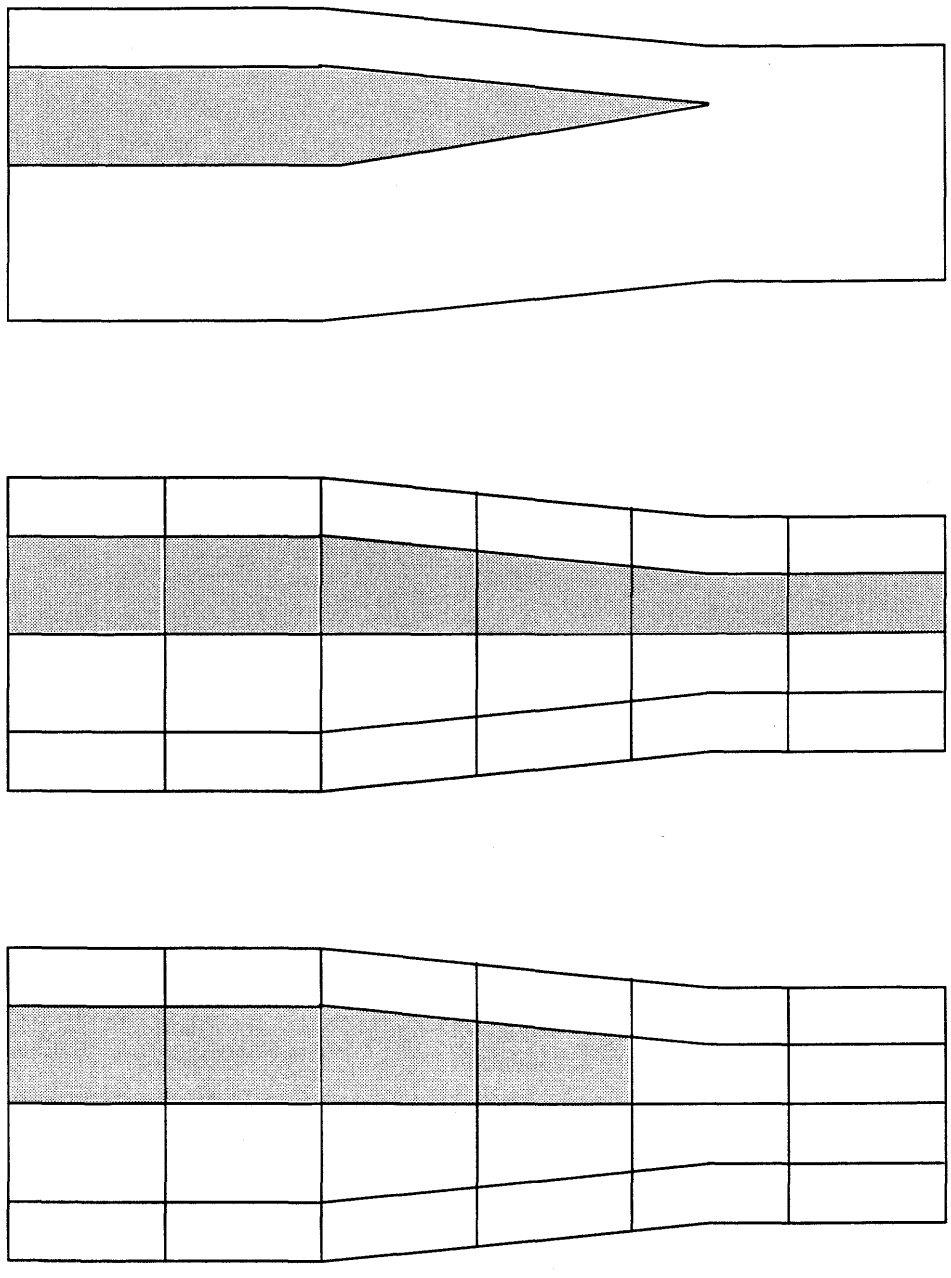

Figure 4.3 - Modelling Lens and Pinchouts in a 3-D Mesh

Table 4.1 - Number of Layers Constructed for the Hydrogeological Units in the 3-D Finite Element Mesh

Hydrostratigraphic Unit	Number of Layers
Surficial Aquifer and Aquitard	2
Floral Aquitard	5
Floral Aquifer	2
Sutherland Aquitard	4
Tyner Valley Aquifer System	2
Lea Park Aquitard	3
TOTAL	**18**

4.1.2 Boundary Conditions

Once the 3-D finite element mesh is designed, boundary conditions can be specified. The types of boundary conditions used in groundwater flow and solute transport models are (Anderson and Woessner, 1992 and Wang and Anderson, 1995):

1. Specified hydraulic head (Dirichlet) boundary conditions;
2. Specified groundwater flow (Neumann) boundary conditions; and
3. Hydraulic head dependent groundwater flow (Cauchy or mixed) boundary conditions.

The perimeter of the study area was located at a considerable distance away from the WMA in order to minimize the influence of boundary effects. The nodes along the perimeter of the mesh were placed at the same location as the grid nodes used in the numerical study of regional groundwater flow west of Saskatoon (Karvonen, 1997). The hydraulic heads determined from the calibrated regional groundwater flow study were used as constant head boundary conditions for the

site-specific model. Constant head boundary conditions determined from the calibrated regional groundwater flow model were only assigned to the aquifers and surficial stratified deposits that intersected the perimeter of the site-specific mesh. Constant head boundary conditions were not applied to the aquitards. The implicit assumption for the aquitards was no flow. Since these units have low hydraulic conductivity, this was an acceptable approximation.

Constant head (Dirichlet) boundary conditions were also assigned to the nodes coinciding with the location of surface hydrological features such as rivers, streams, lakes and perennial sloughs. The values assigned to these features were determined from published information and topographic elevations inferred from Map 1, Appendix F. Constant head boundary conditions were also applied at the tailings pond and beneath the tailings pile. Table 4.2 summarizes the range of constant heads used in the model.

Table 4.2 - Constant Hydraulic Heads Used in the Numerical Model

Surficial Stratified Deposits Boundary	478 m - 521 m
Streams and Perennial Sloughs	476 m - 515 m
South Saskatchewan River	478 m - 479 m
Moon Lake	480 m
Tailings Pond	493 m
Floral Aquifer	478 m - 521 m
Tyner Valley Aquifer	473 m - 510 m
Judith River Aquifer	481 m - 507 m

Constant flux (Neuman) boundary conditions were applied to the centroid of the mesh elements in the top layer of the model in order to represent recharge water infiltrating into the flow system. Flux boundary conditions were not applied to the elements containing constant head nodes, since such fluxes were redundant.

4.1.2.1 Hydraulic Properties and Initial Conditions

After the 3-D model was constructed and the boundary conditions were specified, hydraulic properties and initial conditions for the model were assigned. The first approximation of hydraulic properties for the various aquifer and aquitard units used in the model agreed with the calibrated values determined by Karvonen (1997) and fell within the range of values given by Dominco and Schwartz (1990), Maathuis *et al.*, (1994), Mualem, (1978), Ranjitkar, (1989) and van Genuchten (1980). The hydraulic properties assigned included saturated hydraulic conductivity (Kx, Ky and Kz) and soil-moisture characteristics for the unsaturated zone. The ranges of these values are summarized in Tables 2.2 and 2.3 (Chapter 2).

An initial hydraulic head of 490 m was assigned to the numerical mesh as a preliminary estimate of the hydraulic head distribution in the flow system. By assigning an "average ground surface" initial condition the time required for model convergence was reduced. This value was important for nonlinear unsaturated flow systems where an "average" ground surface or topographic elevation value seemed to provide a good starting point. If the system was suspected to be strongly nonlinear, careful choice of initial conditions was essential since results may have been highly sensitive to this choice.

4.2. Temporal Discretization

Temporal discretization is the process of selecting the time steps that the simulation will use to advance the solution.

When time stepping, large time steps are avoided since the flow and transport processes are nonlinear and properties can change significantly both as a function of hydraulic head and concentration. Large time steps can result in a loss of numerical accuracy and problems with convergence. The magnitude of the time step specified for a coupled simulation is dependent on (Istok, 1989):

1. The size and shape of the elements in the finite element mesh;
2. The specific storage and hydraulic conductivity of the elements;
3. Whether lumped or consistent formulation is used to calculate element capacitance matrices;
4. Boundary conditions; and
5. The relaxation parameter.

Small time steps, along with close spaced nodes provide a better discrete approximation of the partial differential equation governing the physical processes of flow and transport. Reducing the time step can attenuate unstable numerical oscillations that result from nonlinearity. The magnitude of the initial time used for highly nonlinear transient problems can be estimated using equation 4.1 (Bear and Verruijt, 1987):

$$\Delta t \approx \frac{S(\Delta x)^2}{4T} \tag{4.1}$$

where:

Δt	=	time step interval
S	=	storativity of the porous medium
T	=	transmitivity
Δx	=	characteristic measure of the mesh size.

For explicit solution schemes, the time step controls the stability of the solution. For implicit schemes, the time step controls the accuracy of the solution. An implicit time stepping scheme was used to simulate flow and transport at PCS Cory Mine and surrounding area.

4.3 Numerical Formulation

4.3.1 Galerkin's Method

The FEMWATER code uses Galerkin's method to formulate the finite element equations. Galerkin's technique is a Method of Weighted Residuals (MWR) and is the most commonly used procedure for solving groundwater flow and solute transport problems (Bickford, 1990).

In MWR the first step is to find an approximate solution that represents the value of the dependent variable for the problem domain. When the approximate solution is substituted into the system of linear equations, a residual error for each node in the problem domain is calculated (Istok, 1989).

Values of the dependent variables are continuously updated through an iterative process until the residuals are sufficiently small for the solution to be accepted (Bear and Verruijt, 1987). The iteration process continues until the value of the residuals is within a predetermined tolerance criterion. A form of Gauss-Seidel iterations is used to perform the residual minimization in the FEMWATER code.

4.3.2 Pointwise Iterative Matrix Solver

The pointwise iterative matrix solver in FEMWATER was selected for calculating the coupled flow and transport solutions. It adopts a basic successive iteration method, such as Gauss-Seidel, successive over-relaxation or successive under-relaxation, to solve matrix equations (Lin *et al.*, 1996). The pointwise iterative solver produces a convergent solution when the matrix is diagonally dominant. The advantage of this matrix solver is that it is more robust than conjugate gradient methods using either polynomial or incomplete Choleski preconditioners. The disadvantage of the pointwise iterative matrix solver is that convergence can be slower than the other methods (Lin *et al.*, 1996).

A mass lumping formulation was used in conjunction with the pointwise iterative matrix solver to obtain a more accurate solution. Mass lumping tends to increase the potential for numerical instability but tends to avoid problems with mass balance in transport (Lin *et al.*, 1996).

4.3.3 Gaussian/Gaussian Quadrature

Gaussian/Gaussian quadrature was used for integrating the finite element equations. Numerical approximations are obtained for the integrated function within a specified interval by calculating the weighted sum of values of the function at specific points on the interval (Istok, 1989 and Wang and Anderson, 1995). The Gaussian/Gaussian quadrature performs surface and element integration and provides the most accurate integration procedure (Lin *et al.*, 1996).

4.3.4 Backward Difference Weighting Factor

The backward difference method is an implicit numerical scheme (Lin *et al.*, 1996). In this scheme for time stepping, the spatial derivatives of the dependent variable are evaluated simultaneously at a new time. The advantage of an implicit time stepping scheme is its unconditional stability. Equation 4.1 shows the matrix equation for the fully implicit case to solve Laplace's equation (Wang and Anderson, 1995):

$$\{h\} = (1-\alpha)\{h\}^{t} + \alpha\{h\}^{t+\Delta t} \qquad (4.1)$$

where:

{h}	=	Column matrix of nodal hydraulic heads
α	=	1 for backward difference or fully implicit time stepping
t	=	Current time
Δt	=	Time step

4.3.5 Relaxation Parameter

For the solution of nonlinear flow and transport equations an estimate of the initial pressure head and concentration is required to construct the matrix equation. Under-relaxation, exact-relaxation and over-relaxation are the three options available to estimate new pressure heads and concentration distributions. In all cases the estimates are based on previous approximations. For under-relaxation, the relaxation parameter ranges from 0.0 to 1.0. Exact-relaxation, the value of the relaxation parameter is 1.0. For over-relaxation, the ranges from 1.0 to 2.0 (Lin *et al.*, 1996). The exact-relaxation parameter was selected for solving both flow and transport equations in FEMWATER. The equation relating the relaxation parameter to the unknown hydraulic heads for Laplace's equation is given in 4.2 (Wang and Anderson, 1995):

$$h_{i,j}^{m+1} = h_{i,j}^{m} + \left(\tilde{h}_{i,j}^{m+1} - h_{i,j}^{m}\right)\omega \qquad (4.2)$$

where:

$h_{i,j}$	=	value of the hydraulic head at any point
m	=	iteration index
$h^{m}_{i,j}$	=	initial guess for the unknown hydraulic head
ω	=	relaxation parameter

When determining the new hydraulic head values (h^{m+1}) the previously determined hydraulic heads (h^{m}) are modified or corrected. The relaxation parameter controls how much correction is made for each step in the iteration.

If $\omega < 1$, then the correction to the "guess" is reduced and convergence is slow but stabilized. This is called under-relaxation. If $\omega > 1$, then the correction to the "guess" is increased. This accelerates convergence but may lead to "overshoot" and instability.

CHAPTER 5

STEADY-STATE MODEL CALIBRATION AND RESULTS

FEMWATER was used to calculate the steady-state groundwater heads. In steady-state groundwater flow, the volume of fluid entering a mesh element equals the volume of fluid flowing out. Hydraulic head is independent of time for steady-state flow.

When calibrating the steady-state flow model the hydraulic parameters and boundary conditions were adjusted until the simulated hydraulic heads matched the water levels measured in the field. Once the steady-state flow regime was simulated, the transient transport component of model was calibrated by matching the model predictions to the known history of the site.

5.1 Calibration of the Steady-State Groundwater Flow Model

Small changes in material properties, within the constraints of the observed and estimated data, were made to improve the correspondence between the observed and predicted steady-state heads. The boundary conditions changed in the calibration process were those simulating the WMA, surficial water bodies, constant heads and the infiltration fluxes at the surface. Boundary conditions along the perimeter of the model were acquired from a regional hydrogeological flow model (Karvonen, 1997) and were not adjusted.

Calibration of the steady-state groundwater flow model for PCS Cory Mine and surrounding area was based on:

1. Water levels measured in peizometers and monitoring wells;
2. Documented groundwater velocities; and
3. Results of regional groundwater flow numerical studies (Karvonen, 1997).

5.2 Errors Associated with Calibration Heads

All field measurements have associated errors. When calibrating a groundwater flow simulation a calibration target is specified. The calibration target quantifies the allowable difference between the simulated hydraulic head and the hydraulic head observed in the field. The calibration target used for the brine migration study was ±2.47 m. This corresponded to ±5% of the total hydraulic head difference in the model. Errors attributed to field data that affect the value of the acceptable calibration target include:

1. Transient Effects

Calibrating a groundwater flow model with field water level measurements introduces transient effect errors into the model. The transient effect errors occur because the measured water levels are influenced by changes in seasonal and long term in climatic conditions. Maathuis and van der Kamp (1995) indicate that climate change and seasonal fluctuations can vary the hydraulic head by several meters.

2. Density Effects

Hydraulic head measurements used for calibrating the steady-state groundwater flow model are influenced by fluid concentration through the fluid density parameter of the hydraulic head. The more concentrated the fluid within the monitoring well, the more effect it has on the measured water level.

When calculating the steady-state groundwater flow field freshwater concentration (1 g/L) and density (1,000 kg/m^3) were assumed. If the fluid concentration is greater than freshwater or if a dense fluid has infiltrated into the monitoring well, the concentration and density will be greater than 1 g/L and 1,000 kg/m^3 respectively. This results in the observed head being an underestimate of the freshwater head.

3. Measurement Errors

These errors are associated with the accuracy of the water level measuring device, the operator and the location of the survey point. Generally measurement errors are on the order of a few hundredths of a meter, however, the magnitude of such errors can increase for regional surveys (Anderson and Woessner, 1992). Errors in ground level estimates or surveys are the major inaccuracies in reporting water level data. For some data points, ground level was established from topographic maps resulting in a potential error of several meters.

4. Scaling Effects

Anderson and Woessner (1992) describe scaling effects as errors resulting from the mesh elements unable to represent the small scale heterogenities within them. Point field values may not represent the region of a model mesh element.

Scaling effects can introduce errors into the model by using water level measurements obtained from wells having long screen lengths. Numerical simulations require point head data. Field measurements from monitoring wells with long screened zones may not represent the point head data needed for numerical simulations (Anderson and Woessner, 1992).

5. Interpolation Errors

Nodal positions in models should coincide with the location of monitoring wells used in model calibration. If the nodes do not coincide with the well position then interpolation is used to determine the simulated hydraulic head from surrounding nodes. For large regional investigations the errors associated with interpolation errors can be several meters (Anderson and Woessner, 1992). Interpolation error decreases when nodal points are closely spaced .

5.3 Calibration Database

The hydraulic head field data used for calibrating the groundwater flow model was supplied by AGRA Earth and Environmental, the SRC and the Saskatchewan Water Corporation (SWC). Data from twenty-two wells were used for this study. Not all measurements were equally reliable. Table D.1 in Appendix D lists the well name, hydrostratigraphic position and measured hydraulic head used for the flow model calibration. The well location and hydraulic head measurements are shown on Map 2, Appendix F.

5.4 Flow Model Calibration Technique

Calibrating the groundwater flow model for PCS Cory Mine and surrounding area involved a trial and error process. During model calibration hydraulic properties and boundary conditions were assigned to the mesh nodes and elements. Using the assigned values, FEMWATER calculated the steady-state groundwater flow distribution for the region. The simulated hydraulic heads were compared to field measurements. If the simulated heads matched the observed heads within the predetermined range of the calibration target, the model was considered calibrated. If not, then the hydraulic parameters and/or boundary conditions were adjusted. FEMWATER was then used to recalculate the solution. This process continued until the simulated hydraulic heads matched the field conditions within the ranges specified by the calibration target. Figure 5.1 illustrates the trial and error procedure used in steady-state groundwater flow model calibration.

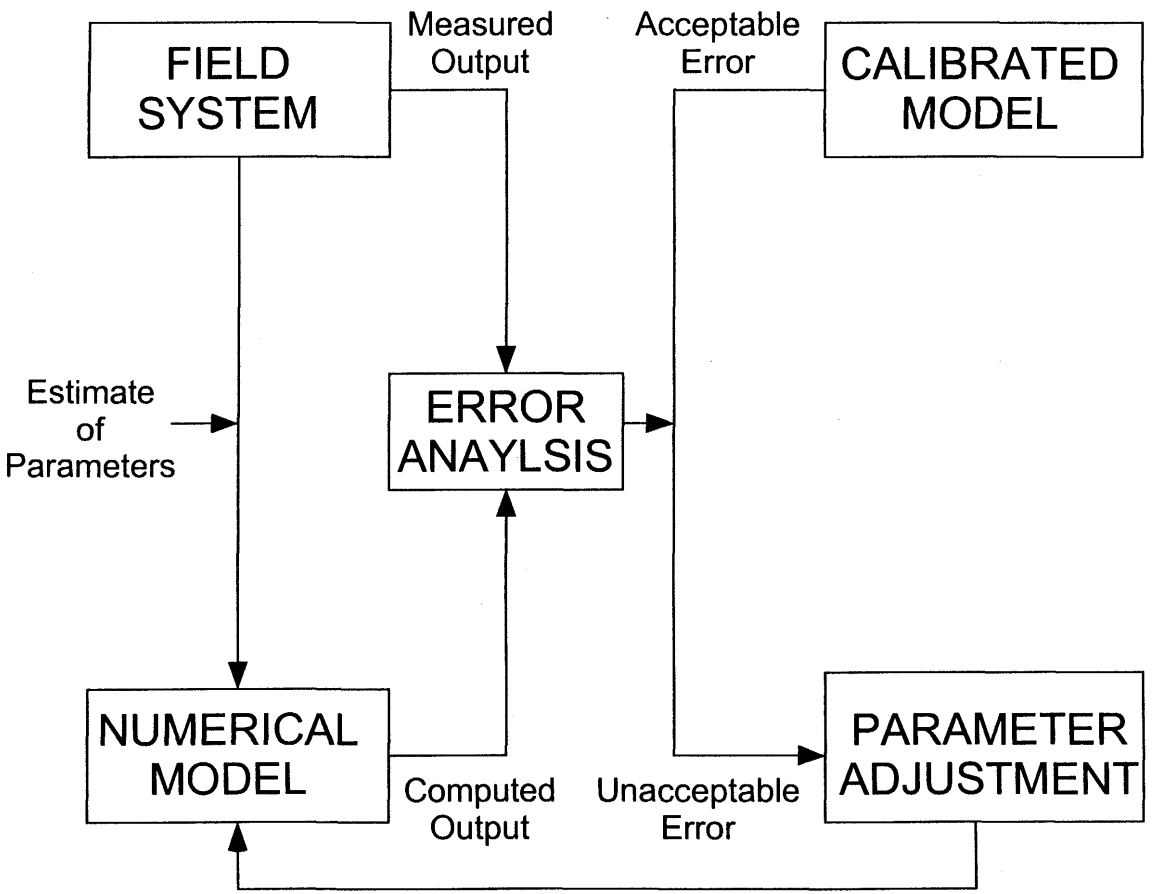

Figure 5.1 Trial and Error Calibration Process (after Anderson and Woessner, 1992)

5.4.1 Evaluation of the Calibrated Steady-State Groundwater Flow Model

The steady-state flow model calibration was evaluated both qualitatively and quantitatively. In the qualitative evaluation attention was given to the flow patterns relative to those indicated by Meneley (1970) and Maathuis *et al.* (1994). The computed results were reviewed and analyzed to ensure that groundwater flow directions, gradients and fluxes were consistent with field evidence.

In the quantitative evaluation of the numerical results, the difference between measured and simulated hydraulic heads were analyzed. There is no standard convention for evaluating calibrated models (Anderson and Woessner, 1992), however there are commonly used measures for evaluating the "average error" resulting from trial and error calibration. "Average error" measures used for quantifying the calibrated steady-state groundwater flow model include:

1. Mean Error

The mean error (ME) quantifies the average difference between the measured hydraulic head (h_m) and the simulated hydraulic head (h_s) for a given number of calibration points (n). The ME is not the preferred method for evaluating calibrated models as both positive and negative differences are included in the mean during averaging. These differences may cancel out the calibration error. A positive ME indicates that the calibrated hydraulic heads are lower than field measurements. A negative ME indicates that the calibrated hydraulic heads are higher than field measurements (Anderson and Woessner, 1992).

$$ME = \frac{1}{n}\sum_{i=1}^{n}\left(h_m - h_s\right)_i \qquad (5.1)$$

2. Mean Absolute Error

The mean absolute error (MAE) is the average of the absolute value of the

measured and simulated hydraulic head differences. The MAE, when compared to the ME, provides a better assessment of how much the measured heads vary with the simulated heads. In the MAE calculation the absolute values of the residual heads are determined prior to averaging. (Anderson and Woessner, 1992).

$$MAE = \frac{1}{n}\sum_{i=1}^{n}\left|\left(h_m - h_s\right)_i\right| \tag{5.2}$$

3. Root Mean Square Error

The root mean square (RMS) error is the square root of the average of the squared differences between the measured and simulated heads. The RMS is the best error estimate available if the errors are normally distributed (Anderson and Woessner, 1992).

$$RMS = \sqrt{\frac{1}{n}\sum_{i=1}^{n}\left(h_m - h_s\right)_i^2} \tag{5.3}$$

5.5 Calibration Results for the Steady-State Flow Model

More than forty trial and error calculations were performed before obtaining a calibrated steady-state groundwater flow model. A graph showing the calibration correlation between measured and simulated hydraulic heads for the monitoring well data used in the trial and error process is shown in Figure 5.2. Figures D.1 to D.4, Appendix D contains the calibration plots for the individual aquifer units.

The solid line shown in Figure 5.2 represents perfect calibration, meaning that simulated hydraulic head exactly matches field data. The two dashed lines parallel to the solid line represent the ±5% (±2.47m) limits of the calibration target.

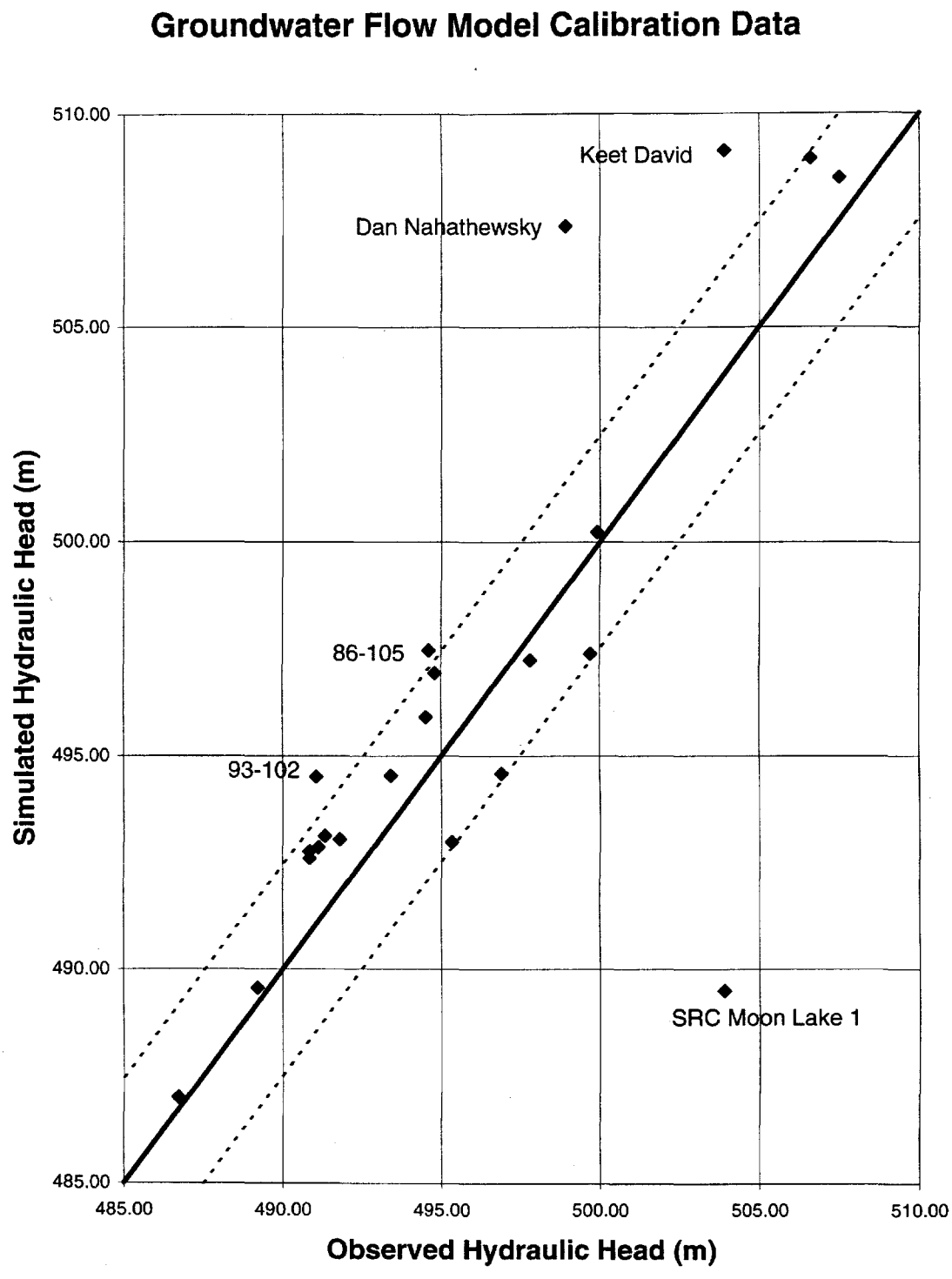

Figure 5.2 – Calibration Plot of the Groundwater Flow Model Calibration Data

Data points lying within the dashed zone were successfully calibrated. The points falling outside this zone were not successfully calibrated.

Table 5.1 summarizes the calibration errors calculated for the steady-state groundwater flow model. The ME, MAE and RMS computed from the steady-state calibrated model were -0.71 m, 2.70 m and 4.71 m respectively. The negative ME indicates that, in general, the simulated hydraulic heads were larger than the measured water levels. The MAE and RMS were high because of large differences between the measured and simulated heads for few of the monitoring wells. Table 5.2 lists the observations wells that were not successfully calibrated.

Table 5.1 - Average Errors Calculated from the Calibrated Flow Model

Hydrogeological Unit	Points	ME (m)	MAE (m)	RMS (m)
Surficial Stratified Deposits	2	7.05	7.35	7.20
Floral Aquifer	6	-1.03	1.81	1.83
Sutherland Aquifer	3	-0.76	2.30	2.49
Tyner Valley Aquifer	5	-3.48	3.48	4.59
Judith River Aquifer	6	-0.41	1.37	1.85
Entire Model	22	-0.71	2.70	4.71

Table 5.2 - Unsuccessfully Matched Calibration Data

Well Name	Hydrogeological Unit	Difference (m)
SRC Moon Lake I	Surficial Stratified Deposits	-14.55
93-102	Sutherland Aquifer	+3.46
Dan Nahathewsky	Tyner Valley Aquifer	+8.80
Keet David	Tyner Valley Aquifer	+5.33
86-105	Judith River Aquifer	+2.74

The simulated hydraulic head for SRC Moon Lake I monitoring well was 14.55 m lower than the water level measured in the field. The SRC Moon Lake I well is located on a hillside that consists of sand underlain by stratified clay. It is possible that the water level measured in this monitoring well is from a locally perched water table. Because of sparse data in the vicinity of SRC Moon Lake I and the coarse mesh outside the WMA, it was difficult to resolve small scale heterogenities in the groundwater flow system. Errors in survey measurements for the SRC Moon Lake I monitoring well are also possible.

The simulated hydraulic head in the Sutherland Aquifer for hole 93-102 was 3.46 m more than the observed head. The discrepancy between the calibrated and measured levels may result from the ambiguity about the thickness and extent of the Sutherland Aquifer below the WMA (Maathuis *et al.*, 1994). Monitoring well 93-102 was measured almost one year after the other monitoring wells completed in the Sutherland Aquifer levels were measured (Maathuis *et al.*, 1994). The hydraulic conditions and fluid concentration affecting well 93-102 at the time of measurement may have been different to those for the other monitoring wells completed in the aquifer.

Domestic wells, Dan Nahathewsky and Keet David, completed in the Tyner Valley Aquifer were not successfully calibrated. The simulated hydraulic head for the Dan Nahathewsky well was 8.80 m higher than the measured level. The calibrated hydraulic head for the Keet David domestic well was 5.33 m above the observed water level. The main reason for the unsuccessful calibration of these wells was that they are located near the perimeter of the study area. Boundary conditions obtained from the regional groundwater flow study (Karvonen, 1997) were consistent to the simulated hydraulic heads for the two domestic wells. These errors were largely inherited from the regional model of Karvonen (1997).

Other reasons for inability to calibrate the simulated heads for the Dan Nahathewsky and Keet David domestic wells include scale effects and surveying error. Near the boundary of the study area the mesh was coarse and the Tyner Valley Aquifer is geologically complex. A coarse numerical mesh cannot account

for the small scale heterogenities where average hydrogeological properties were assigned to large mesh elements.

The calibrated head for monitoring well 86-105 completed in the Judith River Aquifer was 2.74 m greater than the measured water level. A possible reason for this variation was the geological complexity in the vicinity of the well. The average hydraulic properties used to the model Judith River Aquifer may not precisely reflect local geological conditions. Surveying and other measurement errors may have also contributed to the unsuccessful calibration of this well.

5.6 Calibrated Steady-State Groundwater Flow Model

The calibrated steady-state groundwater flow model represents a reasonable approximation of the flow system but not necessarily the correct solution. The trial and error process during calibration does not provide an exact solution for the flow regime in the study area. Further modification of hydraulic properties could still provide many equally calibrated solutions. Furthermore, the steady-state flow regime for the study area incorporated the boundary conditions form a regional groundwater flow investigation (Karvonen, 1997). Biases and errors in the regional flow model will contribute to errors in the calibrated site-specific flow model.

5.6.1 Calibrated Model Parameters

The hydraulic conductivities of the hydrogeological units in calibrated groundwater flow model are summarized in Table 5.3. These calibrated values are in agreement with published information and the values reported by Karvonen (1997) for regional groundwater flow numerical study. The constant head for the tailings pond was 493 m. An infiltration rate of 0.1 mm/yr was used in the calibrated model.

Table 5.4 lists the parameters used to describe the soil-moisture characteristics of the hydrostratigraphic units in the study area. These parameters

were applied to both steady-state and transient calibrated simulations. The soil-moisture characteristic data were obtained from Carsel and Parrish (1988), Mualem (1976), Mualem (1978), Ranjitkar (1989) and van Genuchten (1980).

Table 5.3 - Calibrated Hydraulic Conductivity

Hydrostratigraphic Unit	Kh (m/s)	Kz (m/s)	Kh (m/yr)	Kz (m/yr)
Surficial Stratified Deposits				
Sand	3.00×10^{-4}	6.00×10^{-5}	9.46×10^{3}	1.89×10^{3}
Silt	3.06×10^{-6}	6.11×10^{-7}	9.64×10^{1}	1.93×10^{1}
Clay	3.06×10^{-9}	3.06×10^{-9}	9.64×10^{-2}	9.64×10^{-2}
Floral Aquitard	6.96×10^{-9}	3.06×10^{-8}	5.34×10^{-1}	9.64×10^{-1}
Riddell Aquifer	5.00×10^{-5}	6.85×10^{-6}	1.58×10^{3}	5.26×10^{2}
Floral Aquifer	1.08×10^{-4}	1.48×10^{-5}	3.42×10^{3}	1.14×10^{3}
Sutherland Aquifer	2.00×10^{-4}	6.67×10^{-5}	6.31×10^{3}	2.10×10^{3}
Sutherland Aquitard	7.00×10^{-11}	7.17×10^{-12}	2.21×10^{-3}	2.21×10^{-4}
Tyner Valley Aquifer - High K	8.33×10^{-6}	2.78×10^{-6}	2.63×10^{2}	8.76×10^{1}
Tyner Valley Aquifer - Low K	2.08×10^{-8}	2.08×10^{-9}	6.57×10^{-1}	6.57×10^{-2}
Judith River Aquifer	5.00×10^{-6}	1.67×10^{-6}	1.58×10^{2}	5.26×10^{1}
Lea Park Aquitard	8.33×10^{-12}	8.33×10^{-12}	2.63×10^{-4}	2.63×10^{-4}

Table 5.4 - Calibrated Parameters Describing the Soil-Moisture Characteristics of the Hydrostratigraphy in the Study Area

Stratigraphic Unit	θs (%)	θr (%)	α (m^{-1})	β ( )
Surficial Stratified Deposits				
Sand	46.9	14.9	1.42	2.75
Silt	27.2	9.0	3.83	9.42
Clay	44.6	20.0	0.15	1.17
Floral Aquitard	25.0	16.0	0.80	1.09
Riddell Aquifer	44.0	12.0	7.5	2.01
Floral Aquifer	38.1	10.0	12.4	2.28
Sutherland Aquitard	33.0	16.0	0.60	1.09
Sutherland Aquifer	35.0	9.0	13.10	2.61
Tyner Valley Aquifer - High K	38.0	14.0	3.83	2.60
Tyner Valley Aquifer - Low K	46.9	19.0	1.80	2.06
Judith River Aquifer	25.0	15.3	2.74	10.40
Lea Park Aquitard	8.0	6.0	0.15	1.17
Slurry Trench	45.0(1)	40.0(1)	0.70	1.17

(1) Barbour (1997)

5.7 Steady-State Groundwater Flow Model Results

The hydraulic heads and groundwater flow velocities determined from the calibrated steady-state model were plotted.

Figure 5.3 shows the magnitude of the steady state groundwater flow velocity in the study area plotted on a logarithmic scale. The dark green to light blue regions correspond to the locations of aquitards. Flow velocities at these locations were on the order of 10^{-4} m/yr to 10^{-6} m/yr. Flow velocity in the Lea Park Aquitard represented by the dark blue color ranged from $2x10^{-6}$m/yr to $5x10^{-9}$ m/yr. Major aquifer units denoted by the light green, orange and red colored regions had

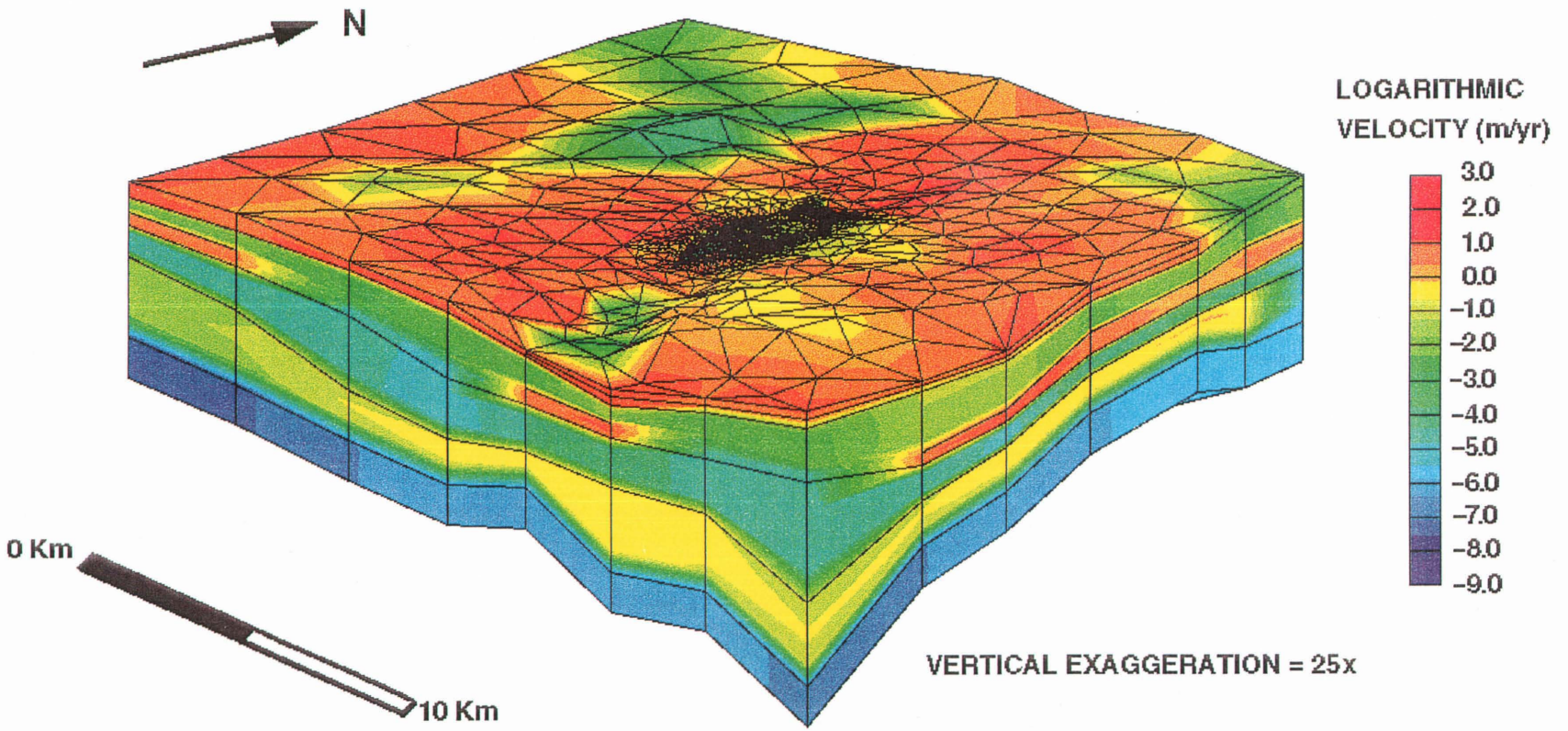

Figure 5.3 - Magnitude of the Steady-State Calibrated Flow Velocity in the Study Area

relatively high flow velocities ranging from approximately 10^{-1} m/yr in the light green areas to 10 m/yr in the red areas.

5.7.1 Tyner Valley Aquifer System

Figures 5.4 and 5.5 show the hydraulic head and flow velocity in Tyner Valley Aquifer System respectively. Permeability restrictions and discontinuities in the Tyner Valley Aquifer System significantly influenced the hydraulic head, hydraulic gradient and the groundwater flow velocity in the study area.

The calibrated hydraulic head in the Tyner Valley Aquifer System varied from over 510 m near the southeast corner of the study area to under 474 m in the north central region. The hydraulic head distribution in the Tyner Valley Aquifer System was complex.

The permeability restriction near Grandora resulted in a large hydraulic gradient in this area. South of Grandora the hydraulic gradient was less but hydraulic head was high and artesian conditions exist. North of Grandora the hydraulic head is governed by the elevation of the North Saskatchewan River (Meneley, 1970).

The flow velocity in the Tyner Valley Aquifer was highly variable throughout the study area. Towards the southwest the average flow velocity was approximately $6x10^{-2}$ m/yr. Flow in the vicinity of the permeability restriction was as low as $4x10^{-4}$ m/yr. North of the permeability restriction flow velocity increased to approximately $4x10^{-1}$ m/yr. Most groundwater flow in the Tyner Valley Aquifer was directed away from the permeability restriction near Grandora.

The hydraulic gradient in the Judith River Aquifer was, in general, more uniform than that in the Tyner Valley Aquifer. The hydraulic gradient in the Judith River Aquifer in northeast portion of the study area increased due to the permeability blockage. A local recharge feature existed in the Judith River Aquifer. In this region the Sutherland Aquitard was relatively thin. The reduction in thickness allowed the Floral Aquifer to recharge the Judith River Aquifer at an increased rate.

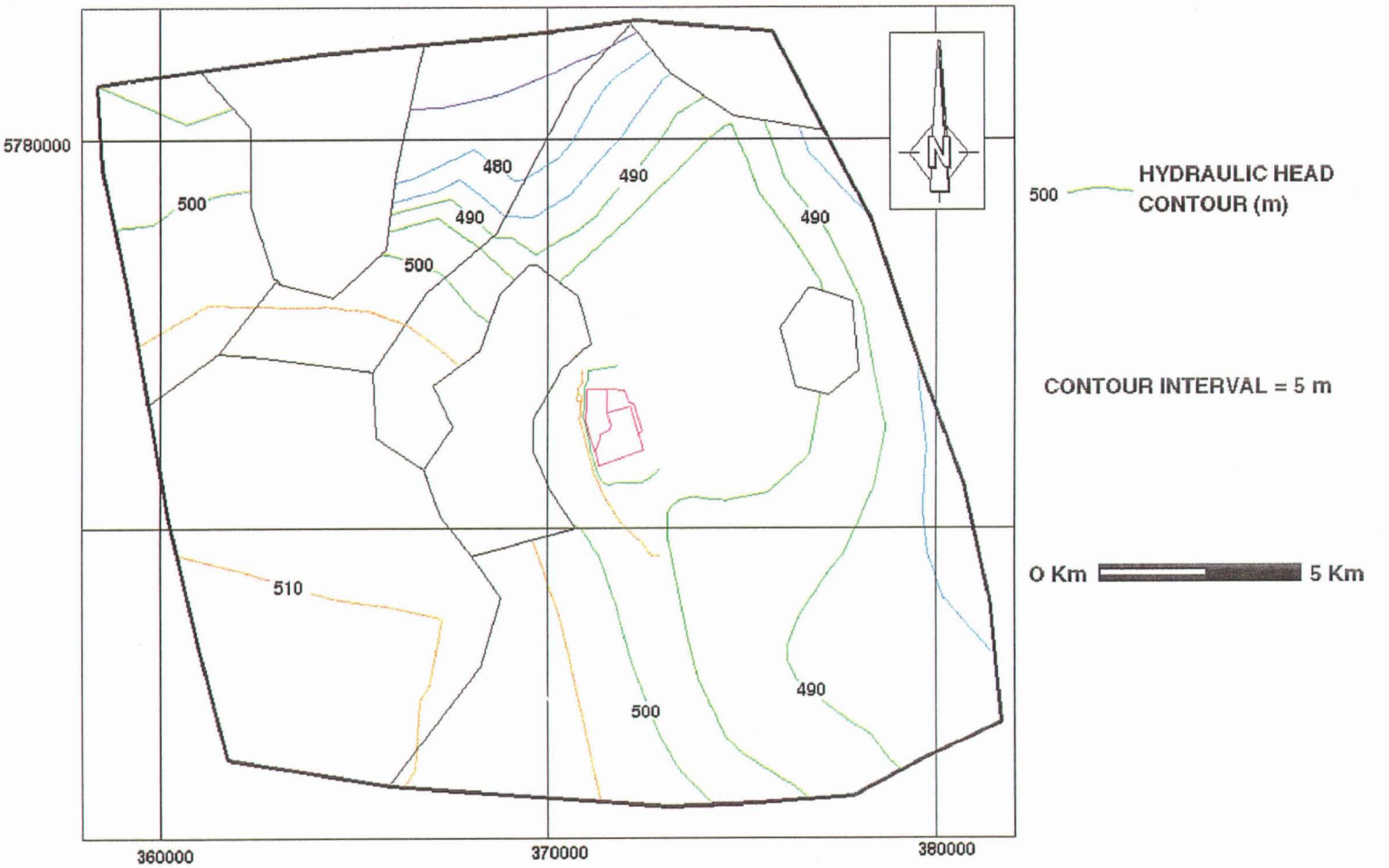

Figure 5.4 - Calibrated Hydraulic Head In the Tyner Valley Aquifer System

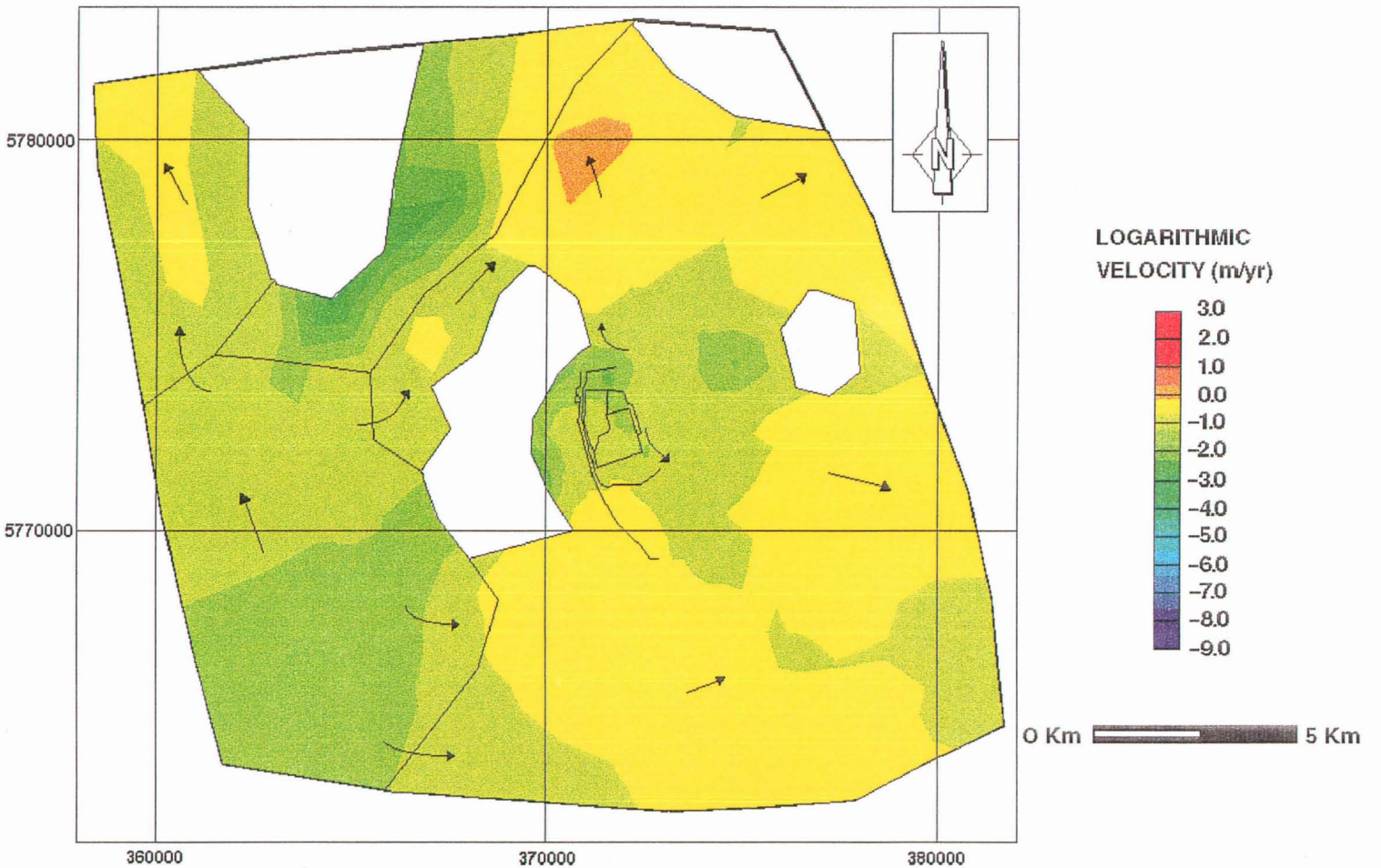

Figure 5.5 - Calibrated Groundwater Flow Velocity in the Tyner Valley Aquifer System

Flow in the Judith River Aquifer varied from approximately $9x10^{-2}$ m/yr to $4x10^{-1}$ m/yr. Some areas in the Judith River Aquifer had localized flow velocities as low as $3x10^{-2}$ m/yr and as high as 1 m/yr. Most groundwater flow south of the WMA discharged into the South Saskatchewan River. Groundwater north of the WMA flowed towards the Tyner Valley Aquifer channel.

5.7.2 Sutherland Aquifer

The calibrated steady-state hydraulic head in the Sutherland Aquifer ranged from 486 to 504 m in the study area. The hydraulic head within the vicinity of the WMA ranged from 493 m in the south to 496 m in the north. The average groundwater flow velocity was $3x10^{-2}$ m/yr and was directed southwards.

5.7.3 Floral Aquifer

Figure 5.6 illustrates the steady-state hydraulic head distribution in the Floral Aquifer. Groundwater originating from the Floral Aquitard and Dalmeny Aquifer recharges the Floral Aquifer (Karvonen, 1997). Flow in the Floral Aquifer was northwest to southeast discharging into the South Saskatchewan River.

Hydraulic head in the Floral Aquifer was approximately 500 m in the northern part of the study area and 476 m to the south. The branch of the Floral Aquifer located along the eastern perimeter of the study area was 503 m in the north and 472 m at its southern extent. The average hydraulic head within the detached aquifer portions located near the northwest and southwest corners of the study area were approximately 500 m and 520 m respectively.

Figure 5.7 shows the steady-state groundwater flow velocity. Flow at the north end of the central Floral Aquifer channel was approximately $6x10^{-1}$ m/yr. As groundwater flowed toward the WMA the flow rate increased to 1 m/yr. North of the WMA the flow rate increased to 9 m/yr.

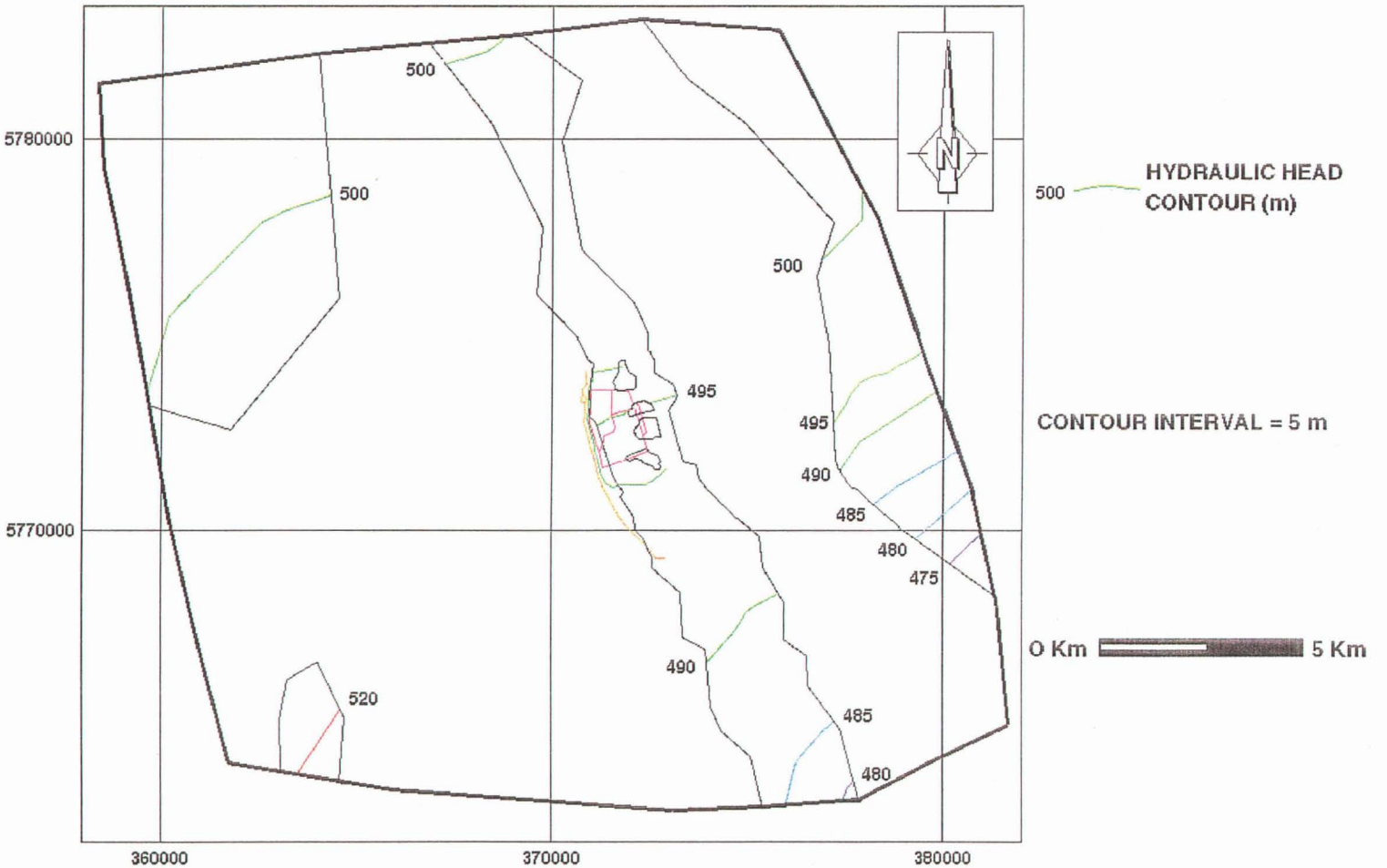

Figure 5.6 - Calibrated Hydraulic Head in the Floral Aquifer

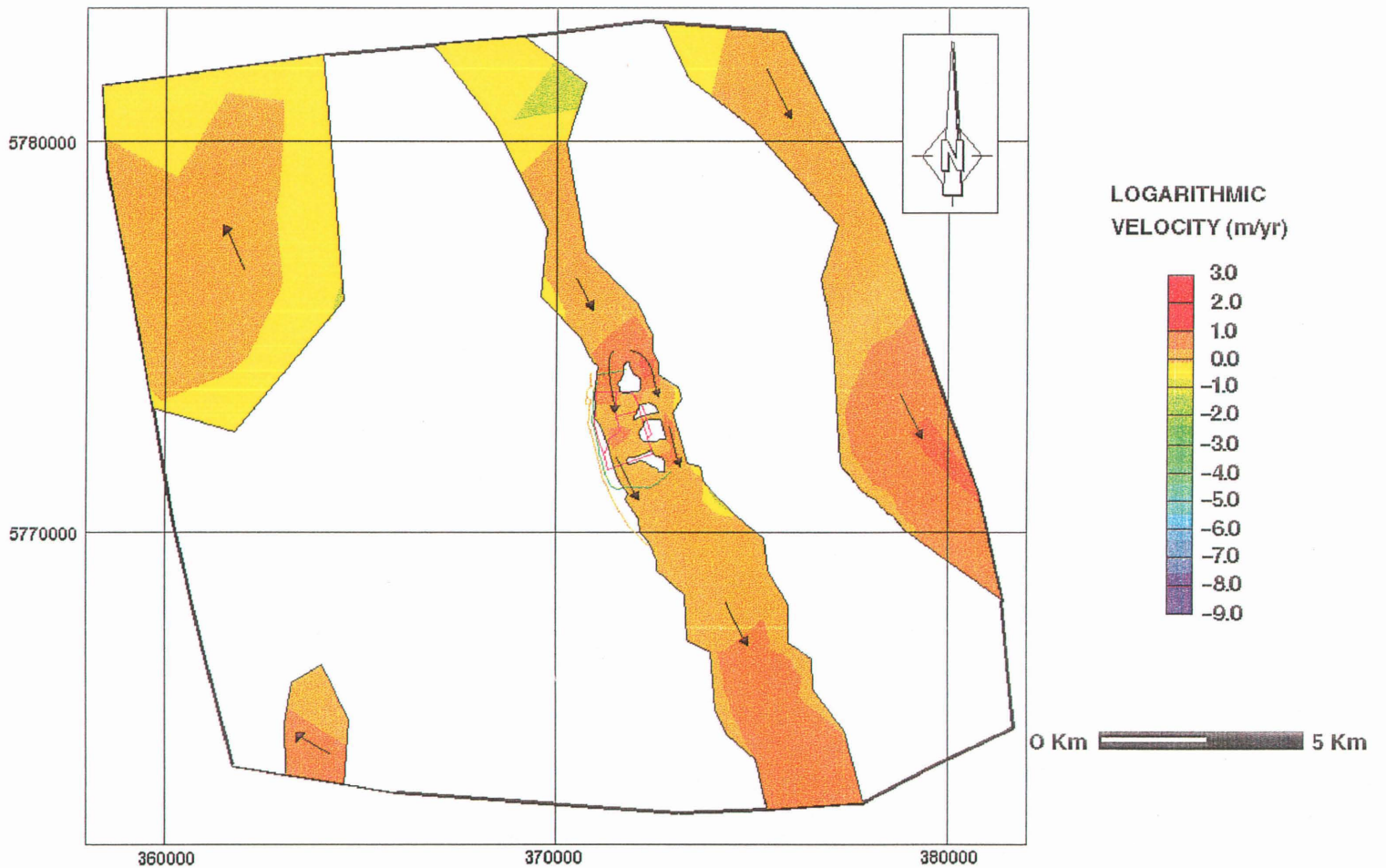

Figure 5.7 - Calibrated Groundwater Flow Velocity in the Floral Aquifer

There was a localized region beneath the WMA where the flow rate was approximately 28 m/yr. Groundwater flow vectors diverted around the aquifer discontinuities in the vicinity of the WMA and velocities increased locally. Beneath most the WMA and to the south of the mine site the flow rate was approximately 1 m/yr. As groundwater approached the South Saskatchewan River Valley the flow rate increased to 9 m/yr.

Groundwater velocity in the Floral Aquifer channel located along the eastern perimeter of the study area increased as it moved towards the South Saskatchewan River. In the northern portion of the channel the flow rate was approximately $6x10^{-1}$ m/yr. As it moved southward, the flow rate increased to 1 m/yr. Groundwater discharging into the river valley varied from 9 to 28 m/yr.

Flow in the detached aquifer at the northwest corner of the study area varied from $9x10^{-2}$ to 1 m/yr. Similarly flow in the detached aquifer located along the southwestern edge of the study area fluctuated from 1 m/yr to 9 m/yr. In both detached portions of Floral Aquifer groundwater was flowing westward, probably discharging at Rice Lake.

5.7.4 Riddell Aquifer

The steady-state hydraulic head in the Riddell Aquifer varied from roughly 493 m in the southern most position to 495 m in the northern area. Groundwater flow in the aquifer was southwards attaining an average velocity of $3x10^{-1}$ m/yr. There was a localized region where the flow velocity increased to approximately 1 m/yr.

5.7.5 Surficial Stratified Deposits

The calibrated steady-state hydraulic head and groundwater flow velocities in the surficial stratified deposits are shown in Figures 5.8 and 5.9 respectively.

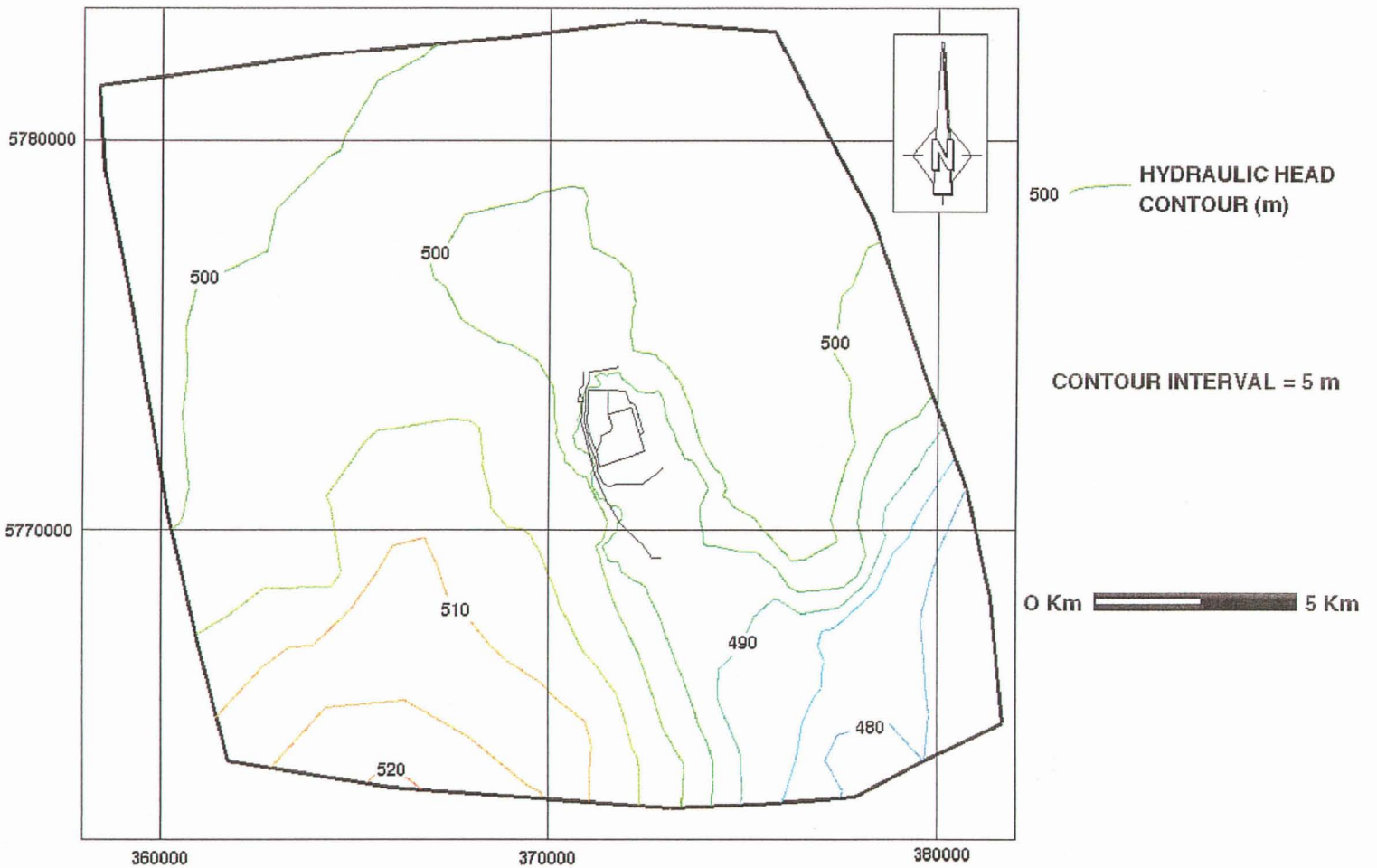

Figure 5.8 - Calibrated Hydraulic Head in the Surficial Stratified Deposits

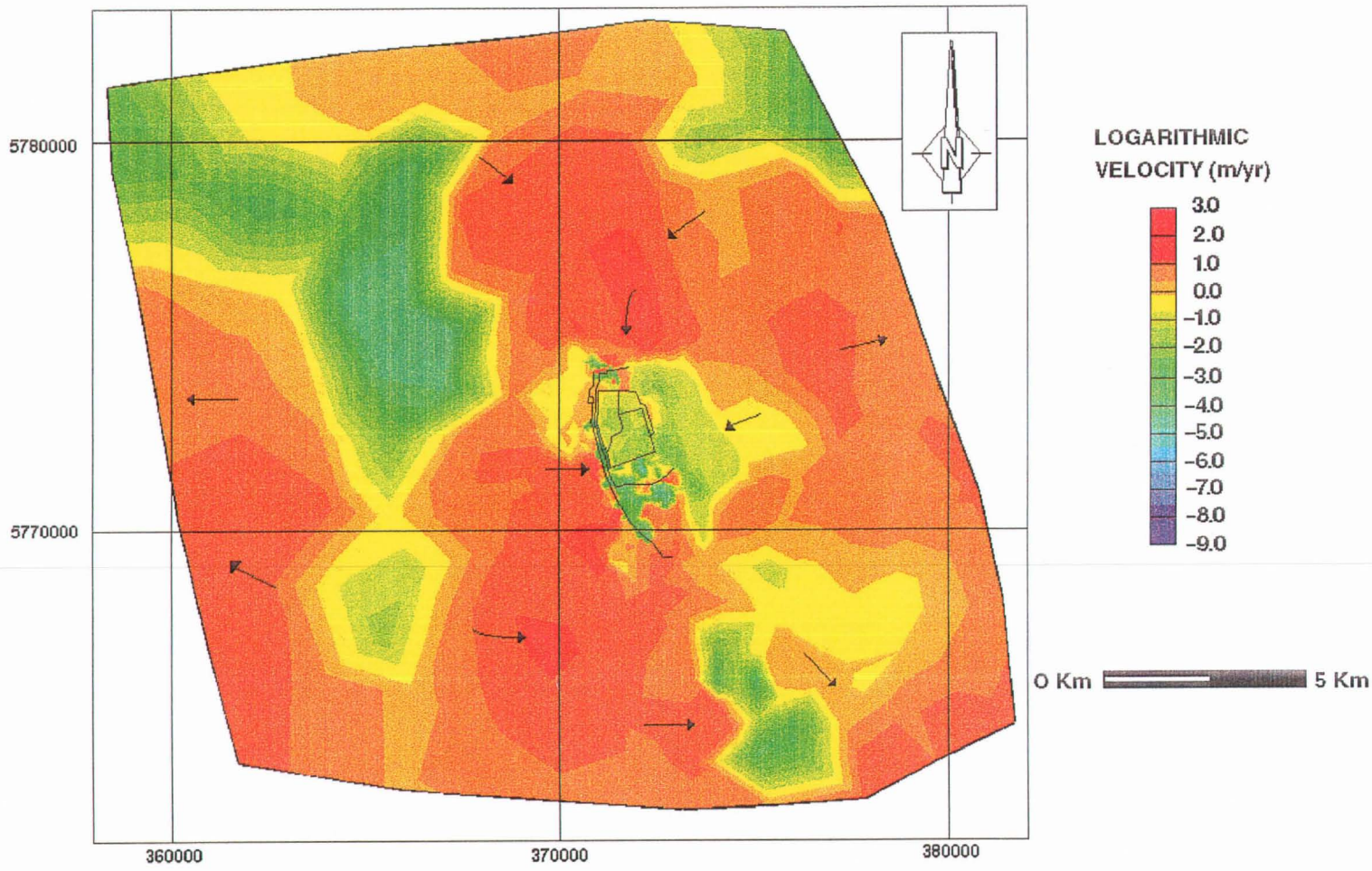

Figure 5.9 - Calibrated Groundwater Flow Velocity in the Surficial Stratified Deposits

Hydraulic head in the surficial stratified deposits was significantly affected by topography and lithology. In southwest region of the study area, where topography is high, the calibrated hydraulic head ranged from approximately 514 m to over 520 m. Where the South Saskatchewan River Valley is located the hydraulic head reduced to 478 m. The calibrated steady-state hydraulic head in the vicinity of the WMA was approximately 493 m.

Throughout most of the study area hydraulic head gradient varied with topography. As topographic elevation decreases the hydraulic gradient generally decreased. Large hydraulic gradients in the surficial stratified deposits were generally found in sands adjacent to clays where the hydraulic conductivity contrast was high.

Figure 5.9 shows that near the western perimeter of the study area groundwater discharged to Rice Lake. To the east, flow was towards the meltwater channel located in the middle of the study area (Figure 1.5). Once in the meltwater channel flow moved southward towards Moon Lake and the South Saskatchewan River. Located near the eastern perimeter of the study area was another surficial groundwater channel.

Flow in the Surficial Aquitard ranged from $9x10^{-6}$ m/yr to $9x10^{-4}$ m/yr. Flow in the Surficial Aquifer varied from $9x10^{-3}$ m/yr to 28 m/yr.

5.8 Transient Brine Transport Parameters

In transient simulations hydraulic head and brine concentration are calculated as a function of time. Transient modelling of flow and brine transport in the study area used the calibrated steady-state flow system as the initial condition for the simulation. Determining when the transient brine transport simulation was calibrated was difficult because only limited anecdotal qualitative information existed regarding the position and concentration of the brine plume with time. In absence of calibration standards, sensitivity analysis was used to evaluate the results of the transient brine transport model.

The material properties used in the transient brine transport model are listed in Table 5.5. The hydraulic conductivities and boundary conditions determined from the calibrated steady state flow model were applied to the transient model. The hydraulic conductivity of the slurry trench was 6.4×10^{-10} m/s (Arun, 1994 and Haug *et al.*, 1988). The dry densities of the hydrostratigraphic units were assumed from the range of values listed in Table 2.1 (Chapter 2). The coefficient of tortuosity for the surficial stratified deposits and underlying consolidated sediments were assumed to be 0.500 and 0.250 respectively. The surficial stratified deposits was assigned a large value because it is unconsolidated. The coefficient of tortuosity for the slurry trench was assumed to be 0.380, the average of the coefficient of tortuosity of the surficial stratified deposits and the more consolidated sediments.

The longitudinal and transverse dispersivity specified in the transient model was 5.00 m. These values were greater than those determined by the empirical expression relating the apparent longitudinal dispersivity to the flow length (equation 3.13). The shortest horizontal and vertical flow length in numerical mesh was approximately 3 m. Using the empirical expression calculated a dispersivity slightly smaller than the one used in the numerical model. By using a higher dispersivity the contaminant plume migrated further from the WMA. This was a conservative design assumption. Numerical dispersion also increased the predicted rates of mixing.

The molecular diffusion coefficient used in the transient model was 1.67×10^{-9} m^2/s. The coefficient used falls within the range 1×10^{-9} to 2×10^{-9} m^2/s documented by Fetter (1992). It was also consistent with the chloride effective diffusivity range of 2.5×10^{-10} to 5×10^{-10} m^2/s determined by Maathuis and van der Kamp (1994) during brine diffusion tests at ambient groundwater temperatures.

The distribution coefficient was set to zero for chloride since it was not significantly modified by ion exchange, adsorption and microbial activity (Davis and DeWiest, 1966).

Table 5.5 - Transient Model Parameters

Hydrostratigraphic Unit	Dry Density (kg/m^3)	Coefficient of Tortuosity
Surficial Stratified Deposits		
Sand	1800	0.500
Silt	1600	0.500
Clay	1300	0.500
Floral Aquitard	2000	0.250
Riddell Aquifer	1900	0.250
Floral Aquifer	1900	0.250
Sutherland Aquifer	1900	0.250
Sutherland Aquitard	2200	0.250
Tyner Valley Aquifer - High K	1900	0.250
Tyner Valley Aquifer - Low K	1950	0.250
Judith River Aquifer	1950	0.250
Lea Park Aquitard	2300	0.250
Slurry Trench	2000	0.380

CHAPTER 6

ANALYSIS OF BRINE MIGRATION

Brine migration at PCS Cory Mine began with the onset of brine storage at the WMA. Concentration and density differences between brine and native groundwater, the hydraulic gradient created by the brine pond constant head and the advective flow velocities in the regional flow system were primary factors affecting brine migration. Containment structures such as perimeter dykes, slurry walls, bypass ditches, drains and storage facilities were installed at various times to inhibit brine migration from the WMA. Conservative numerical results suggest that these structures were sufficient for impeding brine transport in the surficial stratified deposits. These structures, however, were not successful at stopping lateral brine transport in the surficial stratified deposits by diffusion or at inhibiting the downward migration of brine due to its strong negative buoyancy.

FEMWATER was used to simulate 50 years (1969-2019) of brine migration in the study area. All figures showing the position and concentration of the brine plume were plotted using the logarithm of concentration in order to resolve, in detail, the structure of the brine plume with time. The concentration of brine contained in the tailings pond used in the numerical simulation, was 300,000 mg/L or 300 g/L. This corresponded to a logarithmic concentration of 2.48, or $10^{2.48} \approx 300$ g/L. The concentration of native groundwater used in this study was 1,000 mg/L or 1 g/L, which corresponded to a logarithmic concentration of 0.0.

6.1 Overview of Analysis Locations

Numerical results showing the brine plume position and concentration from 1969 to 2019 were computed for PCS Cory Mine and surrounding area. The characteristics of the brine plume after 10, 17, 26 and 50 years in the surficial stratified deposits, Floral Aquifer, Judith River Aquifer and in vertical cross-sections

were computed and examined in detail. Figure 6.1 shows the location the cross-sections used for the assessment of brine migration at PCS Cory Mine and also the nodal locations where breakthrough profiles of the Floral Aquifer were constructed.

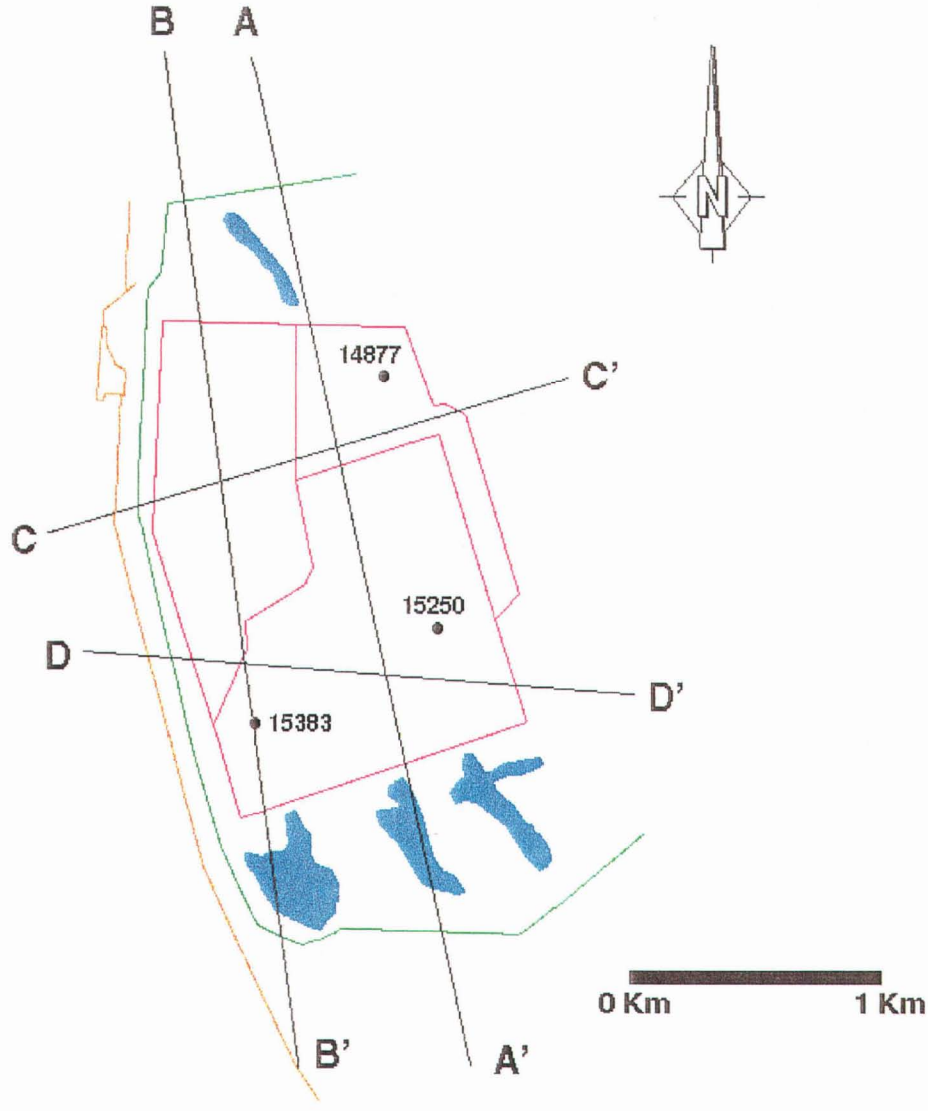

Figure 6.1 - Location of Cross-Sections and Nodal Points Used in the Analysis of Brine Plume Migration

6.2 Overview of Control Measures

In 1969, brine storage at the PCS Cory Mine WMA began. The year 1969 represented time 0 for the transient model study. The constant brine concentration applied to the model for the 50 years of simulated brine transport was 300 g/L at the tailings pond and tailings pile and 250 g/L at the pond sources located immediately north and south of the tailings dam (Figures 1.4 and 6.1). Brine contained in the tailings pond was saturated and therefore assigned 300 g/L. The pond source concentration was assumed to be less than saturated brine since they are diluted by surface run-off, local precipitation and are not in direct contact with the tailings.

The constant hydraulic head simulating the tailings pond and tailings pile was assumed to be 493.0 m and for the run-off ponds, 492.9 m. The constant head boundary conditions and concentrations were based on measured elevations and conductivities. These measurements take into account the effects of seasonal changes by averaging.

In 1979 a slurry trench and freshwater bypass ditch were constructed at the WMA (Figures 1.4 and 6.1). The slurry trench was hydrated with brine at the time of installation. An initial concentration of 300 g/L was assigned to the slurry trench in order to simulate brine hydration. The constant head boundary conditions used to simulate the freshwater bypass ditch ranged from 491.81 m at its southern end to 494.36 m at its northern end. The constant head conditions assigned to the nodes located along the bypass ditch between the northern and southern limits decreased at a constant rate from north to south. All constant head boundary conditions along the bypass ditch were coupled with a concentration boundary condition equal to native groundwater (1 g/L). Both the slurry trench and freshwater bypass ditch were added to the numerical model after 10 years of simulation time.

The east and west drain (Figures 1.4) were added to the numerical model after 17 years of simulated brine migration (1986). The constant head boundary condition applied to the east and west drains were both approximately 492 m. A constant concentration of 1 g/L was also assigned to these drains.

The flood containment pond, slime storage facility and an extension of the west drain (Figure 1.4) were constructed in 1995 and therefore included in the numerical model after 26 years of simulation time. Difficulties were experienced during the construction of a dyke west of the flood containment pond. This resulted in the overflow of brine from the containment pond into a region located between the slurry trench and tailings dam. Brine then pooled along the northwest perimeter of the tailings facility. This surface water ponding was also included in the numerical simulation at this time. Constant head and concentration boundary conditions of 492.9 m and 250 g/L respectively were applied to represent the flood containment pond, slimes storage unit and overflow of brine. The head and concentration boundary conditions added to the extension of the west drain were approximately 492 m and 1 g/L respectively.

6.3 Analysis of Brine Migration

The results discussed here are for the base case model which includes all containment structures and brine sources but does not allow for brine mounding in the tailings pile.

6.3.1 Brine Plume in the Surficial Stratified Deposits

Figure 6.2a to 6.2d shows the contaminant plume in the surficial stratified deposits at 10, 17, 26 and 50 years after the initiation of brine storage at PCS Cory Mine in 1969.

After 10 years (Figure 6.2a) brine migrated outside of the containment dykes surrounding the tailings facility. The contaminant originating from the pond sources dispersed into the surrounding surficial stratified deposits. The slurry trench was easily located by its high concentration resulting from brine hydration during construction. By 1979 the brine plume moved approximately 270 m to the east. The brine plume originating from the WMA also intercepted the slurry trench to the

west. There was an apparent localized advance in the contaminant plume near the west-central edge of the WMA. This radial advance was approximately 300 m from the source and coincided with the location of the Surficial Aquifer. The brine plume has not reached the freshwater bypass ditch after 10 years.

The brine plume in the surficial stratified deposits calculated for the year 1986, after 17 years is shown in Figure 6.2b. The difference between the position of the brine plume after 10 and 17 years was readily apparent especially along the slurry trench and to the north of the WMA. By 1986 brine originating from the slurry trench dispersed and the peak concentration was less than 300 g/L. North of the WMA and near the slurry trench the brine plume expanded considerably. The most significant expansion occurred in the proximity of the Surficial Aquifer (to the north of the WMA). After 17 years the brine plume intercepted the freshwater bypass ditch over much of its length. The western extent of the migration was approximately 450 m west from the southwest corner of the tailings dam. The brine plume has not reached the east and west drain at this time. The brine plume was spreading towards the drains within the Surficial Aquifer near the southwestern edge of the WMA.

Figure 6.2c shows the position of the brine plume within the surficial stratified deposits in the year 1995, after 26 years. The difference between the position of the brine plume after 17 and 26 years was relatively small. More spreading between the tailings facility, the pond sources in the south and the slurry trench north of the tailings pond was evident.

Figure 6.2d shows the predicted location of the brine plume in the surficial stratified deposits for the year 2019, after 50 years. The flood containment ponds, overflow pond and slimes storage facility contributed significantly to the subsequent 24 years of spreading in the surficial stratified deposits.

The brine concentration between the slurry trench and the northwest side of the tailings dam was over 200 g/L except at a few locations where it reduced to approximately 80 g/L. The development of the flood containment area as a source resulted in the further contamination of neighbouring soils. The addition of the slime

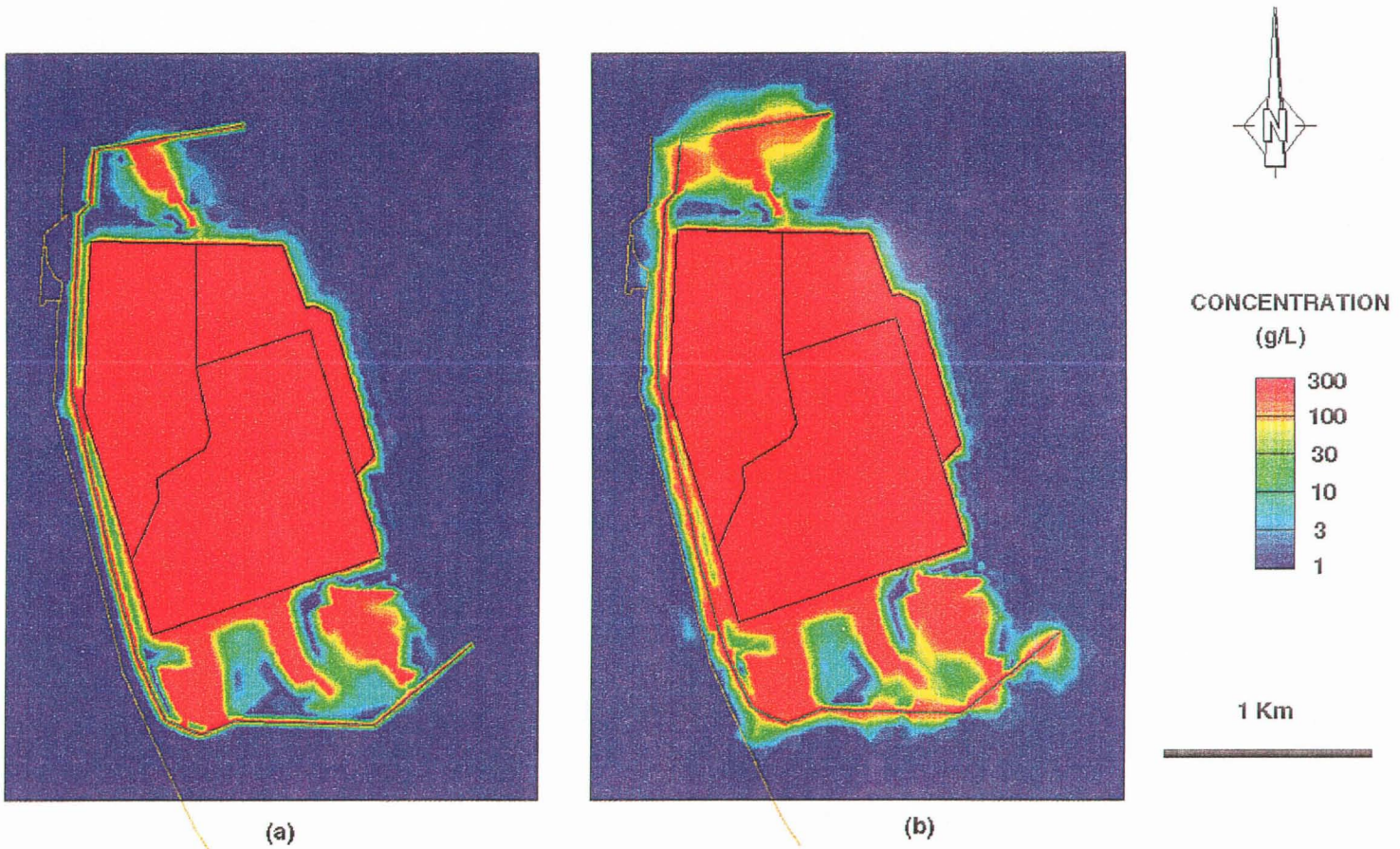

Figure 6.2 - Position of the Brine Plume in the Surficial Stratified Deposits after (a) 10 years and (b) 17 years of Brine Transport

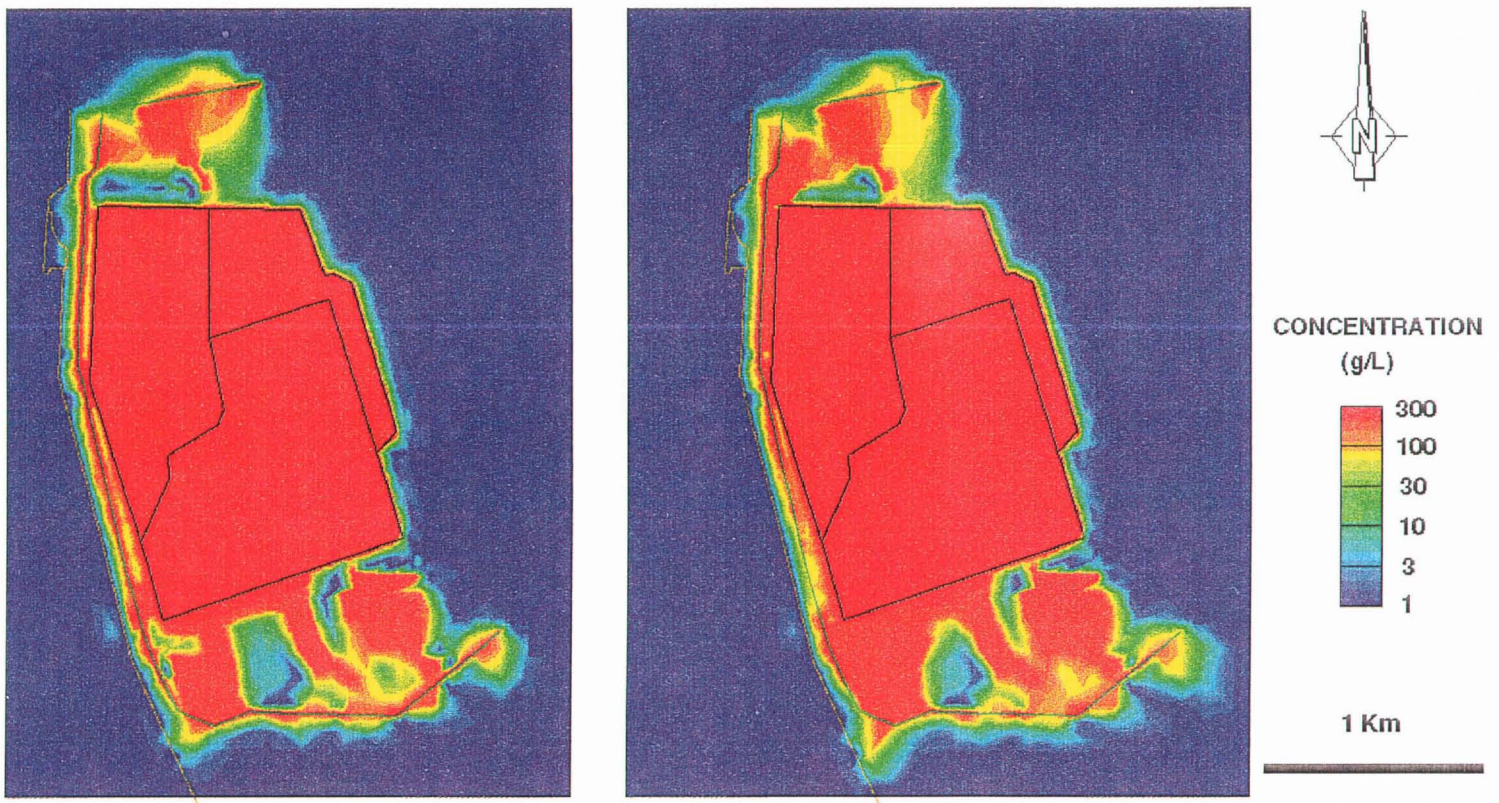

Figure 6.2 - Position of the Brine Plume in the Surficial Stratified Deposits after (c) 26 years and (d) 50 years of Brine Transport

storage facility also contributed to the spreading of the brine plume in the surficial stratified deposits. The predicted concentration of brine reaching the east and west drains were slightly above 1 g/L.

6.3.2 Brine Plume in the Floral Aquifer

Figures 6.3a to 6.3d show the predicted brine concentration in the Floral Aquifer after 10, 17, 26 and 50 years.

Figures 6.3a shows the brine plume for the year 1979, after 10 years. The highest concentration in the Floral Aquifer was approximately 4 g/L and was located below the southwest corner of the tailings facility. The plume also intercepted the aquifer below the northwest corner of the tailings dam, however, the concentration at this location was less than 2.5 g/L.

After 17 years of brine migration (Figure 6.3b) the largest concentrations computed in the Floral Aquifer were below the northwest corner and southwestern region of the tailings facility. The values were approximately 5 g/L and 13 g/L respectively. Brine contamination originating from the hydrated slurry trench construction had, in some places, infiltrated into the Floral Aquifer attaining concentrations greater than 7 g/L both to the north and south.

The extent of predicted brine contamination in the Floral Aquifer was considerably higher by 1995 (Figure 6.3c), after 26 years. Most of the Floral Aquifer below the WMA was contaminated. The largest concentration of the brine in the aquifer was less than 80 g/L and was found below the southwest edge of the tailings dam. Brine from the hydrated slurry trench continued to infiltrate the aquifer and in some places the concentration in the aquifer originating from the trench was greater than 35 g/L. Evidence of contamination from the pond sources was also present in the aquifer. The highest concentration originating from these sources was approximately 12 g/L.

Figure 6.3d illustrates the predicted brine plume in the Floral Aquifer for the year 2019, after 50 years. The maximum concentration simulated in the Floral

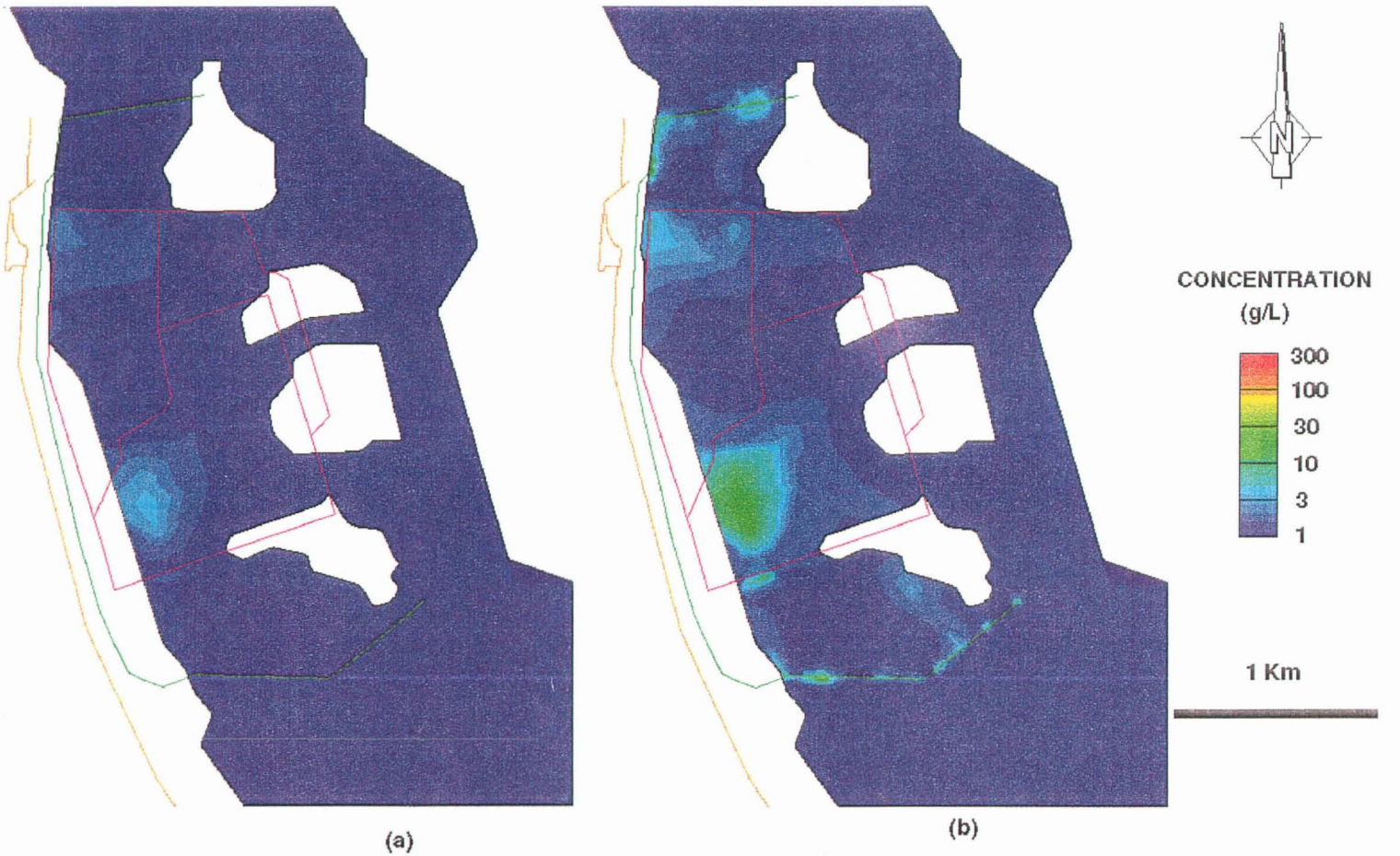

Figure 6.3 - Position of the Brine Plume in the Floral Aquifer after (a) 10 years and (b) 17 years of Brine Transport

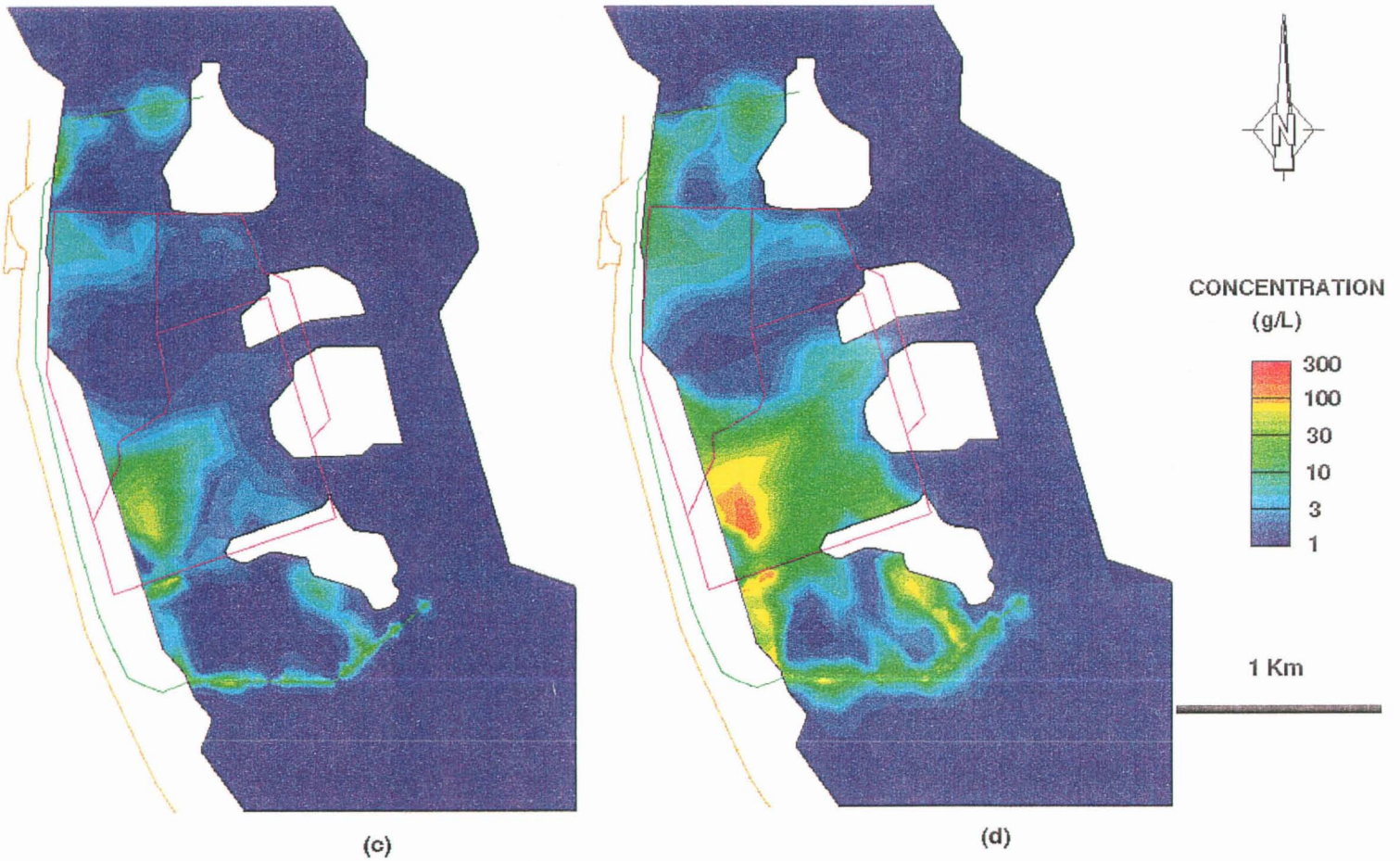

Figure 6.3 - Position of the Brine Plume in the Floral Aquifer after (c) 26 years and (d) 50 years of Brine Transport

Aquifer was approximately 128 g/L. The concentration of brine from the hydrated slurry trench that infiltrated the aquifer was over 80 g/L. The pond sources south of the tailings facility also contributed to the contaminant plume in the channel aquifer.

6.3.2.1 Floral Aquifer Breakthrough Profiles

Logarithmic concentration breakthrough profiles (Figure 6.4) were constructed for nodes 14877, 15250 and 15383 in the Floral Aquifer. The location of these nodes are shown on Figure 6.1. All three profiles show increased brine concentration with time. The maximum concentration reached at nodes 14877, 15250 and 15383 after 50 years of simulated brine migration were approximately 3, 9.5 and 118 g/L respectively.

6.3.3 Brine Plume in the Judith River Aquifer

The maximum concentration predicted the Judith River Aquifer in the year 2019 was less than 1.5 g/L. The location of the concentration maximum was beneath the southeast corner of the WMA. A plan view map showing the concentration distribution was not constructed because the maximum concentration in the aquifer was approximately equalled to background conditions.

6.4 Cross-Section Results

Figures 6.5a to 6.5d show the concentration along section A-A' for the years 10, 17, 26 and 50. The region bounded in white and sandy-yellow shows the limits of the Floral and Judith River Aquifers respectively. Sections B-B', C-C' and D-D' show the brine plume for the year 2019 as a fence diagram in Figure D.5, Appendix D.

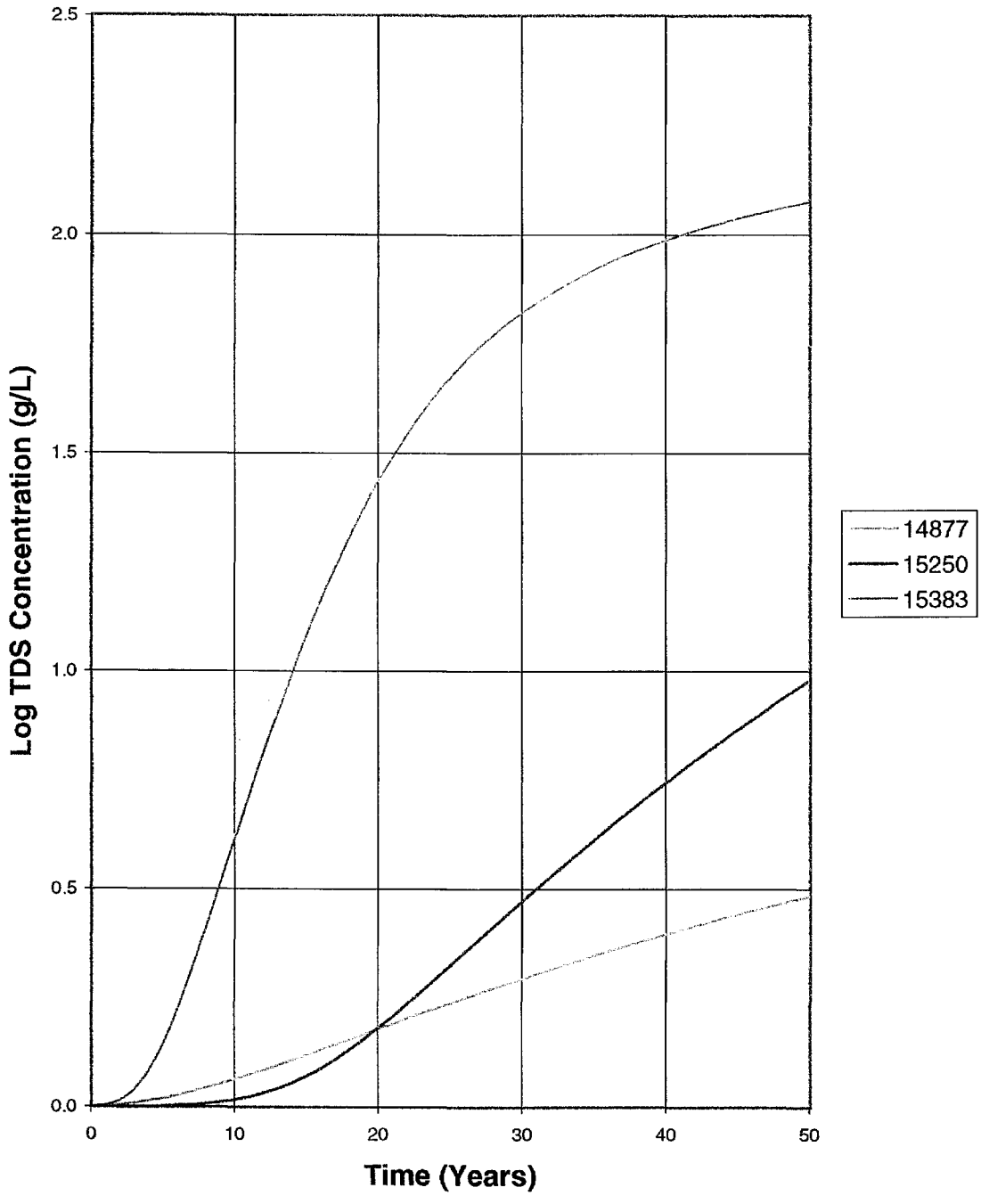

Figure 6.4 - Breakthrough Profiles for the Floral Aquifer

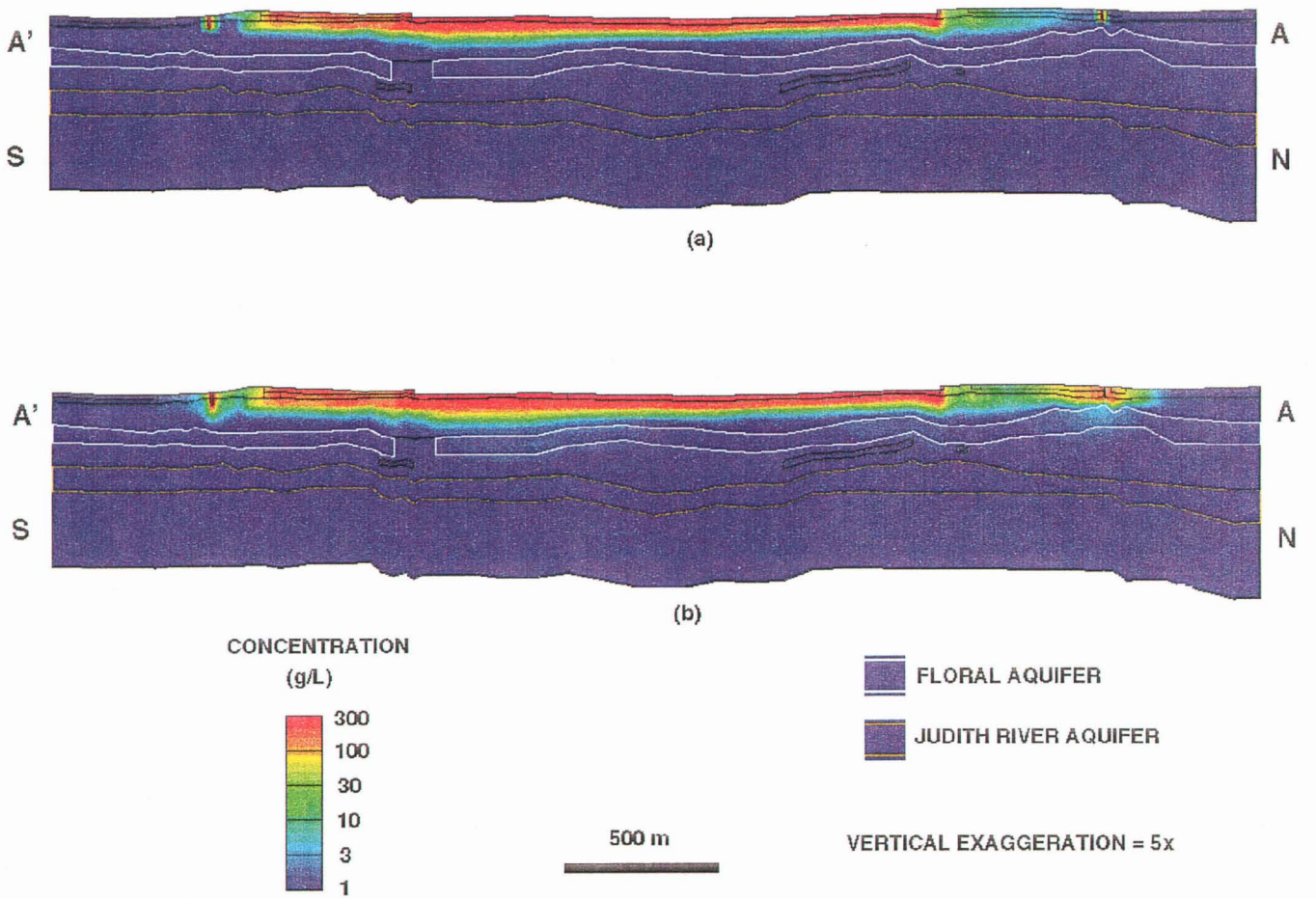

Figure 6.5 - Position of the Brine Plume along Section A-A' after (a) 10 years and (b) 17 years of Brine Transport

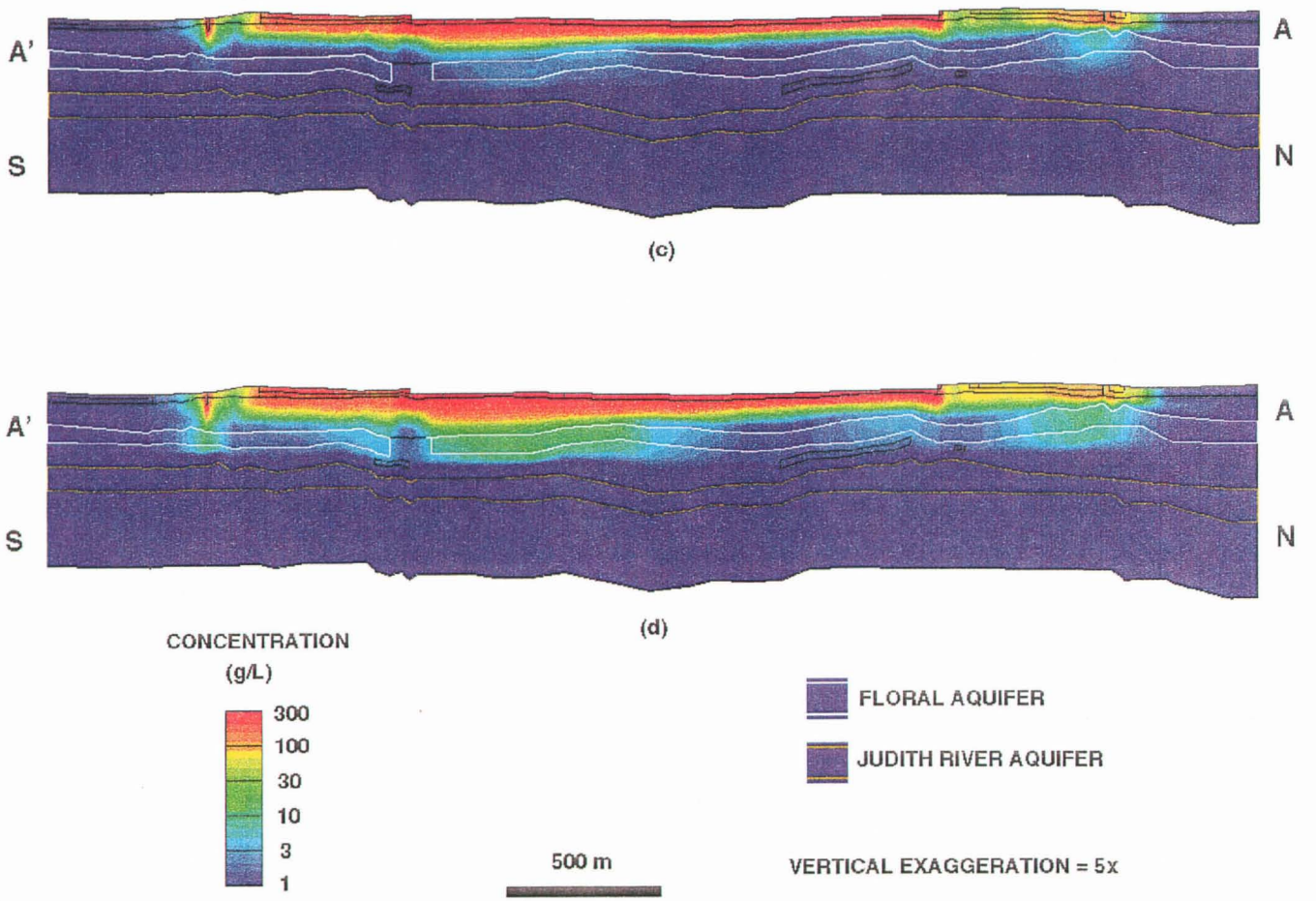

Figure 6.5 - Position of the Brine Plume along Section A-A' after (c) 26 years and (d) 50 years of Brine Transport

Section A-A' (Figure 6.5a) shows the position of the brine plume in 1979, after 10 years. The brine plume infiltrated the Floral Aquitard. Spreading of brine in the surficial stratified deposits was evident north of the tailings facility. Figure 6.5a shows the hydrated slurry trench as isolated sources at both ends of the section. Along section A-A' the brine plume had not migrated into the Floral Aquifer.

The brine plume shown in section A-A' for the year 1986, after 17 years (Figure 6.5b) indicated that further spreading of the plume occurred in all directions. Brine originating from the hydrated the slurry trench had spread especially within the Surficial Aquifer north of the tailings facility. The concentration distribution indicated that by 1986 the brine plume was contaminating the Floral Aquifer. The highest concentration shown in A-A' in the aquifer was nearly 5 g/L near "A" at the north end of the section.

Figure 6.5c shows the brine plume along section A-A' computed for the year 1995, after 26 years. The brine plume had spread laterally and downwards. Saline fluids from the WMA and hydrated slurry trench infiltrated into the Floral Aquifer and also into the underlying Sutherland Aquitard. The highest concentration recorded in the channel aquifer along section A-A' was approximately 7 g/L and was located below the slurry trench north of the tailings facility.

The position of the brine plume predicted for the year 2019, after 50 years, along section A-A' is shown in Figure 6.5d. The contaminant front advanced both radially and vertically. There were several locations where the plume migrated through the Floral Aquifer and infiltrated into underlying Sutherland Aquitard and in some places, the Sutherland Aquifer. The predicted maximum concentration in the channel aquifer and underlying aquitard after 50 years of transient brine migration was over 20 g/L.

6.5 Transport Mechanisms

Molecular diffusion was one of the main transport processes governing brine migration in the surficial stratified deposits. The brine plume diffused radially in the

surficial soils due to the large concentration gradient existing between the brine and native groundwater.

Advective velocities were low in the clay and till aquitards where the hydraulic gradient and hydraulic conductivities were small. The hydraulic gradient between the elevated brine pond and the regional water table induced the dispersive transport.

The density contrast between brine and native groundwater dominated the downward migration of brine at the mine site. Analysis of variable density groundwater flow and solute transport was complex and strongly coupled as the density-driven component of fluid flow was dependent on fluid concentration. Brine in the WMA was highly concentrated and very dense. As the brine plume moved downwards, the vertical extent of the brine slug increased. This resulted in an increased hydraulic head driving fluid vertically. Beneath the plume fluids were forced out radially in the aquifers by increased advective velocities. This allowed for dispersive processes to spread the brine plume in the direction of groundwater flow.

Spreading of the brine plume in the Floral Aquifer was effected by the groundwater flow velocity and hydrodynamic dispersion. The largest advective velocities were generated radially around the sinking plume. Advective transport in the aquifer accelerated the fluid towards the South Saskatchewan River Valley. The brine plume also moved down the channel of the Floral Aquifer, under the action of gravity, in a direction controlled by the elevation of the channel floor.

The shape of the breakthrough curves plotted for various nodes in the Floral Aquifer indicated that dispersive transport processes affect the brine plume. If molecular diffusion and mechanical dispersion did not exist in the aquifer then the breakthrough curve would be a step function.

6.6 Calibration of the Transport Model

The PCS Cory Mine WMA was inspected in September 1997 to aid with the

calibration of the FEMWATER simulation by comparing its results with field conditions. Photographs were taken to assist with interpretation of brine migration predictions. Figures 6.6a and 6.6b show the flood containment pond and the overflow brine pond. Inspection of the PCS Cory Mine WMA revealed that brine probably migrated west of the slurry trench. Evidence for this was the presence of strongly saline soils and salt-tolerant vegetation.

The base case model appears to be a valid approximation of the groundwater flow and brine transport characteristics at the study area. The validity of the transport model in representing field conditions were difficult to confirm because of the limited data. The detailed geometry of the hydrostratigraphic units in the study area and the position and concentration of the brine plume with time were not well constrained.

At PCS Cory Mine, based on water quality information, for 1997, 28 years after the onset of brine storage in the WMA, brine was detected in both east and west drains. The brine concentrations measured at these drains were under 20 g/L. To simulate the brine plume migrating to the east and west drains after 28 years, more detailed information regarding the precise geometry of the Surficial Aquifer in the vicinity of these drains is needed.

Information about the timing of brine infiltration into the Floral Aquifer was limited. Golder Associates (1996) indicate from their numerical modelling studies that the time required for the 250 mg/L isochlor to intercept the Floral Aquifer is between 8 and 50 years after the onset of brine storage. The estimated time of brine plume breakthrough in the Floral Aquifer, computed in the base case model, falls within the 8 to 50 year window reported by Golder Associates (1996).

Karvonen (1997) suggests that the advective front does not leave the WMA after 500 years of brine transport. When density dependent effects are modelled the sinking brine plume generates radial advection of the *insitu* fluids by displacement. The dense plume obstructs regional advection and appears to move down the gradient of the base of the aquifer rather than down the hydraulic gradient.

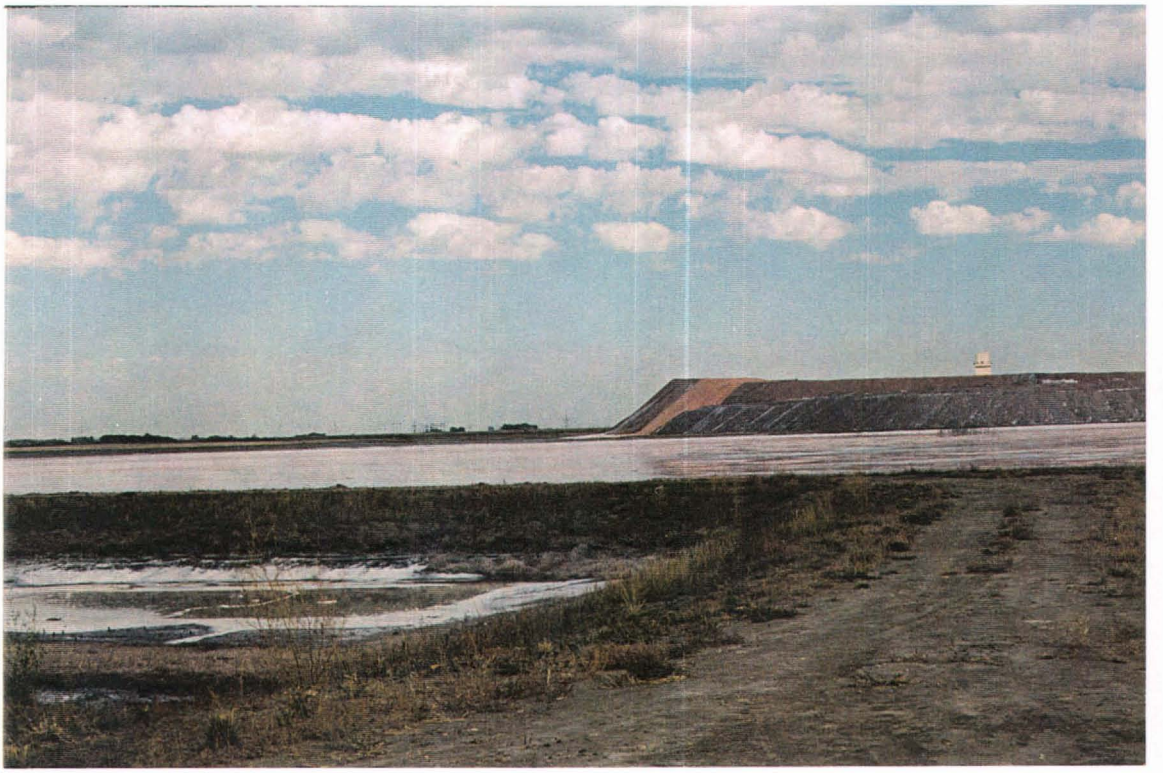

(a)

(b)

Figure - 6.6 Photographs of the (a) flood containment pond and (b) overflow pond

CHAPTER 7

SENSITIVITY ANALYSIS

The purpose of a sensitivity study is to evaluate the uncertainty in the calibrated model resulting from indeterminate estimation of hydraulic properties, changing hydrological stresses and boundary conditions (Anderson and Woessner, 1992). In the sensitivity study model parameters having a significant effect on computed results were identified. The values of these parameters were varied across a plausible range of values that could notably affect the numerical outcome (Istok, 1989).

The sensitivity study was applied to the transient numerical simulation in order to investigate the variability in the computed brine plume position with time. The transient model parameters were varied one at a time to determine their individual effects on the numerical results. A few sensitivity simulations were performed on the calibrated steady-state flow model. All figures showing the concentration of the brine plume were constructed using logarithmic concentration values.

7.1 Time Steps

The first set of sensitivity runs were performed to determine the effects of the time step on numerical accuracy, numerical oscillation and the amount of computational time needed to simulate 50 years of transient brine migration.

Four sensitivity runs were performed. The time step used in the sensitivity analysis were 12 months, 4 months, 2 months and 1 month. Results for different the time steps were summarized by comparing the mean and standard deviation of the computed brine concentrations at various times. Table E.1, Appendix E lists the mean and standard deviation computed for the four sensitivity runs.

The mean and standard deviation values in Table E.1 indicate that using a

smaller time step only slightly decreased the computed mean and standard deviation. A 1 month time step was chosen to simulate brine migration at PCS Cory Mine and vicinity for all subsequent analysis. Reducing the time step further, increased the computational time required to simulate the flow and transport process but did not significantly improve the quality of the results.

7.2 Spatial Parameters

Sensitivity studies were conducted on the spatial domain of the calibrated steady-state groundwater flow and the transient transport model. The majority of the sensitivity runs were performed on the transient model. A detailed sensitivity study was recently carried out on the regional steady-state groundwater flow model west of Saskatoon (Karvonen, 1997). The objective of this thesis was to study transient brine migration in the vicinity of PCS Cory Mine. For this reason, most of the analysis concentrated on the transient performance of the model.

7.3 Steady-State Flow Model

Sensitivity runs were performed on the site-specific, steady-state groundwater flow model. During these sensitivity runs the amount of infiltration, hydraulic conductivity and the brine pond constant head level were altered to determine its impact on the computed flow system. Qualitative and quantitative results (Tables E.2 to E.5, Appendix E) from these simulations indicate that changing either infiltration or hydraulic conductivity had minimal effect on the simulated head levels calculated for the various monitoring wells. Sensitivity results indicated that the constant head level of the brine pond had a considerable effect on the simulated hydraulic heads. Raising the pond level increased the computed hydraulic heads, especially in the Floral Aquifer. The optimum brine pond elevation determined from the calibrated steady-state model and used for all subsequent numerical simulations was 493 m.

7.4 Base Case Transient Model

Numerous sensitivity runs were conducted on the base case model to determine the effect of various modelling parameters on the brine plume. The following simulations were performed and analysed during the sensitivity study:

1. Results for the base case model were compared with the results for a simulation with no brine containment structures to determine the impact of these structures on brine migration;
2. The effect of brine mounding within the tailings pile on the position of the brine plume was studied. Both containment structures and no structures were investigated; and
3. The impact of varying the coefficient of tortuosity on the position of the contaminant plume.

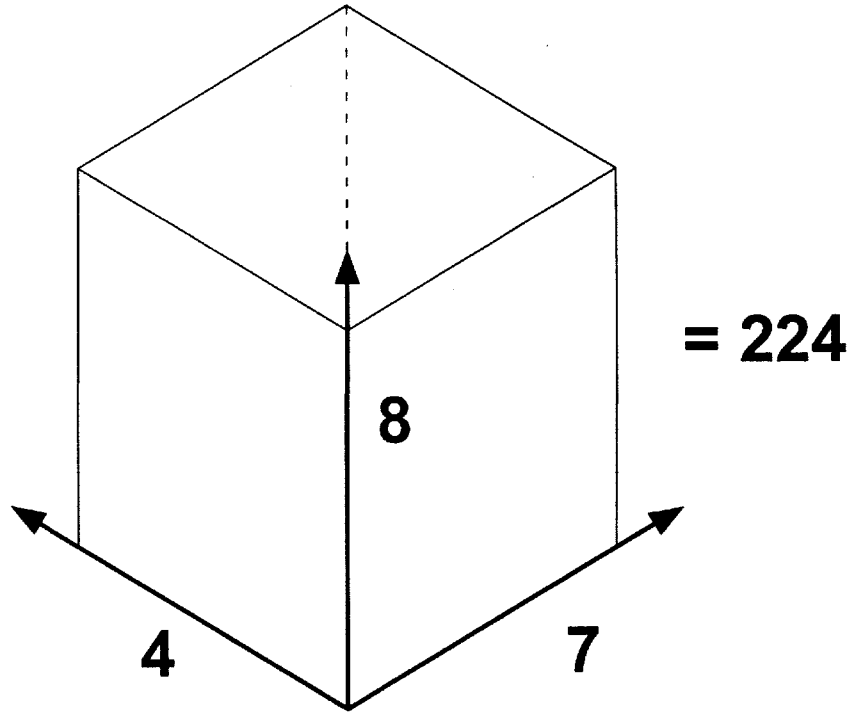

Figure 7.1 - Total Number of sets of results computed for the Sensitivity Analysis

Eight sensitivity models, with concentration distributions saved at four times (year 10, 17, 26 and 50), four cross-sections (A-A', B-B', C-C' and D-D') and three plan views (surficial stratified deposits, Floral Aquifer and Judith River Aquifer) were analyzed in the study. This provided the potential for 224 (8x7x4) sets of results showing the concentration distribution for the sensitivity studies (Figure 7.1). Only a fraction of these results was included in this thesis. Table E.6, Appendix E lists the sensitivity models, times the computed brine plume positions were saved, the plan views and cross-sections that were constructed for the sensitivity analysis.

7.4.1 Brine Migration Without Containment Structures

A sensitivity study was conducted to determine if the slurry trench, freshwater bypass ditch, flood containment pond and slimes storage facility affected the position of the brine plume. The results obtained after 50 years of brine migration were compared with the results of the base case model described in Chapter 6.

Figures 7.2a and 7.2b show the position of the brine plume after 50 years of transient brine migration in the surficial stratified deposits and the Floral Aquifer respectively.

The spreading of the brine plume in the surficial stratified deposits (Figure 7.2a) appeared fairly uniform, with the exception of a localized region west of the tailings facility where brine dispersed more in the Surficial Aquifer.

Comparing the brine plume calculated in this sensitivity simulation (Figure 7.2a) with that of the base case model (Figure 6.2d) showed that the slurry trench, flood containment pond and slimes storage facility contributed significantly to the advancement of the brine plume. Hydrating the slurry trench with brine provided an advanced source for contaminant spreading. If the slurry trench was not hydrated with brine, the plume would not have spread as much. It is difficult to determine at this time whether or not the freshwater bypass ditch impeded brine transport.

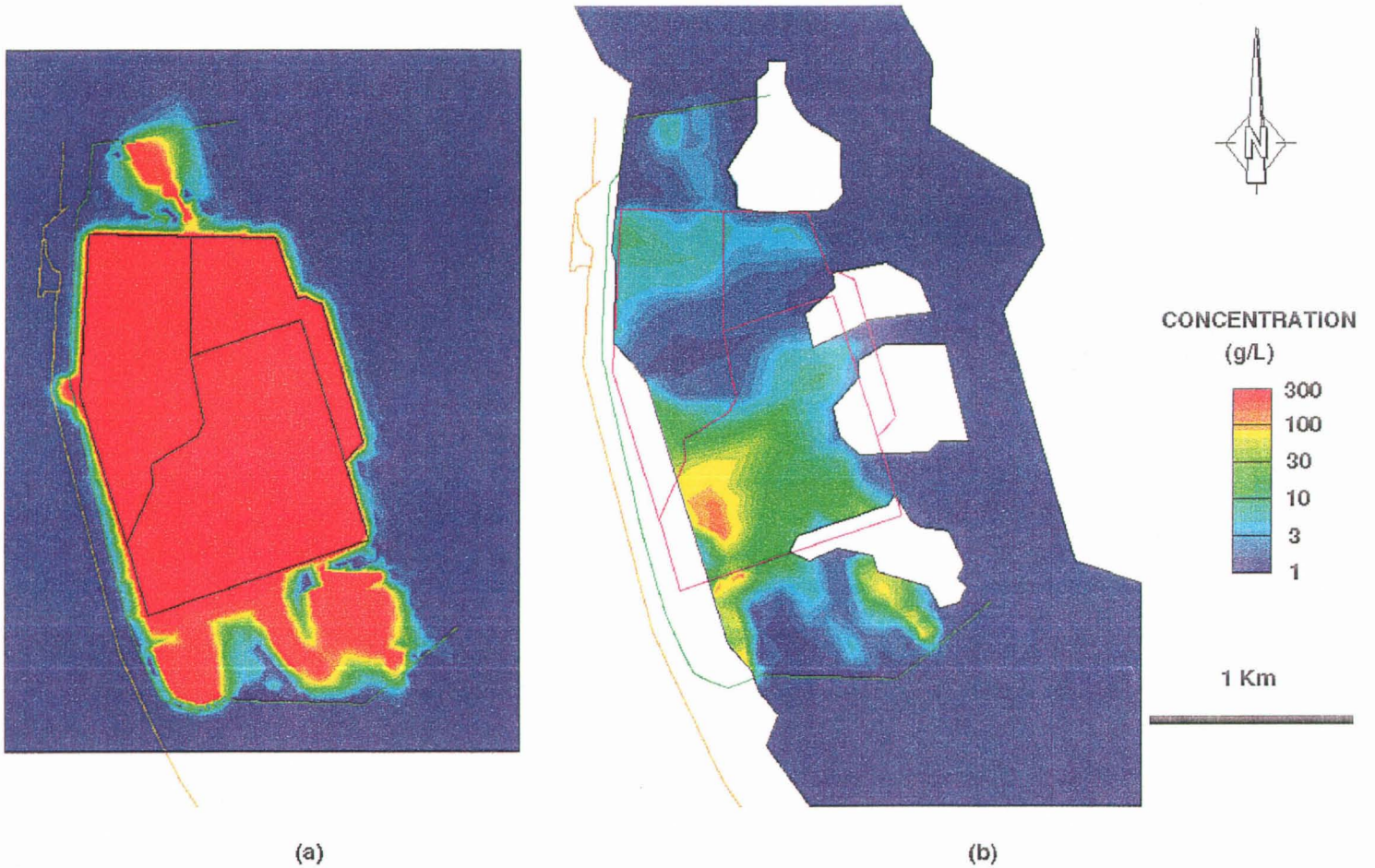

Figure 7.2 - Position of the Brine Plume in the (a) Surficial Stratified Deposits and (b) Floral Aquifer after 50 years of Simulated Brine Transport for a Model Without Containment Structures

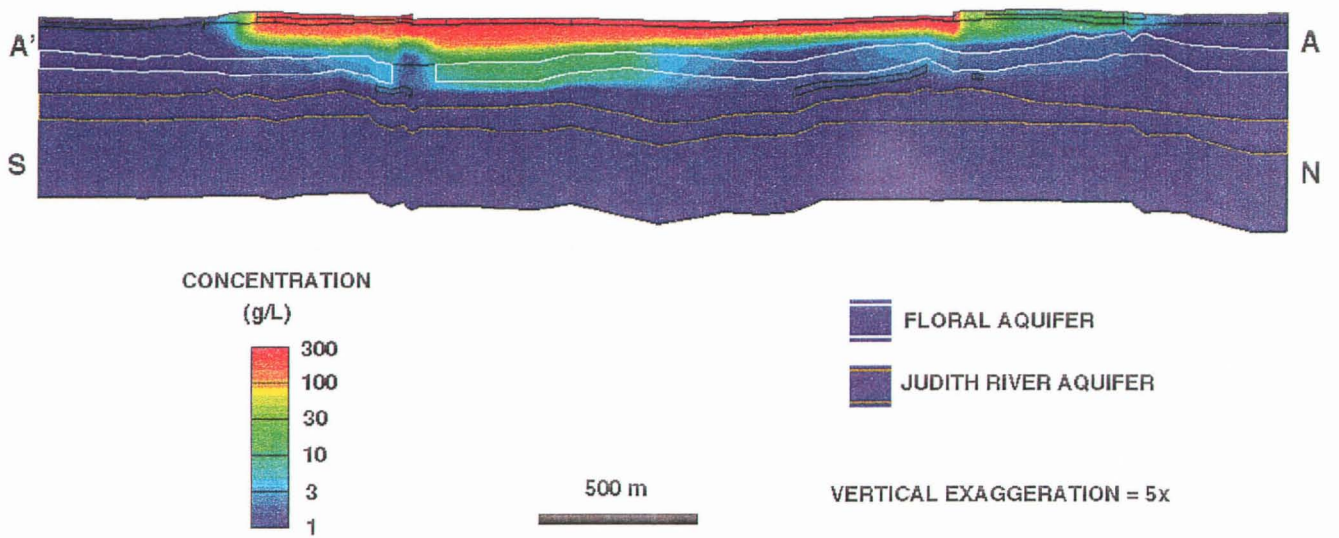

Figure 7.3 - Position of the Brine Plume along Section A-A' after 50 years of simulated Brine Transport for a Model Without Containment Structures

Figure 7.2b shows the position of the brine plume in the Floral Aquifer. The highest concentration was approximately 128 g/L and was situated below the southwest region of the tailings facility. This corresponded with that calculated in the base case model after 50 years of brine transport. A comparison of Figure 6.3d with Figure 7.2b indicated that a significant amount of brine contamination in the Floral Aquifer resulted from the slurry trench, the flood containment pond and slimes storage facility. Figure 7.2b also shows that the brine plume in the channel aquifer for a simulation with no engineering structures was less extensive than that calculated for the base case model.

The highest concentration of the calculated in this sensitivity study for the Judith River Aquifer was less than 1.5 g/L. This was in agreement with the maximum concentration determined in the base case model.

Figure 7.3 shows the brine plume computed along section A-A'. Comparing these results of the base case model (Figure 6.5d) further suggested that the hydrated slurry trench, flood containment pond and slime storage facility contributed significantly to the position of the contaminant plume.

7.4.2 Brine Mounding in the Tailings Pile

Simulations were performed to determine the effect of brine mounding within the tailings pile on the position of the brine plume. The results from these simulations were compared with the results of the base case model. An estimate was made of the rate of increase in brine head with time.

A maximum rate of 0.36 m/yr was estimated for brine mounding and was assigned to nodes in the centre of the tailings pile. The rate of brine mounding assigned around these central nodes was 0.24 m/yr. The nodes near the perimeter of the tailings pile were assigned a mounding rate of 0.12 m/yr. The highest elevation of the simulated mounded brine after 50 years of brine migration was 18 m. The mounding rates were determined from speculation by individuals working at PCS Cory Mine. They were thought to simulate the worst case scenario of brine

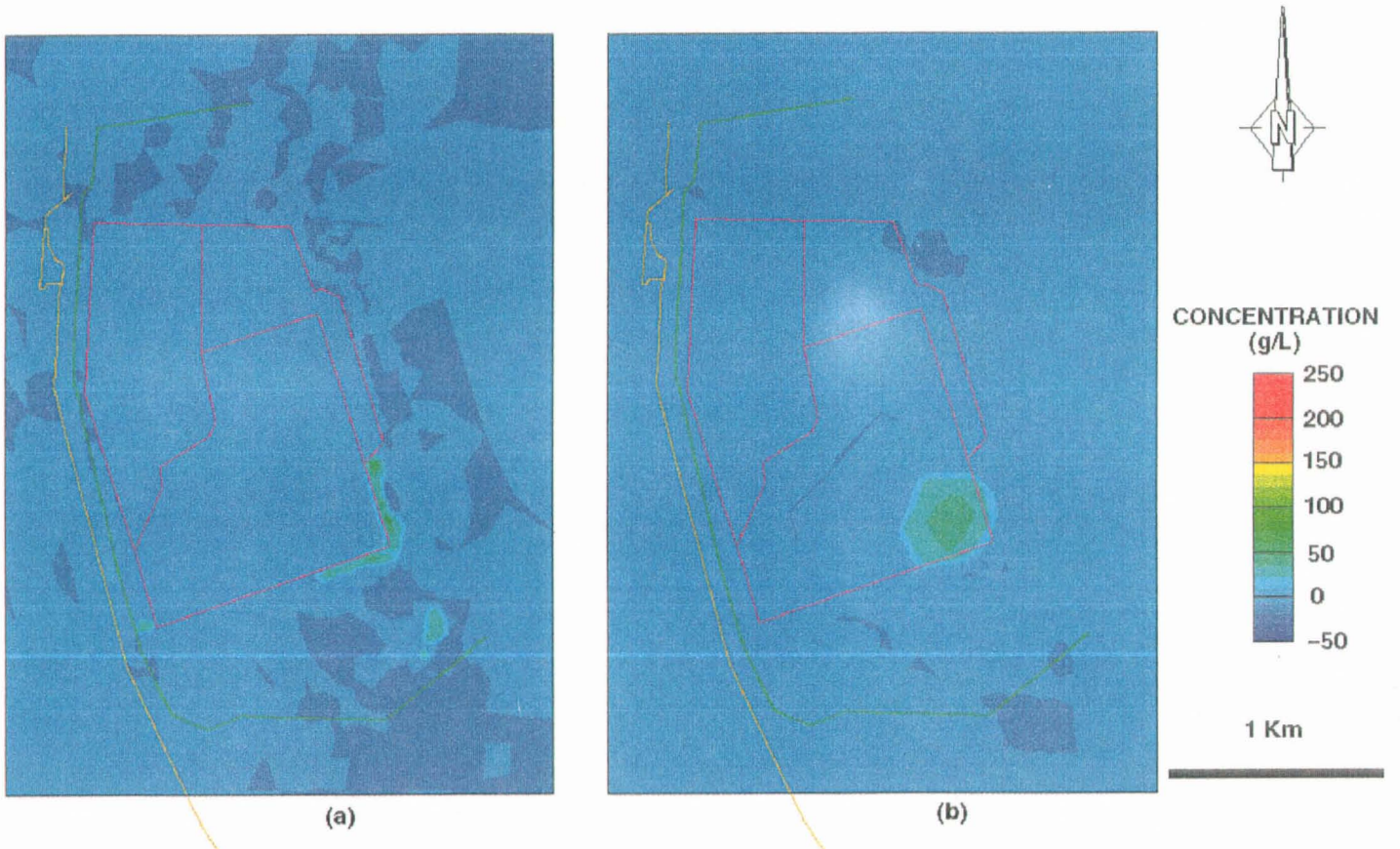

Figure 7.4 - Difference Between the Brine Plume with Brine Mounding and the Base Case Model after 50 Years of simulated Brine Transport in the (a) Surficial Stratified Deposits and (b) Judith River Aquifer.

mounding. All nodes located within the tailings pond and throughout the remainder of the tailings facility maintained a constant hydraulic head of 493 m.

7.4.2.1 Brine Plume in the Surficial Stratified Deposits

The position of the brine plume in the surficial stratified deposits, subjected to brine mounding in the tailings pile is shown in Figures E.1a to E.1d, Appendix E. The difference between the position of the brine plume, subjected to brine mounding and the base case model, after 50 years, is shown in Figure 7.4a. The largest differences in brine plume position were located along the southern perimeter of the tailings pile. The maximum difference in concentration was approximately 4 g/L and was denoted by the light green coloured area.

7.4.2.2 Brine Plume in the Floral Aquifer

The positions of the brine plume infiltrating the Floral Aquifer after 10, 17, 26 and 50 years of brine migration with brine mounding are shown in Figures 7.5a, 7.5b, 7.5c and 7.5d respectively.

The plume position computed within the Floral Aquifer for the year 1979, after 10 years, is shown in Figure 7.5a. An elevated concentration of approximately 60 g/L was found in the southwest region of the aquifer below the tailings facility. The concentration reduced to the northeast of this localized high. The plume was also significant in the Floral Aquifer below the northwest corner of the tailings facility.

The brine plume computed for 1986, after 17 years of brine mounding (Figure 7.5b), indicated that more brine infiltrated into the Floral Aquifer. The region of the aquifer below the tailings pile was almost entirely contaminated. The highest concentration in the aquifer at this time was over 170 g/L. The concentration of the plume in the aquifer below the highest elevations of brine mounding was approximately 40 g/L. Figure 7.5b also shows aquifer contamination resulting from

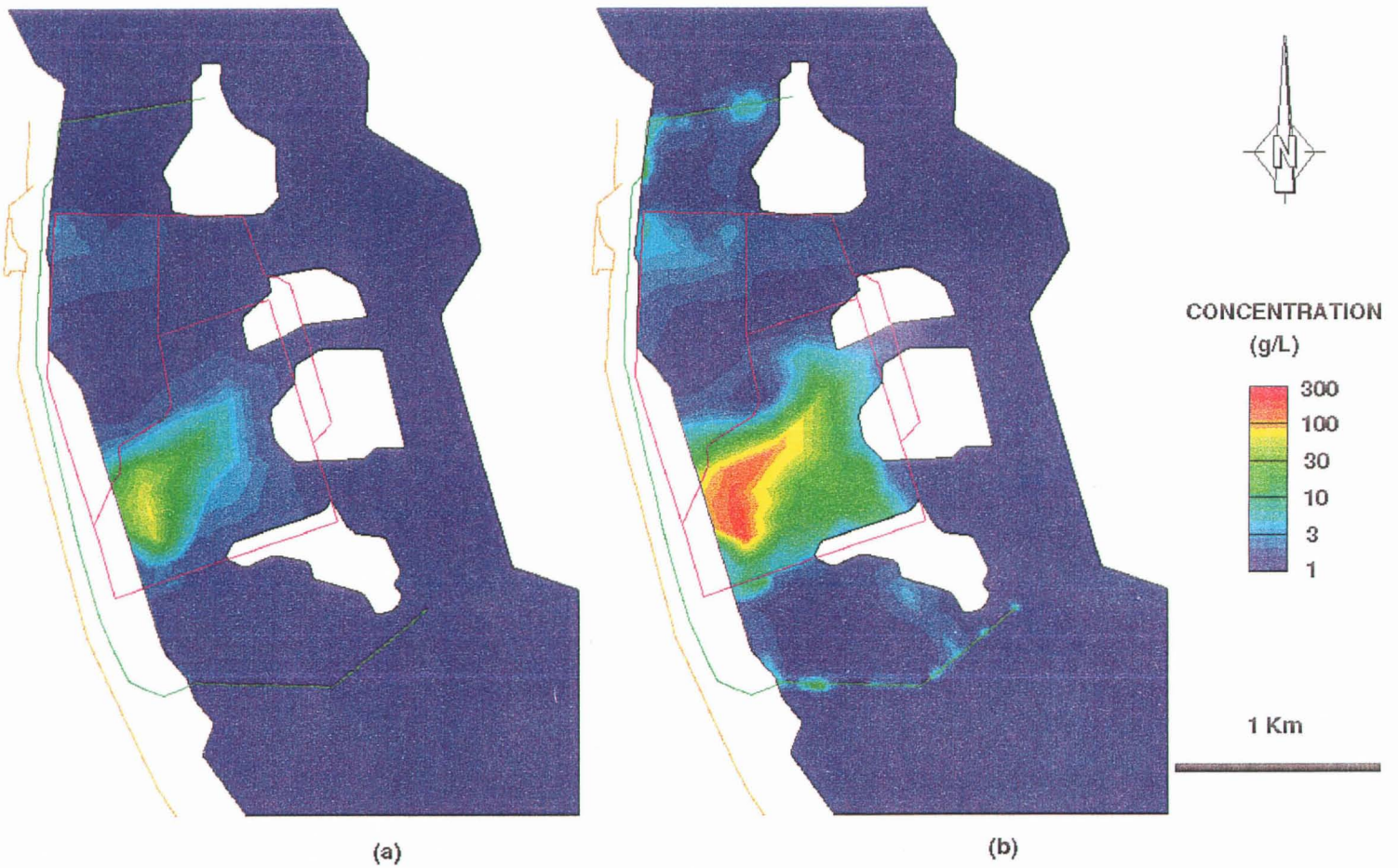

Figure 7.5 - Brine Plume in the Floral Aquifer after (a) 10 years and (b) 17 years of simulated Brine Transport with Brine Mounding in the Tailings Pile

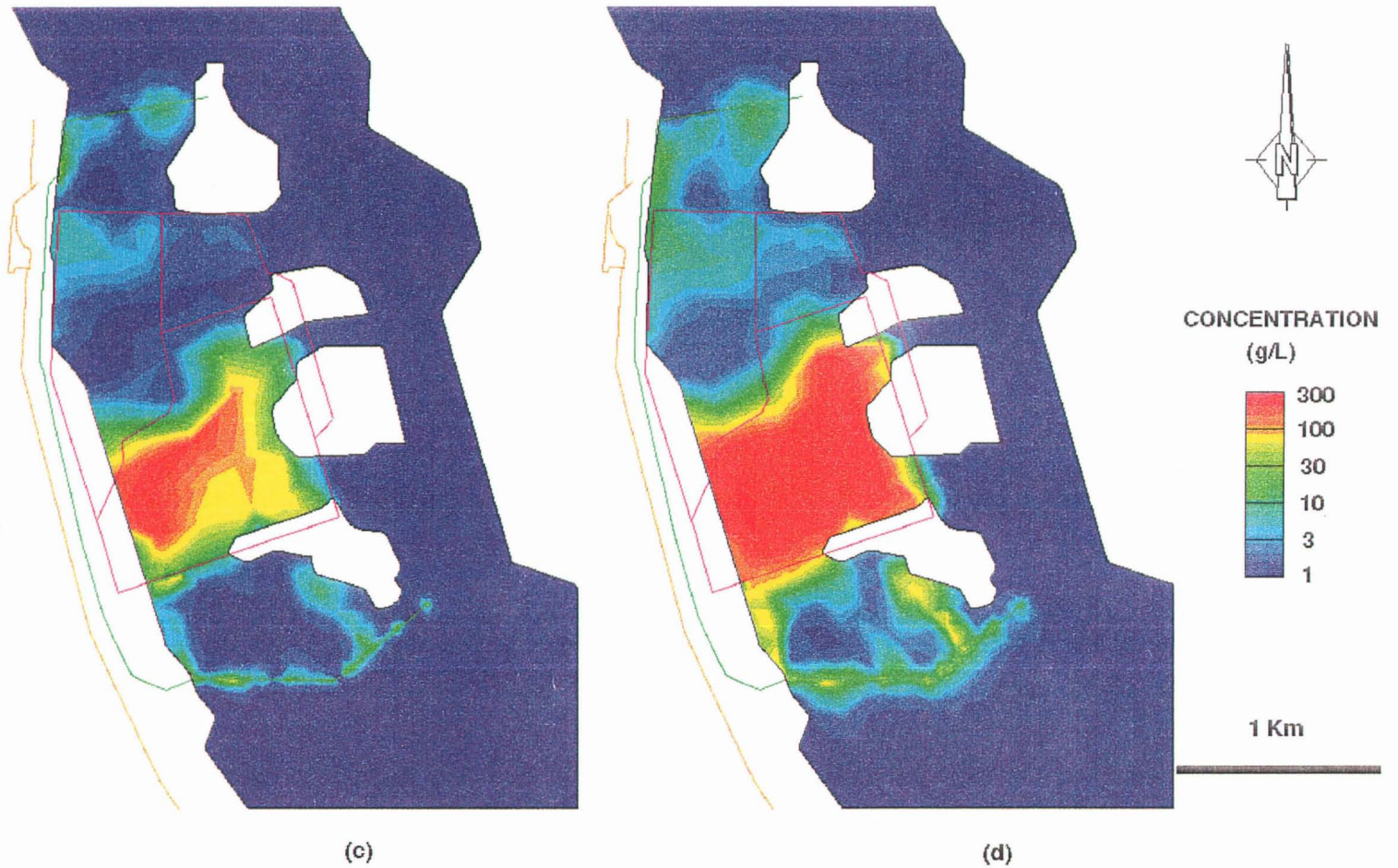

Figure 7.5 - Brine Plume in the Floral Aquifer after (c) 26 years and (d) 50 years of simulated Brine Transport with Brine Mounding in the Tailings Pile

the slurry trench and pond sources.

The brine plume computed in the Floral Aquifer, for the year 1995, after 26 years, is shown in Figure 7.5c. The concentration in the aquifer at this time was over 200 g/L at some locations. The concentration of brine originating from the slurry trench and pond sources also increased in the Floral Aquifer.

The highest brine concentration computed in the Floral Aquifer after 50 years of brine transport with brine mounding was over 275 g/L (Figure 7.5d). Most of the contaminant concentration in the channel aquifer was located below the tailing pile and varied from 60 to 160 g/L. Evidence for increased brine contamination from various containment structures and pond sources are shown in Figure 7.5d.

Differences between the computed position of the brine plume in the Floral Aquifer for the brine mounding and base case model are shown in Figures 7.6a to 7.6d.

After 10 years of brine mounding in the tailings pile, the highest difference in brine concentration within the Floral Aquifer between the brine mounding case and base case model was approximately 50 g/L. The maximum difference was located below the southwest area of the tailings facility. Figure 7.6a also indicated that the concentration over most of the aquifer below the tailings pile computed from the brine mounding sensitivity study was higher than in the base case model.

The difference in the brine plume position and concentration for brine mounding and the base case model, for the year 1986, is shown in Figure 7.6b. The largest concentration difference was nearly 130 g/L and was located below the tailings pile. Again, the extent of brine contamination in the Floral Aquifer was higher than the base case when brine mounding occurred in the tailings pile.

Figures 7.6c and 7.6d show the difference in the brine plume position between the brine mounding and base case model after 26 and 50 years of contaminant transport from the WMA respectively. The maximum difference in brine concentration simulated for the years 1995 and 2019 in the Floral Aquifer were approximately 150 g/L and 190 g/L respectively. Both Figure 7.6c and 7.6d indicate

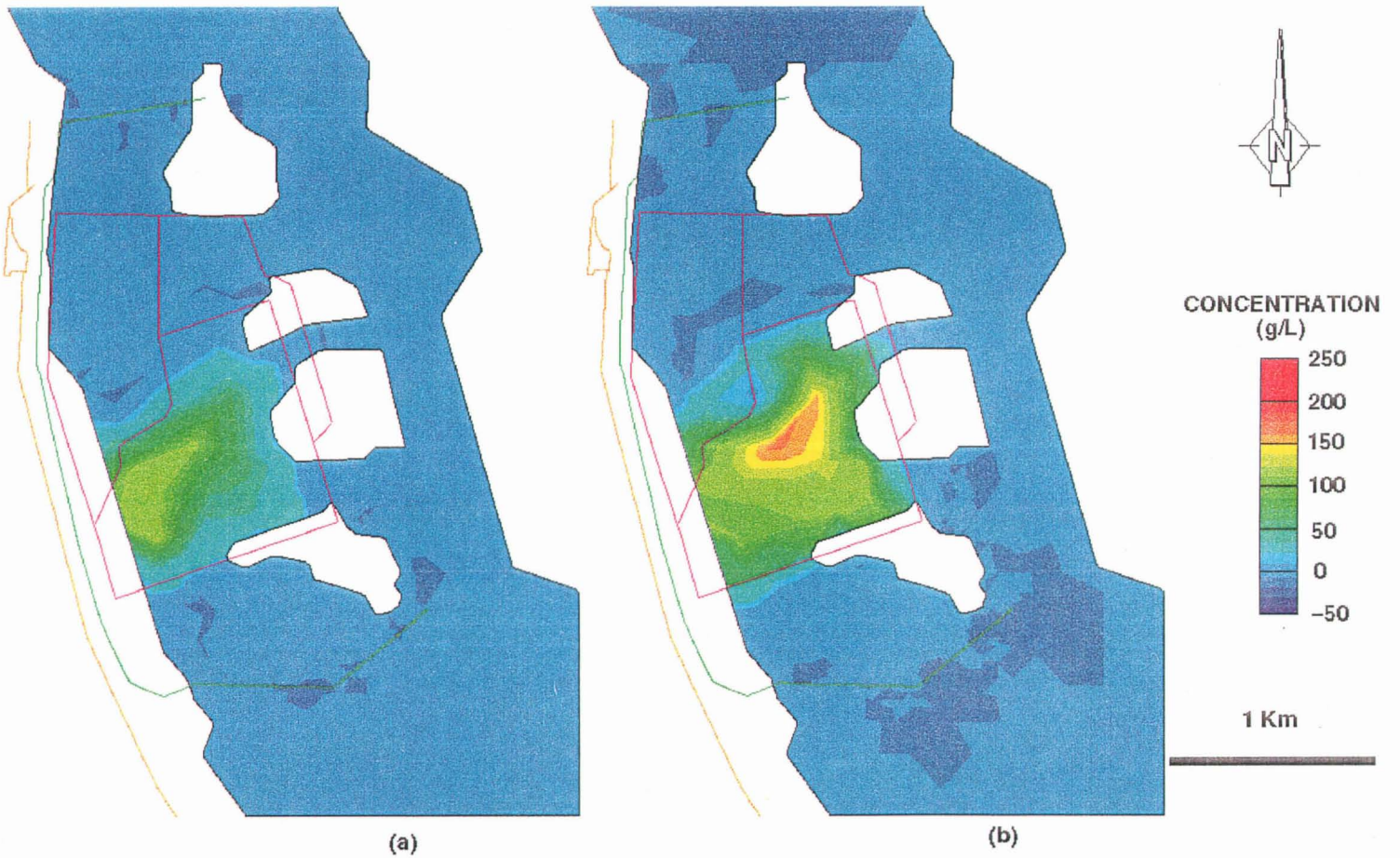

Figure 7.6 - Difference between the Brine Plume Computed from the Brine Mounding and Base Case Model for the Floral Aquifer after (a)10 years and (b) 17 years of simulated Brine Transport

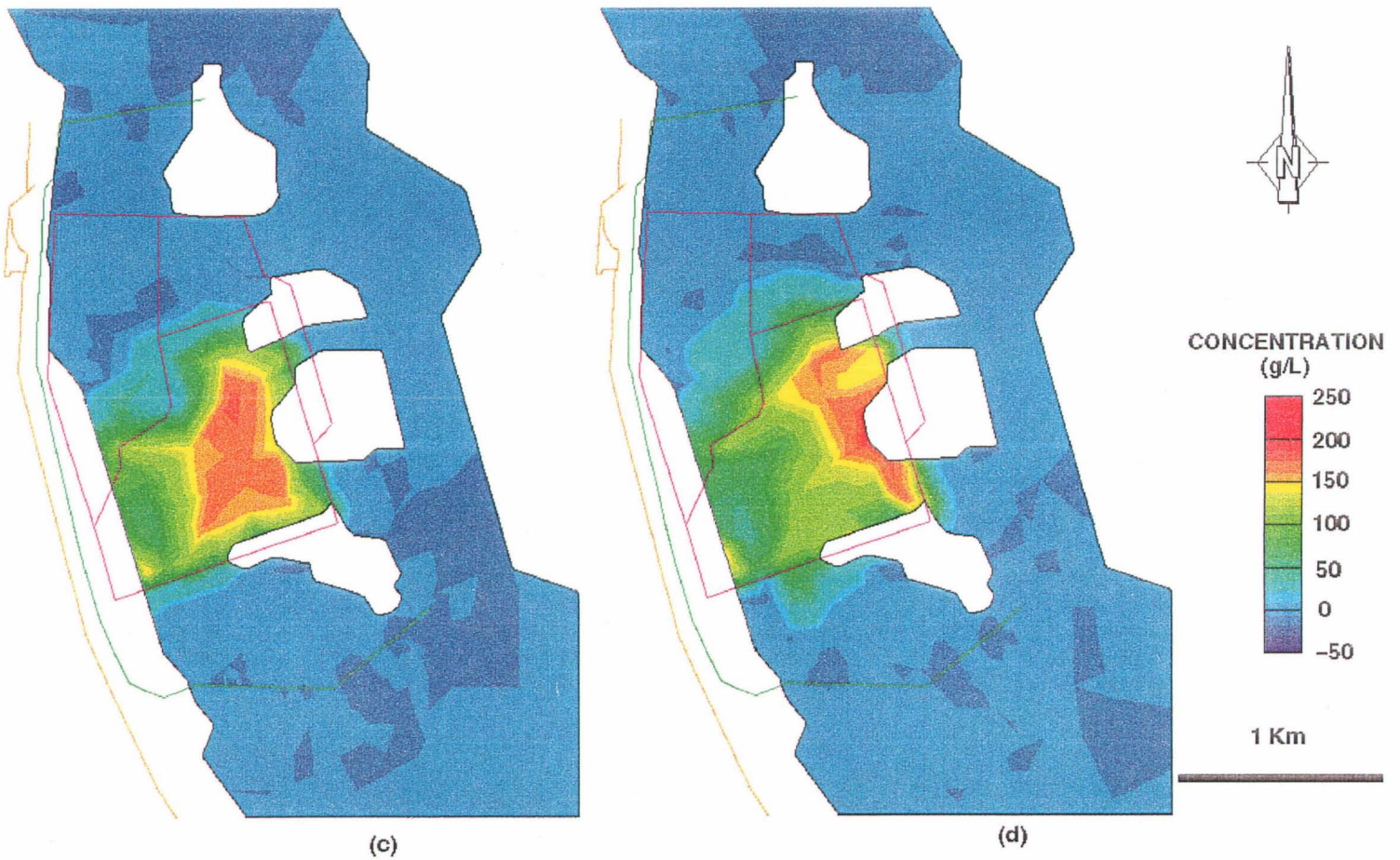

Figure 7.6 - Difference between the Brine Plume Computed from the Brine Mounding and Base Case Model for the Floral Aquifer after (c) 26 years and (d) 50 years of simulated Brine Transport

that when brine mounding occurred, the areal extent of the plume and concentrations in the Floral Aquifer increased.

7.4.2.2.1 Breakthrough Profiles

Logarithmic breakthrough profiles of concentration with time (Figure 7.7) for nodes 14877, 15250 and 15383 in the Floral Aquifer were constructed using the brine mounding values.

The breakthrough curves show that the onset of groundwater contamination in the Floral Aquifer occurred more rapidly in the areas located below the tailings pile. Figure 7.7 also indicated that the concentration of the brine plume in the channel aquifer below the tailings pile was higher than for the rest of the tailings facility. The highest concentration recorded at nodes 14877, 15250 and 15383 after 50 years of simulated brine transport with brine mounding were approximately 3, 203 and 258 g/L respectively. The concentration observed at nodes 15250 and 15383 were considerably higher than the values attained in the base case model (Figure 6.4).

7.4.2.3 Brine Plume in the Judith River Aquifer

The difference in the position and concentration of the brine plume in the Judith River Aquifer computed with brine mounding and the base case model for the year 2019 is shown in Figure 7.4b. The maximum difference in concentration calculated in the aquifer at this time was approximately 4 g/L and was located below the southeast corner of the tailings pile. The maximum concentration of the contaminant in the Judith River Aquifer, after 50 years with brine mounding, was nearly 5.5 g/L (Figure E.2, Appendix E). This was much higher than the 1.5 g/L computed for the base case model.

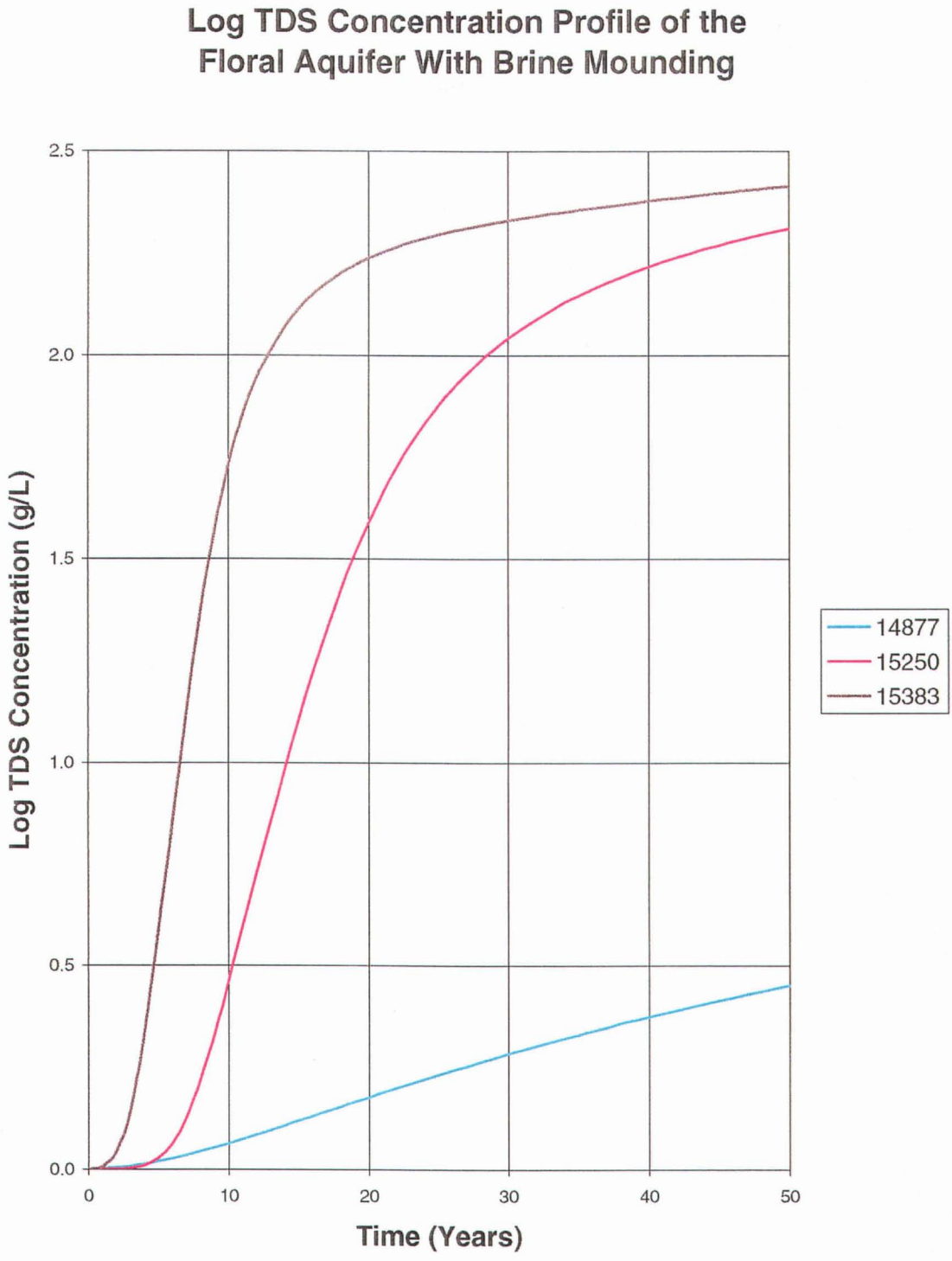

Figure 7.7 - Breakthrough Profiles for the Floral Aquifer when Brine Mounding occurs in the Tailings Pile

7.4.2.4 Cross-Section Results

Figures 7.8a to 7.8d show the position of the brine plume along section A-A' with brine mounding, after 10, 17, 26 and 50 years. Figure E.3, Appendix E shows the position of the brine plume after 50 years of brine mounding for sections B-B', C-C' and D-D'.

After 10 years with brine mounding, the amount of brine migration below the tailings pile increased. The highest concentration in the Floral Aquifer along section A-A' was approximately 3.5 g/L (Figure 7.8a).

The brine plume position in Figure 7.8b shows the concentration along section A-A' for the year 1986. The highest concentration in the Floral Aquifer along this section after 17 years of brine migration with brine mounding was approximately 55 g/L. The plume also migrated into the Sutherland Aquitard attaining a maximum concentration of approximately 10 g/L. Figure 7.8b also showed the radial spread of brine from the hydrated slurry trench.

Figure 7.8c shows the position and concentration of the brine plume, for the year 1995, along section A-A'. By 1995, the maximum concentrations in the Floral Aquifer and underlying Sutherland Aquitard were approximately 125 g/L and 50 g/L respectively.

The computed brine plume position and concentration along section A-A', for the year 2019, is shown in Figure 7.8d. The Floral Aquifer located below the tailings pile was entirely saturated with brine. The highest concentration in the Floral Aquifer is 250 g/L and in underlying Sutherland Aquitard was approximately 160 g/L. The brine plume infiltrated into the Sutherland Aquifer attaining concentrations of approximately 6 g/L.

Figures 7.9a, 7.9b, 7.9c and 7.9d show the difference between the brine plume computed, with brine mounding and the base case along section A-A' for years 1979, 1986, 1995 and 2019 respectively. These figures indicate that the downward rate of brine migration was greater when brine mounding occurred in the tailings pile. Figures 7.9a to 7.9d also shows that downward rate of brine migration

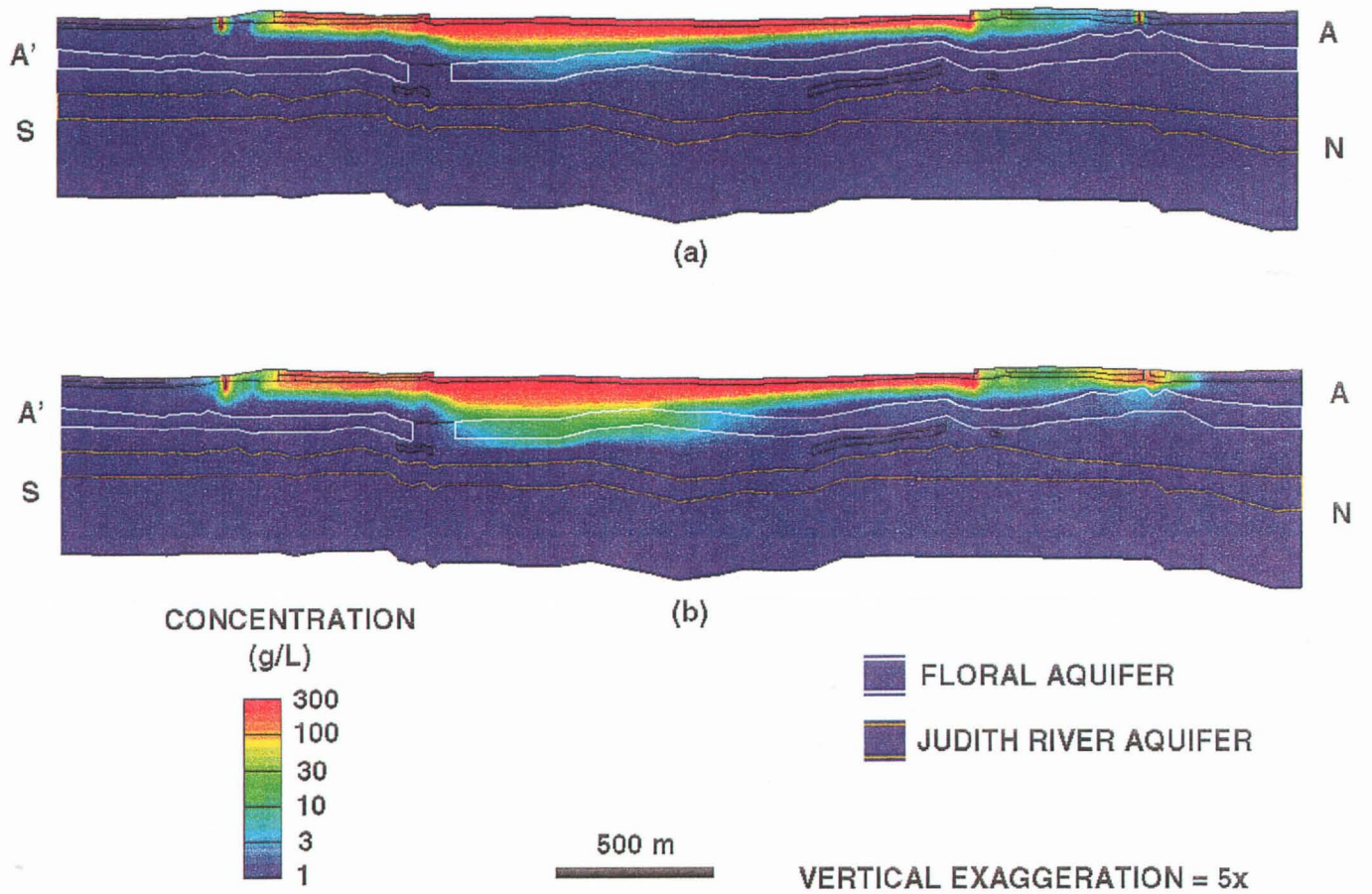

Figure 7.8 - Brine Plume along Section A-A' after (a) 10 years and (b) 17 years of simulated Brine Transport with Brine Mounding within the Tailings Pile

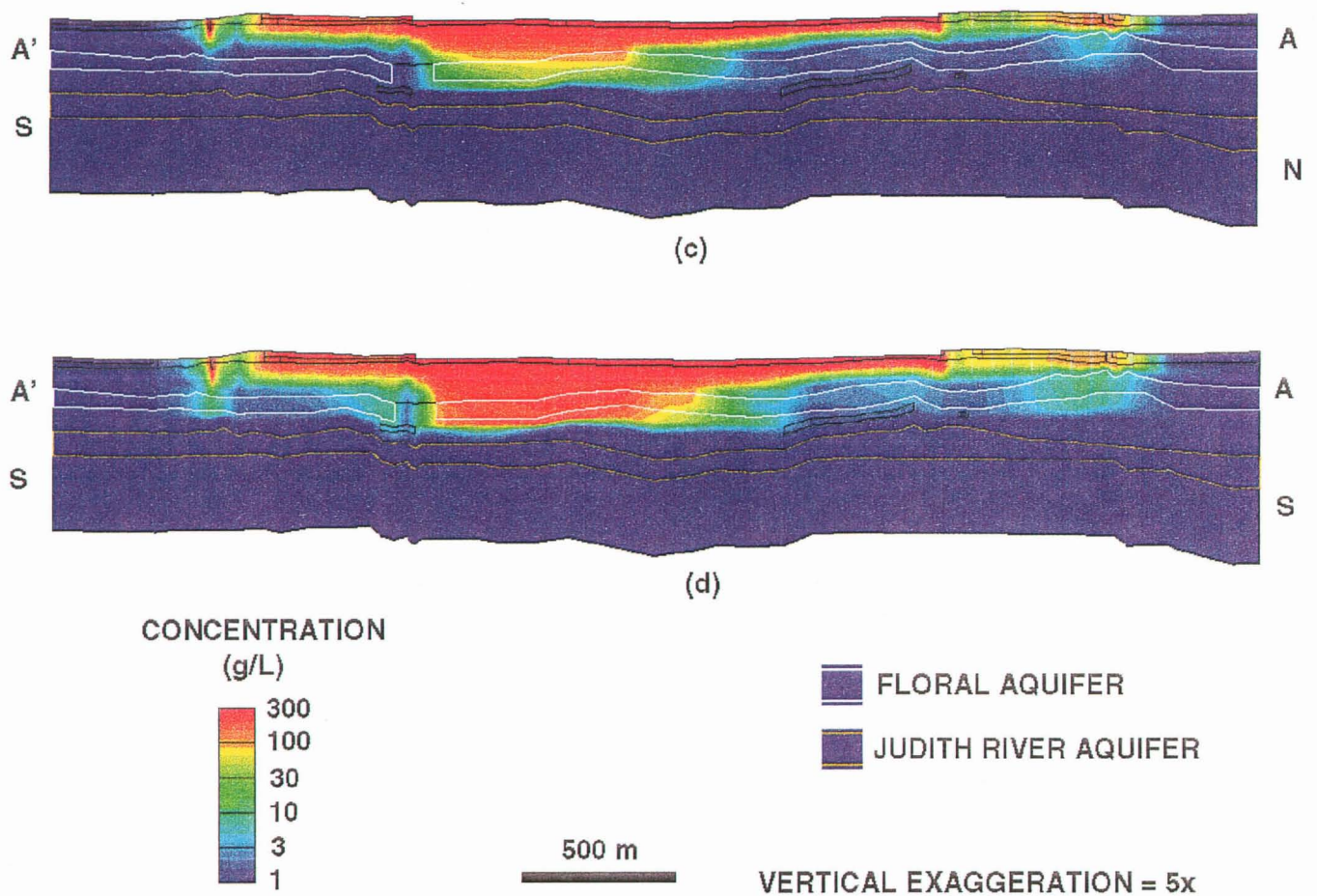

Figure 7.8 - Brine Plume along Section A-A' after (c) 26 years and (d) 50 years of simulated Brine Transport with Brine Mounding within the Tailings Pile

below the mounded brine was greater than the rate below the remainder of the tailings facility. Figure E.4, Appendix E shows the difference in the computed brine plume position for sections B-B', C-C' and D-D' after 50 years of brine transport.

Figures 7.9a and 7.9b indicate that the greatest concentration differences computed for 10 and 17 years of brine migration were in the Floral Aquitard. After 17 years there was also a large concentration contrast computed in the Floral Aquifer. Both Figures 7.9a and 7.9b indicate that the amount of brine in the Floral Aquifer, with brine mounding, was greater than the base case model.

The difference in computed brine plume position for the year 1995, is shown in Figure 7.9c. This figure shows that there was a large concentration difference in both the Floral Aquitard and Floral Aquifer after 26 years of brine migration, with brine mounding. Similarly, Figure 7.9d indicates a large difference in concentration existed after 50 years of contaminant migration.

7.4.3 Brine Mounding Without Containment Structures

Sensitivity runs simulating brine mounding within the tailings pile were carried out for the WMA with no containment structures. The results of these simulations after 50 years are shown in Figure E.5, Appendix E.

The results indicate that the brine plume position in the surficial stratified deposits did not change significantly, when compared to the base case model. The brine plume in the Floral Aquifer was similar to that discussed in Section 7.4.2.2 with the exception that there was no contribution of brine from the containment structures. The concentrations in the Judith River Aquifer obtained from this sensitivity simulation were similar to the computed values in Section 7.4.2.3.

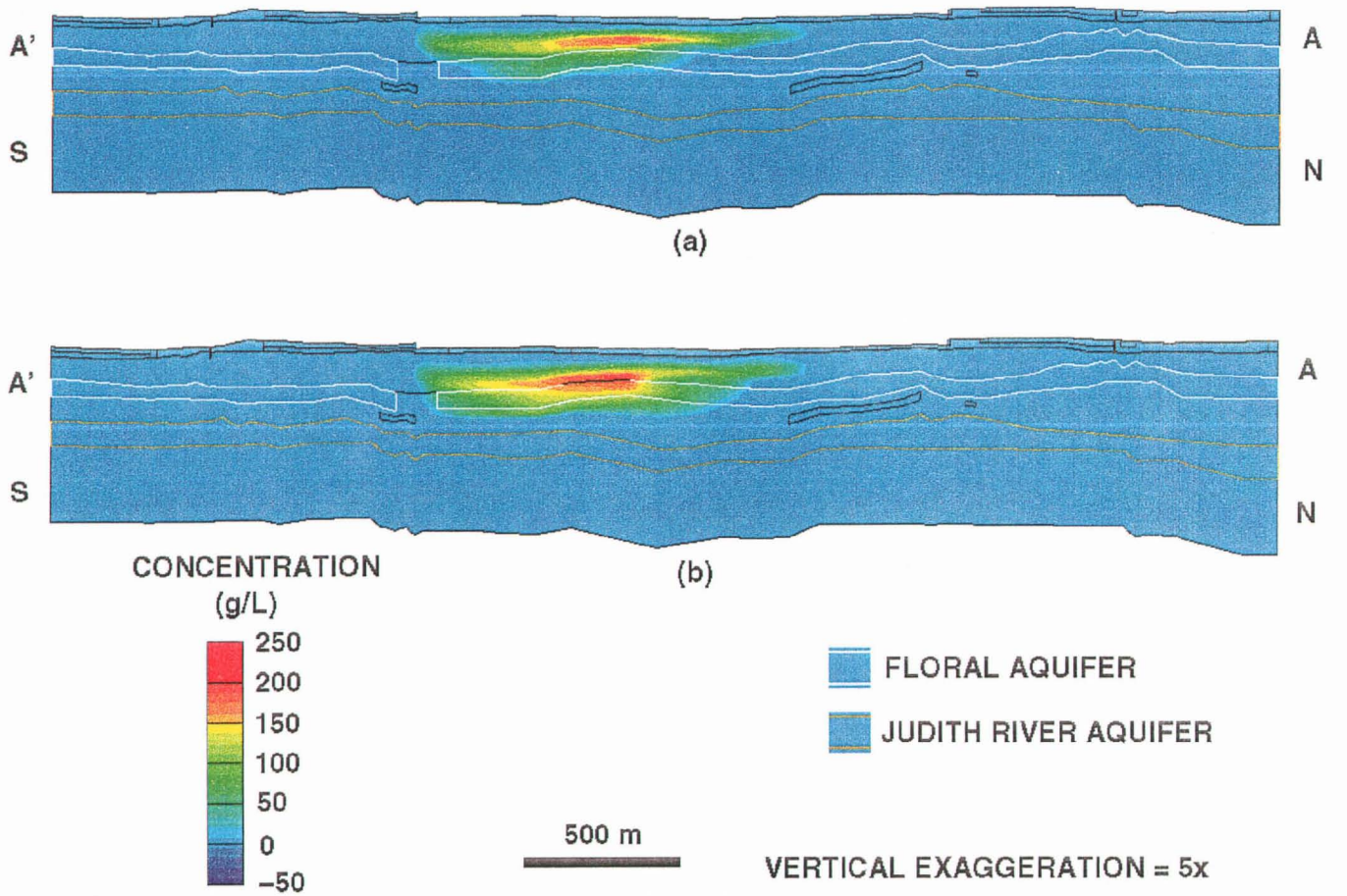

Figure 7.9 - Difference in the Brine Plume along Section A-A' for the Brine Mounding and Base Case Model after (a) 10 years and (b) 17 years of simulated Brine Transport

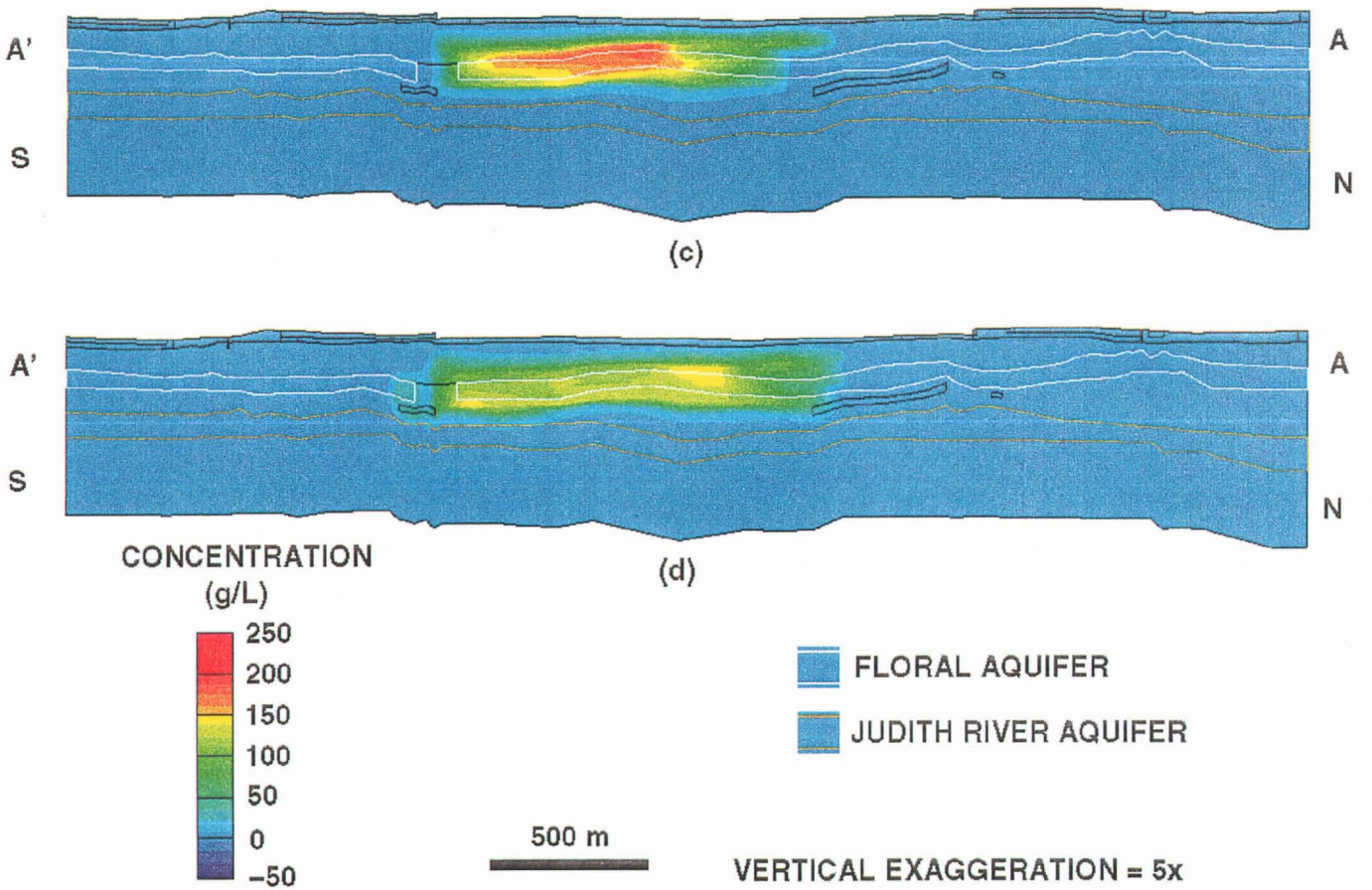

Figure 7.9 - Difference in the Brine Plume along Section A-A' for the Brine Mounding and Base Case Model after (c) 26 years and (d) 50 years of simulated Brine Transport

7.4.4 Varying the Coefficient of Tortuosity

The final set of sensitivity simulations varied the coefficient of tortuosity for the hydrostratigraphic units in the study area. Two sensitivity simulations were performed; one had high coefficients of tortuosity and the other had low coefficients of tortuosity. The coefficients used in the sensitivity study represented the extreme limits for porous media. By using the upper and lower bounds of tortuosity values, the best and worst case scenarios were simulated and analyzed. The coefficient of tortuosity assigned to the slurry trench was the average of those assumed for surficial and consolidated soils. Table 7.1 lists the coefficient of tortuosity values used in the sensitivity analysis.

Table 7.1 - Coefficient of Tortuosity Values Used in the Sensitivity Study

Porous Media Unit	High Coefficient of Tortuosity	Low Coefficient of Tortuosity
Surficial Stratified Deposits		
Sand	1.0000	0.2500
Silt	1.0000	0.2500
Clay	1.0000	0.2500
Floral Aquitard	0.5	0.125
Riddell Aquifer	0.5	0.125
Floral Aquifer	0.5	0.125
Sutherland Aquifer	0.5	0.125
Sutherland Aquitard	0.5	0.125
Tyner Valley Aquifer - High K	0.5	0.125
Tyner Valley Aquifer - Low K	0.5	0.125
Judith River Aquifer	0.5	0.125
Lea Park Aquitard	0.5	0.125
Slurry Trench	0.75	0.1875

The calculated brine plume in the surficial stratified deposits, Floral Aquifer and in vertical section (Figures E.6 to E.8, Appendix E) after 50 years of brine transport using high and low coefficients of tortuosity were fairly similar. Figure 7.10 illustrates the difference in the computed brine plume position using the high and low coefficient of tortuosity values. The figure indicates that changing the coefficient of tortuosity of the soil had little affect on the position and concentration of the brine plume for the year 2019, after 50 years. Section A-A' (Figure 7.11) indicated that the largest difference in brine plume concentration after 50 years of contaminant transport was in the vertical direction. The maximum concentration difference between the high and low coefficient of tortuosity values was less than 30 g/L. This was computed only at a few nodes directly below the tailings facility.

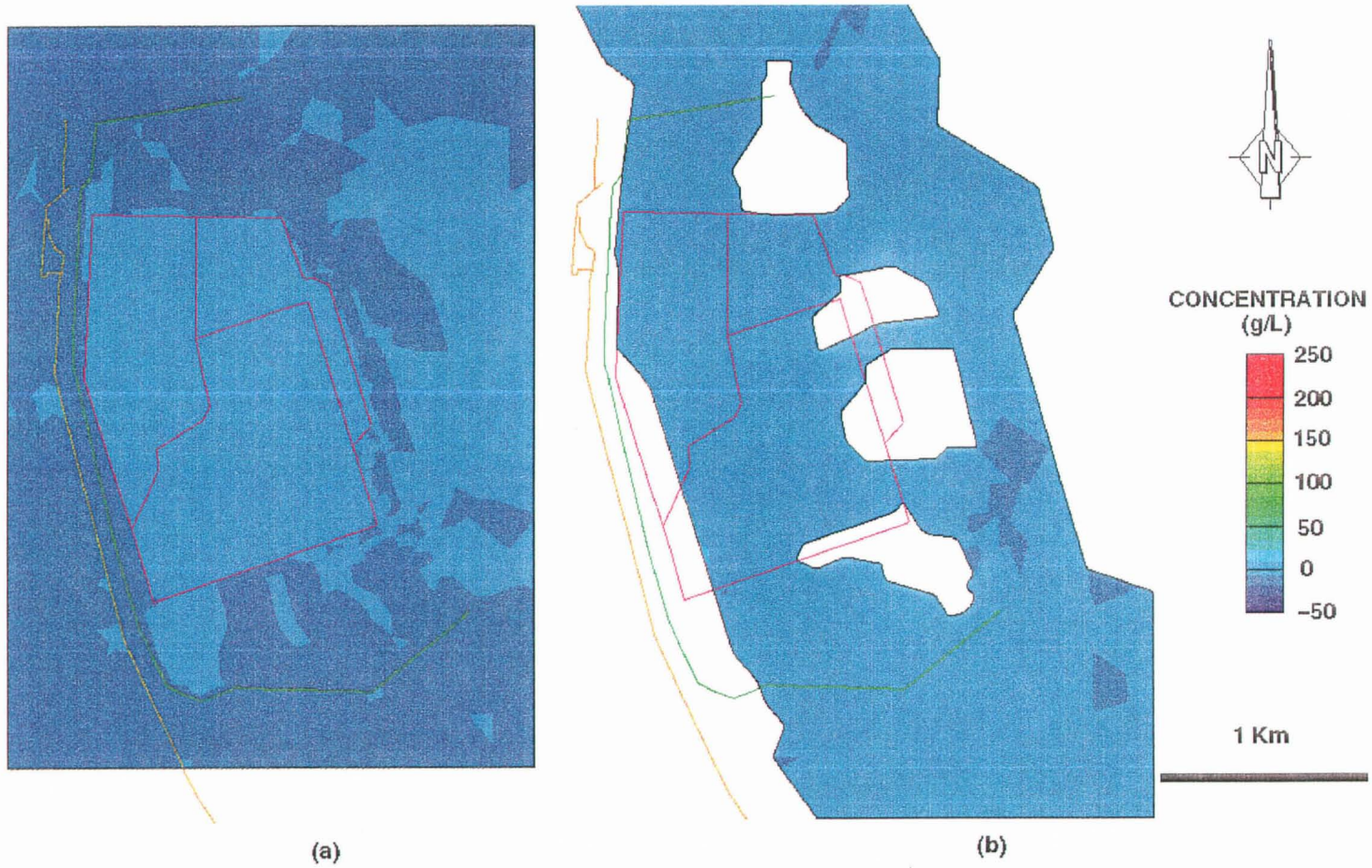

Figure 7.10 - Difference in the Brine Plume Concentration computed in the (a) Surficial Stratified Deposits and (b) Floral Aquifer for the High and Low Tortuosity Cases after 50 years of simulated Brine Transport

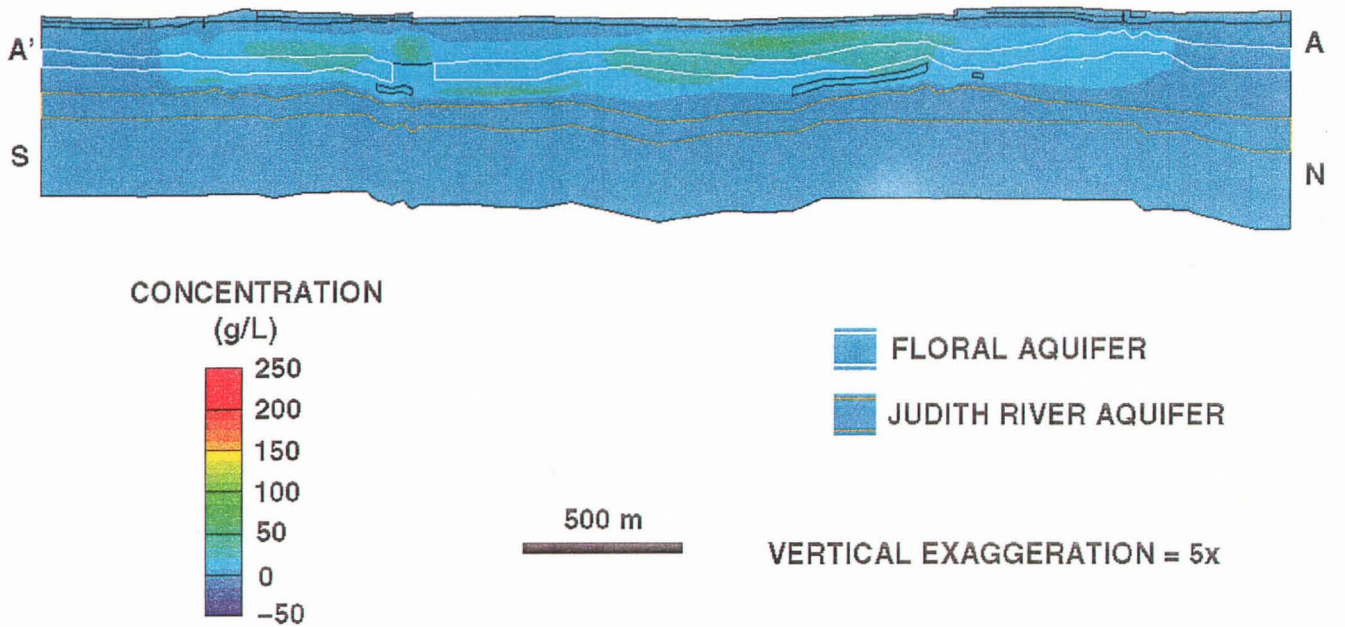

Figure 7.11 - Difference in the Brine Plume Concentration computed along Section A-A' for the High and Low Tortuosity Cases after 50 years of simulated Brine Transport

CHAPTER 8

SUMMARY AND CONCLUSION

A site-specific investigation of brine migration in the vicinity of PCS Cory Mine located southwest of Saskatoon, Saskatchewan, Canada was conducted using FEMWATER, a variable density groundwater flow and solute transport numerical code. The primary objective of this numerical study was to simulate long term brine migration from the PCS Cory Mine WMA in order to assist with the environmental impact assessment evaluation of brine contamination.

The specific project objectives, listed in Section 1.1, Chapter 1, were met in this study. A 3-D hydrogeological conceptual model representing the groundwater flow system and solute transport mechanisms at PCS Cory Mine and surrounding area was developed (Chapters 2 and 3). This conceptual model was then transformed into a mathematical model that numerical simulated the flow and transport regime of the study area (Chapter 4).

The steady-state groundwater flow system computed by the numerical model was calibrated using available hydrogeological data, results from regional groundwater flow studies and direct observations of the brine plume at the mine site (Chapter 5). Following model calibration, 50 years of transient brine migration at the WMA was simulated using FEMWATER (Chapter 6). The effectiveness of existing engineered containment structures at impeding brine plume migration was investigated in detail (Chapter 7). Sensitivity analyses were also performed to determine the limitations of the numerical study (Chapter 7).

8.1 Hydrostratigraphy

Geological information was extracted from numerous drillholes and geophysical logs obtained for the study area. Porous media having similar physical and chemical properties were combined to form a 3-D hydrostratigraphic conceptual

model required for the numerical study. The hydrostratigraphic units identified in the study area were, in ascending order:

1. Lea Park Aquitard;
2. Tyner Valley Aquifer System which included the;
    - Judith River Aquifer, and
    - Tyner Valley Aquifer,
3. Sutherland Aquitard;
4. Sutherland Aquifer;
5. Floral Aquifer;
6. Riddell Aquifer;
7. Floral Aquitard; and
8. Surficial Aquifer and Surficial Aquitard.

8.2 Site-specific Groundwater Flow Model

A finite element numerical mesh was constructed from the 3-D hydrostratigraphic conceptual model using the graphical interface, GMS. The numerical mesh used to simulate groundwater flow and transport in the vicinity of PCS Cory Mine consisted of 44,673 nodes and 84,058 elements. A total of 18 layers were constructed.

8.2.1 Calibrated Steady-State Groundwater Flow Model

The steady-state groundwater flow model was calibrated using a trial and error process. This process involved matching the simulated hydraulic heads, within ±2.47 m, with the water levels measured from numerous monitoring wells in the study area. Hydraulic conductivity, infiltration and brine pond elevation were systemically altered until the flow model was calibrated. The mean error (ME), mean absolute error (MAE) and root mean square error (RMS) were computed at

the end of each calibration run. The calibrated hydraulic conductivities used in the numerical study are listed in Table 8.1.

Table 8.1 - Calibrated Hydraulic Conductivity

Hydrostratigraphic Unit	Kh (m/s)	Kz (m/s)	Kh (m/yr)	Kz (m/yr)
Surficial Stratified Deposits				
Sand	3.00×10^{-4}	6.00×10^{-5}	9.46×10^{3}	1.89×10^{3}
Silt	3.06×10^{-6}	6.11×10^{-7}	9.64×10^{1}	1.93×10^{1}
Clay	3.06×10^{-9}	3.06×10^{-9}	9.64×10^{-2}	9.64×10^{-2}
Floral Aquitard	6.96×10^{-9}	3.06×10^{-8}	5.34×10^{-1}	9.64×10^{-1}
Riddell Aquifer	5.00×10^{-5}	6.85×10^{-6}	1.58×10^{3}	5.26×10^{2}
Floral Aquifer	1.08×10^{-4}	1.48×10^{-5}	3.42×10^{3}	1.14×10^{3}
Sutherland Aquifer	2.00×10^{-4}	6.67×10^{-5}	6.31×10^{3}	2.10×10^{3}
Sutherland Aquitard	7.00×10^{-11}	7.17×10^{-12}	2.21×10^{-3}	2.21×10^{-4}
Tyner Valley Aquifer - High K	8.33×10^{-6}	2.78×10^{-6}	2.63×10^{2}	8.76×10^{1}
Tyner Valley Aquifer - Low K	2.08×10^{-8}	2.08×10^{-9}	6.57×10^{-1}	6.57×10^{-2}
Judith River Aquifer	5.00×10^{-6}	1.67×10^{-6}	1.58×10^{2}	5.26×10^{1}
Lea Park Aquitard	8.33×10^{-12}	8.33×10^{-12}	2.63×10^{-4}	2.63×10^{-4}

8.2.1.1 Tyner Valley Aquifer System

Analysis of the calibrated steady-state flow model provided information about the groundwater flow velocity within the study area. Most groundwater flow in the Judith River Aquifer north of the mine recharged the Tyner Valley Aquifer while flow in the south discharged in the South Saskatchewan River. Flow in the Judith River Aquifer was recharged by the Floral Aquifer near the eastern perimeter of the study area. Groundwater flow in the Tyner Valley Aquifer was significantly affected by a permeability reduction near Grandora. This reduction in the Tyner Valley channel caused the development of artesian conditions in the aquifer within the vicinity of

PCS Cory Mine. The magnitude of groundwater flow velocities in the Judith River and Tyner Valley Aquifer varied from $3x10^{-2}$ m/yr to 1 m/yr and $4x10^{-4}$ m/yr to $4x10^{-1}$ m/yr respectively.

8.2.1.2 Floral Aquifer

Groundwater flow in the Floral Aquifer discharged in the South Saskatchewan River. The magnitude of the flow velocity varied from $6x10^{-1}$ m/yr to 9 m/yr. Localized areas below the WMA had flow rates as high as 28 m/yr.

8.2.1.3 Surficial Aquifer

The majority of groundwater flow in the surficial stratified deposits was directed towards the central meltwater channel in the study area (Figure 1.5). There appeared to be a groundwater divide in the surficial stratified deposits parallel to the central meltwater channel. Groundwater in the surficial stratified deposits reaching the central meltwater discharged in the South Saskatchewan River Valley. The magnitude of groundwater flow velocities in the surficial stratified deposits were highly variable. The flow velocity in the Surficial Aquitard varied from approximately $9x10^{-6}$ m/yr to $9x10^{-4}$ m/yr, while in the Surficial Aquifer it ranged from $9x10^{-3}$ m/yr to 28 m/yr.

8.3 Base Case Transient Transport Model

The following section refers to the base case model where brine mounding was not included but all engineering structures were present.

8.3.1 Surficial Stratified Deposits

The positions of the brine plume at the WMA were analyzed for the years

1979, 1986, 1995 and 2019. The brine plume calculated after 50 years of simulated brine migration showed that in the surficial stratified deposits the plume had spread past the freshwater bypass ditch. The brine plume originating from the flood containment pond, slime storage facility, pond sources and the slurry trench also advanced radially.

8.3.2 Floral Aquifer

The brine plume within the Floral Aquifer spread and its concentration increased with time. After 10, 17, 26 and 50 years of brine migration, the maximum concentrations in the channel aquifer originating from the tailings facility were approximately 4, 13, 80 and 128 g/L respectively. Brine originating from the surficial pond sources, hydrated slurry trench, flood containment pond and slime storage facility also contributed to the brine plume in the Floral Aquifer.

8.3.3 Judith River Aquifer

The concentration calculated for the year 2019, after 50 years, in the Judith River Aquifer below the WMA was marginally greater than native groundwater (1g/L). The maximum concentration simulated in the Judith River Aquifer was under 1.5 g/L.

8.3.4 Cross-Section Results

Characteristics of the brine plume in the vertical direction were observed along cross-sections through the WMA. These cross-sections indicated after 50 years of brine migration the plume had infiltrated the Sutherland Aquitard and the Sutherland Aquifer.

8.4 Sensitivity Analysis

Numerous sensitivity runs were conducted. Few sensitivity runs were performed on the steady-state flow model since an earlier, detailed sensitivity analysis was performed on the regional groundwater flow system that included the study area.

Sensitivity simulations varied the time step used to simulate 50 years of brine migration. Results indicated that reducing the time step from 12 months, to 4 months, to 2 months and finally 1 month only slightly reduced the mean and standard deviations of the calculated concentrations. This analysis indicated that results were generally insensitive to the time step used. A 1 month time step was used to simulate the 50 years of brine migration in the base case model.

Sensitivity simulations were performed to compare the position and concentration of the brine plume calculated from a simulation without containment structures, to the results obtained from the base case model. Analysis indicated that the slurry trench had little effect on the attenuation brine migration in the surficial stratified deposits. Analysis also indicated that hydrating the slurry trench with brine created a contaminant source that contributed to the advancement of the brine plume in the surficial stratified deposits and also the extent of groundwater contamination in the Floral Aquifer. The flood containment pond and slimes storage facility, installed in 1995, also contributed to the advancement of the brine plume in the surficial stratified deposits and the Floral Aquifer.

The effect of brine mounding within the tailing pile was also analyzed. Comparing the computed brine plumes indicated that there was little difference in the surficial stratified deposits, however there was significant differences in the Floral Aquifer. The maximum concentration in the Floral Aquifer, when subjected to 50 years of brine mounding within the tailings pile, was over 275 g/L (compared to 128 g/L without mounding). Almost all of the Floral Aquifer below the tailings pile, after 50 years, was contaminated with dense brine when mounding was included. After 50 years the concentration of most of the groundwater in the Floral Aquifer

(away from the mounded core) was less than seawater (35 g/L). The maximum concentration in the Judith River Aquifer after 50 years, with brine mounding, was approximately 4 g/L (compared with 1.5 g/L in the base case model).

Brine mounding studies were also performed without containment structures. The results were compared with the base case model and also the previous sensitivity studies simulating brine mounding in the WMA. Analysis of the compared results confirmed that the slurry trench had little effect on preventing the spread of brine in the surficial stratified deposits. The results also indicated that brine mounding in the tailings pile increased the downward rate of brine migration.

The final sensitivity runs involved changing of the coefficient of tortuosity of the aquifer and aquitard units. The results indicated that varying the coefficient of tortuosity had relatively little effect on the characteristics of the brine plume.

8.5 Future Work

Outlined below are a number of areas where additional research could be conducted.

8.5.1 Hydrostratigraphy of the PCS Cory Mine WMA

1. The hydrogeology of the surficial stratified deposits within the vicinity of the WMA should be mapped in detail. Detailed hydrostratigraphic information about the surficial soils will increase the reliability of computed brine plume.

2. Fluid levels in the monitoring wells at PCS Cory Mine should be remeasured and water samples taken. This data will provide information about the environmental hydraulic head and also the position and concentration of the brine plume. This will also assist with the calibration of subsequent groundwater flow and contaminant transport models.

3. Further investigation of the Floral Aquitard in the vicinity of the mine should be conducted to establish the extent of possible fracturing on the position of the brine plume. This information will assist in the characterization of the Floral Aquitard in model studies.

4. Inclined drilling and installation of monitoring wells should be completed in the Floral Aquifer to help determine the extent of the brine plume in the channel aquifer beneath the tailings pile. This will help determine if brine mounding is present in the tailings pile. The recommended localities for inclined drilling are near the northern perimeter and also the southwestern and southeastern regions of the tailings facility.

8.5.2 Additional Numerical Modelling

1. The concentration of the pond sources, flood containment facility and slimes storage area used in the numerical model should be altered to match the concentration determined from systematic conductivity measurements.

2. Sensitivity to changes in the longitudinal and transverse dispersivity should be investigated to determine how it affects the simulated brine plume.

3. Changes to the boundary conditions along the western perimeter of the Tyner Valley Aquifer System should be reviewed in order to better fit the observed groundwater flow system.

4. The calibrated steady-state and transient flow and transport models should be recalibrated as more information regarding position and concentration of the brine plume is obtained.

5. As computer systems become more powerful and are able to model sophisticated problems, the numerical mesh should be refined in the vertical direction, directly below and within the vicinity of the WMA. Refining the mesh in this manner will reduce numerically induced dispersion and also provide more detailed information about the vertical migration of the brine plume.

REFERENCES

AGRA Earth and Environmental and Saskatchewan Research Council, 1996. Potash Corporation of Saskatchewan, Inc. Cory Mine Division, Regional Geological and Hydrogeological Framework, Saskatoon.

Anderson, M.P., and Woessner, W.W., 1992. Applied Groundwater Modeling: Simulation of Flow and Advective Transport. Toronto, Academic Press, Inc., 381pp.

Arun, B.G., 1994. Control of brine migration with used of vertical barriers: a computer simulated study. MSc. Thesis, University of Saskatchewan.

Bachu, S., 1995. Flow of variable-density formation water in deep sloping aquifers: review of methods of representation with case studies. Journal of Hydrology, **164**, 19-38.

Barbour, S.L., 1990. The impact of sodium-chloride solutions on the geotechnical properties of clay soils: a review of clay-brine interactions: Saskatoon, Saskatchewan, 172 p.

Barbour, S.L., 1997. Personal Communication. University of Saskatchewan, Saskatoon, Saskatchewan

Barbour, S.L., and Fredlund, G., 1989. Mechanisms of osmotic flow and volume change in clay soils. Canadian Geotechnical Journal, **26**, 551-562.

Barbour, S.L., and Yang, N., 1993. A review of the influence of clay-brine interactions on the geotechnical properties of Ca-montmorillonitic clayey soils from Western Canada. Canadian Geotechnical Journal, **30**, 1167-117.

Bear, J., 1972. Dynamics of Fluids in Porous Media. New York, American Elsevier Publishing Company, Inc., 764 p.

Bear, J., and Verruijt, A., 1987. Modeling groundwater flow and pollution: with computer programs for some cases. Boston, Kluwer Academic Press, 414 p.

Bell, F.D., 1993. Engineering Geology. Don Mills, Oxford University Press, 359 p.

Domenico, P.A., and Schwartz, F.W., 1990. Physical and Chemical Hydrogeology: Toronto, John Wiley and Sons, 824 p.

Elder, J.W., 1967. Transient convection in a porous medium. Journal of Fluid Mechanics, **27** (3), 609-623.

Engineering Computer Graphics Laboratory (ECGL), 1996. The Department of Defense Groundwater Modeling System: Reference Manual. Brigham Young University, Provo, Utah.

Eyles, N., 1983. Glacial Geology, An Introduction for Engineers and Earth Scientists: Toronto, Pergamon Press, 409 p.

Fetter, C.W., 1992. Contaminant Hydrogeology: Toronto, Maxwell Macmillan Canada, 458 p.

Fortin, G., van der Kamp, G., and Cherry, J.A., 1989. Hydrology and hydrochemistry of an aquifer-aquitard system within the glacial drift, Saskatchewan, Canada. Saskatchewan Research Council.

Frind, E.O., 1982. Simulation of long-term transient density-dependent transport in groundwater. Advanced Water Resources, **5**, 73-78.

Freeze, R.A., and Cherry, J.A., 1979. Groundwater: Toronto, Prentice-Hall of Canada, Ltd., 604 p.

Golder Associates, 1996. Regional groundwater flow and solute transport modelling: PCS Cory. Technical Supporting Document in Support of Decommissioning Plan #962-6400.

Haug, M.D., Barbour, S.L., and Longval, P., 1988. Design and construction of a prehydrated sand-bentonite liner to contain brine. Canadian Journal of Civil Engineering, **15** (6), 955-963.

Henry, H.R., 1964. Effects of dispersion on salt encroachment in coastal aquifers. United States Geological Survey Water Supply Paper, 1613-C, C71-C84.

Ho, Y.A., Pufahl, D.E., and Barbour, S.L., 1989. The effects of brine contamination on volume change behavior of fine grained soils. 42nd Canadian Geotechnical Conference, 272-279.

Holtz, R.D., and Kovacs, W.D., 1981. An Introduction to Geotechnical Engineering: Toronto, Prentice-Hall of Canada, Ltd., 733 p.

Hubbert, M.K., 1940. Theory of ground water motion. Journal of Geology, **48**, 785-944.

Huyakorn, P.S., and Taylor, C., 1983. Finite element models for coupled groundwater flow and convective dispersion. In: Finite Elements in Water Resources, 1.131-1.151.

INTERA, 1979. Revision of the documentation for a model for calculating effects of liquid waste disposal in deep saline aquifers. U.S. Geological Survey, Water Resources Investment, Rep.79-96, 73 p.

Istok, J., 1989. Groundwater Modeling by the Finite Element Method: Water Resources Monograph 13. Washington, American Geophysical Union, 495 p.

Karvonen, A., 1997. Numerical Modelling of the regional groundwater system in the west Saskatoon District. MSc. Thesis, University of Saskatchewan.

Keller, C.K., van der Kamp, G., and Cherry, J.A., 1989. A multi-scale study of permeability of thick clayey till. Water Resources Research, **25**, (11), 2299-2317.

Keller, C.K., van der Kamp, G., and Cherry, J.A., 1988. Hydrogeology of two Saskatchewan tills, I. fractures, bulk permeability, and spatial variability of downward flow. Journal of Hydrology, **101**, 97-121.

Keller, C.K., van der Kamp, G., and Cherry, J.A., 1986. Fracture permeability and groundwater flow in clayey till near Saskatoon, Saskatchewan. Canadian Geotechnical Journal, **23**, 229-240.

Kestin, J., Khalifa, H.E., and Correia, R.J., 1981. Tables of the dynamic and kinematic viscosity of aqueous NaCl solutions in the temperature range 20-150 °C and the pressure range 0.1-35 MPa., Journal of Physical and Chemical Reference Data, **10** (1), 71-87.

Lin, H-C.J., Richards, D.R., Yeh, G-T., and Jones, N.L., 1996. FEMWATER: A three dimensional finite element computer model for simulating density driven flow and transport. Technical Report HL-95. Brigham Young University.

Lennox, D.H., Maathuis, H., and Pederson, D., 1988. Region 13, Western Glaciated Plains. In Hydrogeology Vol, O-2, The Geology of North America, Geological Society of America, p. 115 - 128.

Lusczynski, N.J., 1961. Head and flow of ground water of variable density. Journal of Geophysical Research, **66** (12), 4247-4256.

Maathuis, H., and van der Kamp, G., 1994. Prediction of brine movement. Volume II: modelling and sand-tank experiments. Saskatchewan Research Council and National Hydrology Research Institute, Publication R-1220-6-C-95. 71p.

Maathuis, H., and van der Kamp, G., 1984. Theory of groundwater flow in the vicinity of brine ponds and salt tailings piles. SRC Technical Report No. 152, 39p.

Maathuis, H., van der Kamp, G., Campbell, J., and Schreiner, B., 1994. Prediction of brine movement. Volume I: Hydrogeology of the PCS Cory Division potash waste storage facility and region. Saskatchewan Research Council and National Hydrology Research Institute, Publication R-1220-6-C-95. 74p.

Meneley, W.A., 1970. Geotechnology: Groundwater Resources. In Physical environment of Saskatoon, Canada, Christiansen, E.A. (Ed.), National Research Council of Canada, NRC Publication No. 11378, pp.

Meneley, W.A., 1989. The Environmental Impact of Potash Mining in Saskatchewan. Proceedings of the Potash Tailings and Site Decommissioning Options, Saskatoon, Saskatchewan. Saskatchewan Mining Association, 13 p.

Mualem, Y., 1976. A new model for predicting the hydraulic conductivity of unsaturated porous media. Water Resources Research, **12** (3), 513-522.

Mualem, Y., 1978. Hydraulic conductivity of unsaturated porous media: generalized macroscopic approach. Water Resources Research, **14** (2), 325-334.

Neuman, S.P., 1990. Universal scaling of hydraulic conductivities and dispersivities in geological media. Water Resources Research, **26**, 1749-1758.

Oberland, P.L., 1989. Head and flow of groundwater of variable density. Journal of Geophysical Research, **66** (12), 4247-4256.

Oldenburg, C.M., and Pruess., K., 1995. Dispersive transport dynamics in a strongly coupled groundwater-brine flow system. Water Resources Research, **6** (3), 875-882.

Penner, L.A., 1986. Fracture patterns and their influence on the strength and hydraulic conductivity of Floral Till, Saskatchewan. M.Sc. thesis, University of Saskatchewan, Saskatoon, Saskatchewan.

Pinder, G.F., and Cooper, H.H., 1970. A numerical technique for calculating the transient position of the saltwater front. Water Resources Research, **6** (3), 303-311.

Ranjitkar, S.S.B., 1989. Prediction of hydraulic properties of unsaturated granular soils based on grain size data. Ph.D. Thesis. Bell & Howell Information Company, Ann Arbor.

Rowe, A.M.Jr., and Chou, J.C.S., 1970. Pressure-volume-temperature-concentration relation of aqueous NaCl solutions. Journal of Chemical and Engineering Data, **15** (1), 61-66.

Rowe, R.K., 1996. The role of diffusion and the modelling of its impact on groundwater quality. Advances in Groundwater Pollution Control and Remediation, 371-403.

Sauer, E.K., Egeland, A.K., and Christiansen, E.A., 1993. Preconsolidation of tills and intertill clays by glacial loading in southern Saskatchewan, Canada. Canadian Journal of Earth Sciences, **30**, 420-433.

Sauer, E.K. and Christiansen, E.A., 1991. Preconsolidation pressures in the Battleford Formation, southern Saskatchewan, Canada. Canadian Journal of Earth Sciences, **28**, 1613-1623.

Segol, G., Pinder, G.F., and Gray, W.G., 1976. A Galerkin finite element technique for calculating the transient position of the saltwater front. Water Resources Research, **11** (2), 343-347.

SkwaraWoolf, T., 1980. Biostratigraphy and paleoecology of Pleistocence deposits (Riddell Member, Floral Formation, Late Rancholabrean), Saskatoon, Canada. Canadian Journal of Earth Sciences, **18**, 311-322.

Stauffer, M.R., and Gendzwill, D.J., 1987. Fractures in the northern plains, stream patterns, and the midcontinent stress field. Canadian Journal of Earth Sciences, **24**, 1086-1097,

Stephenson, D.A., Fleming, J.H., and Mickelson, D.M., 1988. Glacial deposits. In Hydrogeology Vol, O-2, The Geology of North America, Geological Society of America, p. 301 - 314.

Tallin, J.E., Pufahl, D.E., and Barbour, S.L., 1990. Waste management schemes of potash mines in Saskatchewan. Canadian Journal of Civil Engineering, **17** (4), 528-542.

Therrien, R., and Sudicky, E.A., 1996. Three-dimensional analysis of variable-saturated flow and solute transport in discretely-fractured porous media. Journal of Contaminant Hydrology, **23**, 1-44.

Tóth, J., 1963. A theoretical analysis of groundwater flow in small drainage basins. Journal of Geophysical Research, **68**, 4795-4812.

Tóth, J., 1962. A theory of groundwater motion in small drainage basins in central Alberta, Canada. Journal of Geophysical Research, **67**, 4375-4387.

van der Kamp., G., 1989. General salt migration processes in groundwater. The Environmental Impact of Potash Mining in Saskatchewan. Proceedings of the Potash Tailings and Site Decommissioning Options, Saskatoon, Saskatchewan. Saskatchewan Mining Association, 13 p.

van der Kamp, G., and Maathuis, H., 1985. Excess hydraulic head in aquitards under solid waste emplacements. International Association of Hydrogeologists. Volume XVII, Part I. Proceedings in the Hydrogeology of rocks of low permeability, Tucson, 118-129.

van Genuchten, M.T., 1980. A closed-form equation for predicting the hydraulic conductivity of unsaturated soils. Soil Science Society of America Journal, **44**, 892- 898.

Voss, C.I., 1984. SUTRA: A finite-element simulation model for saturated-unsaturated fluid-density-dependent ground-water flow with energy transport of chemically-reactive single-species solute transport. U.S. Geological Survey Water Resources Investment, Rep. 84-4369, 409 p.

Voss, C.I., and Souza, W.R., 1987. Variable density flow and solute transport simulation of regional aquifers containing a narrow freshwater-saltwater transition zone. Water Resources Research, **23** (10), 1851-1866.

Wang, H.F., and Anderson, M.P., 1995. Introduction to Groundwater Modelling: Finite Difference and Finite Element Methods. Toronto, Academic Press, Inc., 237pp.

Whitaker, S.H., and Christiansen, E.A., 1972. The Empress Group in Southern Saskatchewan. Canadian Journal of Earth Sciences, **9**, 353-360.

Yang, N., and Barbour, S.L., 1992. The impact of soil structure and confining stress on the hydraulic conductivity of clays in brine environments. Canadian Geotechnical Journal, **29**, 730-739.

Bickford, W.B., 1990. A First Course in the Finite Element Method. Boston, R.R. Donnelley & Sons Company, 649 p.

Braitsch, O., 1971. Salt Deposits: Their Origin and Composition. Springer-Verlag, New York, 232 p.

Carsel, R.F., and Parrish, R.S., 1988. Developing joint probability distributions of soil water retention characteristics. Water Resources Research, **24** (5), 755-769.

Christiansen, E.A., 1967. Collapse structures near Saskatoon, Saskatchewan, Canada. Canadian Journal of Earth Sciences, **4**, 757-767.

Christiansen, E.A., 1970. Geology. In Physical environment of Saskatoon, Canada, Christiansen, E.A. (Ed.), National Research Council of Canada, NRC Publication No. 11378, pp.3-17.

Christiansen, E.A., 1979. The Wisconsinan deglaction of southern Saskatchewan and adjacent areas. Canadian Journal of Earth Sciences, **16,** 913-938.

Christiansen, E.A., 1992. Pleistocene stratigraphy of the Saskatoon area, Saskatchewan, Canada: an update. Canadian Journal of Earth Sciences, **29**, 1767-1778.

Christiansen, E.A., and Sauer, E.K., 1994. Geotechnique of Saskatoon and Surrounding Area, Saskatoon, Saskatchewan, Canada: Proceedings of the Annual GAC/MAC meeting.

Davies, P.B., 1987. Modeling areal, variable density, ground-water flow using equivalent freshwater head - analysis of potentially significant errors. Proceedings of the NWWA-IGWMC Conferences - Solving Groundwater Problems with Models, 888-903.

Davies, S.N., and DeWiest, R.J.M., 1966. Hydrogeology. John Wiley & Sons, Inc. New York, 463 p.

Desai, C.S., and Contractor, D.N., 1977. Finite element analysis of flow, diffusion and salt water intrusion in porous media. In: Formulation and Computational Algorithms in Finite Element Analysis, 958-983.

Diersch. H.J., 1996. Interactive, graphics-based finite-element simulation system FEFLOW for modeling groundwater flow, contaminant mass and heat transport processes. WASY Institute for Water Resources Planning and System Research Ltd..

APPENDIX A

FEMWATER - FLOW AND TRANSPORT CODE VERIFICATION

When modelling a groundwater flow system parameters are needed to characterize the system. Coupled groundwater flow and solute transport problems are often studied and analyzed using numerical models.

The numerical codes require specification of boundary conditions, hydraulic head, concentration distributions and material properties. The codes compute the transient hydraulic head and contaminant concentration. The numerical codes solve for a series of discrete nodal points and elements in two steps; one for the flow field and the other for the contaminant transport.

Before numerical investigations are conducted, the numerical code must be verified to ensure that it accurately simulates coupled flow and transport for the particular kind of problem investigated. The FEMWATER code used in this thesis was verified using the classic Henry (1964) seawater encroachment problem and the Elder (1967) buoyancy-driven flow problem. Simple 3-D groundwater flow and brine transport problems were also solved using FEMWATER to gain insight about brine migration and experience in the convergence characteristics of the code for site-specific purposes.

A.1 FEMWATER

FEMWATER was developed in the early 1990s by combining the two numerical codes, 3DFEMWATER (flow) and 3DLEWASTE (transport), into a single groundwater flow and solute transport code (Lin *et al.*, 1995).

FEMWATER is a 3-D finite element code simulating saturated-unsaturated, variable density, groundwater flow and solute transport. The selection of FEMWATER, for simulating groundwater flow and solute brine transport at PCS

Cory Mine, was based on the following capabilities:

1. Solution of 3-D density-driven flow and transport problems;
2. Supported by the GMS graphical interface;
3. Effective incorporation of saturated and unsaturated conditions; and
4. Ability to model fluid density and dynamic viscosity as a function of concentration (equations 3.1 and 3.2).

A.2 Numerical Verification of Classic Examples

To successfully simulate density-dependent, groundwater flow and solute transport, the numerical code must represent the physical system through a set of governing equations in a stable fashion (Voss and Souza, 1987). Numerical codes must be validated to ensure that it accurately simulates flow and transport processes.

There are a limited number of published 3-D problem verifications. Often 3-D numerical codes are verified using 2-D analytical and numerical solutions. This section discusses the classic "Henry Problem" for seawater encroachment (Henry, 1964) and "Elder Problem" for buoyancy-driven fluid flow (Elder, 1967).

A.2.1 Henry's Seawater Encroachment Verification

Henry (1964) studied the interaction between freshwater and seawater in a confined aquifer near the coast of Florida. In particular, Henry analyzed the characteristics of the transition zone existing between freshwater and seawater. The flow conditions were such that freshwater was moving over a diffuse saltwater wedge that encroached the aquifer and discharged into the sea (Voss and Souza, 1987).

Often variable density flow and transport codes are verified by comparing the numerical results with those of Henry's (1964) approximate solutions for steady-

state saltwater intrusion into an aquifer. To date, numerical models such as the 2-D particle tracking model of Pinder and Cooper (1970), the finite difference model by INTERA (1979) and the finite element models by Segol *et al.* (1975), Huyakorn and Taylor (1976), Desai and Contractor (1977), Frind (1982), SUTRA (Voss, 1984) and FEFLOW (Diersh,1996) have not matched Henry's analytical solution. This may indicate that some of Henry's approximate results may be inaccurate. Although numerical codes do not exactly match Henry's analytical results, confidence in the accuracy for solving nonlinear problems involving highly dispersed transition zones, is gained provided that the code matches results of other numerical models (Diersch, 1996 and Voss and Souza, 1987).

The problem domain and boundary conditions used to verify the Henry problem are presented in Figure A.1. Table A.1 lists the parameters used in the numerical simulation. The maximum density contrast in the Henry Problem was 2.5% (Oldenburg and Pruess, 1995) since the density of seawater is 1.025 Mg/m^3.

The numerical results calculated with FEMWATER, like most other variable density codes [e.g., Voss and Souza (1984) and Diersch (1996)] matched the early results published by Pinder and Cooper (1970).

There are several problems with the Pinder-Cooper solution as a verification standard. First, the solution is not entirely converged after 100 minutes, the simulation time. Second, the computational grid generates significant numerical dispersion.

Table A.2 lists the spatial discretization characteristics of the 3-D meshes used in this verification exercise. The results of the 20x10x1 3-D mesh design were compared with that of Pinder-Cooper, SUTRA and FEFLOW. The results demonstrated good agreement with these published results.

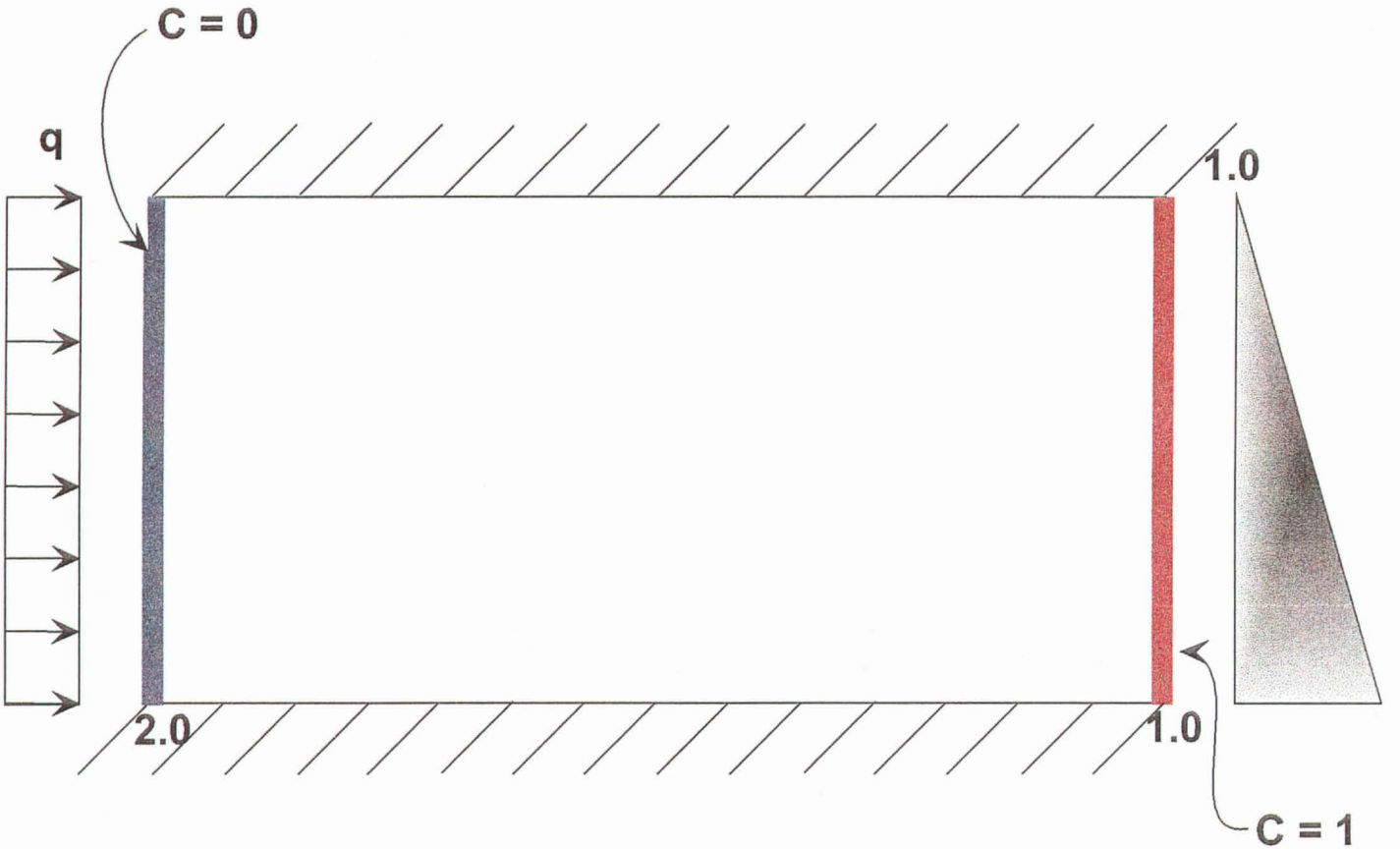

Figure A.1 - Problem domain and boundary conditions for the Henry (1964) seawater intrusion problem

Table A.1 - Parameters used in the Henry (1964) Seawater Intrusion Verification (after Oldenburg and Pruess, 1995)

Quantity	Value
Porosity	0.35
Permeability	1.02×10^{-9} m^2
Viscosity	1.0×10^{-3} Pa·s
Gravity	9.81 m/s^2
Longitudinal Dispersivity	0 m
Transverse Dispersivity	0 m
Molecular Diffusivity	6.6×10^{-6} m^2/s
Tortuosity	1
Density of Pure Water	1000 kg/m^3
Density of Pure Brine	1025 kg/m3
Mass Source on Left Side	6.6×10^{-2} kg/m·s

Table A.2 -Spatial Discretization Characteristics of the Finite Elements Meshes Used to Simulate the Henry (1964) Solution with FEMWATER

3-D Mesh Design	# of Nodes	# of Elements
20x10x1	231	200
40x20x1	861	800
80x40x1	3321	3200

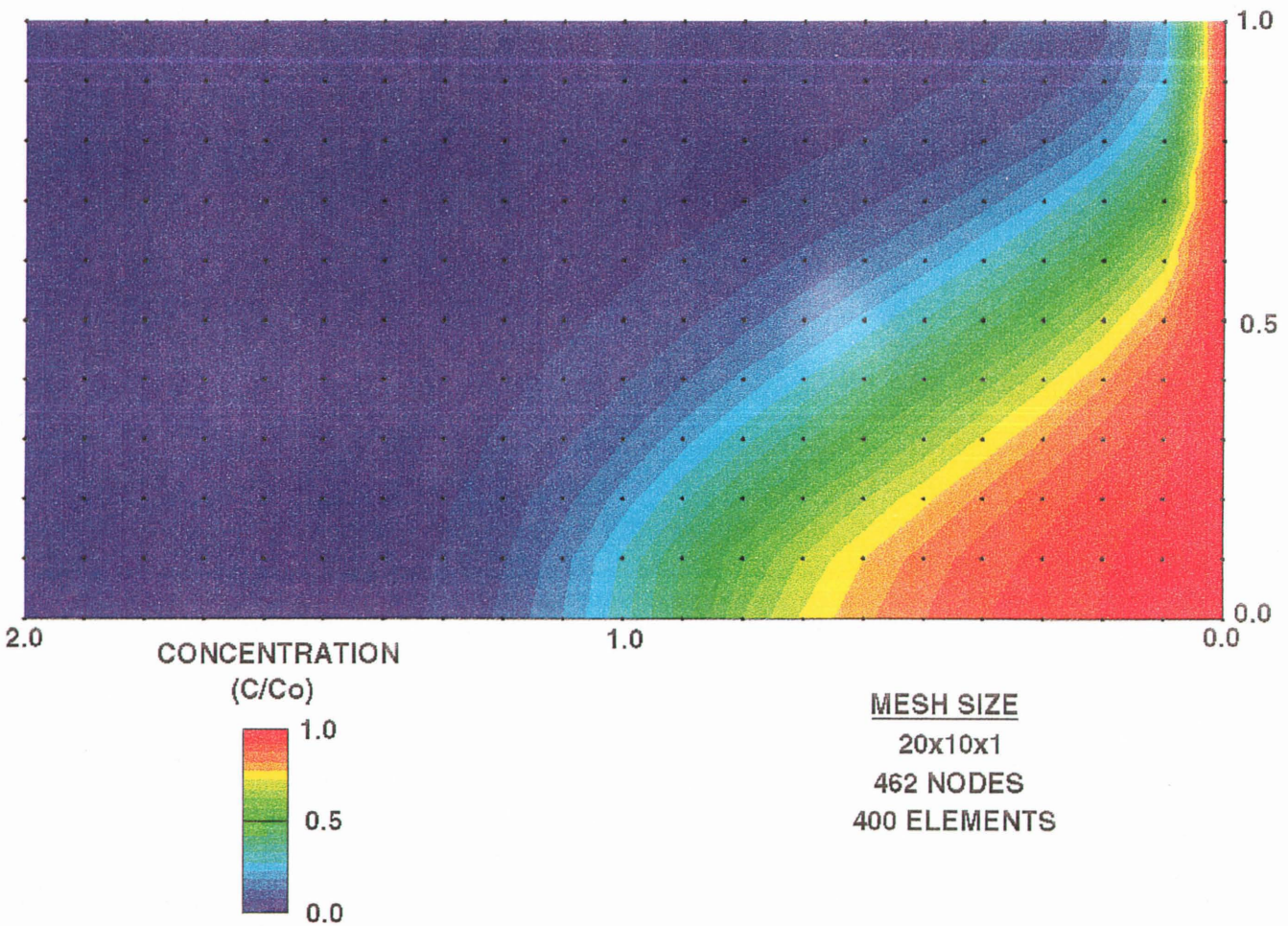

Figure A.2a - Concentration Profile of the Henry Problem computed by FEMWATER for the 20x10x1 Mesh

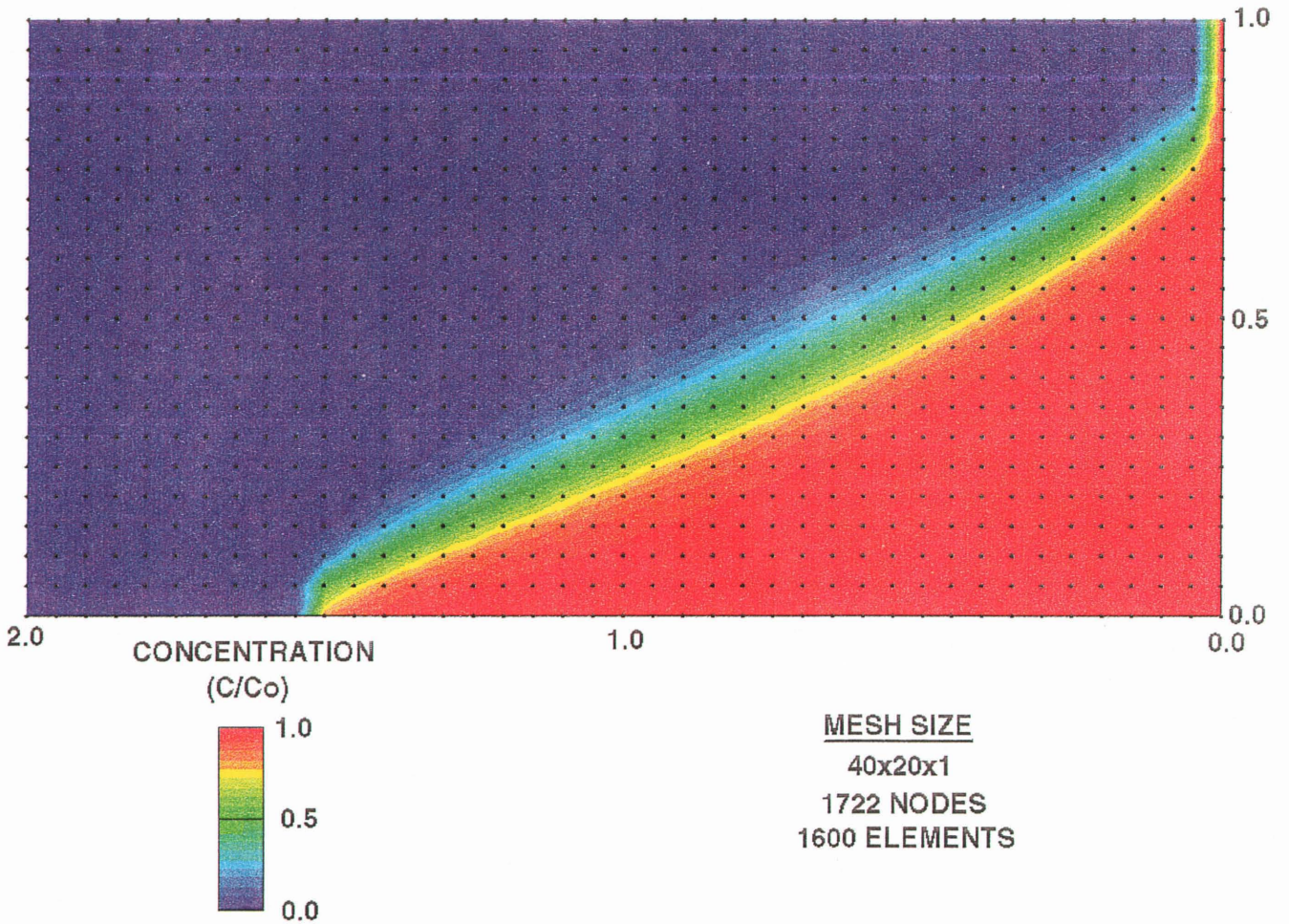

Figure A.2b - Concentration Profile of the Henry Problem computed by FEMWATER for the 40x20x1 Mesh

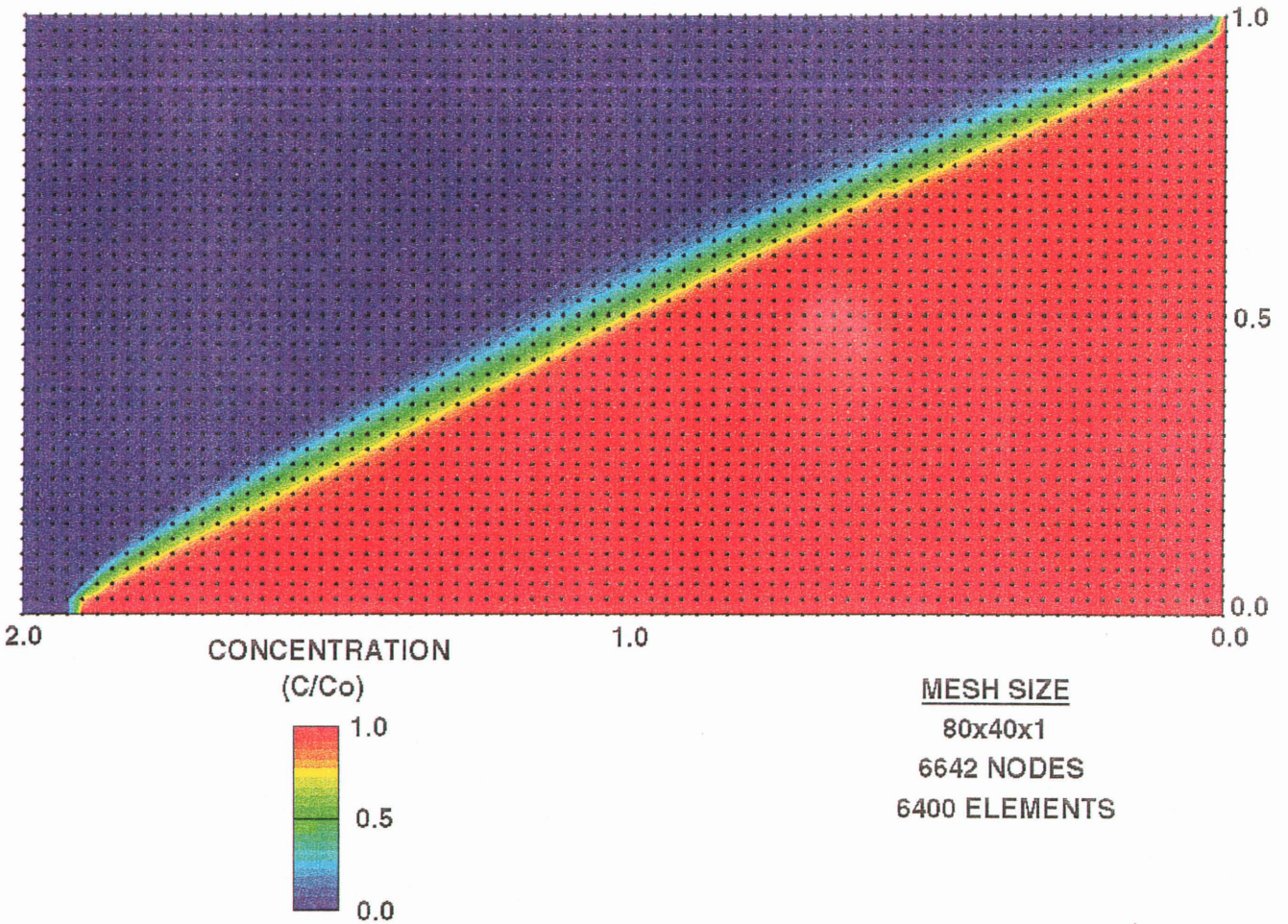

Figure A.2c - Concentration Profile of the Henry Problem computed by FEMWATER for the 80x40x1 Mesh

The Henry problem (1964) simulated with FEMWATER converged after 180 minutes of simulation time. The concentration distribution computed from the various mesh designs are shown in Figures A.2a to A.2c. The concentration profile indicated that the interface between freshwater and seawater narrowed as the nodal spacing in the numerical grid reduced. The attenuation of this interface occurred because numerical dispersion reduced. Numerical dispersion being a discretization artifact resulting in the smearing of sharp interfaces. Refining the numerical grid decreased the amount of numerical dispersion thereby allowing for the more accurate representation of narrow transition zones (Oldenburg and Pruess, 1995).

A.2.2 Elder's Buoyancy-Driven Fluid Flow Verification

Elder (1967) experimentally and numerically studied fluid flow caused by heating a basal porous layer. The physics of the Elder's study involves a nonlinear system of that can be simulated using equations coupling free convection flow and heat transfer (Diersch, 1996).

The numerical results from Elder's study of thermal convection can be used, by analogy, to verify fluid flow driven only by density variations (Oldenburg and Pruess, 1995 and Voss and Souza, 1987). The problem domain and boundary conditions used for simulating Elder's problem are shown in Figure A.3. The parameters used for the FEMWATER verification simulations are listed in Table A.3. The maximum density change within the model was more than 20% for saturated brine, making the Elder problem a very challenging validation test for coupled flow and transport numerical codes.

The concentration profiles computed for various times by FEMWATER are shown in Figure A.4. Figure A.5 demonstrates the flow field vectors the show the direction of convective flow at 20 years. The convective flow system calculated by FEMWATER matches, both spatially and temporally, that calculated with FEFLOW. The concentration distribution and flow field shown in Figures A.4 and A.5 represents a strongly coupled problem. The computed flow field was very complex

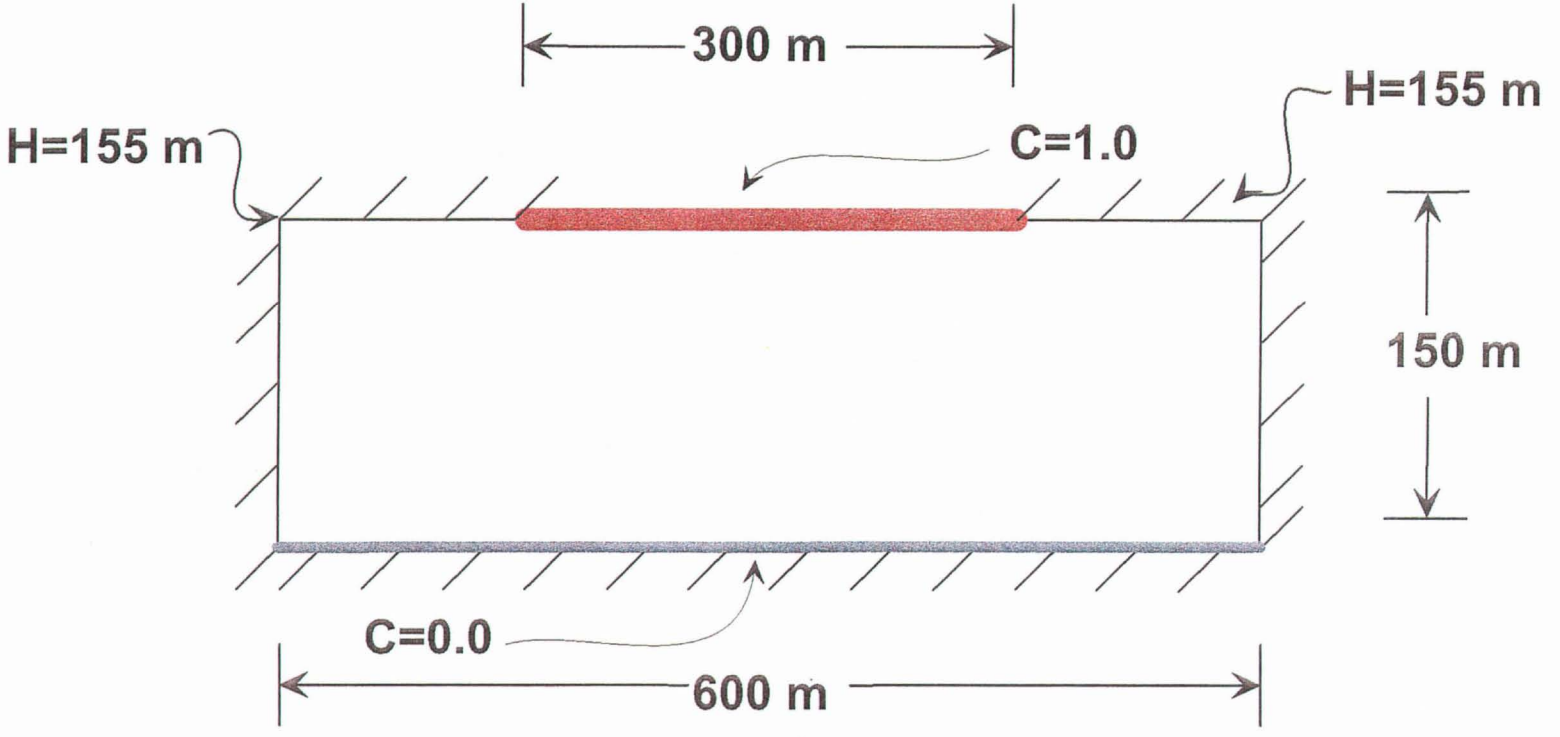

Figure A.3 -Problem domain and boundary conditions for the Elder (1967) free convection problem

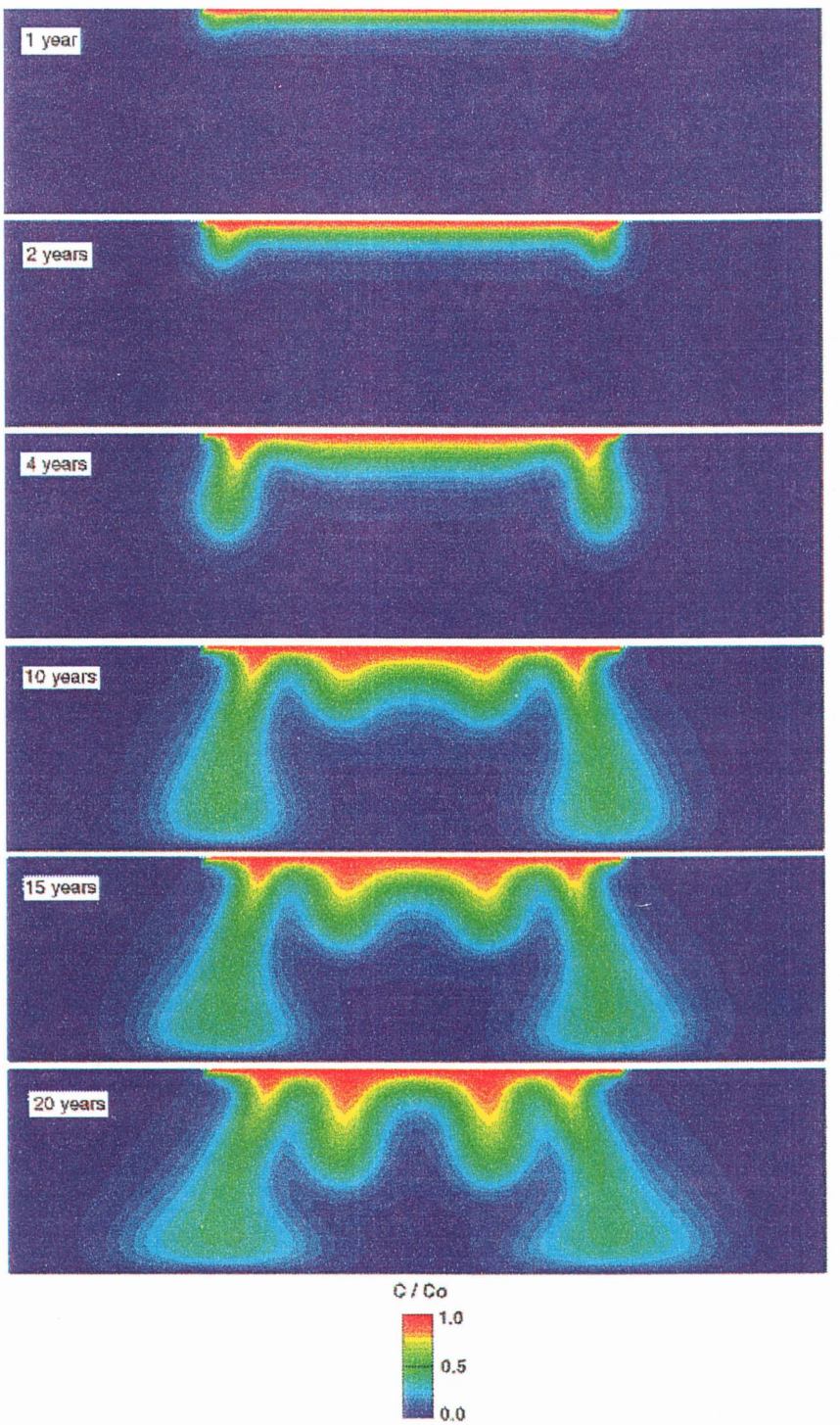

Figure A.4 - Brine Plume calculated by FEMWATER at various Elapsed Times for the Free Convective Flow

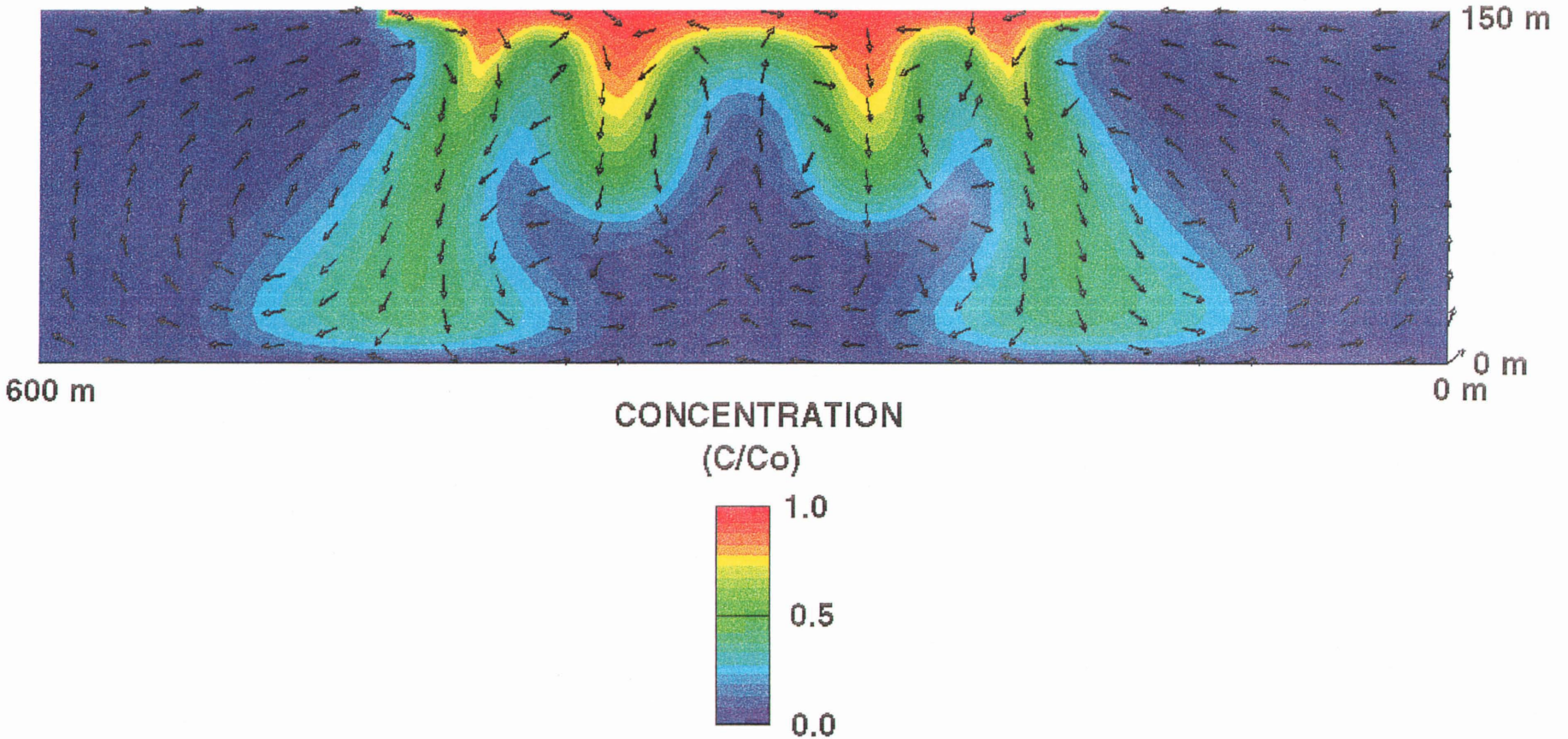

Figure A.5 - Vectors calculated after 20 Years of Simulated Free Convective Flow

and evolved through a series of transient clockwise and counterclockwise vortices (Voss and Souza, 1987).

The FEMWATER results for Elder's problem demonstrated that spatial and temporal discretization were crucial. Mesh discretization used for the FEMWATER verification was similar to that used by Voss and Souza (1987). Analysis indicated that at large elapsed times the numerical results were sensitive to mesh discretization and the time stepping scheme but appeared less sensitive to the choice of solver.

Table A.3 - Parameters used for the Elder (1967) Problem (after Oldenburg and Pruess, 1995)

Quantity	Value
Porosity	0.1
Permeability	4.845×10^{-13} m^2
Viscosity	1.0×10^{-3} Pa·s
Gravity	9.81 m/s^2
Transverse Dispersivity	0 m
Longitudinal Dispersivity	0 m
Molecular Diffusivity	3.565×10^{-6} m^2/s
Tortuosity	1
Density of Pure Water	1000 kg/m^3
Density of Pure Brine	1200 kg/m^3

A.3 Forced Convection Simulations

A series of forced convection simulations were performed using FEMWATER. Boundary conditions used for the forced convection simulations (Figure A.6) are similar to Elder's free convection simulation (Figure A.3) but were modified by coupling the constant concentration boundary condition with a constant

hydraulic head. The parameters used in the forced convection simulations were the same as those in the free convection problem (Table A.3). The importance of the forced convection simulation was that it provides information about the characteristics fluid flow when both constant hydraulic head and concentration were applied. This was the case that applied to brine ponds.

In the forced convection simulation, fluid convection was affected by the constant hydraulic head boundary condition. The driving force governing fluid flow was influenced by the hydraulic gradient and density variations (equation 3.7). Figure A.7 illustrates the location of the brine plume at various of elapsed times. Figure A.8 shows the flow vectors calculated after twenty years.

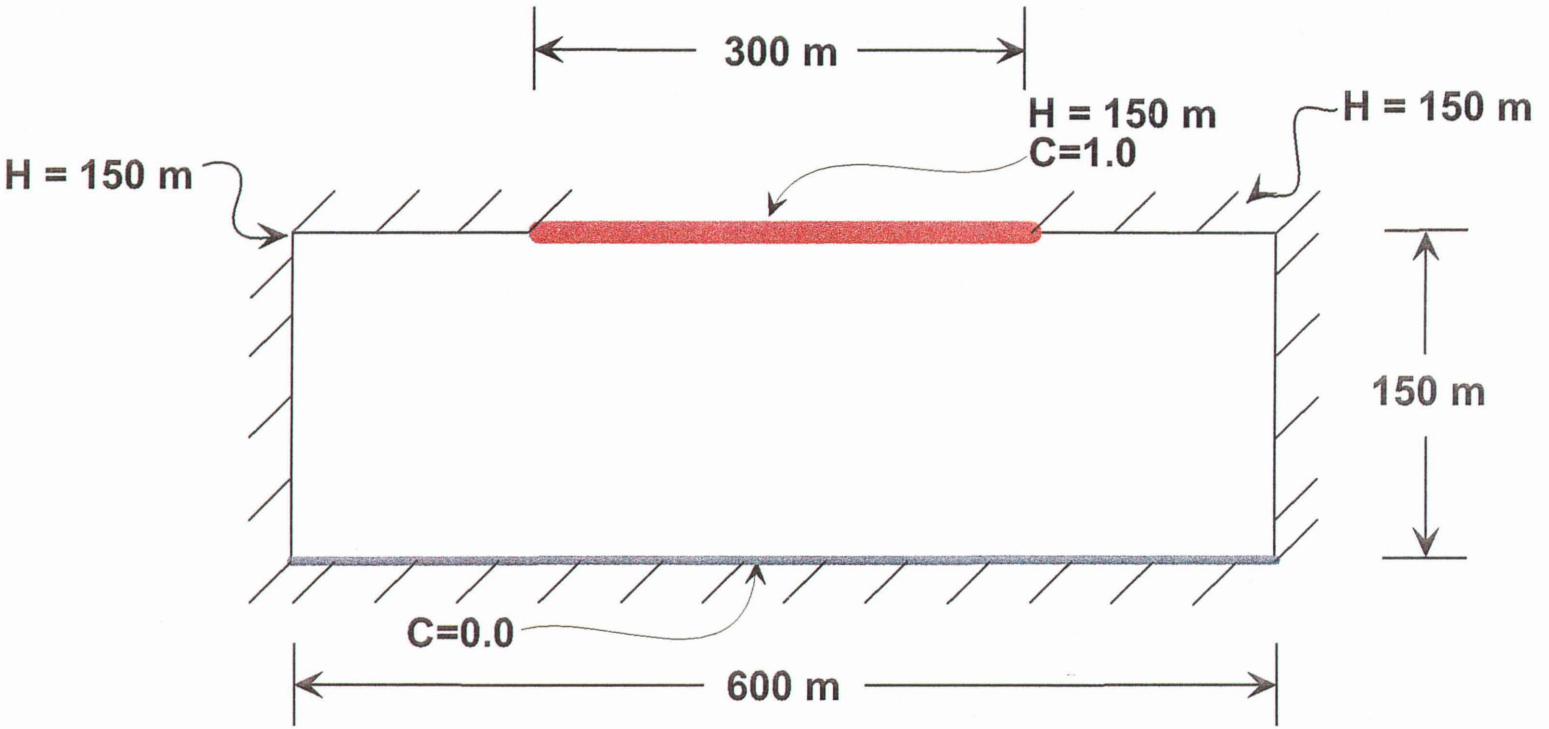

Figure A.6 - Boundary Conditions for the Forced Convection Simulation

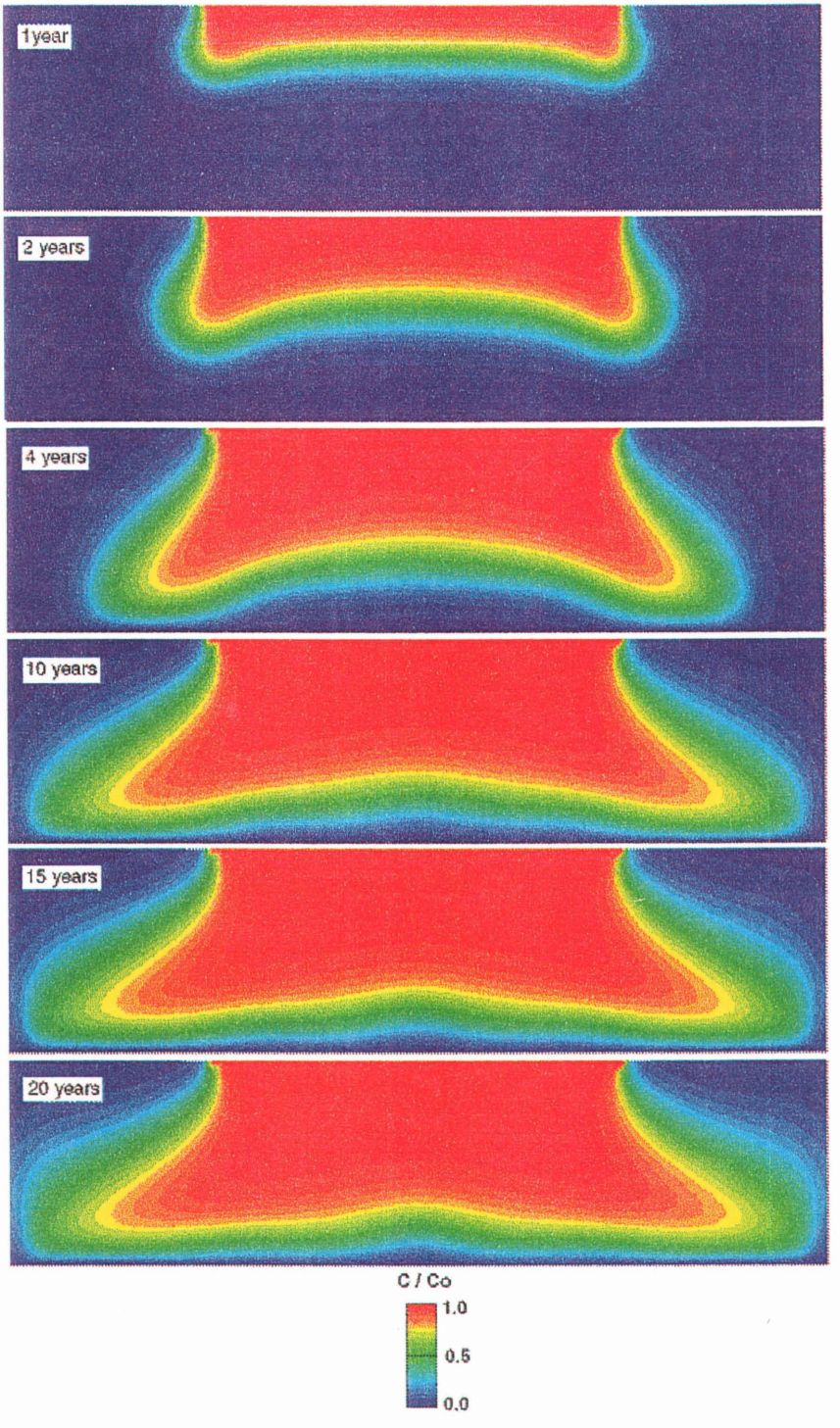

Figure A.7 - Brine Plume calculated by FEMWATER at various Elapsed Times for the Forced Convective Flow

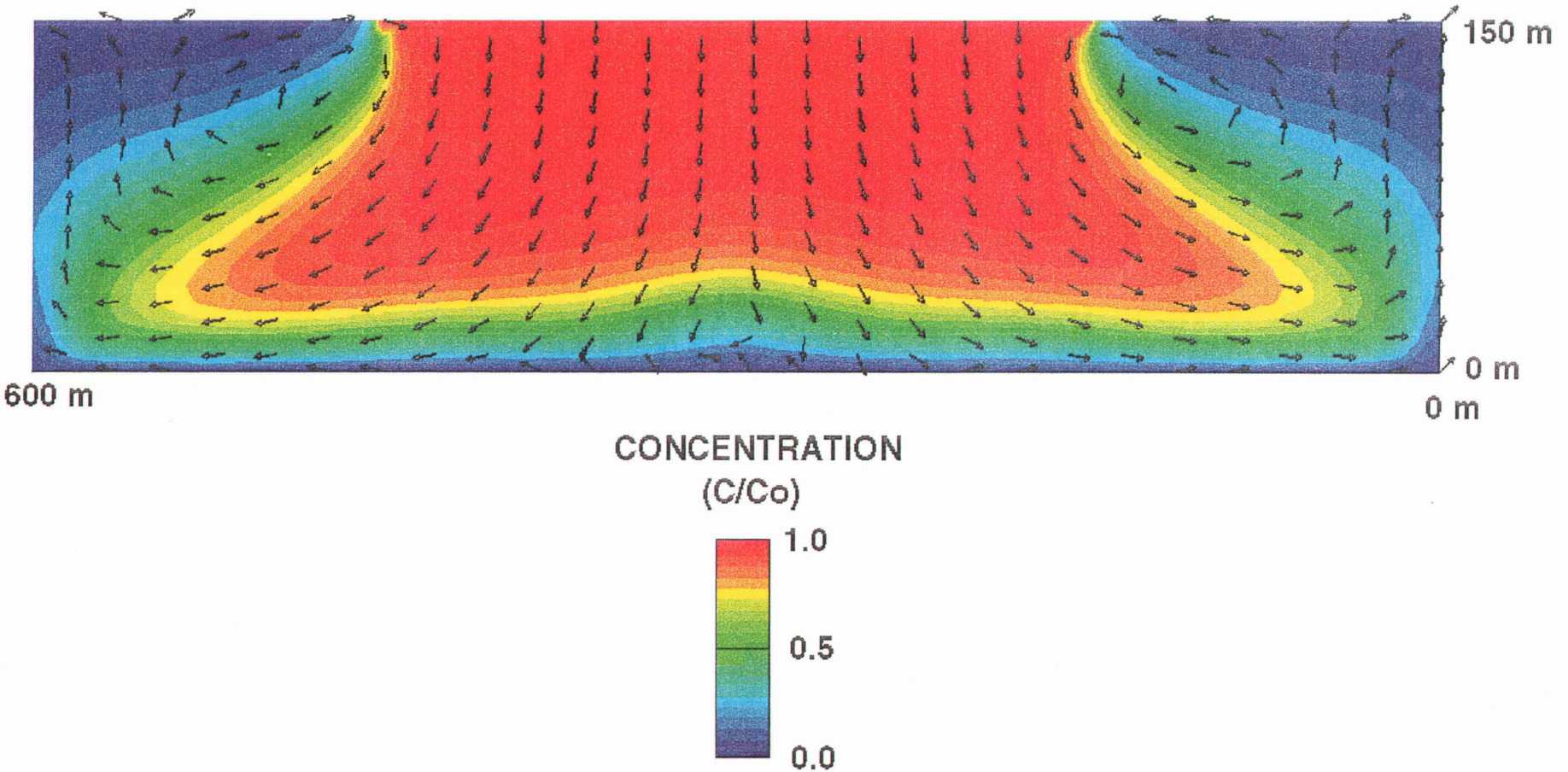

Figure A.8 - Vectors calculated after 20 Years of Simulated Forced Convective Flow

APPENDIX B

THREE DIMENSIONAL COUPLED BRINE TRANSPORT SENSITIVITY STUDIES

The groundwater flow and brine transport numerical study for PCS Cory Mine and vicinity was complex, highly nonlinear and significantly influenced by hydraulic gradients, density contrasts and the hydrogeological system. In order to understand this complexity small scale groundwater flow and brine transport simulations were performed for a simple layered porous media geometry. The purpose of these 3-D simulations was to provide an understanding of the mechanisms affecting brine migration and to gain insight into processes controlling solute transport.

Numerous flow and transport simulations were conducted using 2 g/L, 20 g/L and 200 g/L contaminant source TDS concentrations. One hundred years of brine migration was simulated using FEMWATER. The model parameters are listed in Table B.1. The hydraulic conductivity of the porous media was not changed throughout the simulations, with the exception of the clay unit. This unit was assigned either a relatively high value to represent fractured till or relatively low value to represent unfractured till. The dispersivity values for all hydrostratigraphic units were assigned either a relatively high or relatively low value.

Figures B.1 and B.2 show the problem domain and boundary conditions used for Simulations A to C and D and E respectively. The base of the sand aquifer modelled in Simulations A to C was horizontal while the base of the aquifer modelled in Simulations D and E was dipping 1° in a direction opposing groundwater flow. Simulations D and E were modelled using only the 200 g/L TDS source concentration. Figures B.3, B.4, B.5, B.6 and B.7 show the results of Simulations A, B, C, D and E respectively.

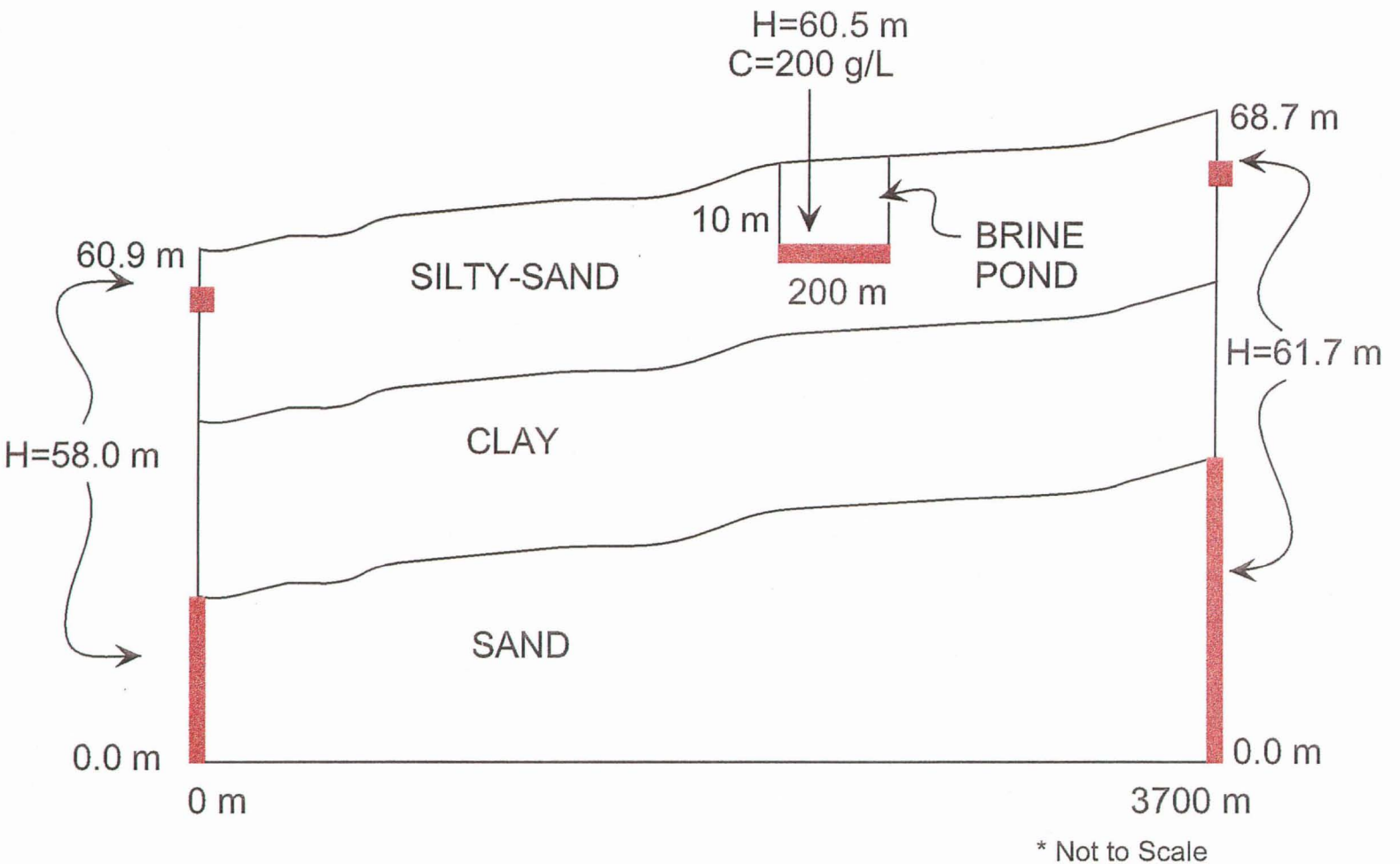

Figure B.1 - Problem Domain and Boundary Conditions For Simulations A to C

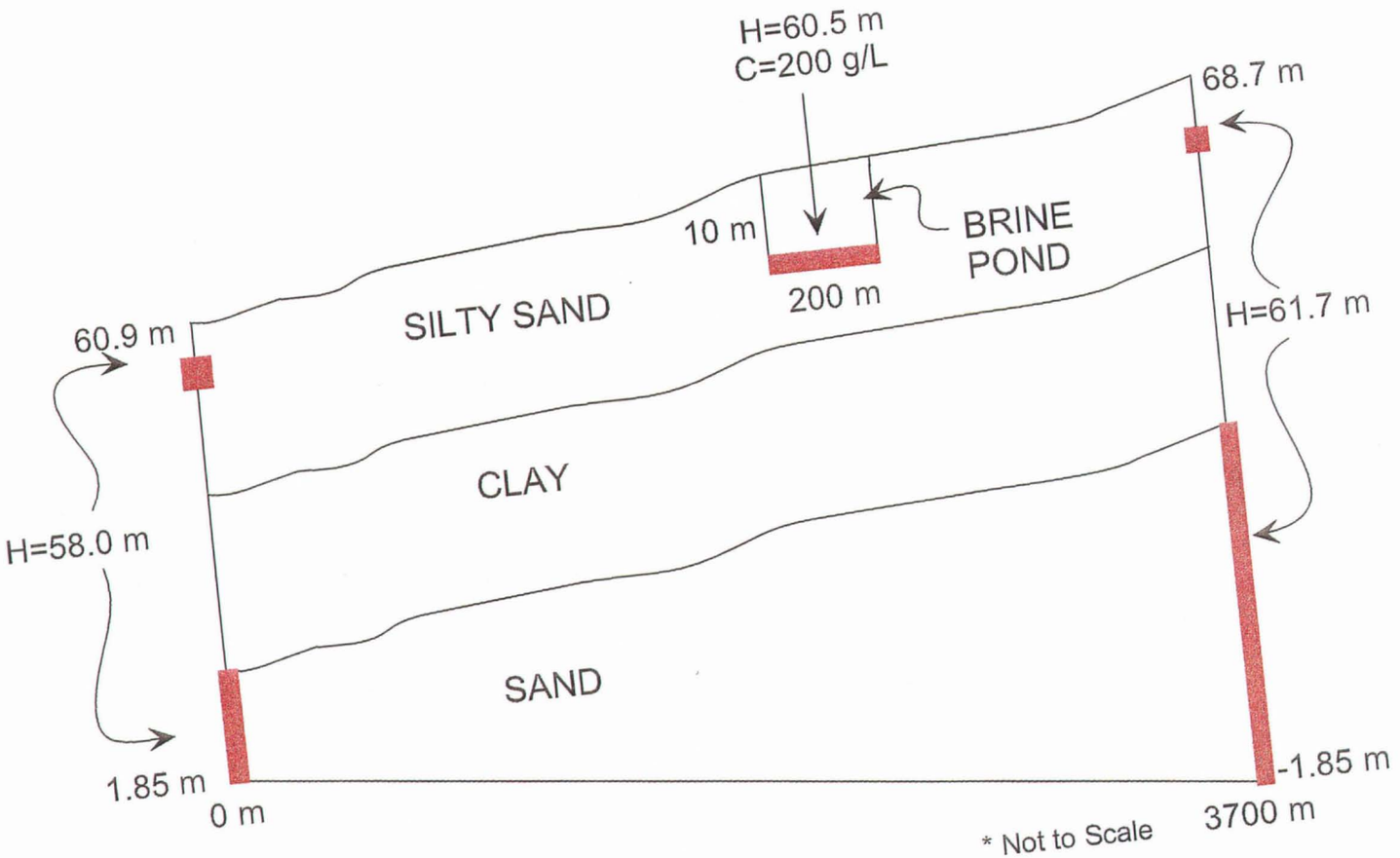

Figure B.2 - Problem Domain and Boundary Conditions For Simulations D and E

Table B.1 - Hydraulic Properties used for the Brine Flow and Transport Problems

Quantity	Value
Hydraulic Conductivity (K) Silty Sand Clay (High) Clay (Low) Sand	 4.2×10^{-6} m/s = 131.4 m/yr 2.8×10^{-7} m/s = 8.8 m/yr 1.4×10^{-8} m/s = 4.4×10^{-1} m/yr 1.4×10^{-4} m/s = 4415.0 m/yr
Dispersivity (α_L) Low High	 15 m 150 m
Molecular Diffusion Coefficient (D_d)	5.0×10^{-10} m^2/s = 1.6×10^{-2} m^2/yr

* Note : $\alpha_L = 10 \times \alpha_T$

Table B.2 - Summary of the Brine Plume Simulations Conducted

Simulation A	Low K	Low α_L	$\theta = 0$
Simulation B	Low K	High α_L	$\theta = 0$
Simulation C	High K	High α_L	$\theta = 0$
Simulation D	Low K	Low α_L	$\theta = \theta_1$
Simulation E	High K	High α_L	$\theta = \theta_1$

Figure B.3 shows the results of Simulation A, the low hydraulic conductivity clay and low dispersivity case. The results showed that the denser the plume, the more rapid the downward movement. Only the contaminant plume for the 200 g/L source reached the basal boundary and begun to spread laterally. Most plume development occurred in the basal aquifer due to the higher groundwater flux. By contrast, little spreading occurred in the low hydraulic conductivity clay.

Figure B.4 shows the results for Simulation B, the low hydraulic conductivity clay and high dispersivity case. For all cases, spreading was greater than that of Simulation A. The differences between Simulations A and B illustrated the sensitivity of the predictions to the dispersivity parameter.

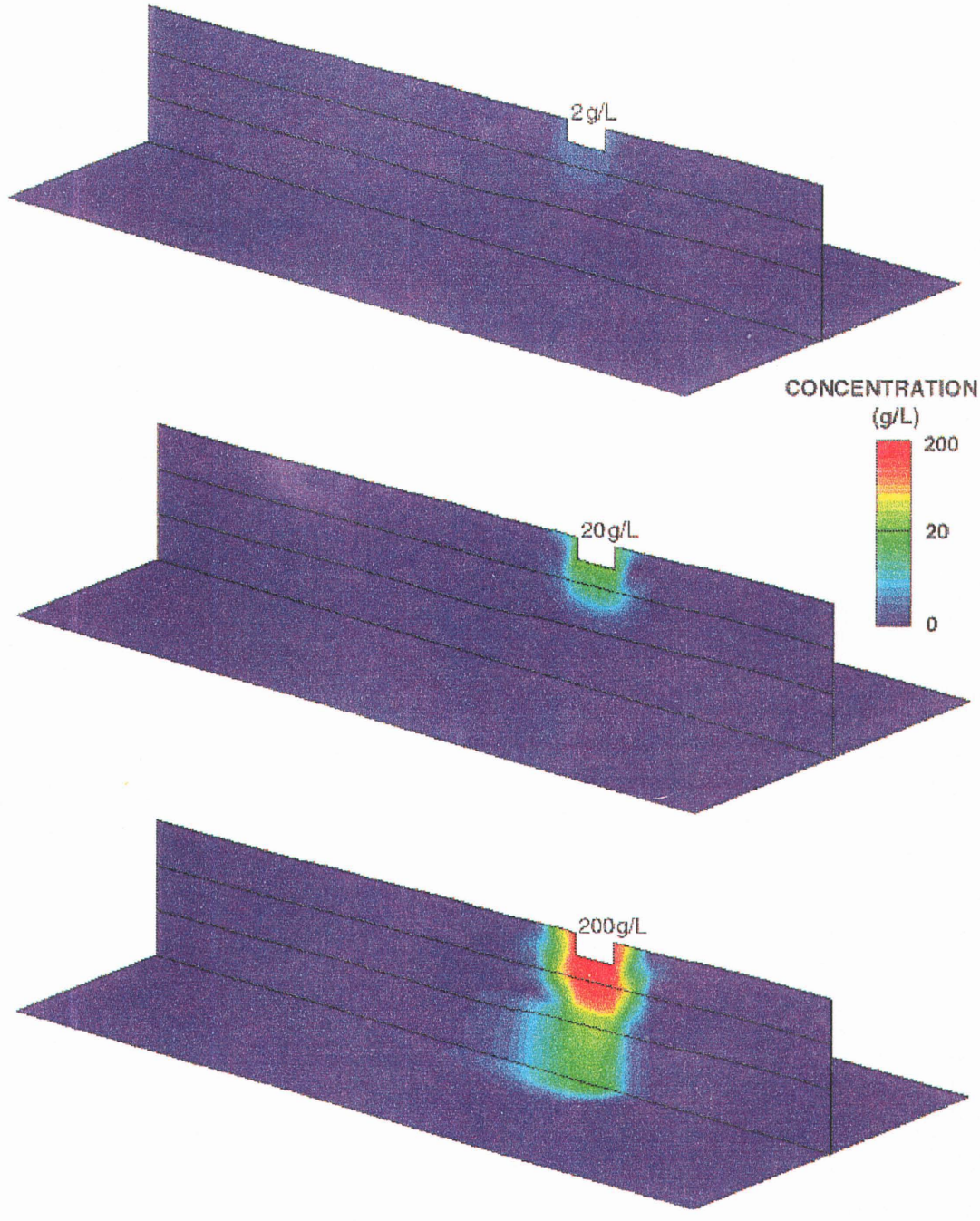

Figure B.3 - Position and Concentration of the Brine Plume for Simulation A

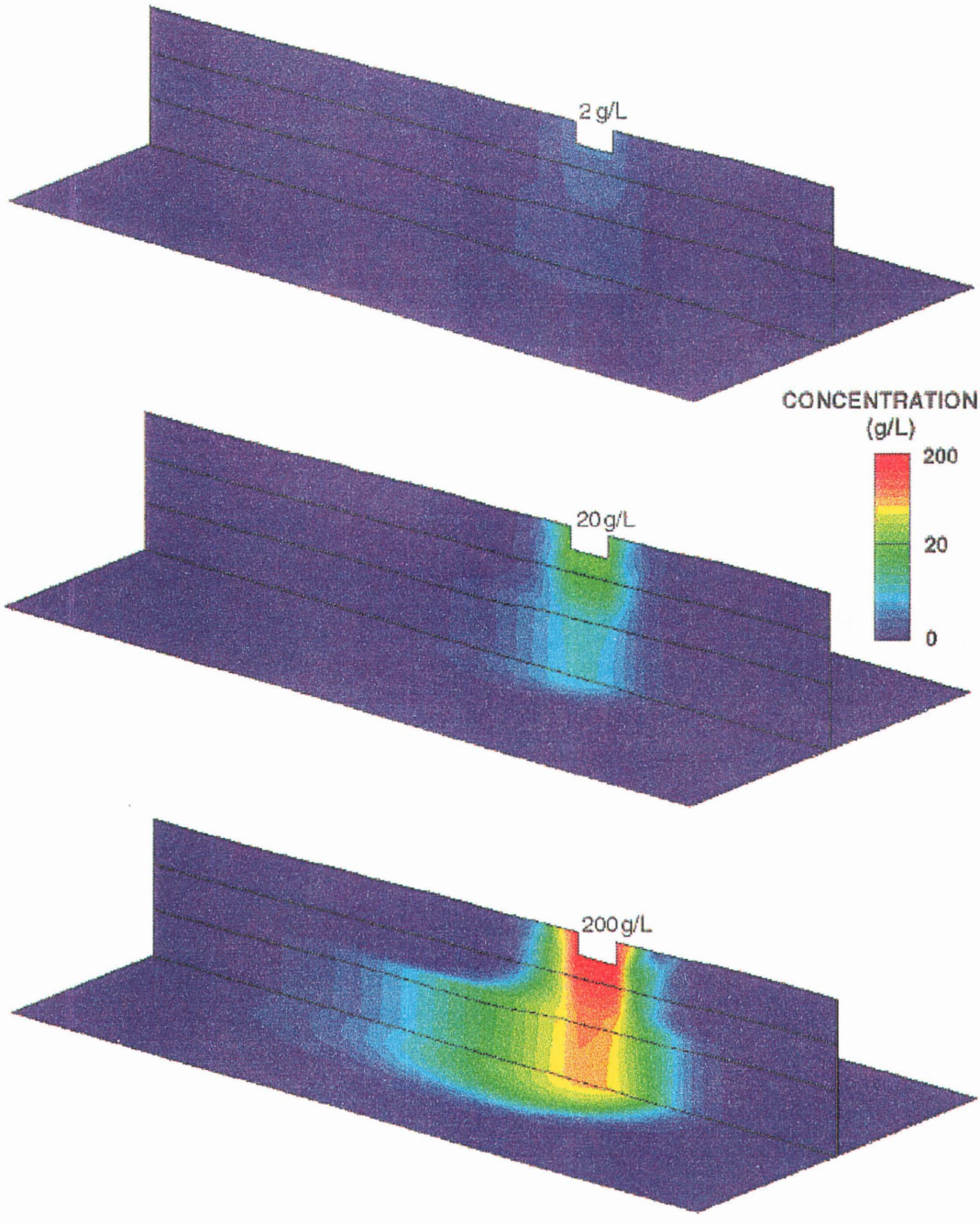

Figure B.4 - Position and Concentration of the Brine Plume in Simulation B

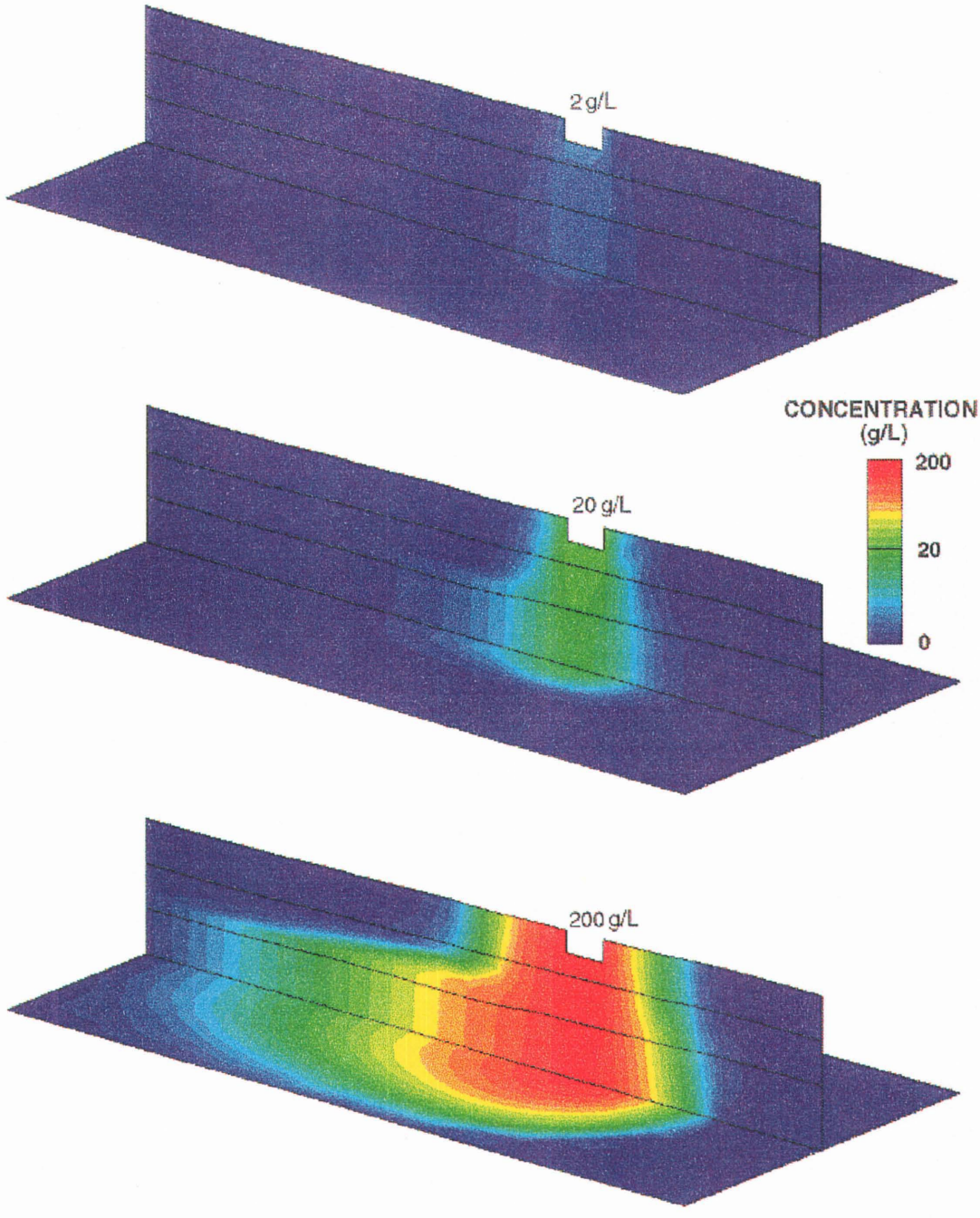

Figure B.5 - Position and Concentration of the Brine Plume in Simulation C

The results of Simulation C, the high hydraulic conductivity clay and high dispersivity case, are shown in Figure B.5. The differences between Simulations B and C illustrated the sensitivity of the predications to the clay hydraulic conductivity.

Figure B.6a shows the results of Simulation D which introduced a gently dipping aquifer and contained a 200 g/L source concentration. Figure B.6b shows the 200 g/L case from Simulation A with no aquifer dip. The difference in contaminant plume position between the two figures isolated the effect of the aquifer dip. The relatively uniform green color in Figure B.6c, showing the difference between B.6a and B.6b, indicated that a dipping basal aquifer had little effect on the contaminant plume for a hydrostratigraphic section with low dispersivity soils and a low hydraulic conductivity clay unit.

Figure B.7a shows the results of Simulation E. Differences between B.7a and B.7b, for the high clay hydraulic conductivity and high dispersivity cases, were the result of the aquifer dip. Significant variations in contaminant plumes characteristics were highlighted by the blue and red colored regions (Figure B.7c). The blue area indicated that the brine plume calculated in the dipping aquifer case did not spread as much in the direction of groundwater flow when the aquifer was horizontal. The area in red showed that brine plume computed from the dipping aquifer case advanced more downslope, in a direction opposing groundwater flow, when compared to the horizontal aquifer case.

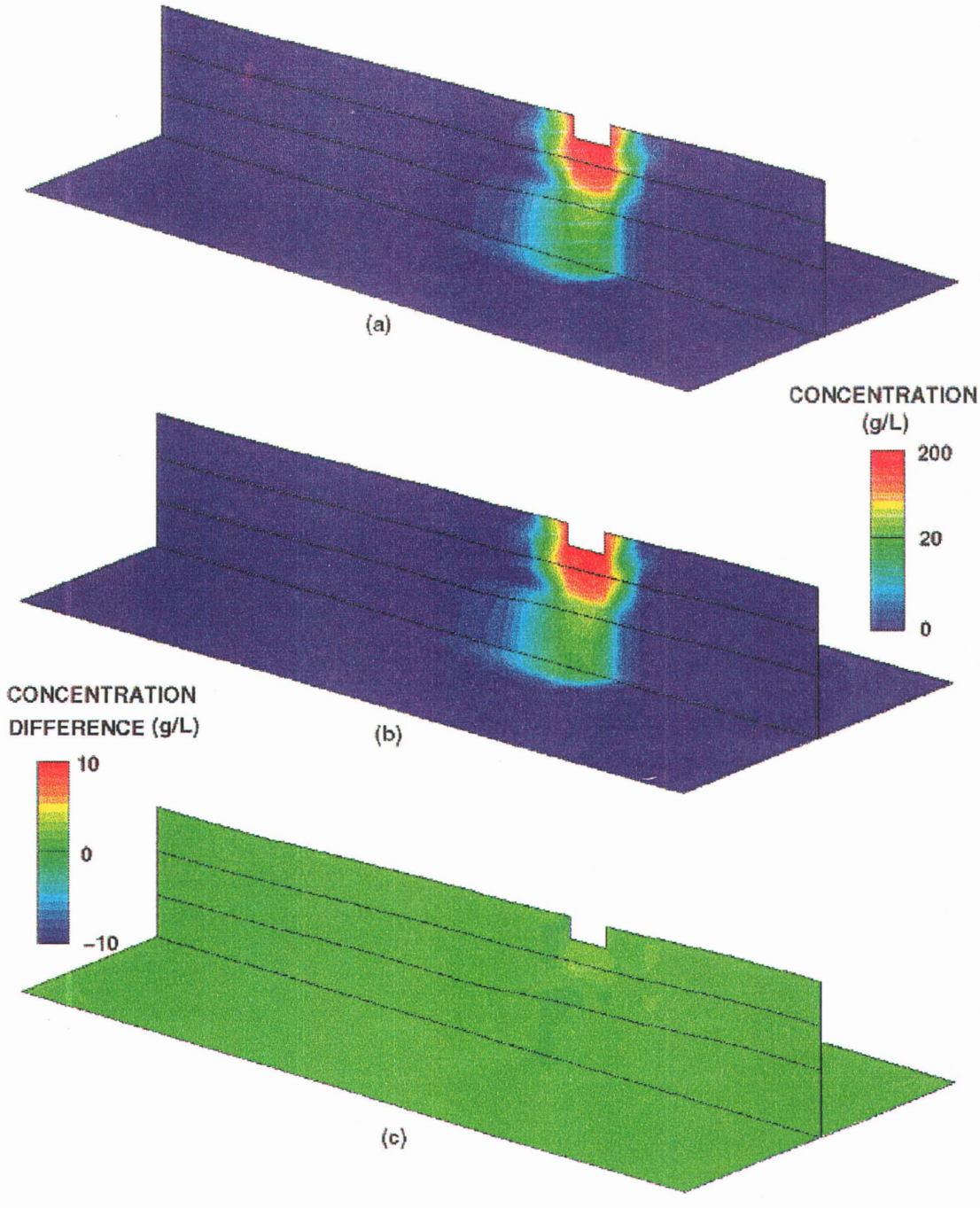

Figure B.6 - Difference in the Brine Plume Position for the Dipping and Horizontal Basal Aquifer (Low Clay Hydraulic Conductivity, Low Dispersivity Case)

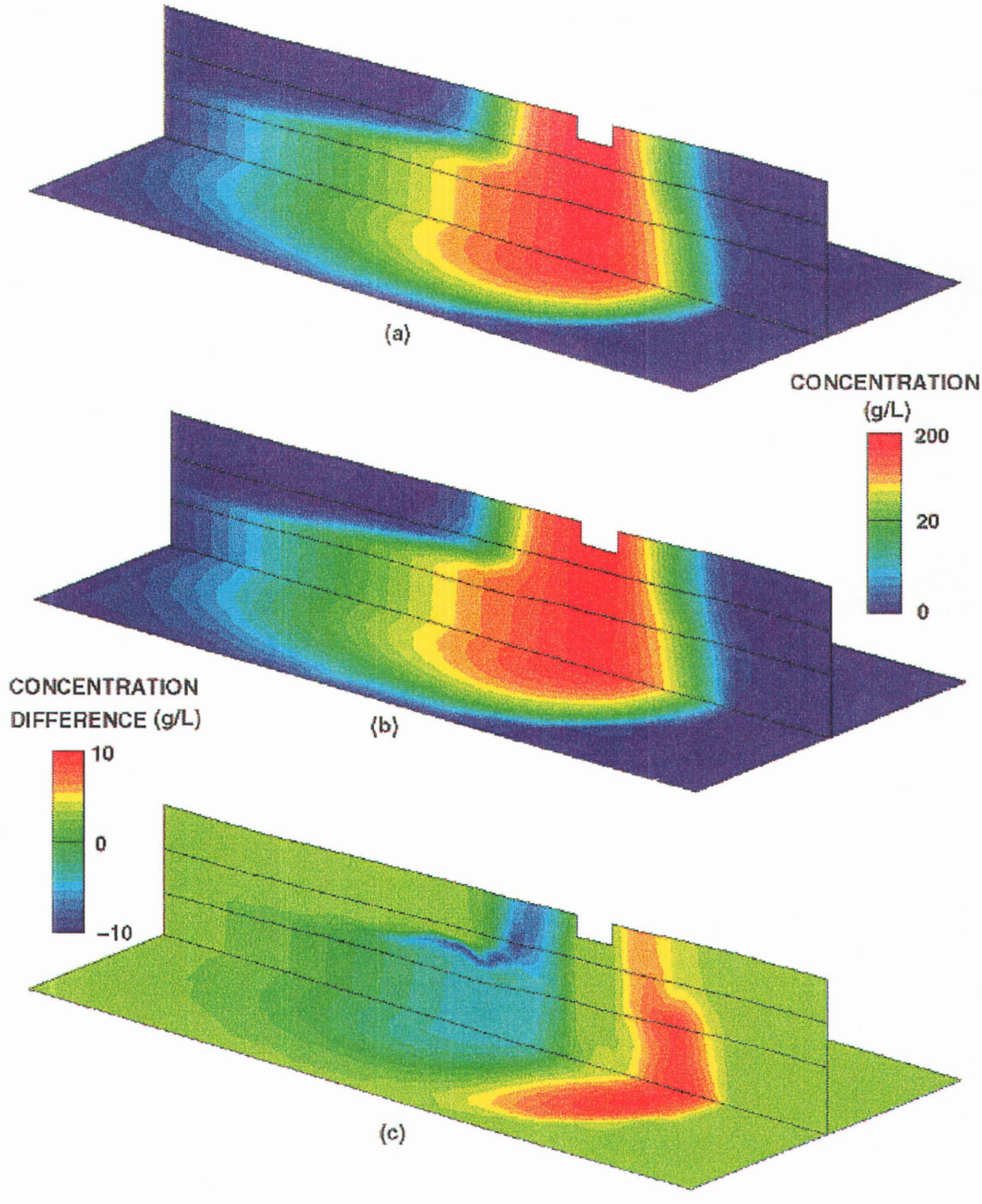

Figure B.7 - Difference in the Brine Plume Position for the Dipping and Horizontal Basal Aquifer (High Clay Hydraulic Conductivity, High Dispersivity Case)

B.1 Conclusions From The Couple Brine Transport Simulations

The results of the coupled brine transport simulations provided information about the sensitivity of the movement of brine in the groundwater flow system to basal aquifer dip, dispersivity and clay hydraulic conductivity. Simulations A, B and C indicated that rate of downward brine migration and also the amount of dispersion was sensitive to low dispersivity soils and low hydraulic conductivity clay units. The results from Simulations A and B indicated that increasing the dispersivity of the porous media by a factor of 10 resulted in significant differences. The results of Simulations B and C further indicated that for high dispersivity, the system was sensitive to the increased clay hydraulic conductivity.

Comparing the results of Simulation A with Simulation D showed that when the dispersivity of the porous media and the hydraulic conductivity of the confining unit was low, the amount of spreading the contaminant plume down dip was minimal. If soil dispersivity and hydraulic conductivity of the clay unit were high, brine would move down dip, against the direction of groundwater flow. The down dip migration of the brine plume against groundwater flow occurred because the density-driven component of flow was greater than the component of flow resulting from the hydraulic head gradient.

APPENDIX C

ISOPACHS

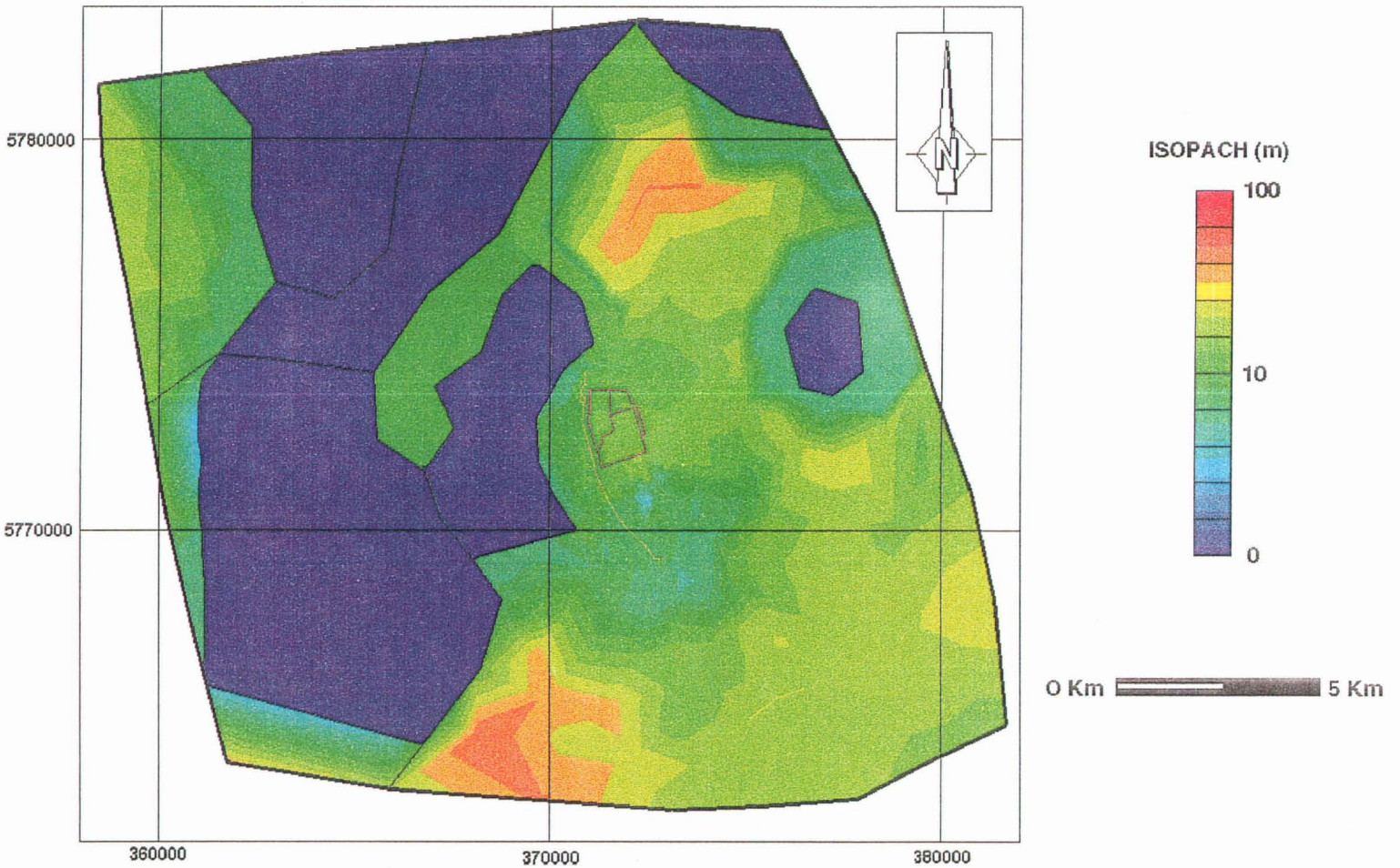

Figure C.1 - Judith River Aquifer Isopach Map

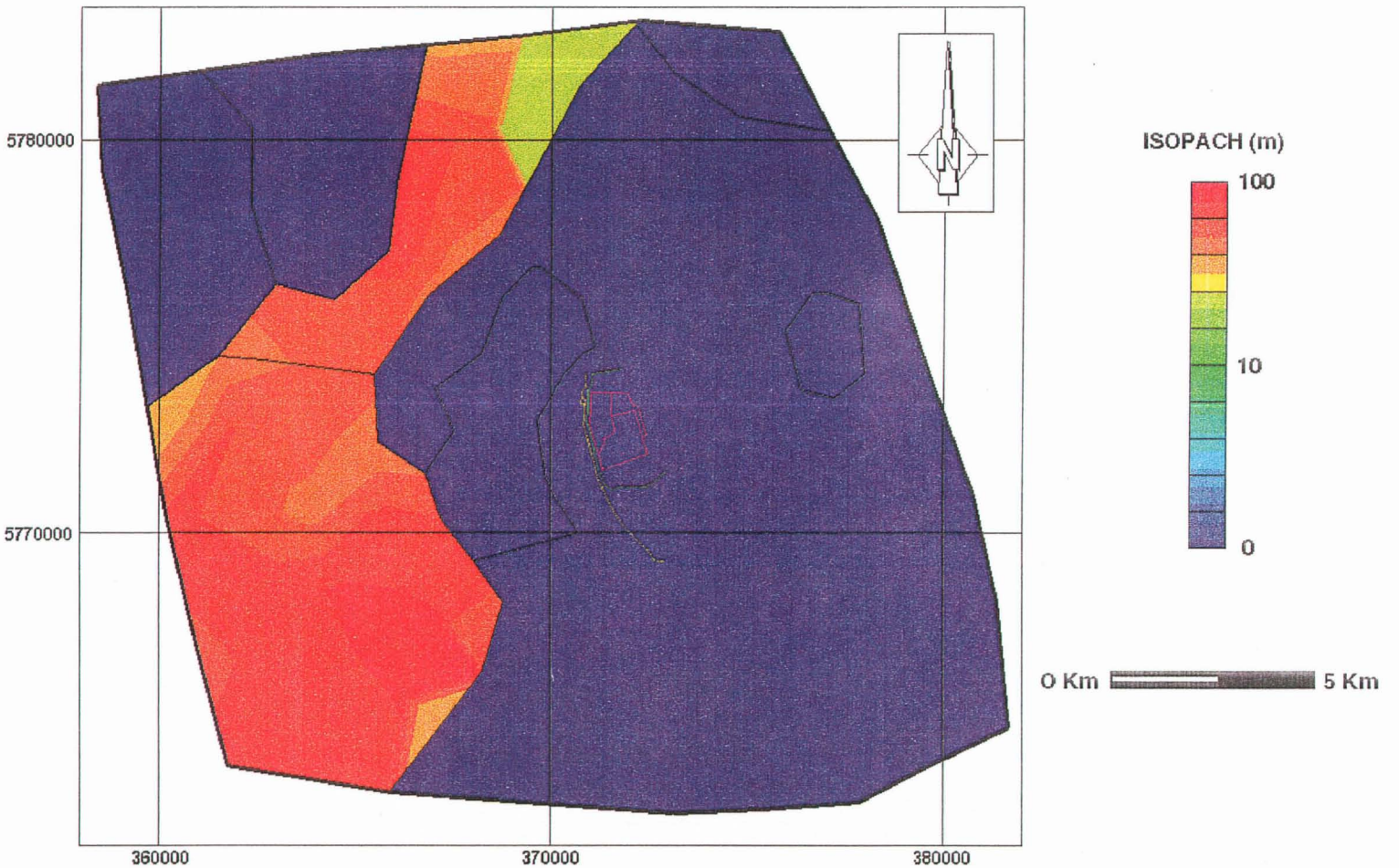

Figure C.2 - Tyner Valley Aquifer Isopach Map

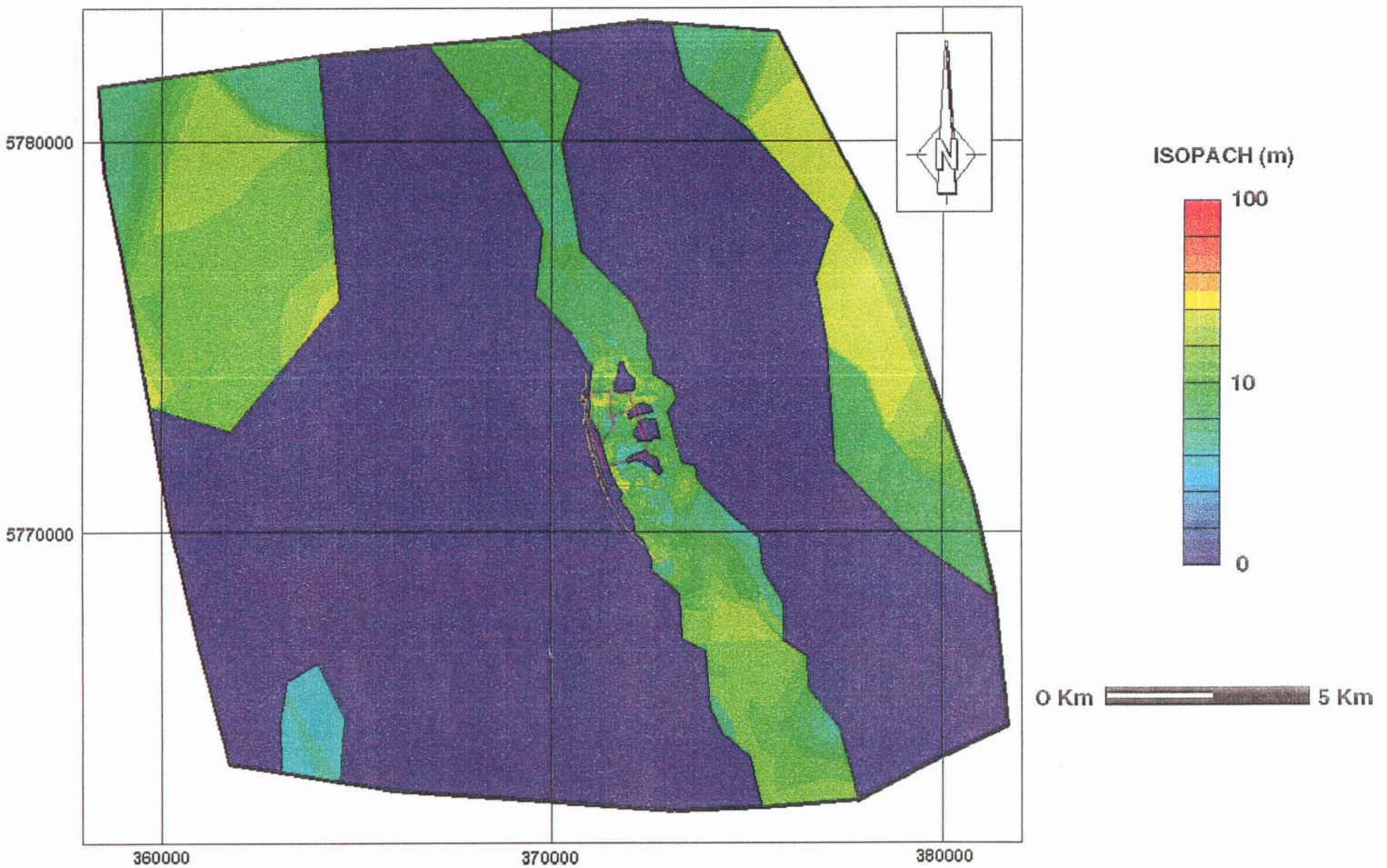

Figure C.3 - Floral Aquifer Isopach Map

APPENDIX D

CALIBRATED STEADY-STATE AND TRANSIENT MODEL

TABLE D.1 - WATER LEVEL DATA USED IN THE STEADY-STATE MODEL CALIBRATION

MONITORING WELL NAME	AQUIFER UNIT	EASTING	NORTHING	MEASURED WATER LEVEL (m)
77-702	Judtih River	370902	5773589	499.7
77-802	Floral	372478	5771153	491.11
77-804	Floral	372150	5771552	491.31
77-805	Floral	372806	5770828	490.84
86-101	Sutherland	372272	5773577	496.9
86-103	Judith River	370861	5773368	497.8
84-104	Sutherland	370892	5772053	493.4
86-105	Judith River	371680	5770495	494.6
86-107	Floral	372917	5771596	495.32
86-109	Judith River	373278	5772750	494.8
93-102	Sutherland	372590	5770985	491.05
93-103	Floral	372585	5770993	490.83
D13/MW#18	Floral	372073	5771158	491.79
Dan Nahathewsky	Tyner Valley	363925	5775000	489.9
Gittings Fred	Tyner Valley	361650	5772200	506.6
Gossen Marv	Tyner Valley	364775	5773425	507.5
Keet David	Tyner Valley	364300	5771700	503.9
Keet Nelson	Tyner Valley	367100	5778500	489.2
Miller Daryl	Judith River	361400	5778900	499.9
MW#20	Judith River	372650	5771013	494.52
SRC Moon Lake I	Surficial Drift	375650	5767500	503.9
SRC Moon Lake II	Surficial Drift	375600	5764500	486.7

CALIBRATION PLOT FOR THE JUDITH RIVER AQUIFER

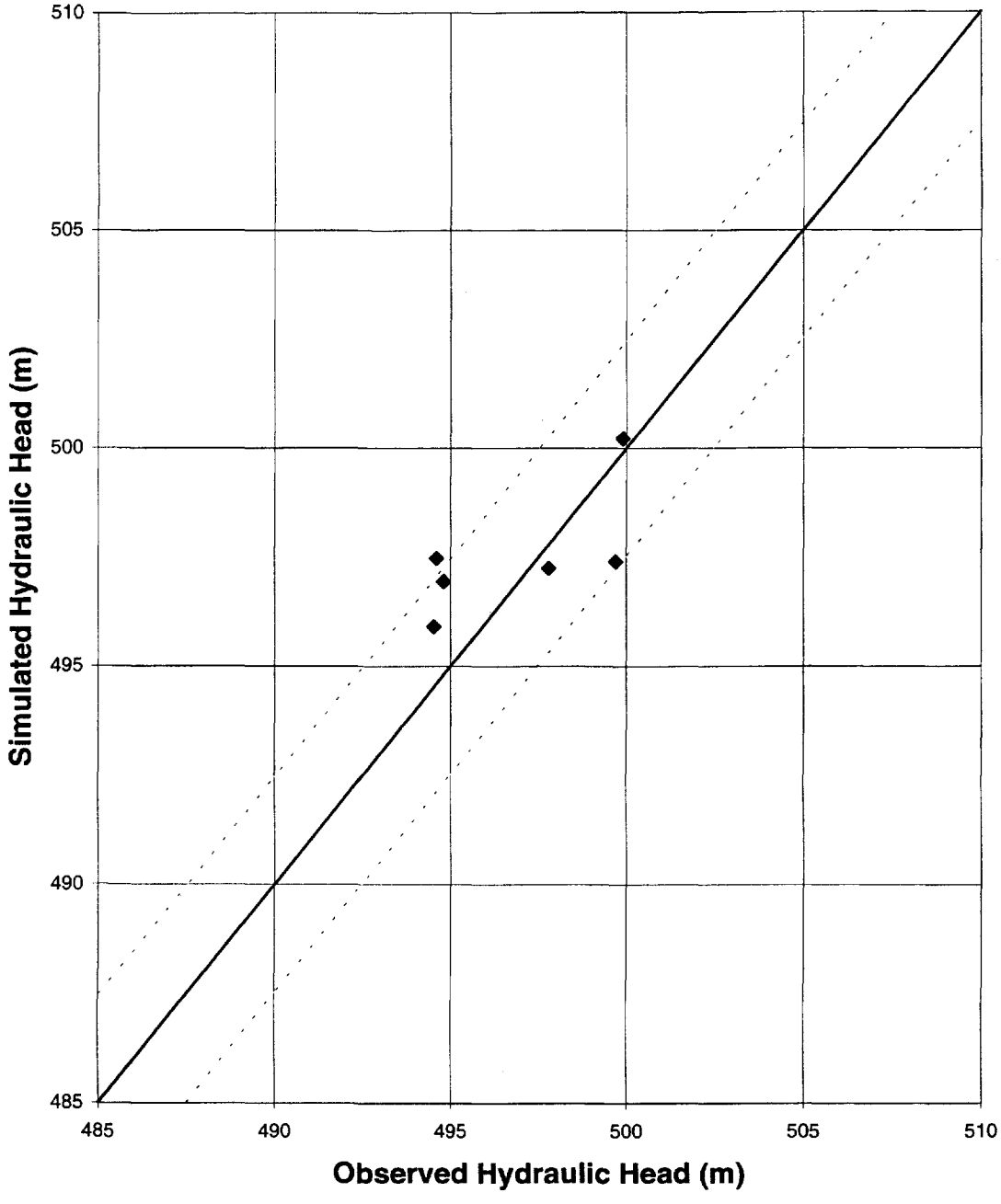

Figure D.1 - Calibration Plot for the Judith River Aquifer

CALIBRATION PLOT FOR THE TYNER VALLEY AQUIFER

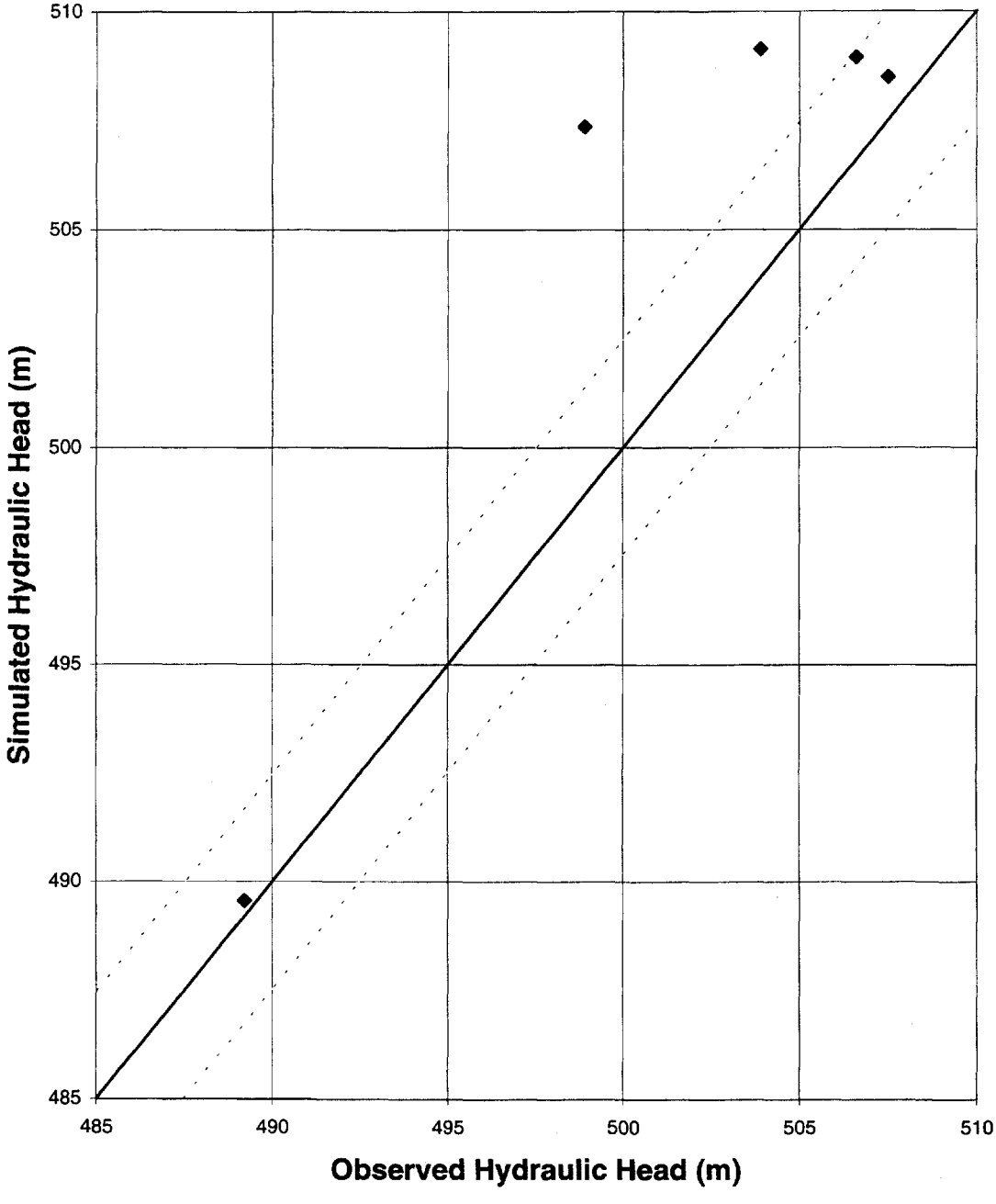

Figure D.2 - Calibration Plot for the Tyner Valley Aquifer

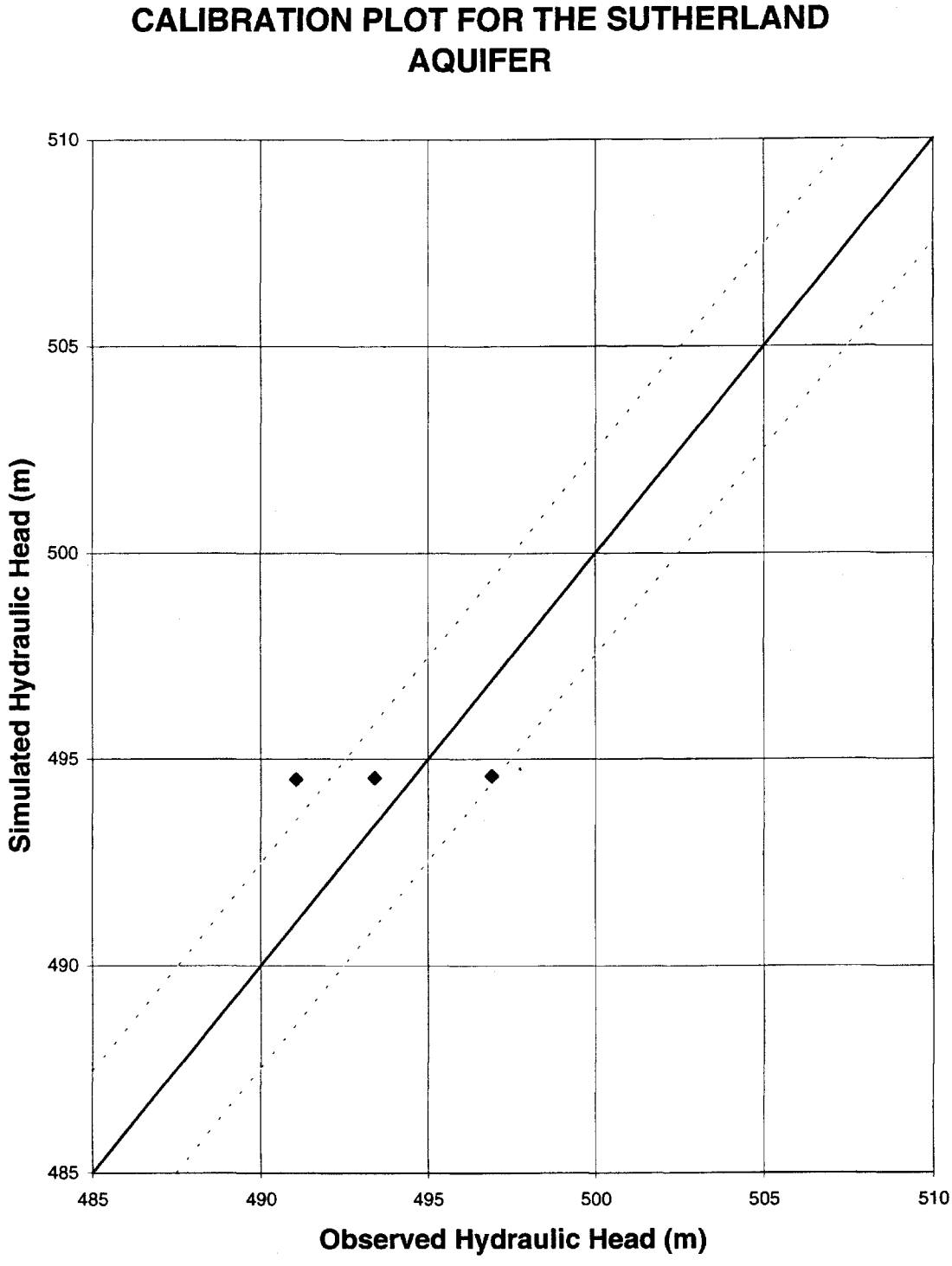

Figure D.3 - Calibration Plot for the Sutherland Aquifer

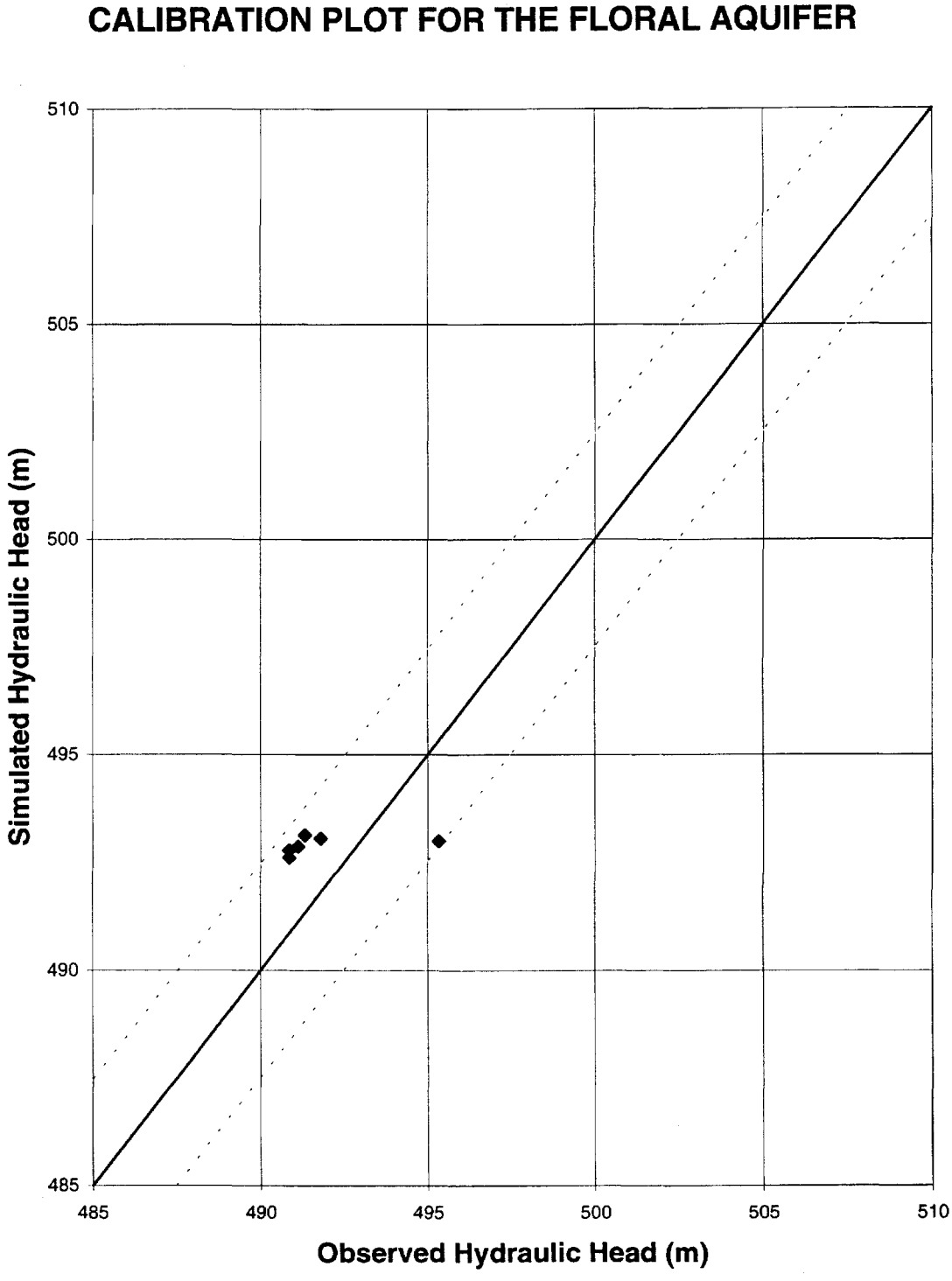

Figure D.4 - Calibration Plot for the Floral Aquifer

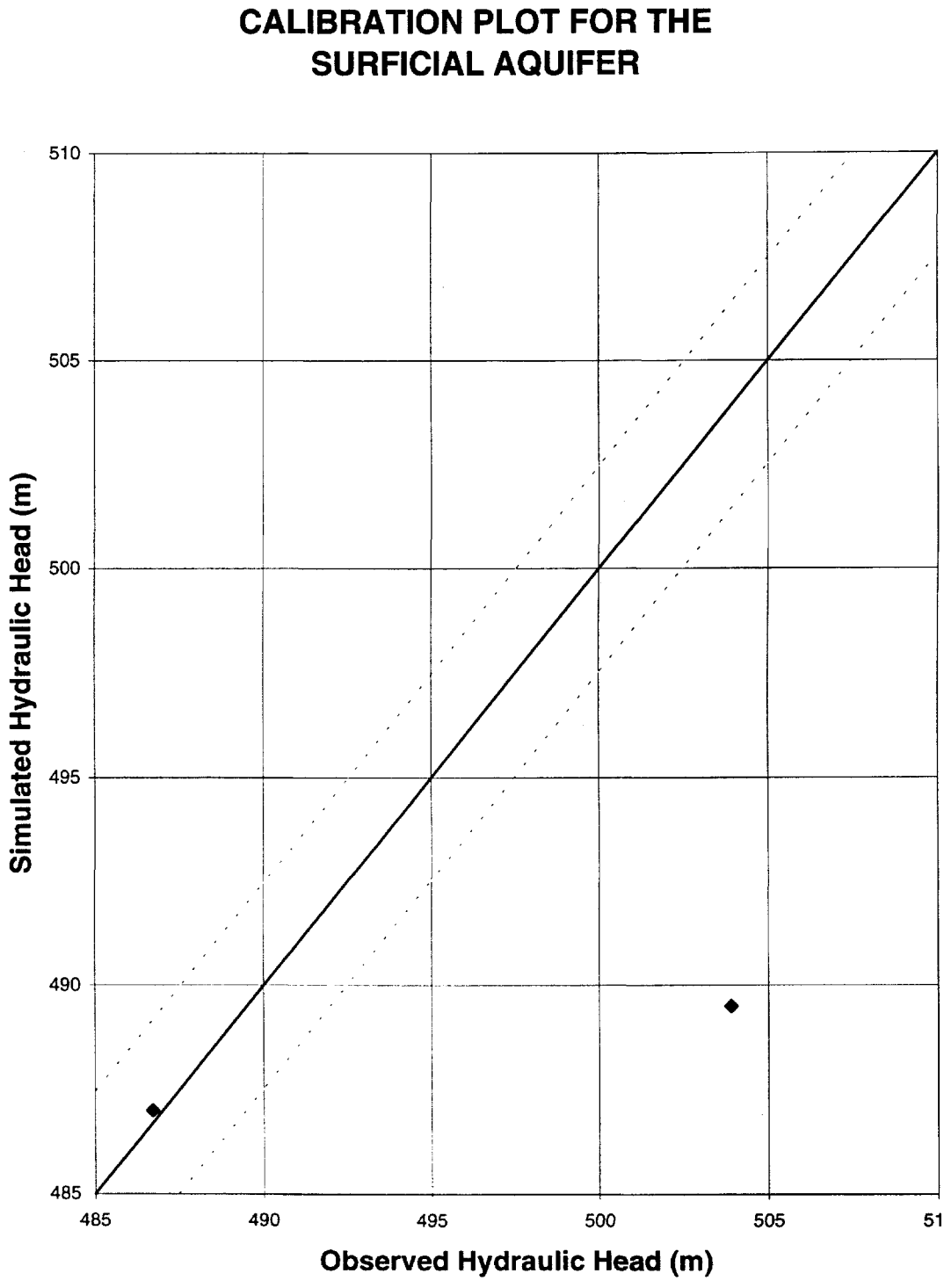

Figure D.5 - Calibration Plot for the Surficial Aquifer

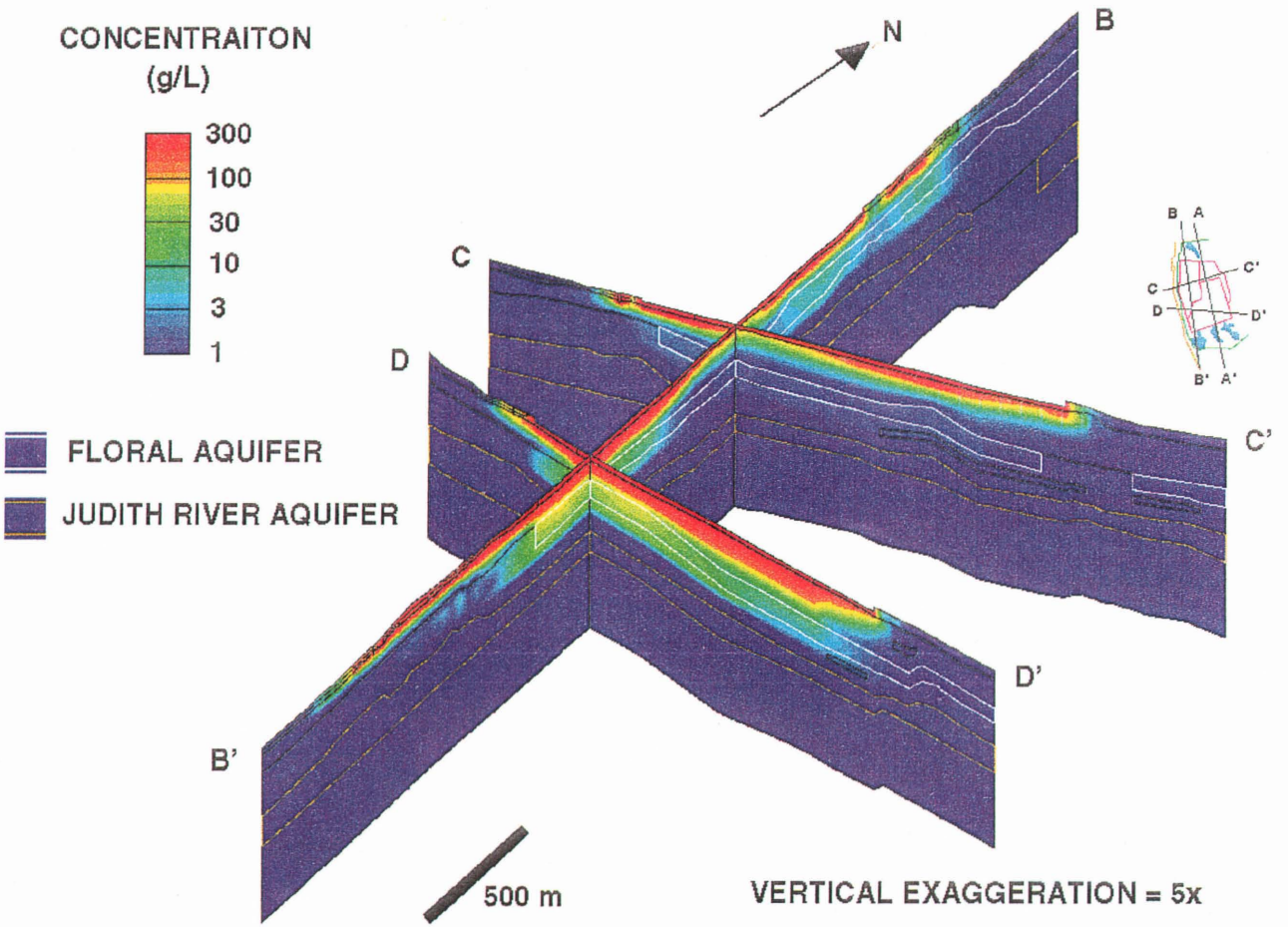

Figure D.6 - Position of the Brine Plume along Sections B-B', C-C' and D-D' after 50 years of Brine Transport

APPENDIX E

SENSITIVITY ANALYSIS

TABLE E.1 - Time Domain Sensitivity Analysis

	12 Months Time Step		4 Months Time Step		2 Months Time Step		1 Month Time Step	
YEAR	Mean	Standard Deviation	Mean	Standard Deviation	Mean	Standard Deviation	Mean	Standard Deviation
0	1.815	12.711	1.815	12.711	1.815	12.711	1.815	12.711
1	2.801	16.303	2.801	16.303	2.801	16.303	2.780	16.215
2	3.104	17.706	3.104	17.706	3.085	17.626	3.031	17.382
3	3.290	18.563	3.290	18.563	3.229	18.295	3.186	18.100
4	3.442	19.225	3.412	19.105	3.346	18.823	3.311	18.656
5	3.544	19.664	3.500	19.487	3.445	19.260	3.416	19.117
6	3.614	19.958	3.576	19.815	3.531	19.630	3.507	19.502
7	3.697	20.262	3.645	20.099	3.607	19.949	3.586	19.832
8	3.771	20.535	3.706	20.348	3.675	20.228	3.658	20.123
9	3.836	20.772	3.762	20.569	3.737	20.476	3.722	20.379
10	3.877	20.913	3.813	20.768	3.793	20.696	3.780	20.609
15	4.096	21.887	4.018	21.517	4.015	21.519	4.008	21.463
20	4.218	22.123	4.179	22.077	4.172	22.027	4.166	22.002
25	4.350	22.543	4.310	22.492	4.299	22.454	4.285	22.367
30	4.394	22.812	4.418	22.759	4.410	22.702	4.381	22.631
35	4.511	23.062	4.509	23.043	4.488	22.968	4.460	22.839
40	4.597	23.285	4.590	23.260	4.571	23.104	4.549	22.981
45	4.677	23.495	4.661	23.423	4.652	23.313	4.590	23.100
50	4.751	23.678	4.727	23.562	4.725	23.428	4.654	23.197

TABLE E.2 - INCREASE BRINE POND HEAD TO 498 m

HYDROGEOLOGICAL UNIT	ME (m)	MAE (m)	RMS (m)
SURFICIAL DRIFT	7.01	7.36	7.18
FLORAL AQUIFER	-3.24	3.46	3.73
SUTHERLAND AQUIFER	-0.83	2.33	2.52
TYNER VALLEY AQUIFER	-3.56	3.56	4.64
JUDITH RIVER AQUIFER	-0.49	1.39	1.89
ENTIRE MODEL	-1.37	3.18	4.51

TABLE E.3 - DECREASE BRINE POND HEAD TO 488 m

HYDROGEOLOGICAL UNIT	ME (m)	MAE (m)	RMS (m)
SURFICIAL DRIFT	7.09	7.35	7.22
FLORAL AQUIFER	1.25	1.25	1.91
SUTHERLAND AQUIFER	-0.70	2.30	2.49
TYNER VALLEY AQUIFER	-3.40	3.40	4.54
JUDITH RIVER AQUIFER	-0.32	1.35	1.81
ENTIRE MODEL	-0.03	2.52	6.00

TABLE E.4 - INCREASE INFILTRATION TO 25 mm/yr

HYDROGEOLOGICAL UNIT	ME (m)	MAE (m)	RMS (m)
SURFICIAL DRIFT	6.75	7.37	7.06
FLORAL AQUIFER	-1.11	1.87	1.89
SUTHERLAND AQUIFER	-0.76	2.30	2.49
TYNER VALLEY AQUIFER	-3.51	3.51	4.62
JUDITH RIVER AQUIFER	-0.43	1.38	1.86
ENTIRE MODEL	-0.77	2.73	4.65

TABLE E.5 - EVAPORATION RATE EQUALED TO 25 mm/yr

HYDROGEOLOGICAL UNIT	ME (m)	MAE (m)	RMS (m)
SURFICIAL DRIFT	7.28	7.33	7.31
FLORAL AQUIFER	-0.96	1.77	1.81
SUTHERLAND AQUIFER	-0.76	2.30	2.49
TYNER VALLEY AQUIFER	-3.43	3.43	4.56
JUDITH RIVER AQUIFER	-0.40	1.37	1.85
ENTIRE MODEL	-0.66	2.68	4.76

Table E.6 - Figures Constructed For the Sensitivity Analysis

Year / Model	10	17	26	50
Base Case Model	2/1	2/1	2/1	3/4
No Containment Structures	-	-	-	2/1
Base Case Model and Brine Mounding	1/1	1/1	1/1	3/4
Difference Between Brine Mounding and Base Case Model	1/1	1/1	1/1	3/4
No Containment Structures and Brine Mounding	-	-	-	2/0
Base Case with a High Coefficient of Tortuosity	-	-	-	1/1
Base Case Model with a Low Coefficient of Tortuosity	-	-	-	1/1
Difference Between the High and Low Coefficient of Tortuosity	-	-	-	2/1

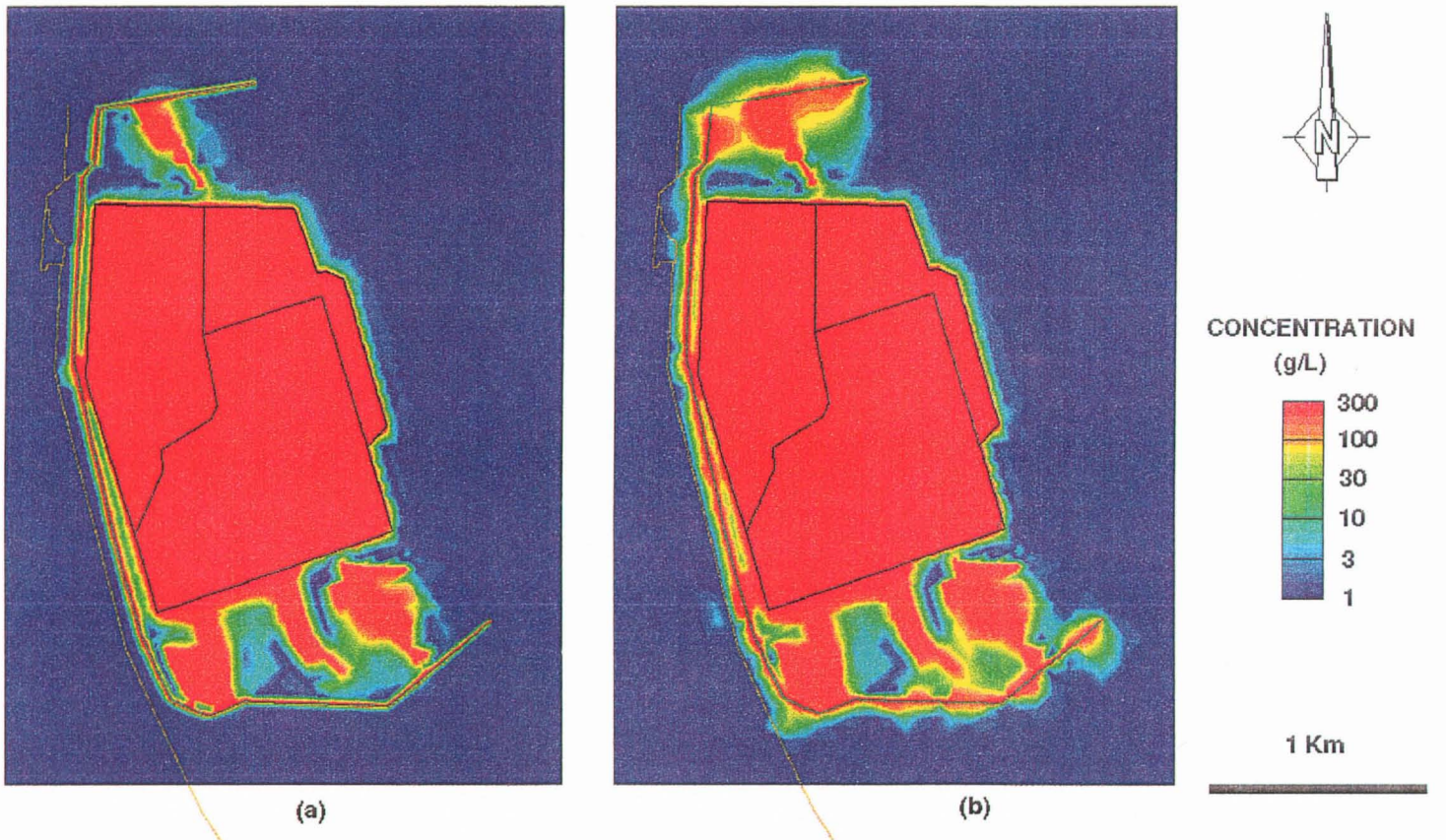

Figure E.1- Brine Plume in the Surficial Stratified Deposits after (a) 10 years and (b) 17 years of simulated Brine Transport with Brine Mounding in the Tailings Pile

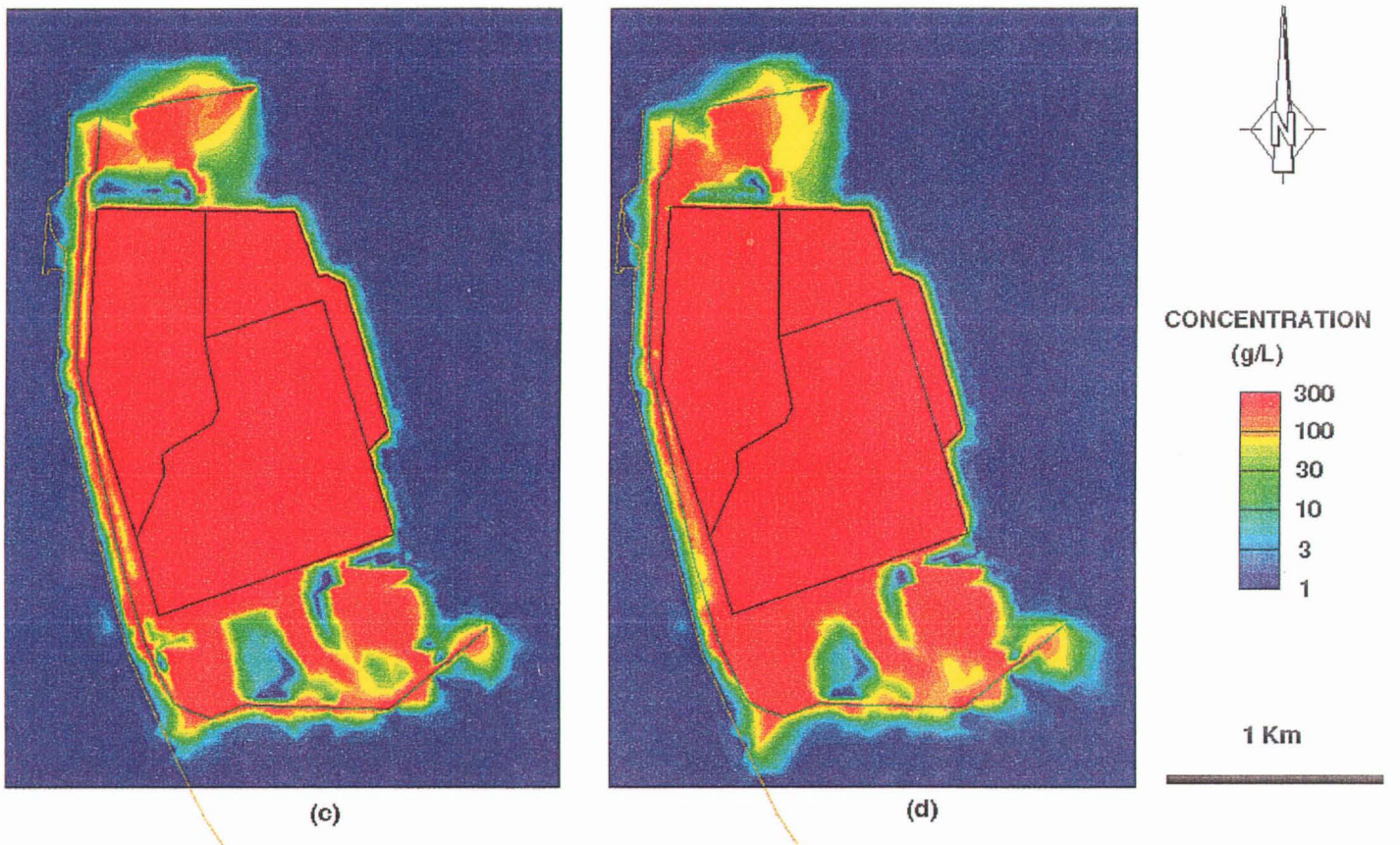

Figure E.1- Brine Plume in the Surficial Stratified Deposits after (c) 26 years and (d) 50 years of simulated Brine Transport with Brine Mounding in the Tailings Pile

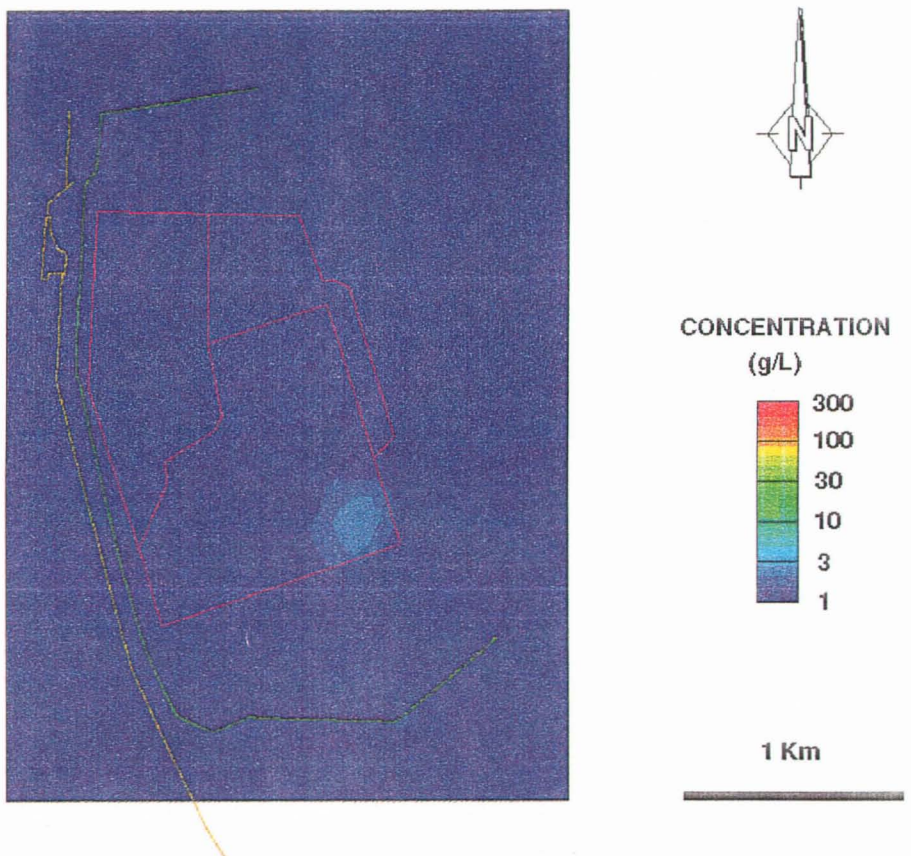

Figure E.2 - Brine Plume in the Judith River Aquifer after 50 years of simulated Brine Transport with Brine Mounding in the Tailings Pile

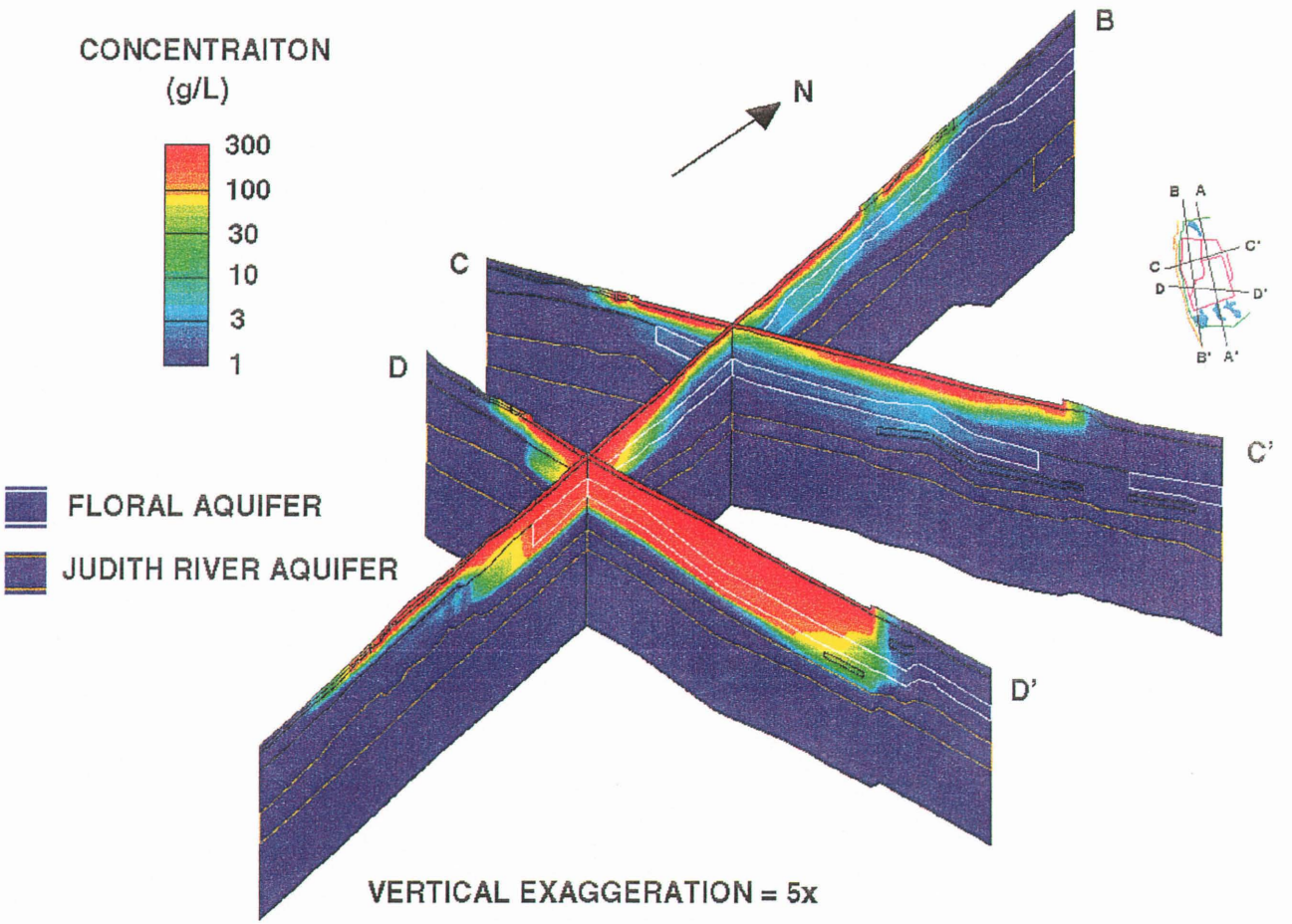

Figure E.3 - Position of the Brine Plume along Sections B-B', C-C' and D-D' after 50 years of simulated Brine Transport with Brine Mounding in the Tailings Pile

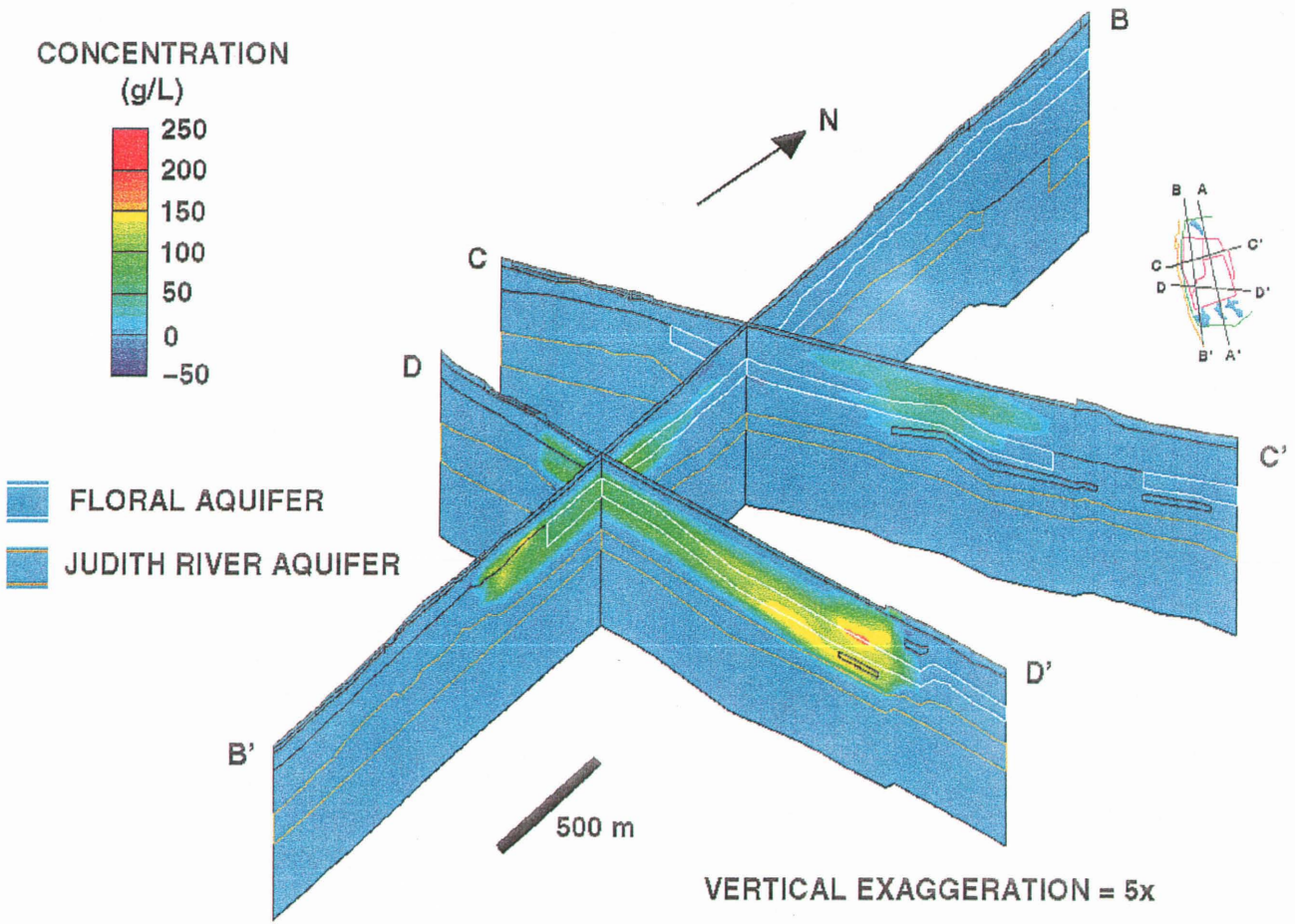

Figure E.4 - Difference between the Brine Plume along Section B-B', C-C' and D-D' for the Brine Mounding and Base Case Model after 50 years of simulated Brine Transport

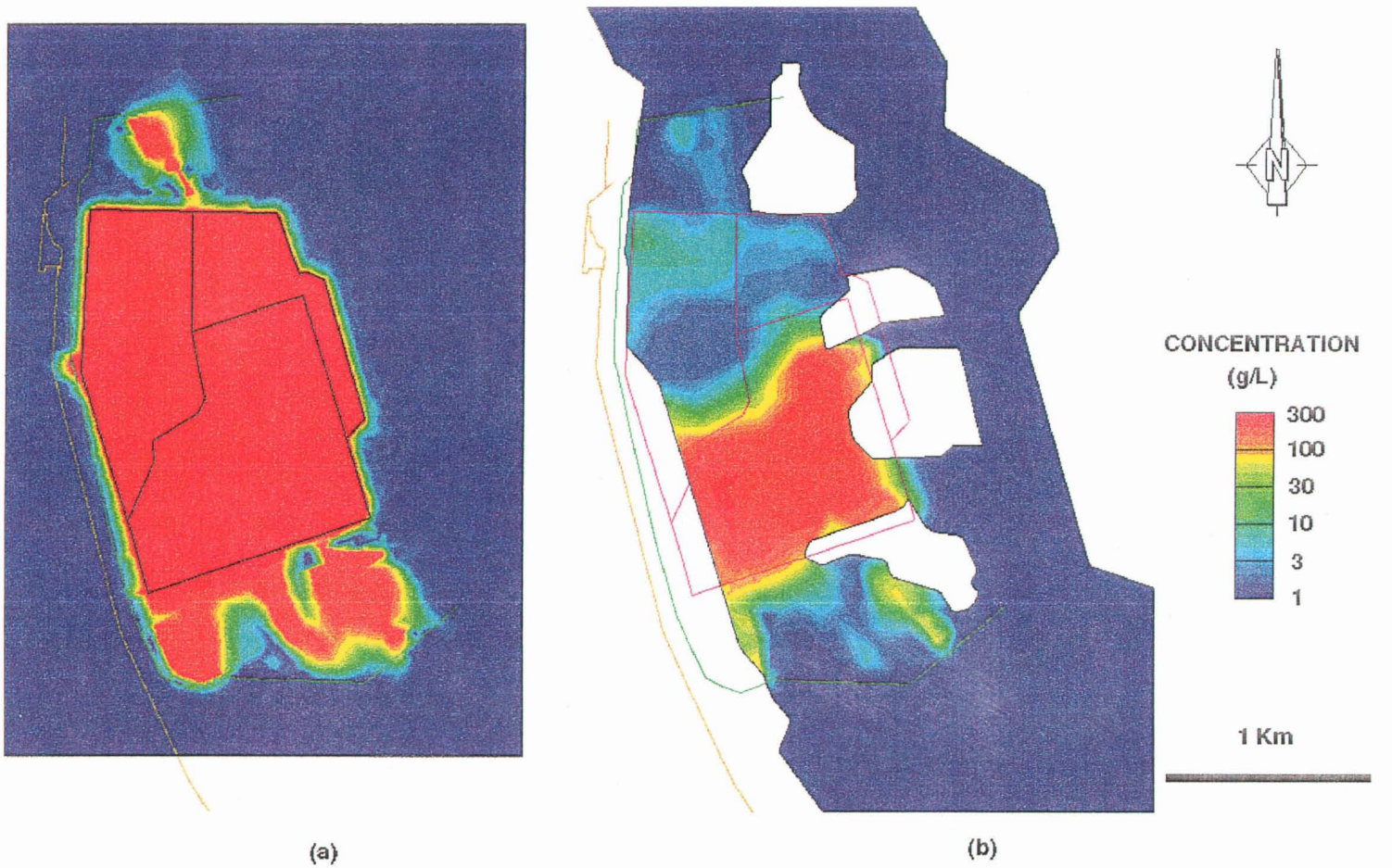

Figure E.5 - Brine Plume in the (a) Surficial Stratified Deposits and (b) Floral Aquifer after 50 years of simulated Brine Transport for the Brine Mounding Case Without Containment Structures

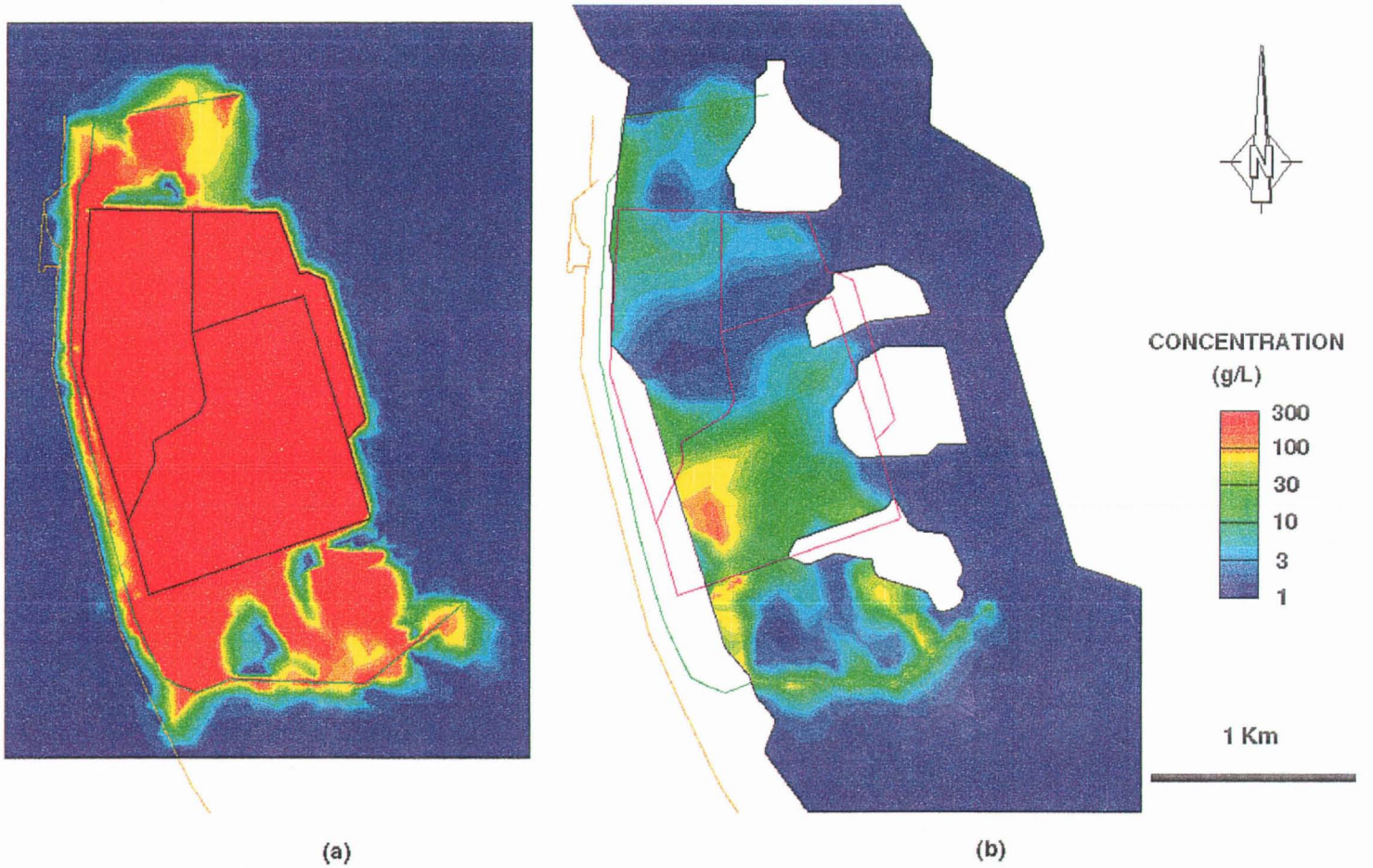

Figure E.6 - Brine Plume in the (a) Surficial Stratified Deposits and (b) Floral Aquifer after 50 years of simulated Brine Transport for the High Coefficient of Tortuosity Case

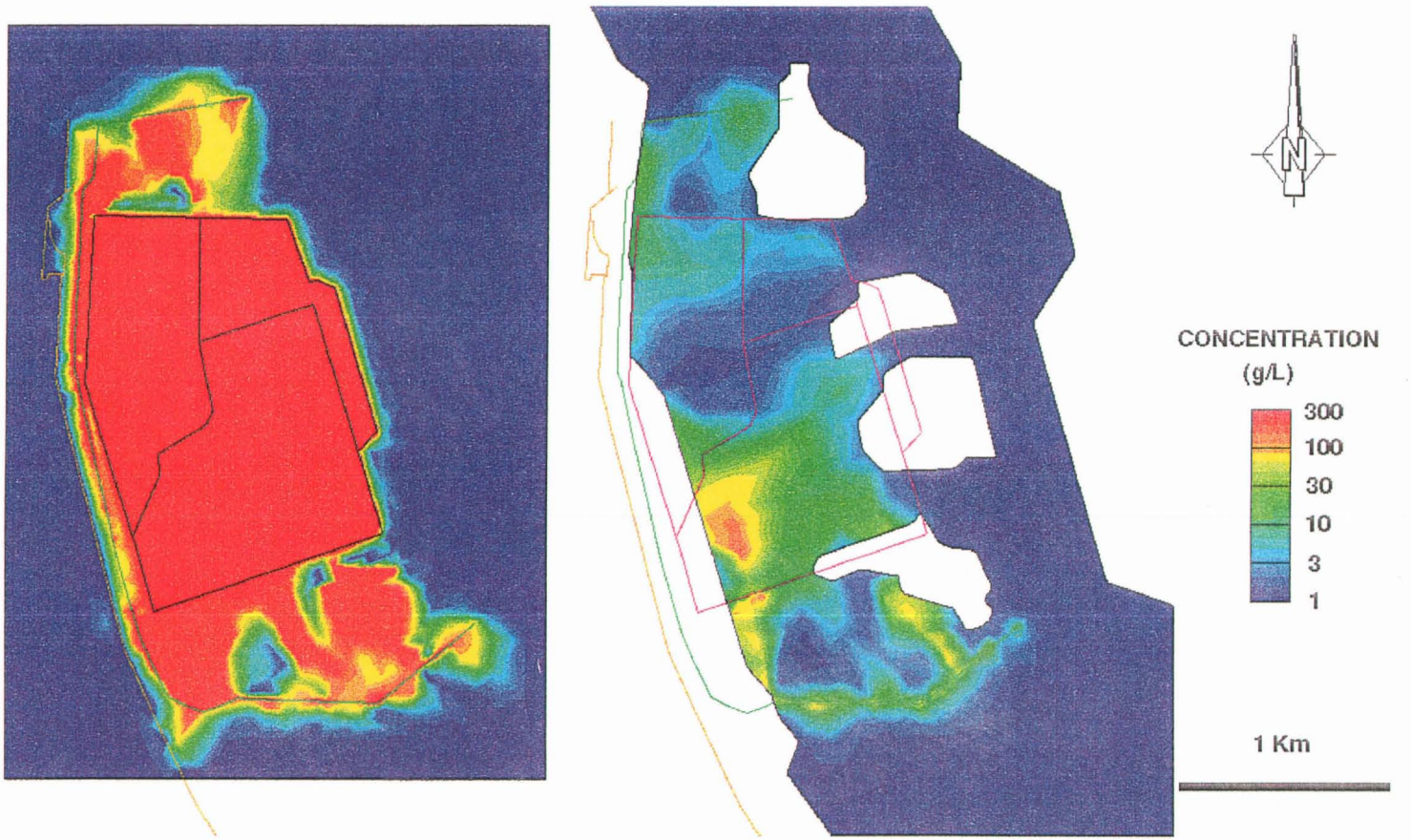

Figure E.7 - Brine Plume in the (a) Surficial Stratified Deposits and (b) Floral Aquifer after 50 years of simulated Brine Transport for the Low Coefficient of Tortuosity Case

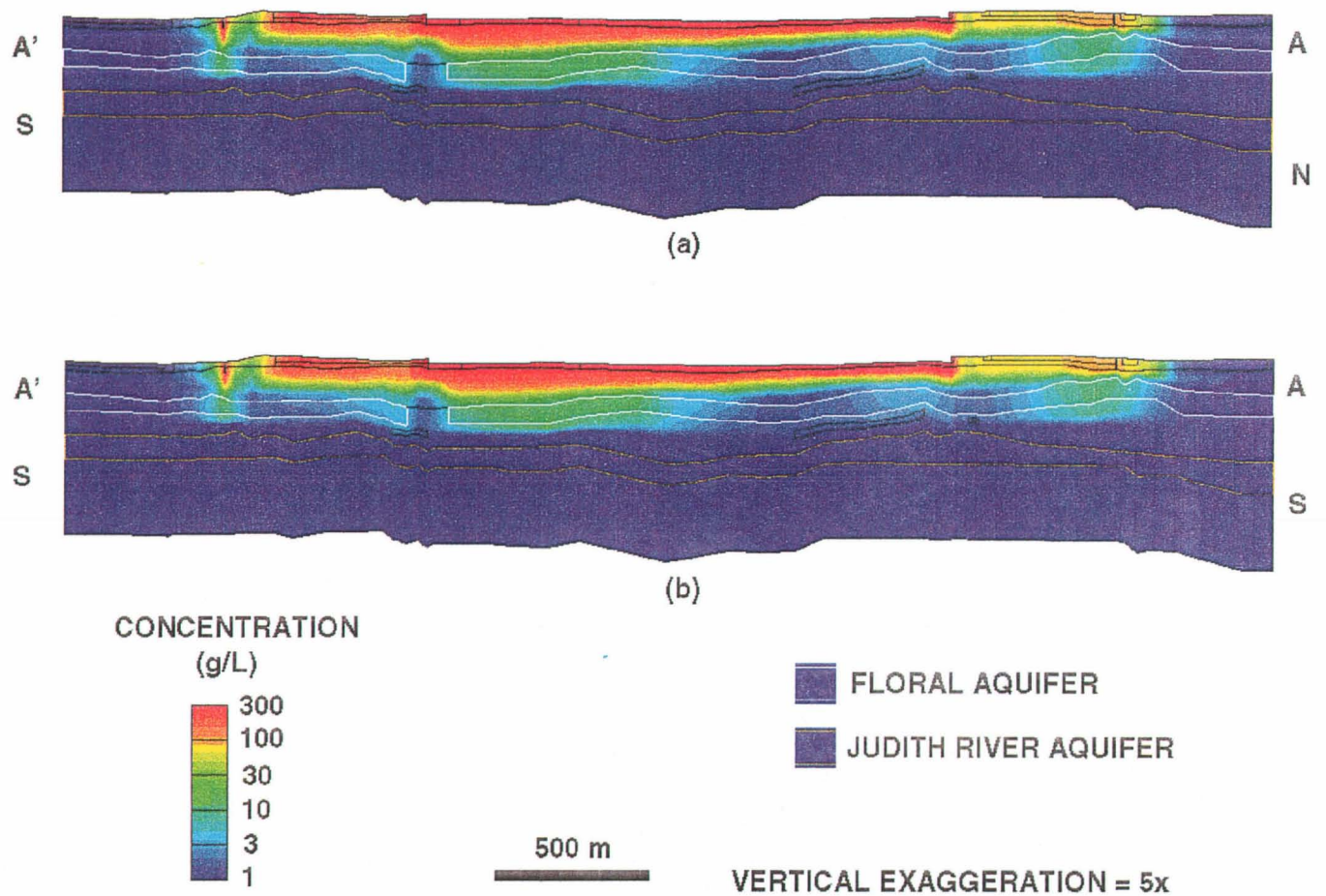

Figure E.8 - Brine Plume along Section A-A' after 50 years of simulated Brine Transport for the (a) High and (b) Low Coefficient of Tortuosity Cases

APPENDIX F

STUDY AREA MAPS